琉球大学学術リポジトリ

アフガニスタンにおける地震のリスクと構造物の振動特性評価に関する基礎的な研究

メタデータ	言語: en
	出版者: 琉球大学
	公開日: 2020-04-09
	キーワード (Ja):
	キーワード (En):
	作成者: NASIRY, NASIR ZIA
	メールアドレス:
	所属:
URL	http://hdl.handle.net/20.500.12000/45547

Doctoral Dissertation of Engineering

A FUNDAMENTAL STUDY
ON
THE SEISMIC RISK IN AFGHANISTAN
AND
VIBRATION CHARACTERISTICS OF
STRUCTURES

March 2020

by

Nasir Zia Nasiry

Civil Engineering

Material, Structural and Energy Engineering

Graduate School of Engineering and Science

University of the Ryukyus

Doctoral Dissertation of Engineering

A FUNDAMENTAL STUDY
ON
THE SEISMIC RISK IN AFGHANISTAN
AND
VIBRATION CHARACTERISTICS OF
STRUCTURES

March 2020

by

Nasir Zia Nasiry

Civil Engineering

Civil and Architecture Engineering Course

Graduate School of Engineering and Science

University of the Ryukyus

Supervisor: Prof. (Dr.) Ömer Aydan

We, the undersigned, hereby, declare that we have read this thesis and we have attended the thesis defense and evaluation meeting. Therefore, we certify that, to the best of our knowledge this thesis is satisfactory to the scope and quality as a thesis for the degree of Doctor of Engineering (Science/Philosophy) in Civil Engineering and Architecture department under Material, Structural and Energy Engineering, Graduate School of Engineering and Science, University of the Ryukyus.
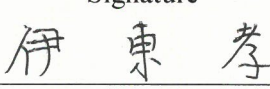
THESIS/DISSERTATION REVIEW & EVALUATION COMMITTEE MEMBERS

Signature

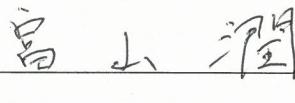**(Chairman) Prof. Dr. Ömer Aydan**

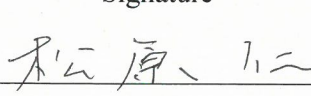Signature

伊 東 孝

(Committee) Prof. Dr. Takashi Ito

Signature

池 田 隆 明

(Committee) Prof. Dr. Takaaki Ikeda

Signature

富 山 潤

(Committee) Assoc. Prof. Dr. Jun Tomiyama

Signature

松 原 仁

(Committee) Assoc. Prof. Dr. Hitoshi Matsubara

ABSTRACT

Earthquakes are major threats for life and infrastructure in Afghanistan in addition to the numerous natural and human-made disasters. The death toll from earthquakes since 1998 is more than 8,000 people in this country. Hundreds of thousands of people were left homeless. Death and damage loss from earthquakes are global problem; however, it is considerably high when it comes to Afghanistan in comparison to other countries in the world. Shallow earthquakes have a relatively high impact all over the world, and the impact considerably decreases when the earthquake is a deep event. The problem that needs to be addressed for the future in Afghanistan region is the shortcomings that result the intermediate-magnitude deep and small size shallow events also cause a considerably high impact on life and properties. A shallow earthquake of magnitude 6.0 will maximum cause deaths in the order of 10 to 100 people in countries like Japan, USA, UK and other developed countries; however, the twine earthquakes of 1998 Mw 6.0 and Mw 5.9 of Rustaq in Takhar province of Afghanistan killed almost 4,000 people, destroyed 7 and damaged more than 30 other villages. The 2015 Mw 7.5, 210 km deep earthquake of Afghanistan and Pakistan in Hindu Kush region killed about 400 people in both countries and damaged about 12,000 houses. The considerably high life and property loss from this earthquake remarks the need of a thorough earthquake hazard assessment in the region.

The primary goals of this thesis are to assess the seismic hazard analysis and seismic vulnerability of common type buildings in Afghanistan. First and foremost, this requires identification of the earthquake sources, the crustal deformations, straining and stresses, strong ground motion and the shortcomings of the common type buildings during past earthquakes in Afghanistan region. To provide a precise answer for each of the above goals, theoretical studies, site investigations as well as huge amount of laboratory experiments are required. To document the past earthquakes, data was retrieved and analyzed from international agencies operating for a long time. Unfortunately, there is very little understood about the historical earthquakes of Afghanistan. Although, Afghanistan started to develop in the beginning of 21st century, very little or almost no data/study is published about the extent of the damage of earthquakes in about last two decades. To predict the future damage and to evaluate the collapse mechanisms of the common type buildings in future earthquakes, data is also analyzed from the reports/studies of earthquakes occurring in neighboring countries and elsewhere in the world. However, enough site visits couldn't be conducted as it is little challenging when it comes to Afghanistan due to security circumstances.

The energy for earthquakes in Afghanistan is mainly released from two regional earthquake sources: namely, the Eurasia-Indian global plate boundary movements in the SE, and the deep earthquake region of Hindu Kush and Pamir in the NE. There are three main fault systems in

Abstract

Afghanistan that accommodates most of their movements from the regional sources, mainly from the Eurasia-Indian global plate boundary movements. Chaman fault system is more active among other two and based on evidence, it is capable of releasing energy for devastating earthquakes in the future. Although, most of the earthquakes in Hindu Kush region are deep events (depth>50 km), the 1998 Rustaq earthquakes and the 2002 Nahrin earthquake were shallow events. However, both shallow and deep earthquakes from this source have had high impact on life and property in the past.

To analyze the earthquake hazard of Afghanistan, first a homogenized earthquake catalogue is developed. The instrumental seismicity has the major contribution in the homogenized earthquake catalogue. Although, the historical earthquake record is almost nil for Afghanistan, information about historical events from the surviving earthquake catalogue is also included. The first historical earthquake that is documented in Afghanistan is reported to be in the year 734. The homogenized earthquake catalogue includes earthquakes of a broader area bounded by $27.0 \leq Latitude \leq 39.5$, $58.5 \leq Longitude \leq 75.0$, and $M \geq 4.0$. The earthquakes are reported in different magnitude scales. We converted them to moment magnitude (Mw).

The earthquake recurrence parameters were calculated for the two instrumental earthquake catalogues as well as for the 9 earthquake domains in Afghanistan: respectively. These parameters are used to analyze the seismic hazard. The results show that the ground acceleration can be up to 1.0 g for Kabul city. The Peak Ground Acceleration (PGA) for Kabul city corresponding to 2% and 10% Probability of Exceedance (PE) in 50 years are 32%g and 19%g, respectively. Maximum spectral acceleration in Kabul city at 2% and 10% PE in 50 years are 82%g and 42%g corresponding to 0.2-second, respectively. Ground motion from a hypothetical earthquake in Kabul City is 0.9g. The results for the whole Afghanistan are presented in the form of ground motion contour maps, acceleration, velocity and displacement time series and earthquake hazard curves. Although, the Chaman fault has not released energy for a big earthquake neither in the instrumental era nor in the historical era, the regional geologic activities remark the potential for occurrence of a devastating earthquake near Kabul city. Considering these values of ground motion and ongoing geologic activities, the SE boundaries of Afghanistan is identified with the very high earthquake hazard followed by the NE with the high seismic hazard. Although, instrumental earthquakes as big as $Mw \geq 7.0$ have not happened in North Afghanistan, few events are reported in the historical catalogue, therefore the North Afghanistan is subjected to moderate earthquake risk and the remaining Afghanistan which is the SW has the lowest hazard as there is no considerable fault movements nor past major earthquake events.

Unavailability of reports or studies about the damage of buildings in past earthquakes of Afghanistan is another serious problem in the path of understanding their collapse mechanisms.

Abstract

Although there is a considerable change in the administrations from the conventional documentation system to the electronic filing system, little information is published or left open to the researchers for analysis and lesson-learns, almost in every field. The collapse mechanism of the common type buildings from the pictures of past earthquakes in Afghanistan, Pakistan, India and Iran are analyzed. The construction methods in these countries as well as in Turkey and Nepal are also studied. Photo-elasticity tests are conducted on masonry buildings, frames and framed structures with various structural systems to identify the weaknesses.

The structural members plinth/foundation beam (B), Columns (C), and ceiling slab (S), and partition walls (W) of reinforced concrete buildings in Afghanistan are constructed in three different models classified by the construction order of these elements; namely, model 1 BCSW, model 2 BCWS and model 3 BWCS. Photo-elasticity tests are carried out and FEM analysis are conducted on the RC bare frames, frame with infill wall and soft-story and frame with full infill walls in order to evaluate the response of these models, respectively. The model 3 provides better response as the structural members and walls start to react as a unit system whereas in model 1 and model 2 the walls start to react when the column, beam and slab undergo certain amount of bending.

Photo-elasticity tests were also conducted on masonry structures. Model test were conducted as well as test were conducted on shaking table. The models consisted of masonry walls only, masonry walls with opening. Lintels were added to both masonry models. We changed spacing and number of the lintels to evaluate their effect. FEM analysis of were also conducted. The masonry buildings provide more ductile response when continuous beams are constructed in regular distance intervals, below and on top of the windows/openings as well as on the top of the wall.

Last but not the least, this study evaluates the structural integrity of some of the common type of structures using the natural frequency and vibration characteristics. Model tests are conducted on towers, frames, frame buildings, beams as well as data of actual wooden buildings, concrete and composite bridges in Japan and in Afghanistan are analyzed. Four different vibration methods; namely, free vibration, forced vibration, micro-tremor devices and Fourier Amplitude are used. From the results it is clearly observed that most of the structures undergo certain amount of degradation with time. Comparison of the data for some bridge structures in Afghanistan with some structures in Japan indicates that those structures in Afghanistan have also degraded. In most of the case, particularly for the slender structures it is seen that all these methods give very close results. This implies that the free vibration and sandbag drop test are appropriate alternatives to regularly monitor structural integrity, particularly for the areas and countries where lack of advance experimental devices are scarce, and the budget limitations are major problems to conduct quality researches.

ACKNOWLEDGMENT

TABLE OF CONTENTS

LIST OF FIGURES

LIST OF TABLES

List of Tables

CHAPTER 1   INTRODUCTION

1.1 Motivation and Background

Earthquakes in Afghanistan have killed about 8,000 people in since 1998. The major events include the 2015 Mw 7.5 Hindu Kush earthquake of Afghanistan and Pakistan, the 2002 M 6.0, M 5.1, M 5.8 Nahrin earthquakes of Baghlan and the twin earthquakes of 1998 M 5.9 & M 6.5 Rustaq of Takhar Province. Shallow and intermediate-depth high magnitude earthquakes result in considerable casualties and damage; however, in Afghanistan region, earthquakes as deep as 200 km and as big as M 6.0 shallow earthquakes usually kill thousands of people and result into huge damage. Earthquakes as low as M 6.0 and deep earthquakes although being high magnitude seems to have little impact in other parts of the world like Japan, United States, Turkey and Italy; however, similar earthquakes cause tremendous impact on life and infrastructures in Afghanistan. A good example is the Rustaq and Nahrin events, both destroying number of villages and killing several thousands of people. The huge impact remarks the need of a thorough study of the seismic hazard and seismic vulnerability of structures, particularly buildings in Afghanistan.

The primary goal of the seismic risk in Afghanistan and vibration characteristics of structures is to identify the nature and extent of the earthquake hazard and earthquake preparedness of structures, particularly buildings against large earthquakes anticipated to be occurring in Afghanistan in the future. First and foremost, it requires a comprehensive record of the historical earthquakes as well as the instrumental past earthquakes and the details of failure mechanisms of the buildings in the past earthquakes. With the invention of the modern seismographs since 1880s, the record of instrumental earthquakes of almost all regions in the world is close to complete; however, the record of the historical earthquakes remain vague in most of the regions of the world, particularly when it comes to Afghanistan region making it difficult to give a precise guide about future seismicity of the region. To provide guidelines about construction of earthquake resistant buildings, it is necessary to evaluate the damage and collapse mechanisms of the buildings in the past earthquakes. Unfortunately, detailed records about buildings' performance in the past earthquakes of Afghanistan are scarce or they are probably not disclosed.

With the help of conventional and statistical seismic hazard analysis methods, idea can be drawn about the earthquake hazard of any region; however, most of these approaches are based on the past seismicity of the target region. The bases of these approaches are the earthquake catalogues of the past earthquakes which are close to complete for the past about a century and half. The seismicity of far future is difficult to predict because of the incompleteness of the historical seismicity. It should be noted that the recurrence interval for some of the earthquakes span to several thousands

of years and unfortunately the records of earthquakes of several thousand years in the past doesn't exist. The 2011 Great East Japan Earthquake of M9.0-9.1 doesn't have its example recorded in the earthquake history so far available. To address this problem, deterministic approaches provide better result. With the help of later approach, we can calculate the time histories and Fourier Amplitude Spectra for any earthquake anticipated to be happing in any location provided that the ground characteristics of the target region are understood.

Decades of violence in the region have left the seismic hazard and seismic safety of buildings in Afghanistan unexplored. With the help of studying the seismicity and earthquake damage to buildings in the other parts of the world that are in similar geologic setting like Afghanistan, effort is made to address the earthquake hazard in Afghanistan and earthquake vulnerability of common structures, particularly buildings in Afghanistan. Numerous model tests are conducted on towers, frames, frame buildings, bridges and photo elasticity tests on frame buildings to evaluate the earthquake performance of different structures. Test on actual structures are also conducted and based on the findings, proposals are made for construction of earthquake-resistant buildings models in Afghanistan for the future.

1.2 Objectives

The primary objectives of this research are to (1) develop earthquake hazard maps and earthquake risk zonation for Afghanistan, and to (2) propose earthquake-resistant building models corresponding to earthquakes anticipated to be taking place in future in Afghanistan. The latter is obtained by evaluating the collapse mechanisms of the buildings in past earthquakes in other parts of the world and from the results of some of the experimental works. More specifically the objectives of this study and the contribution of this work are below.

1. To prepare an up-to-date earthquake catalogue in order to evaluate the seismicity of Afghanistan region and reproduction of some of the previous seismic zoning and risk maps as they are still used by some of the government ministries. The aim in this is to develop a map with distribution of historical and instrumental earthquakes with explanation of their impact on life and properties.

2. To analyse the crustal deformation, strain and stresses in Afghanistan region its interrelationship with the regional seismicity.

3. To develop probabilistic seismic hazard maps and earthquake risk zonation of Afghanistan based on the distribution of the past earthquakes as well as the regional geologic activities.

4. To assess the strong ground motion in Kabul city from earthquakes in Pamir and Hindu Kush region as well as from a hypothetical earthquake anticipated to be occurring along Chaman fault segment near Kabul city.

5. To evaluate the seismic vulnerability of common type of buildings, material and construction methods in Afghanistan. Additionally, the objective is to study the typical seismic damage mechanisms of buildings in Afghanistan and some other countries to propose earthquake-resistant common type building models to increase life and property safety.

6. To propose easy applicable and cheap experimental methods for countries like Afghanistan in order to understand the stress distribution under different kind of loadings on masonry buildings, frames, frame structures through conducting photo elasticity tests on models of these structures.

7. And to evaluate the integrity of common type of structures using the natural frequencies and vibration characteristics.

1.3 Scope

This thesis focuses on assessing the overall impact of future earthquakes on life and property in the country. This work is proposing earthquake resistant models for masonry and framed buildings. We also discuss the typical seismic vulnerability of common buildings in Afghanistan and neighboring countries and a model corresponding to these inadequacies is proposed for the seismic prone areas of Afghanistan. The seismic risk and seismic vulnerability of common type buildings developed in this study are limited to Afghanistan and the finings can be applied for the structural design in this country. The vibration characteristics of common type structures are generally applicable to structures in the Afghanistan region. Although the collapse mechanisms, experimental and analytical data from other parts of the world are utilized, the results correspond to the seismic risk and seismic vulnerability of buildings in Afghanistan.

1.4 Organization and Outline

This thesis is based on compilation of research papers published and submitted for publication within the period of this study. Chapters 2-5 present detailed regional tectonics and crustal deformations, past seismicity, development of earthquake hazard maps and risk zonation of Afghanistan, and the strong ground motion estimation for Kabul city. Chapter 6 evaluates the common building types, construction material and construction methods in Afghanistan and

neighboring countries. The typical seismic damage of common type buildings in past earthquakes are assessed. In Chapter 7 the performance of various structures under normal and normal and shear forces is evaluated by conducting photo-elasticity model tests on fault slits, masonry buildings, frames and framed buildings. And finally, in Chapter 8 the integrity of common type structures is assessed using the natural frequency and vibration data from numerous experimental works and site visits. Following is a brief explanation of Chapter 2 to Chapter 10.

Chapter 2 discusses the tectonic settings and regional geologic activities. The seismicity is discussed in details and some previous earthquake zoning and risk maps have been reproduced. The historical and instrumental earthquake catalogues are summarized. A homogenized earthquake catalogue of about 39,330 events is presented in the form of earthquake distribution maps. Focal mechanisms for some of the devastating earthquakes are discussed.

Chapter 3 presents the crustal deformations, straining and stresses utilizing the GPS data from the GPS Stations installed in Afghanistan and nearby countries. Strain and stress rates are determined as well as their relationship with the regional seismicity is discussed. The faults' activities are also related with the strain and stress rate and seismicity.

Chapter 4 presents the probabilistic seismic hazard maps for Afghanistan. Earthquake data from various international agencies operating in the region for a century and more are analyzed from which the seismic hazard analysis parameters are identified. The catalogue completeness periods are found and with the help of earthquake analysis computer program, the hazard maps with 2% and 10% Probability of Exceedance (PE) in 50 years are developed, respectively. Earthquake hazard curves corresponding to these return periods are presented, and a seismic risk zonation based on the earthquake distribution and regional geologic activities are presented.

Chapter 5 presents the deterministic strong ground motion estimation for Kabul city from the 2015 Mw 7.5 Hindu Kush earthquake and a hypothetical earthquake along Chaman fault segment near Kabul city, respectively. Three different deterministic earthquake hazard analysis methods are utilized, and strong ground motion is presented in the form of contour maps and ground motion time series.

Chapter 6 discusses the construction material and construction methods in Afghanistan as well as the typical seismic damage of common type buildings in past earthquakes in Afghanistan, Pakistan, Iran and India and some other countries. Application of some construction methods in Turkey and Nepal to buildings in Afghanistan are assessed. The collapse mechanisms of masonry and frame buildings in past earthquakes of those countries are discussed and some modifications to the current construction techniques in Afghanistan are proposed.

Chapter 7 presents the results of photo elasticity tests as well as physical test on faults, slits, masonry buildings, frames and framed buildings representing various construction techniques. The results for some techniques are prevailing on others. The attempt is made to modify the construction techniques utilizing the locally available workmanship and material. A series of test are conducted on RCC frame models with different structural orientation as well as on the masonry models with and without lintels.

Chapter 8 looks at the structural integrity of common type buildings as well as towers, frames, and bridges using the natural frequency characteristics of structures. Site visits are conducted in Japan, Turkey, Nepal and Afghanistan and vibration data analyzed. Model tests are also conducted on tower, frame, frame building using four different vibration methods. The response of actual wooden buildings, reinforced concrete, masonry buildings and bridges are also discussed.

Chapter 9 presents proposals and recommendations to increase seismic resistance of common type buildings, modification in construction techniques and general remarks. Seismic risk zoning, strong motion zoning, seismic design spectra and some applicable retrofitting methods for the possible and necessary upgrading of the existing structures are discussed.

Chapter 10 presents the summary and conclusions of this work as well as the limitations and future research scope.

CHAPTER 2   TECTONICS AND SEISMICITY

2.1 General

Ground shake, landslide and many other earthquake-induced events are threatening live and infrastructure in Afghanistan. Obviously, the high-magnitude earthquakes result in much higher damage worldwide; however, in Afghanistan deep and intermediate shallow earthquakes cause considerable fatality and destruction. NE and SE parts of the country are highly aseismic where most of the damage is caused not only by the strong ground motion and surface rupture, but also from liquefaction and extensive and successive landslides (Benz, et al., 2005). The history of destructive earthquakes in Afghanistan goes back to more than four thousand years (Boyd, et al., 2007). Decades of violence and strife have left the country with few scientists and limited resources to address geo-hazard. At least, 609 landslide sites near the lifelines are only identified in Badakhshan province where landslides usually take lives and hide villages under earth (Zhang, et al., 2015).

Enough details about the rates and directions of faults characteristics are not known as in last few years only one GPS station is installed in the country; however, based on the studies of faults elsewhere in the world (the San Andreas fault in the western U.S., the Wasatch fault, Utah and Karakoram fault of western China) that are in similar geologic and climatic settings as Afghanistan, the faults in Afghanistan probably have slip rates on the order of 10mm/year, (Ruleman, et al., 2007).

The surviving macro-seismic data of Afghanistan region appears to be incomplete making it difficult to give a clear guide about Afghanistan's seismicity. Afghanistan is laced with faults (Wheeler, et al., 2005) and seismicity is distributed over a broader area which make it problematic to associate them with the activity of certain faults or inactivity of others (Prevot, et al., 1980). The pre-21st century earthquake hazard and risk zoning literature provide somewhat a biased geographic view of Afghanistan's seismicity. Historical earthquakes, particularly the earlier ones have been assigned by different authors' widely different locations, magnitudes and depths most of which provide circumstantial, telegraphic and occasionally misleading information (Ambraseys & Bilham, 2003). There are regions that are currently seismically quiescent also indicated in most of the previous seismicity maps inactive, but occurrence of earthquakes has been reported in the only surviving historical earthquake catalogue. Afghanistan has earthquakes as high as $M_w7.4$ in the North, $M_w7.7$ in the NE, $M_w7.7$ in the SE borders with Pakistan, and $M_w7.0$ in the West side borders with Iran. The death toll and damage from the earthquakes in the last 20 years inside and near

Afghanistan borders is an alarm for earthquake preparedness and precautions, particularly against future large earthquakes close to the population centers and infrastructures.

2.2 Tectonic Setting

Afghanistan is located in the Eurasian orogenic belt, Figure 2.1, one of the two most seismically active belts in the world. Modern fault movements, deformations, and earthquakes in Afghanistan are driven by the northward subduction of Indian plate beneath Eurasia plate, Figure 2.2. These movements cause moderate-to-large magnitude, potentially damaging earthquakes in the Afghanistan region. These earthquakes will likely cause serious damage, not only from strong ground shaking and faults rupturing the ground surfaces, but also from liquefaction and extensive land sliding as occurred during the devastating 2005 M7.6 Kashmir earthquake (Harp & Crone, 2006).
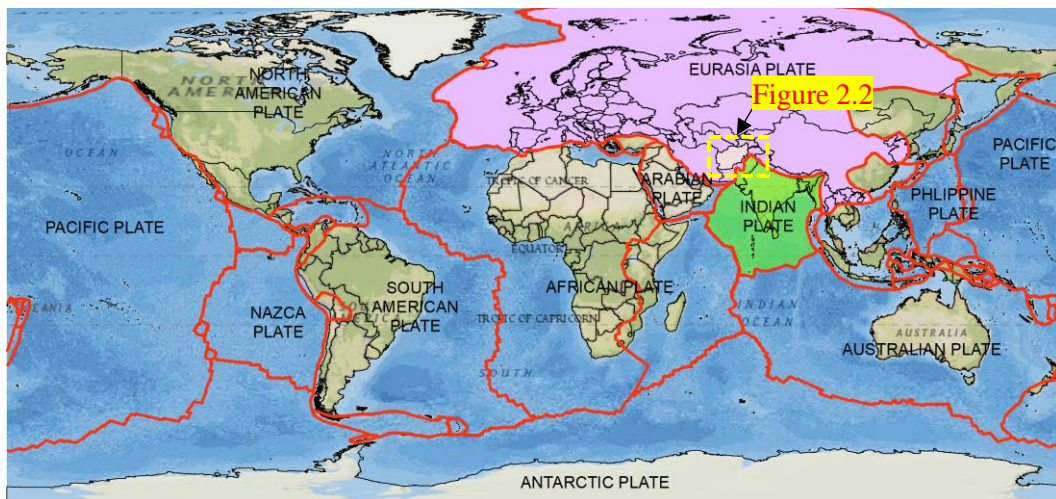
Figure 2.1 Tectonic plate, global faults and location of Afghanistan.
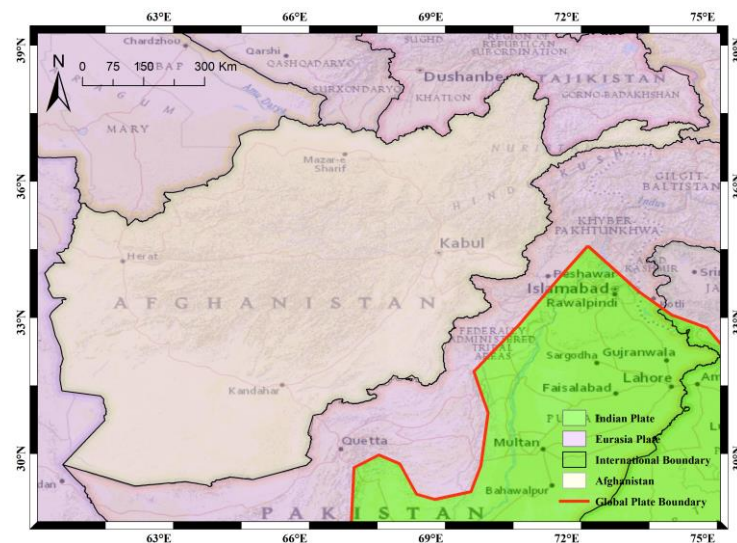
Figure 2.2 Location of Afghanistan and Eurasia-Indian global plates' boundary.

7

The active faults in Afghanistan are divided into 3 fault systems: namely, Chaman, Hari-rud and Central Badakhshan fault systems. In the southeastern Afghanistan and adjacent Pakistan, the Chaman fault system accommodates much of the differential movements between the Indian and Eurasian plates. The main Chaman fault has a reported slip rate of 2-20mm/year and higher where it enters western Pakistan (Lawrence, et al., 1992). The Indian plate has a 20-40mm/year velocity where it comes close to a 300-400 km segment of Chaman fault between (31°N-33.5°N), suggesting that M>7.0 could occur at 200 years interval along this segment. This segment of Chaman fault is silent both historically and in the record of recent seismicity making it similar to the Balakot Bagh (B-B) fault of Pakistan where the 2005 M7.6 Kashmir earthquake occurred remarking that similar earthquakes may occur and may have consequent results particularly it occur near Kabul and other lifelines along the fault. Scarps are present on piedmont and valley alluvium and vary from east- and west-facing, arcuate discontinuous scarps to northeast-and northwest-trending lineaments which shows to be active thrust and tear faults that have developed as a result of northwest-southeast-directed compression (Bernard, et al., 2000). In the eastern Afghanistan, there is a high level of scattered seismicity over a broad area. The activity is not concentrated on well-defined faults, nor does it define new faults (Prevot, et al., 1980). In central Afghanistan, the Hari-rud fault extends from north of Kabul westward to Iran border with a slip rate of 2mm/year, but evidence for active faulting remain controversial, and in northern Afghanistan, for central Badakshan fault in Pamir and Hindu Kush, slip rate is not known; however, a slip rate of 12mm/year is assigned by (Boyd, et al., 2007). The Darvoz fault in NE Afghanistan extends to Tajikistan with a slip rate of 7mm/year, Figure 2.3.
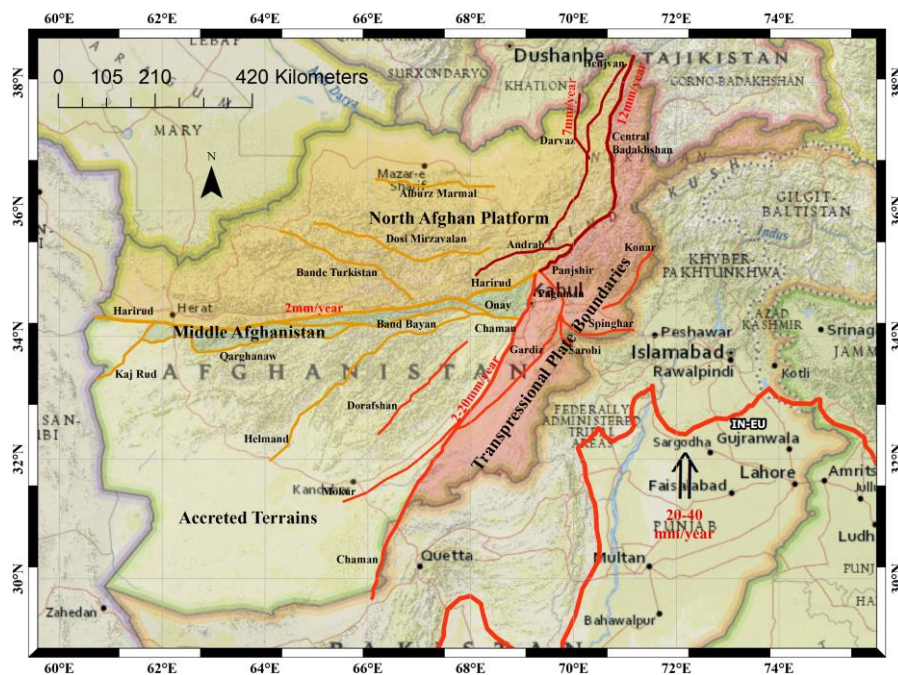
Figure 2.3 Three main fault systems and seismotectonic division of Afghanistan

2.2.1 Pamir and Hindu Kush

Pamir and Hindu Kush of Afghanistan is one of the few places in the world where continental earthquakes as deep as 300 km usually take place. Kabul is located in about 300 km distance from Hindu Kush; however, earthquakes in Hindu Kush induce powerful shocks in the nearby metropolitan city of Kabul, Figure 2.4. The tectonic setting of Afghanistan involves fundamentally the northward motion of the Indian plate sub-ducting beneath Eurasia plate in the Tibet. Movement of the Indian plate is accommodated in Afghanistan and Pakistan by the Chaman fault through mainly sinistral faulting. However, the tectonic setting is more complex in the vicinities of Hindu Kush mountains. Figure 2.5 shows a cross-section depicting the subduction of the Indian plate beneath the Eurasia plate in the vicinity of the Hindu Kush mountains. It is noted that the Indian plate is steeply bended, and it is probably in the process of detachment and sinking into the upper mantle, which would affect the seismicity of the region for decades from now on.
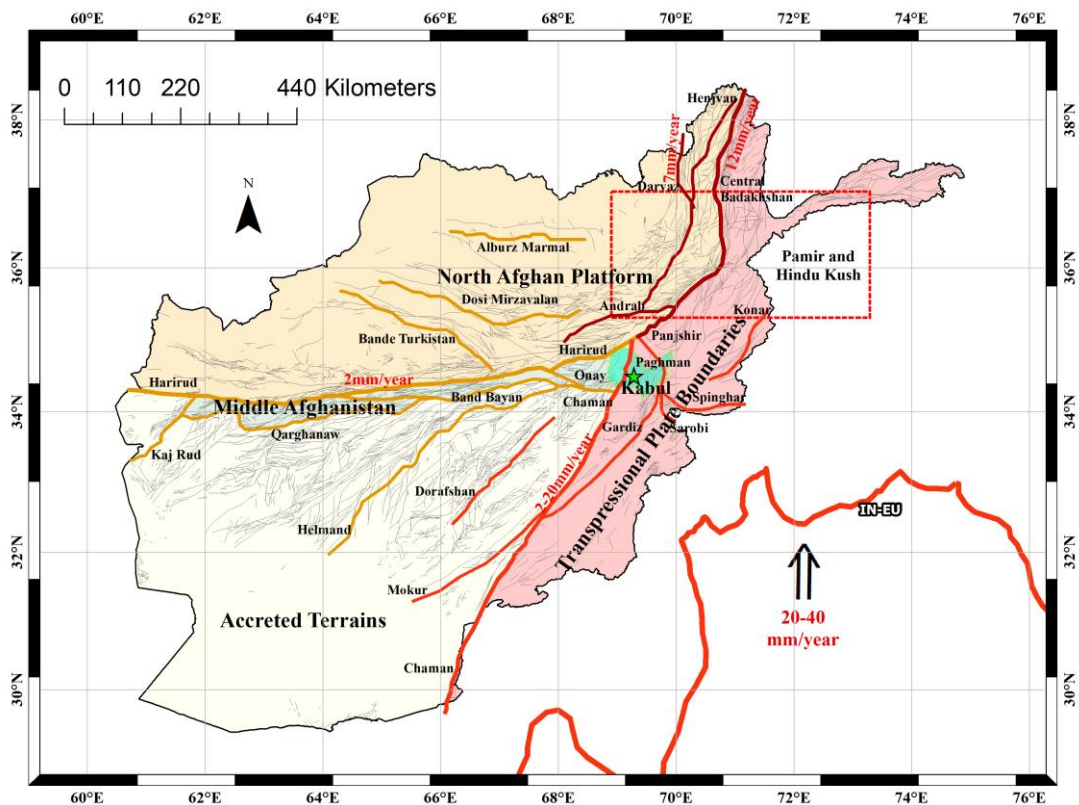
Figure 2.4 Active faults in Afghanistan, location of Kabul, Pamir and Hindu Kush. The lines in grey are the many seismically unidentified faults. Faults modified from (Wheeler, et al., 2005).
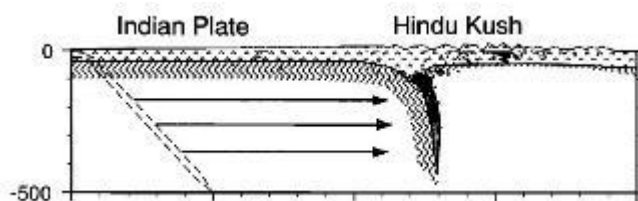
Figure 2.5 Illustration of subduction of Indian Plate beneath Hindu-Kush mountains. Modified from (Pavlis & Das, 2000).

2.3 Seismicity

To evaluate the seismicity of a region, earthquake catalogues play an important role. Recurrence interval of the big earthquakes are more than thousand years. Although there are many international organizations that operate over a long period of time; however, the historical earthquake record is a major problem for many regions in the world, particularly Afghanistan region. The historical earthquakes for Afghanistan region have been reported by different authors with different depth, magnitude, casualties, damage, etc. implying the inaccuracy and incompleteness of the record, (Ambraseys & Bilham, 2003). The incompleteness of the surviving macro-seismic data of Afghanistan region makes it difficult to give a clear guide about seismicity of this region.

2.3.1 Earthquake Zoning and Earthquake Risk Maps

There are several earthquake zoning and earthquake risk maps used by different organizations in Afghanistan. The map developed by Stenz (1945) is probably the first strong earthquake zoning map for Afghanistan, Figure 2.6. This is some other maps have been referred to in the manual of the Ministry of Education (MoE) as a reference for construction of school building as well as in the manual of Ministry of Housing and Urban Development (MHUD) for construction of structures, mainly buildings. Most of those maps handwriting and provided in the form of scan copies with quite low quality. Although, the maps are prepared decades before from when the seismicity has quite changed, we digitalized them for ease of understanding and comparing with the seismicity presented in this study. The maps are presented in Figure 2.7 to Figure 2.10.
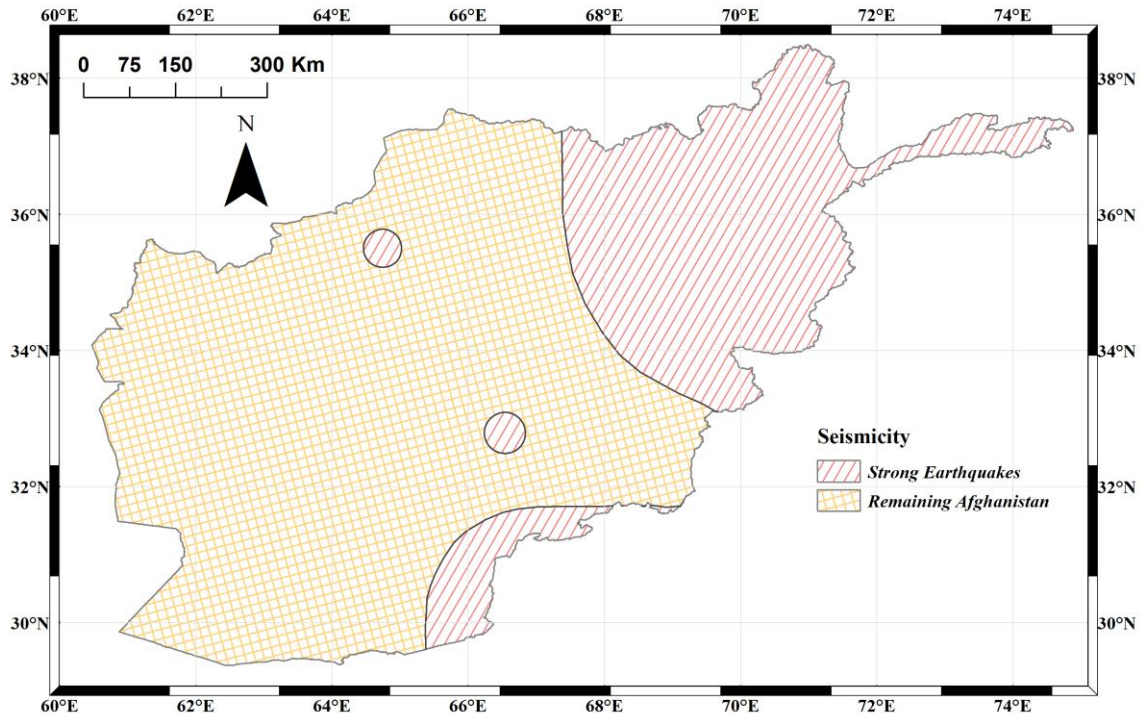
Figure 2.6 Strong Earthquakes Zoning Map, Modified from (Stenz 1945).
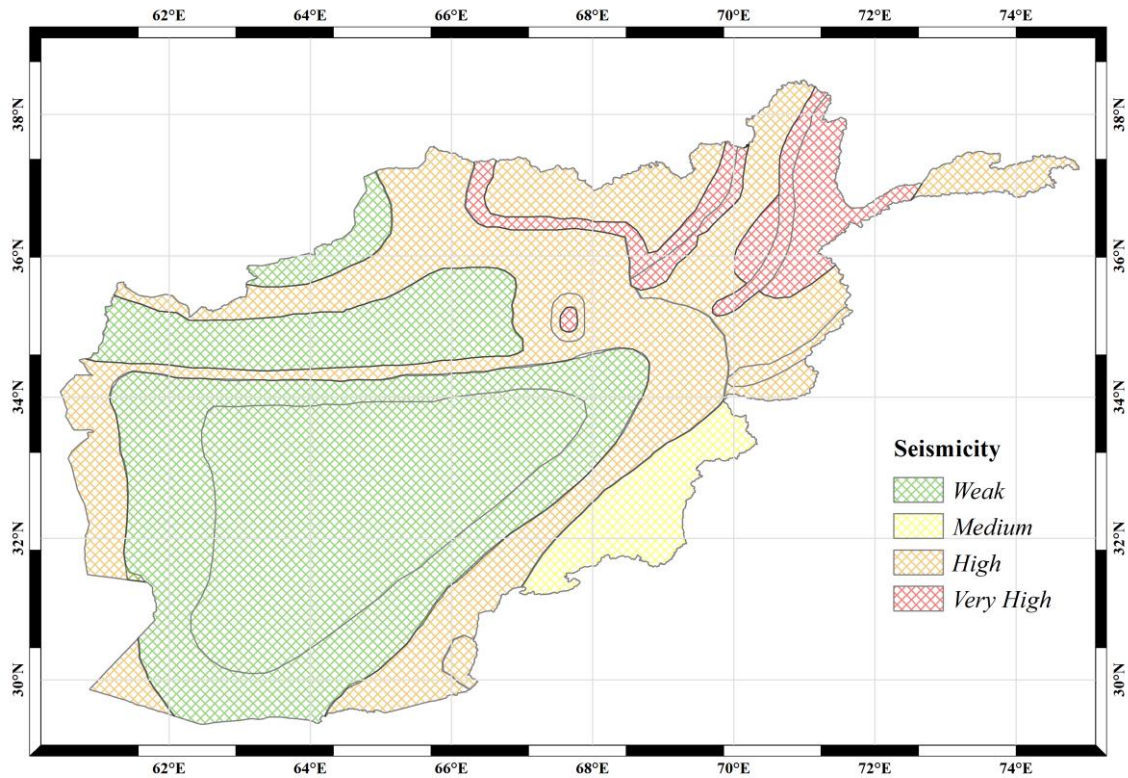
Figure 2.7 Earthquake Zoning Map, Modified from Shareq Abdullah 1993.
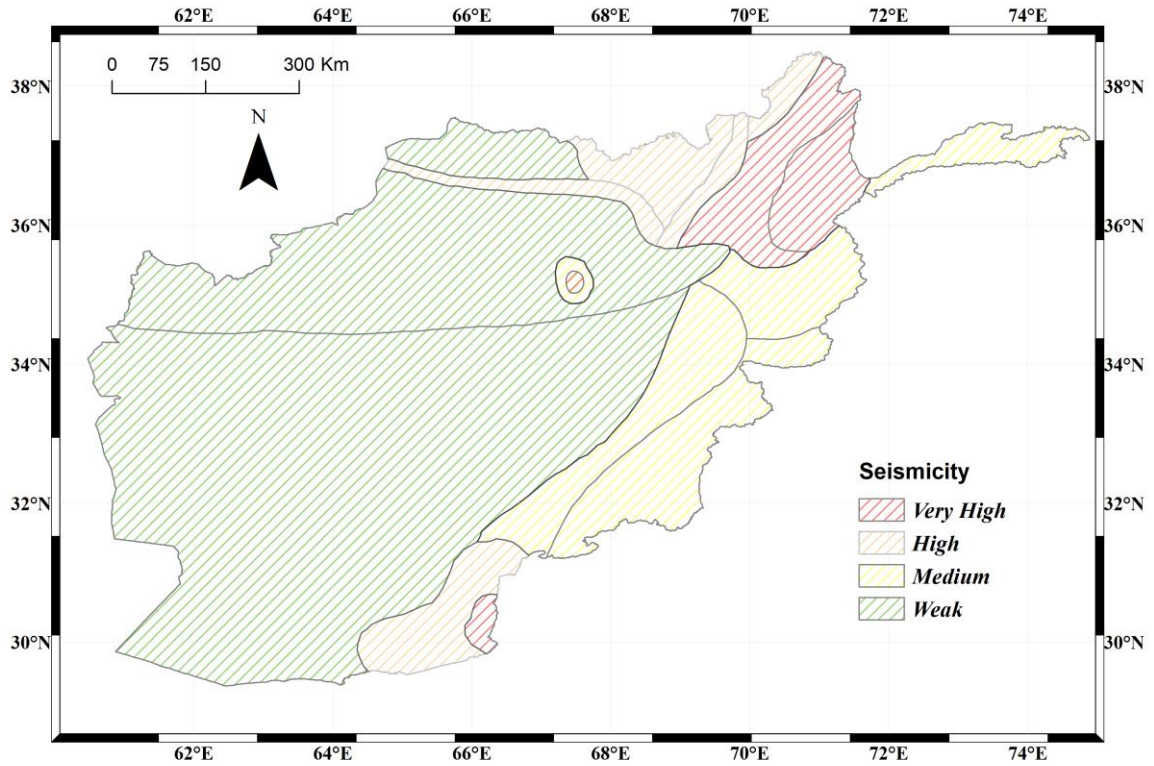
Figure 2.8 Earthquake Zoning Map, Modified from Shareq Abdullah 1981.
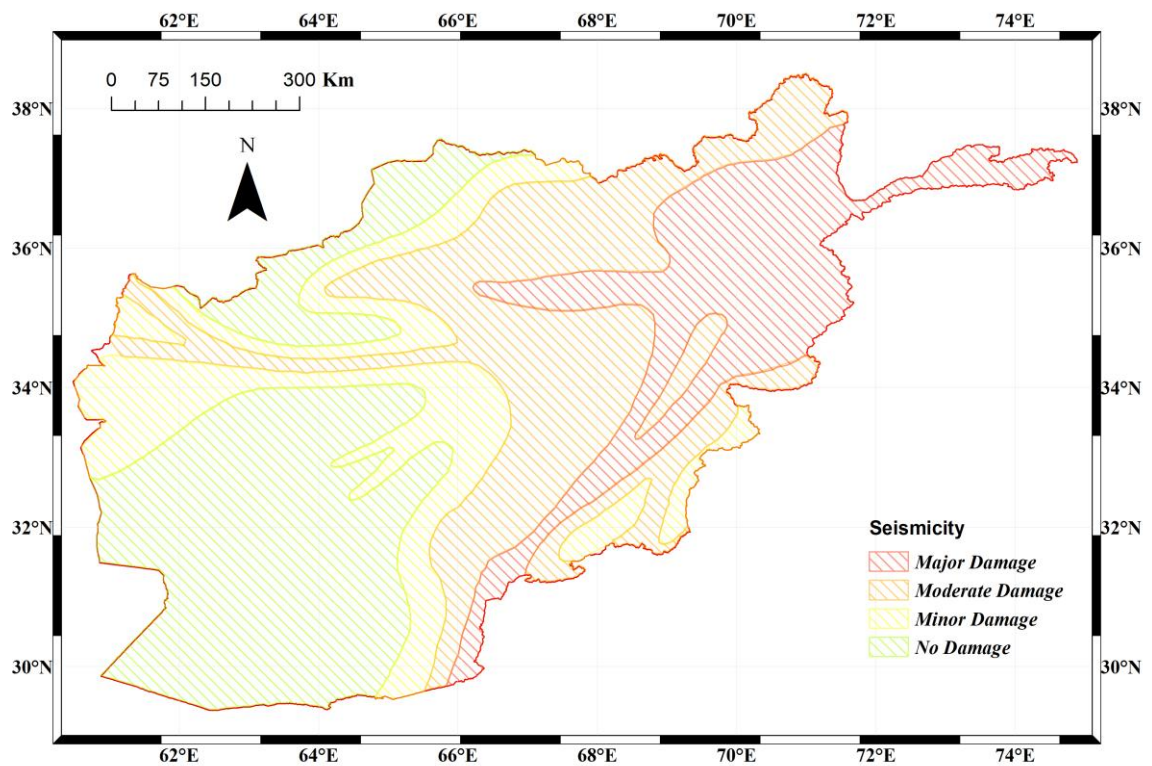
Figure 2.9 Earthquake Zoning Map used in MoE manual used for construction of school Modified from Heuckroth & Karim, 1970.
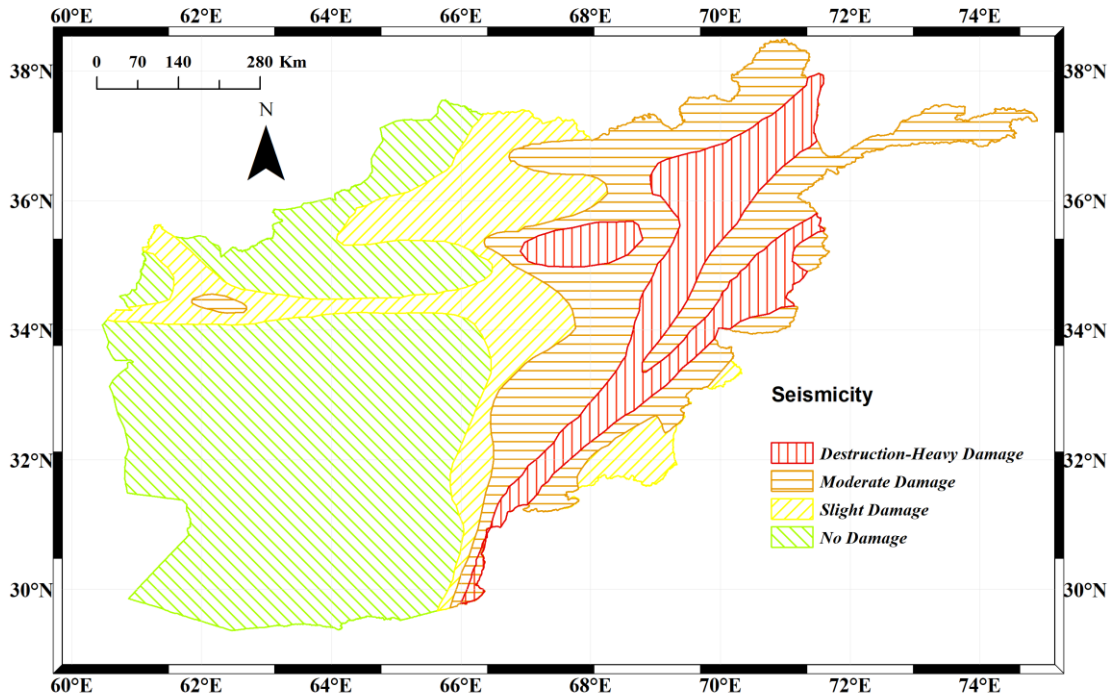
Figure 2.10 Earthquake Zoning used in the Ministry of Housing and Urban Development referred for construction of buildings in their construction manual, Modified from (MUDH, 2003).

2.3.2   Past Large Earthquakes

Several $M_w{\geq}7.0$ earthquakes have occurred within 300 km or more of Hindu Kush area and in Mazar-e-Sharif, Figure 2.11. The most recent being a $M_w7.6$ on 26 October 2015 that killed about 400 people. Another earthquake in this region occurred in 2002 just 20 km to the west of the 26 October 2015 event, and with a similar depth and thrust fault orientation (Hayes, 2017). The 2002 event caused more than 150 fatalities and the damage or destruction of over 400 houses in relation to an associated landslide. A $M_w7.4$ event in December 1983 at a similar depth just 8 km to the south of the October 26, 2015 earthquake resulted in 26 fatalities, hundreds of injuries and extensive damage in the region. The deadliest recent event ($M_w7.5$) in the region occurred 330 km to the southeast of the 26 October 2015 earthquake in the Kashmir region of Pakistan on October 8, 2005. This event killed about 86,000 people and caused extensive damage. The 2005 Kashmir earthquake was a shallow event (26 km) and was caused by geologic forces that are distinctly different than those driving deep earthquakes in the Hindu Kush region. An event of $M_w7.0$ in 819 in Faryab and $M_w7.0$ in 1505 in Kabul both with unidentified depths but less then 40km has been reported in the historical catalogue of (Ambraseys & Bilham, 2003), and $M_w7.0$ in 1842 in Konar, and $M_w7.0$ 1956 in Bamiyan are reported in instrumental earthquake catalogues (ISC, 2016) and (USGS). All these earthquakes caused considerable damage and fatalities. The impact of these earthquakes is explained in Table 2.1.
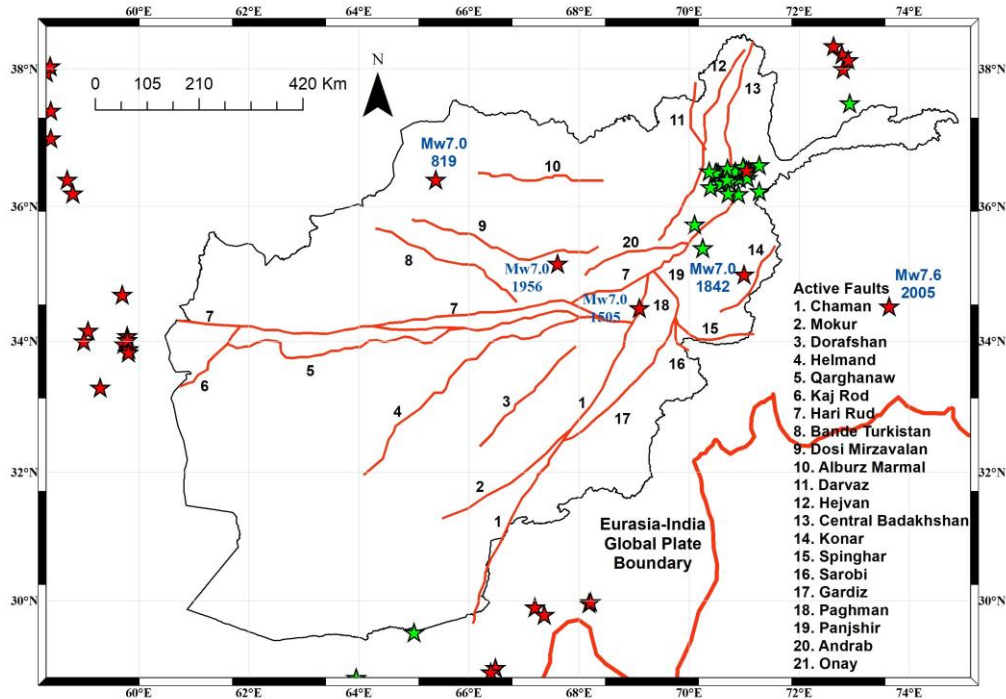
Figure 2.11 Distribution of past large earthquakes (Mw≥7.0 and active faults in Afghanistan. Red stars are shallow earthquakes and green stars are deep earthquakes.

2.3.3 Earthquake Catalogue

Past earthquakes are one of the main elements while it comes to the seismicity evaluation of a region. For the seismicity of the Afghanistan region, we retrieved data from two international earthquake catalogues for instrumental earthquakes that are operating in the world for a long time. The record for historical earthquakes is a challenging problem not only in Afghanistan region but almost all over the world; namely, International Seismological Center (ISC, 2016) and United States Geological Survey (USGS). The historical earthquake catalogue for Afghanistan is also very incomplete. The first earthquake occurred in Afghanistan is reported to be in the year 734. Most of the historical earthquake have been retrieved from books, journals and reports of the travelers which make the events inaccurate. Following we have discussed the historical as well as the instrumental earthquake catalogues for Afghanistan region. The catalogues include earthquakes of a broader area bounded by 27.0≤Latitude≤39.5, 58.5≤Longitude≤75.0, and M≥4.0.

2.3.3.1 *Historical Earthquake Catalogue*

The earthquakes before the instrumental era for Afghanistan region have been documented by (Ambraseys & Bilham, 2003). This document is the only surviving historical earthquake catalogue for Afghanistan region. The first event reported on it is in the year 734 and it contains about 45 events until 1980 where the first modern seismograph was developed by John Milne. Although this number of events in the historical era is good comparing to the historical earthquake catalogues of

other countries, however, it is quite negligible when it comes to the instrumental era in hundred to thousand earthquakes are reported only in a century. For most of these events the earthquake characteristics are unknown. It has been calculated by different authors which are again providing somewhat a biased information about the characteristics of these events. The depth for most of these earthquakes have been reported to be less than 40 km falling into shallow earthquake category. And for most of them the magnitude is also unknown. For those provided, they have been assigned based on the extent of severity of the reports and magazines available at that time. The catalogue also contains the instrumental events until 2002. A total number of 1312 of earthquakes are reported comprising from 46 historical and the 1266 instrumental events. Distribution of the earthquakes in the region is presented in Figure 2.14.
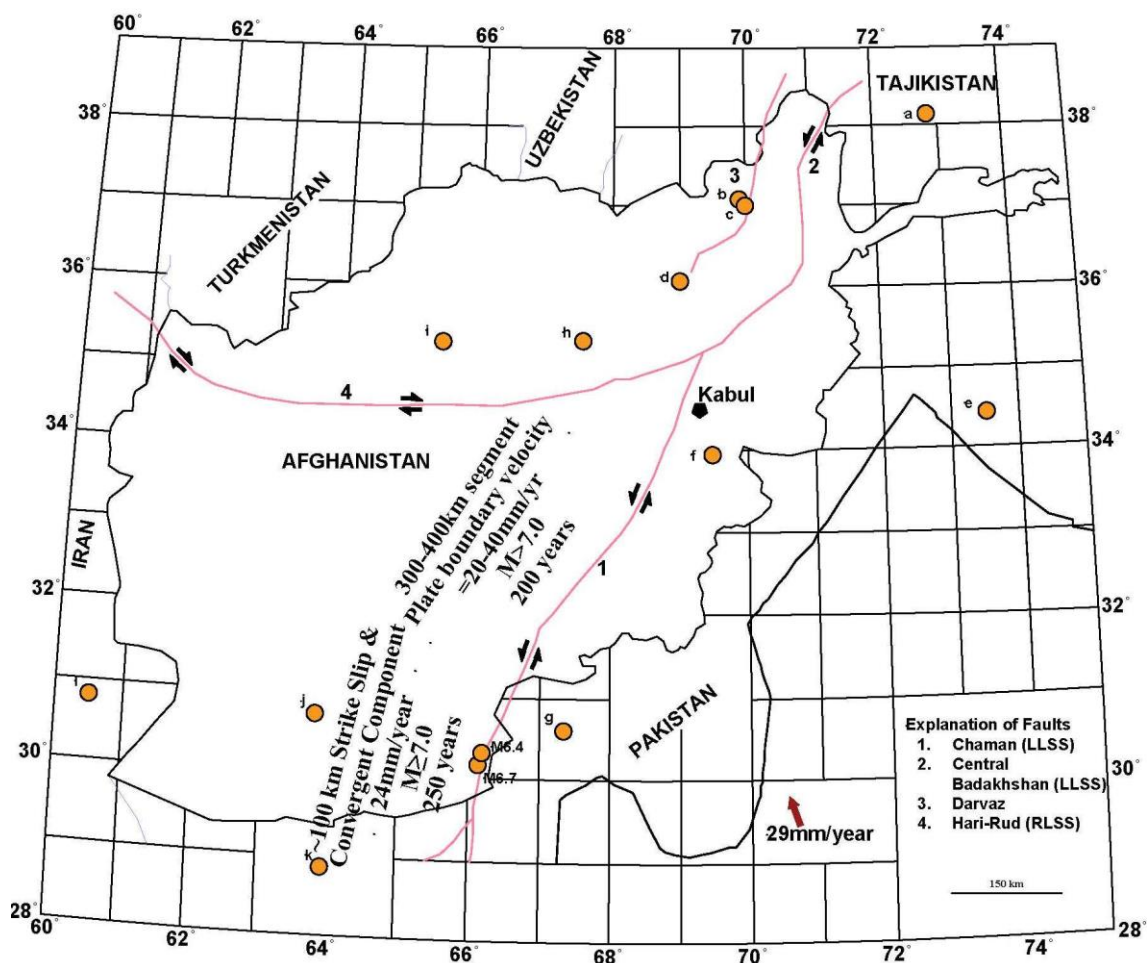
Figure 2.12 Location of big earthquakes in Afghanistan

Table 2.1 Significant Afghan Historical and Instrumental Earthquakes (819-2015)[1]

Year	M$_w$	Estimated Depth (km)	Lat.	Lon.	Description
819	7.3	<40	36.4	65.4	This earthquake in northern Afghanistan destroyed a quarter of Balkh city, and ruined the masjid-i-jami. Sidreh desert (36.75N, 66.22E) was flooded by an excessive rise of the water table and turned the area into a fertile land. It damaged many tens of kilometers to the west which is considered unlikely.
1102	5.6	<40	34.4	62.2	These are the 2nd and 3rd destructive earthquakes in Herat each of which ruined most of the buildings in the city, particularly the tall structures with casualties in the city. The masjid-e-jami in the city which was repaired after 2nd earthquake was again damaged.
1364	5.9	<40	34.4	61.7	
1505	7.2	<40	34.5	69.1	This earthquake ruined the ramparts of the fort, even the walls of gardens in Kabul. All houses in Paghman were destroyed and 70-80 people died. Most of the houses in Tipa (34.68°N, 69.01°E) were leveled with ground. Accounts suggest this earthquake occurred on Paghman fault, with at least 40 km of surface rupture of the fault, and vertical offsets up to 3meter.
1832	7.3	<40	36.7	69.9	This earthquake centered in Badakhshan province. It destroyed most of the nearby villages killing thousands of people and was strongly felt in Kabul and Lahore. Half the population of the nearby villages (156 person) were killed. This earthquake has been interpreted by Russian researchers as a sub-crustal event of focal depth of 180km, consistent with depth of recent large events in the region. The aftershocks triggered numerous landslides and rock falls that blocked valleys in Badakhshan, a rather unusual characteristics of deep earthquakes.
1842	7.4	<40	35	71	This strong prostrated everyone. The collapse of tall houses choked the streets leaving no room for escape. Few local inhabitants were killed as well as 4 British men were killed in a British garrison. Along the Kabul river, the ground opened in several places and water appeared on the surface. Several hundreds of people were killed in Laghman and Kunar. Landslides and rock falls triggered from hills in the Kunar valley. The shock destroyed one tenth of adobe houses in Peshawar killing 40-50 people. At an epicentral distance of 410km, the shock was strong enough to be mentioned

[1]The information in this table is derived from tables 1 and 2 and the Electronic Supplement of Ambraseys and Bilham (2003), Boyd and others (2007) and UNISDR DRR sitrep (2015).

					in official dispatches. The large number of aftershocks and the prolonged duration of the aftershock sequence which extended for months, suggest a crustal event.
1874	6.9	<40	35.1	69.2	This earthquake occurred near north terminus of Paghman fault where the ground opened, presumably due to liquefaction, in the vicinities of Jabal Saraj (35.13N, 69.24E). It caused causalities in villages ~ 70km north of Kabul.
1892	6.5	<40	30.9	66.5	This earthquake occurred near the Afg-Pak border and caused considerable deformation of the newly laid railroad crossing Chaman fault.
1909	7.0 6.0	<40	36.5	70.5	Double shocks: shallow and deep earthquakes centered in Badakhshan. The damage in Badakhshan, Konar and some parts of Pakistan were considerable.
1911	7.6	26	36.5	66.5	This large earthquake occurred in northern Afghanistan, followed four hours later by an aftershock of Ms=6.5, and caused collapse of hundreds of houses and killing of hundreds of people in the mountains north of Kabul.
1935	7.7	33	28.9	66.5	This earthquake occurred near the SE border of Afghanistan and was the largest with fatalities in the last two centuries in the Indian plate or its boundaries. In addition to the town of Quetta and Mustung, at least 100 villages in Quetta subdivision and Kalat State were destroyed. None of the local could recall any similar event in the past. Altogether, the earthquake could have killed 35,000, consisting of 26,000 in Quetta and 9000 of other areas people but reliable figures are lacking.
1956	7.3	33	35.2	67.7	This earthquake was centered in Bamyan and killed fewer than 70 people. The shock caused landslides and rock falls. An estimated 100,000 cubic meters of limestone and marls slid down holding back 8 million cubic meter of water for four days. After sweeping away of the flood, it drowned 350 people.
1982	6.5	36	36.1	69	This earthquake destroyed 7,000 houses, killed 450 people and injured more than 3,000 in Baghlan province.
1998	5.9		37.1	69.8	This destructive earthquake was centered in Rustaq of Badakhshan, northeast of Afghanistan. It killed about 2,300 people, injured 800 and destroyed about 8,100 houses and making 8,000 homeless. The shock triggered extensive landslides adding to the damage and killing more than 6,000 livestock.
1998	6.5	29	37.1	69.8	Main shock of Feb. 4 earthquake, killed about 4,000 people injuring many thousands in Badakhshan and Takhar.

2002	7.2	195	36.5	70.5	Earthquake in Hindu Kush region caused damage and fatalities. Six fatalities were noted in Kabul and extensive damage in few villages. USGS notes 13 fatalities in Kabul and Rostaq, and 150 people killed by landslide.
2002	6.0	10	35.94	69.31	A series of shallow earthquakes hit Nahrin village of Baghlan province. The shock resulted in approximately 1,200 deaths.
	5.4	10	36.0	69.27	
	5.9	10	35.91	69.23	
2012	5.4,	50	36	69.3	Successive earthquakes occurred in North Afghanistan and caused landslide burying town of Sayi Hazara, Burka district of Baghlan province, killing 71 people.
	5.7	16			
2015	7.5	210	36.4	70.7	This earthquake centered in Hindu Kush near Badakhshan province of Afghanistan. This 212km deep earthquake killed 115 people in Afghanistan, 267 people in Pakistan and injured 538 and 1856 in Afghanistan and Pakistan respectively. The earthquake damaged a total of 11, 389 houses in Pakistan.

2.3.3.2   *Focal Mechanisms*

The focal mechanism for the large earthquake in Afghanistan is provided in Figure 2.12 and Figure 2.13. From the focal mechanisms, it is noted that most of the faults in NW and SW have a strike slip movement. The main Chaman fault is a strike slip fault with a slight thrust fault
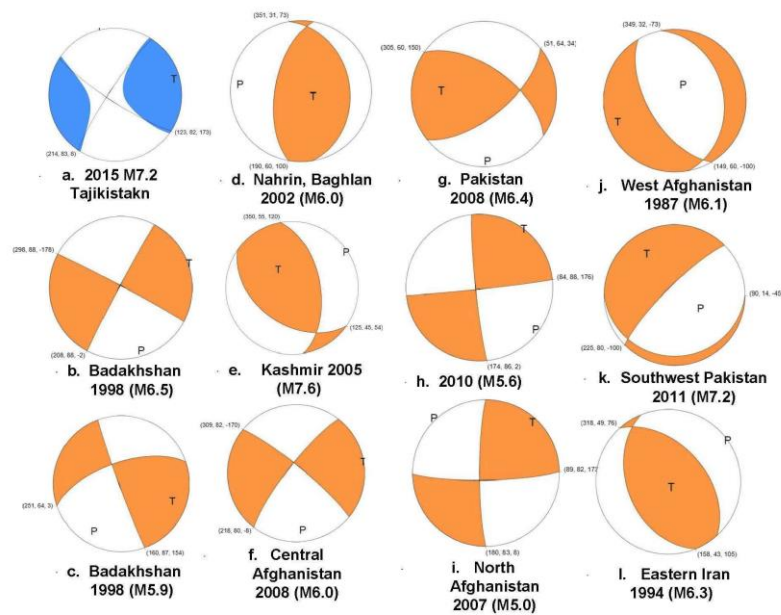
Figure 2.13 Focal mechanisms for the earthquakes with
considerable impact on life and infrastructure

component at the Northern end when it connects the Hari-rud fault. Hari-rud fault itself and its components are also strike slip faults. The faults in the Northern-east part of Afghanistan are mainly thrust faulting. The Darvaz fault, Central Badakhshan fault and their components are mainly thrust faulting as it is also noted from the movement of Eurasia-India plate movement.

2.3.3.3 *Instrumental Earthquake Catalogue*

The International Seismological Centre earthquake catalogue is the most complete one for the region of study of this work. It contains about 26212 events with complete earthquake characteristics. For most of the events, the characteristics have been reported by several authors. Some of the events have been reported by Moment Magnitude (M$_w$). Events have also been
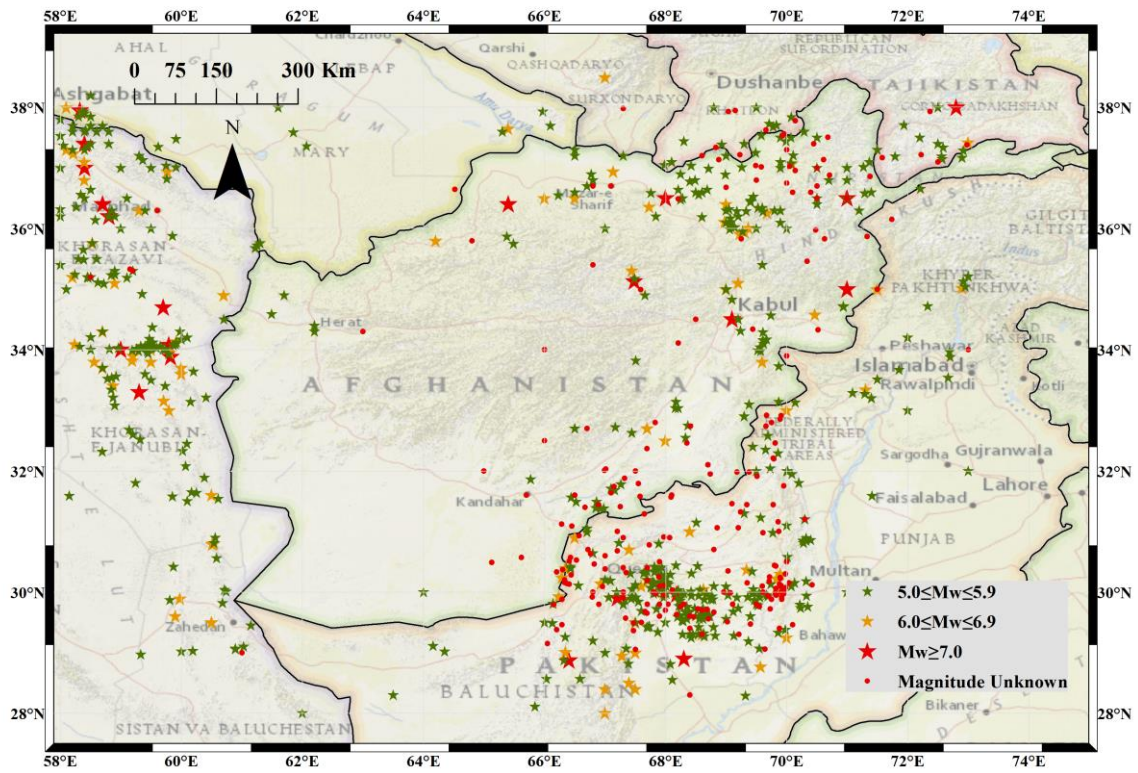
Figure 2.14 Distribution of the historical and instrumental earthquakes between 734-2002, in Afghanistan region from catalogue of (Ambraseys & Bilham, 2003).

reported by Body Wave Magnitude mb, Surface Wave Magnitude M$_S$ and Local Magnitudes M$_L$. We used the relationships of (Scordilis, 2006) to convert the M$_S$ and mb to M$_w$ using equations, *1, 2* and *3*. We also used the relationship of (Zare, 2014) to convert M$_L$ to M$_w$ using equation *4* to create a homogenized earthquake catalogue, Distribution of the ISC catalogues is presented in

$$M_W = 0.67 M_S + 2.07 \qquad\qquad (1)$$
$$3.0 \leq M_S \leq 6.1$$
$$M_W = 0.99 M_S + 0.08 \qquad\qquad (2)$$
$$6.2 \leq M_S \leq 8.2$$

$$M_W = 0.85mb + 1.03 \qquad (3)$$
$$3.5 \leq mb \leq 6.2$$
$$M_W = 1.01 * M_L - 0.05 \qquad (4)$$
$$4.0 \leq M_L \leq 8.3$$
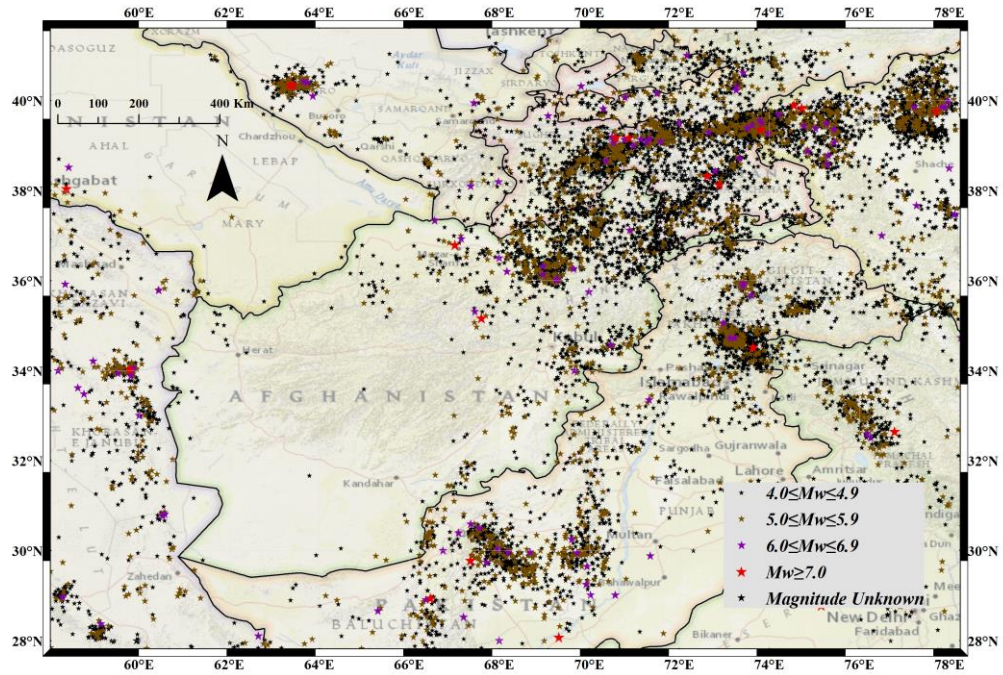
Figure 2.15 Shallow Earthquakes depth≤50 km, ISC Catalogue
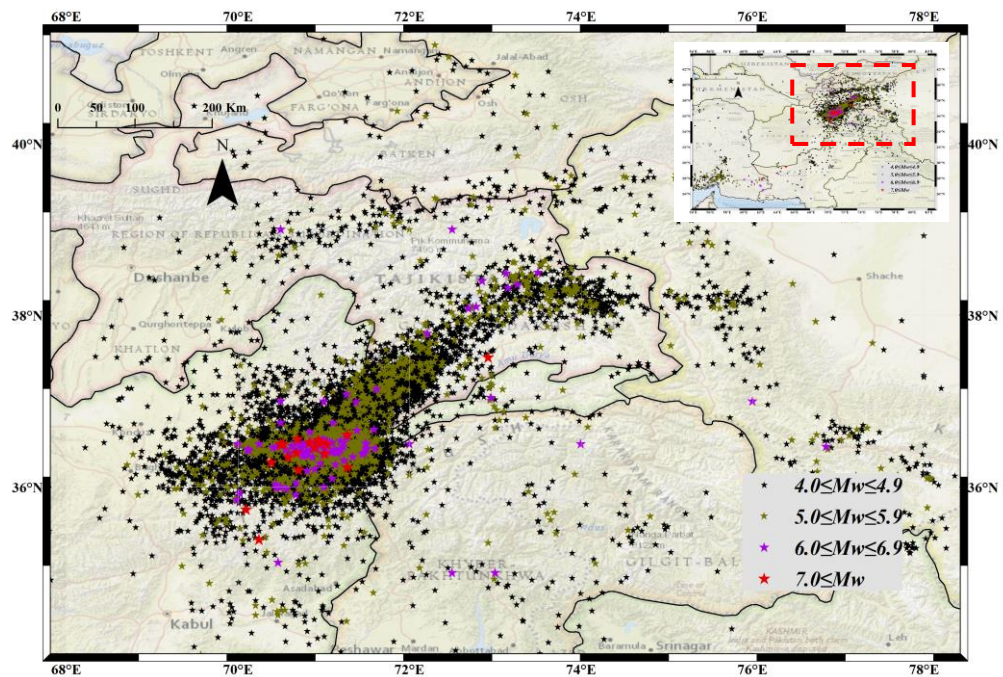
Figure 2.16 Deep Earthquakes depth>50km ISC Catalogue
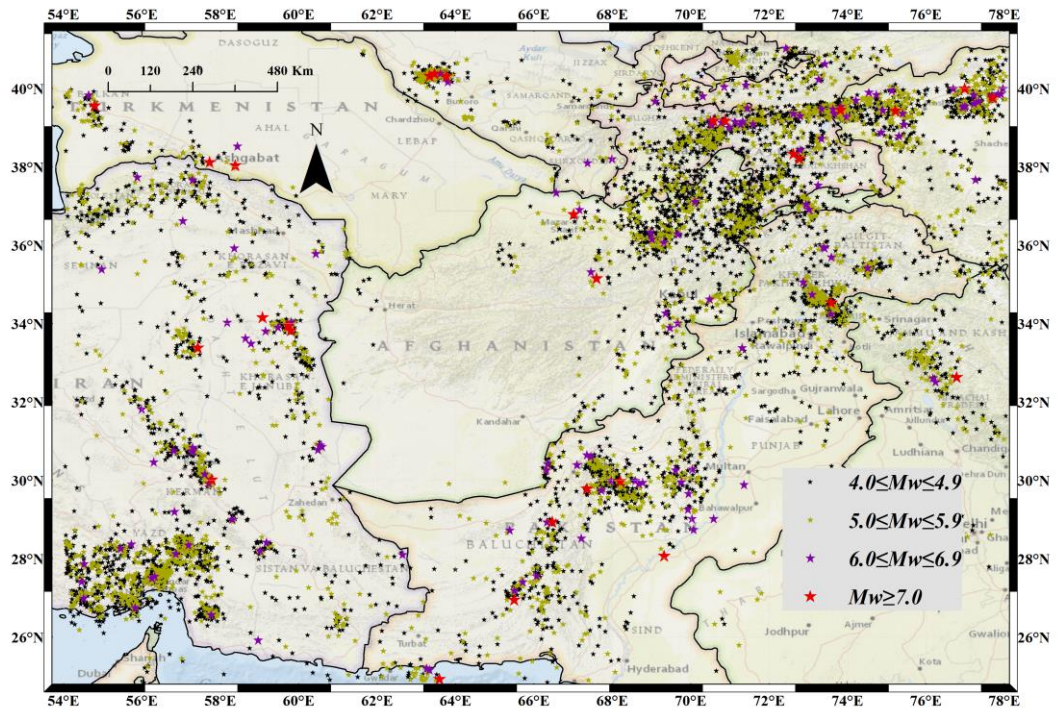
Figure 2.17 Shallow earthquakes depth≤50km USGS catalogue
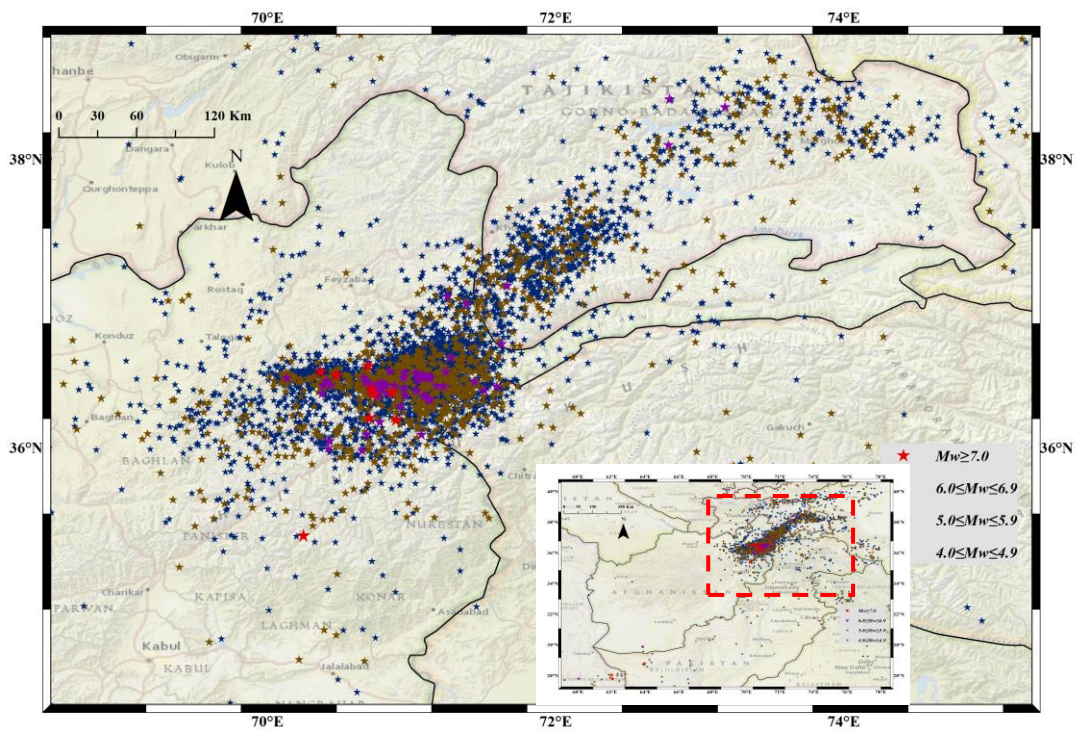
Figure 2.18 Deep earthquakes depth>50km USGS catalogue

2.3.3.4   *Combined Homogenized Earthquake Catalogue*

The catalogues for instrumental earthquakes consist of International Seismological Center (ISC, 2016) and United States Geological Survey (USGS). For the historical earthquakes, we used the only catalogue of Ambraseys and Bilham 2003. We combined the three catalogues and produced a homogenized earthquake catalogue of moment magnitude (Mw) using the equations 1-4, Figure 2.19 to Figure 2.21. The catalogue includes earthquakes of a broader area bounded by 27.0≤Latitude≤39.5, 58.5≤Longitude≤75.0, and M≥4.0. The duplicate events were removed. Many events in the homogenized catalogue are retrieved from the International Seismological Centre (ISC, 2016) and the United States Geological Survey (USGS) global catalogues.
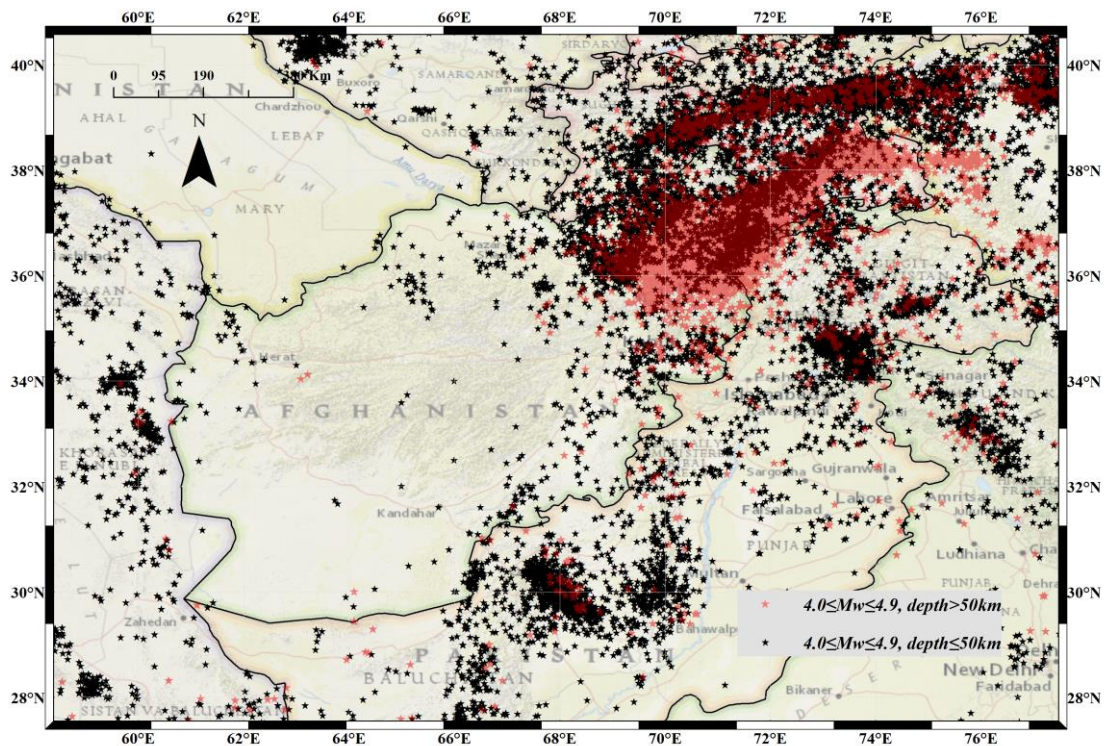
Figure 2.19 Combined catalogue, 4.0≤Mw≤4.9
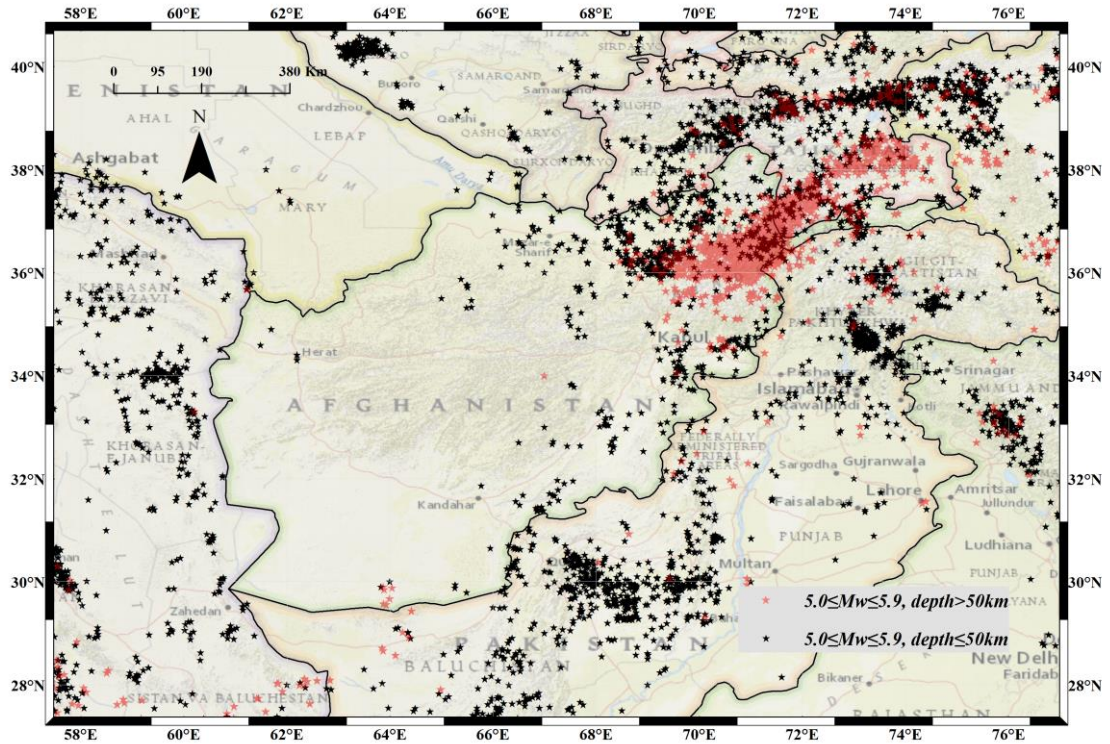
Figure 2.20 Combined Catalogue, 5.0≤Mw≤5.9
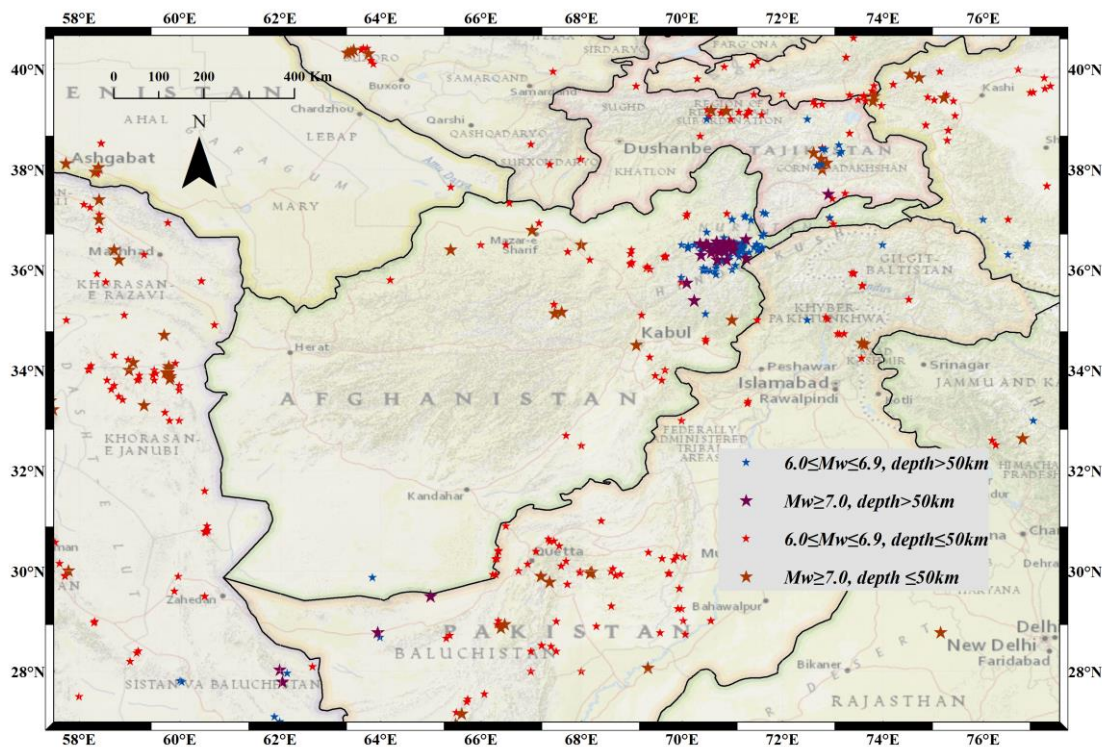
Figure 2.21 Combined Catalogue, 6.0≤Mw≤6.9 and Mw≥7.0

CHAPTER 3   CRUSTAL DEFORMATION, STRAINING AND STRESSES

3.1 Crustal Deformation Measurements by GPS

Crustal deformations worldwide are measured using Global Positioning System (GPS) worldwide. This system fundamentally based on the satellites deployed by United States of America. The Global Positioning System (GPS) consists of satellites moving around the earth at a given orbit, Figure 3.1. It is possible to compute the global position of stations which receive the signals from these orbiting satellites in space and in time. Although there are different applications of the GPS system, the GPS is also used in plate tectonics to monitor the movement of plates and internal deformations of the plates. In plate tectonics, the difference between the positions of a station at different times correspond to the motion of the plate at that station. It is generally said that at least an accurate and reliable measurement of the position of a station at a given time requires the station to be able to receive signals from 4 satellites simultaneously, Figure 3.2. The position of the station is geometrically computed from the arrival times and the position of satellites emitting signals. From this measurements it is possible to measure three components of deformation. The GPS method could be also used for earthquake prediction and a fundamental approach has been described by Aydan (Aydan, 2000; Aydan, 2013; Aydan, et al., 2011).
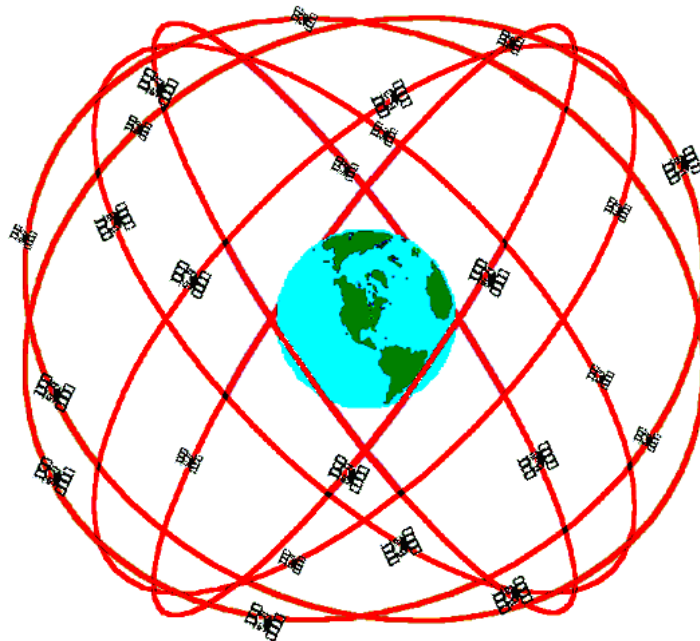
Figure 3.1 A simple illustration of Global Positioning System (GPS)
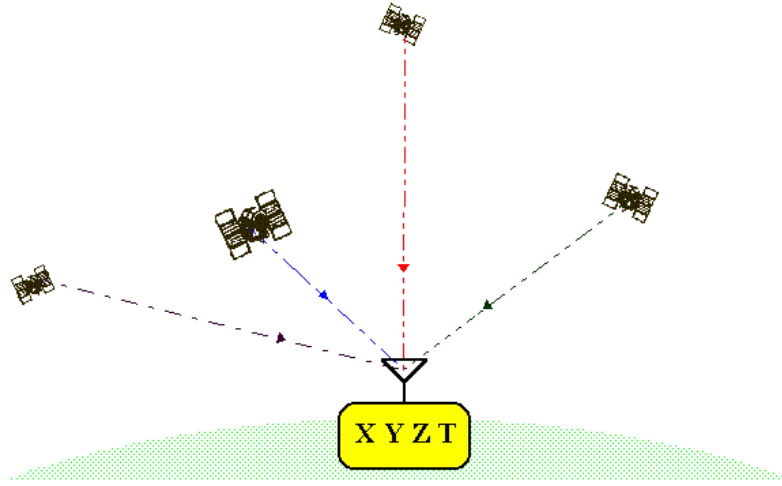
Figure 3.2 Necessary number of satellites for a reliable displacement measurement

3.2 A Method for Computing Tangential Strain and Stress Rates of the Earth's Crust

It is geometrically possible to compute strain rate components on a plane tangential to the earth's surface from the variation of positions of stations at a given time interval (Aydan, 2000; Aydan, 2003a; Aydan, 2003b; Aydan, 2006; Aydan, 2008; Aydan, 2013; Aydan, 2014). For this purpose, one may utilize a procedure used in the finite element method. The method to be presented in this section is based on such a procedure. The simplest approach for this purpose is the use of triangular elements. If the number of GPS stations are quite dense, one may also use higher order elements for computing the strain rates. In this article, triangular elements are chosen to illustrate the fundamental concept of the method since the algebra is less involved. Furthermore, one can work out the computations by manually if necessary.

The strain rate components can be related to the deformation rates through the geometrical relations as given below (Figure 3.3)

$$\dot{\varepsilon}_{xx} = \frac{\partial \dot{u}}{\partial x} ; \quad \dot{\varepsilon}_{yy} = \frac{\partial \dot{v}}{\partial y} ; \quad \dot{\gamma}_{xy} = \frac{\partial \dot{v}}{\partial x} + \frac{\partial \dot{u}}{\partial y} \qquad (3.1)$$

where $\dot{u}$ and $\dot{v}$ are displacement rates in the direction of x and y, respectively. $\dot{\varepsilon}_{xx}$ and $\dot{\varepsilon}_{yy}$ are strain rates normal to the x and y planes and $\dot{\gamma}_{xy}$ is shear strain. Let us assume that the stations of the GPS are arranged in a manner that a mesh of triangular elements are constituted. Furthermore, it is assumed that the displacement rates within a typical element is interpolated by a linear function as given below,
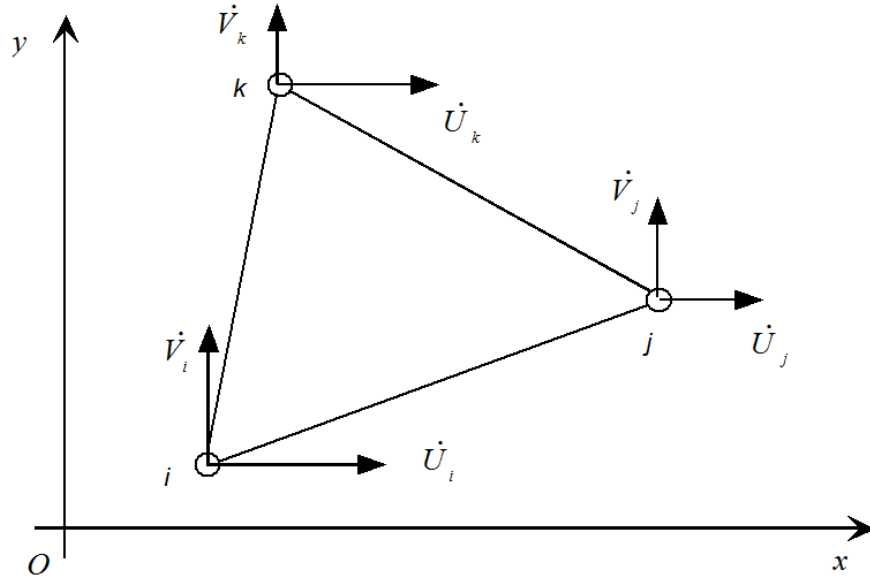
Figure 3.3 Coordinate system and the definition of displacement rates for a triangular element

$$
\left\{ \begin{matrix} \dot{u} \\ \dot{v} \end{matrix} \right\} = \begin{bmatrix} 1 & 0 & x & 0 & y & 0 \\ 0 & 1 & 0 & x & 0 & y \end{bmatrix} \left\{ \begin{matrix} a_1 \\ a_2 \\ b_1 \\ b_2 \\ c_1 \\ c_2 \end{matrix} \right\}
\tag{3.2}
$$

If one requires that displacement rates to be equivalent to those at the nodal points *i,j,k* of a typical element, one can easily obtain the following relation after some algebraic manipulations

$$
\left\{ \begin{matrix} \dot{u} \\ \dot{v} \end{matrix} \right\} = \begin{bmatrix} N_i & 0 & N_j & 0 & N_k & 0 \\ 0 & N_i & 0 & N_j & 0 & N_k \end{bmatrix} \left\{ \begin{matrix} \dot{U}_i \\ \dot{V}_i \\ \dot{U}_j \\ \dot{V}_j \\ \dot{U}_k \\ \dot{V}_k \end{matrix} \right\}
\tag{3.3}
$$

where

$$
N_i = E_{11} + E_{21}x + E_{31}y , \; N_j = E_{12} + E_{22}x + E_{32}y , \; N_k = E_{13} + E_{23}x + E_{33}y
$$

$$E_{11} = \frac{1}{\Delta}\left(x_j y_k - x_k y_j\right), \ E_{12} = \frac{1}{\Delta}\left(x_i y_k - x_k y_i\right) \ E_{13} = \frac{1}{\Delta}\left(x_j y_i - x_i y_j\right)$$

$$E_{21} = \frac{1}{\Delta}\left(y_j - y_k\right), \ E_{22} = \frac{1}{\Delta}\left(y_k - y_i\right), \ E_{23} = \frac{1}{\Delta}\left(y_i - y_j\right)$$

$$E_{31} = \frac{1}{\Delta}\left(x_k - x_j\right), \ E_{32} = \frac{1}{\Delta}\left(x_i - x_k\right), \ E_{33} = \frac{1}{\Delta}\left(x_j - x_i\right)$$

$$\Delta = \left(x_j y_k - x_k y_j\right) + \left(x_k y_i - x_i y_k\right) + \left(x_i y_j - x_j y_i\right)$$

From Eq. (3.3) and Eq. (3.1), one can easily show that the following relation holds among the components of the strain tensor and displacement rates at nodel points *i,j,k*:

$$\begin{Bmatrix} \dot{\varepsilon}_{xx} \\ \dot{\varepsilon}_{yy} \\ \dot{\gamma}_{xy} \end{Bmatrix} = \begin{bmatrix} E_{21} & 0 & E_{22} & 0 & E_{23} & 0 \\ 0 & E_{31} & 0 & E_{32} & 0 & E_{33} \\ E_{31} & E_{21} & E_{32} & E_{22} & E_{33} & E_{23} \end{bmatrix} \begin{Bmatrix} \dot{U}_i \\ \dot{V}_i \\ \dot{U}_j \\ \dot{V}_j \\ \dot{U}_k \\ \dot{V}_k \end{Bmatrix} \tag{3.4}$$

To obtain stress rates from strain rates, a physical relation called constitutive law is required. The simplest constitutive law is Hooke's law based on the concept of elasticity. The other simple constitutive laws are Newton's law for viscos materials and Kelvin's law for visco-elastic materials. In this particular application, it is assumed that Hooke's law is valid. The Hooke's law can be written in the following form

$$\begin{Bmatrix} \dot{\sigma}_{xx} \\ \dot{\sigma}_{yy} \\ \dot{\sigma}_{xy} \end{Bmatrix} = \begin{bmatrix} \lambda + 2\mu & \lambda & 0 \\ \lambda & \lambda + 2\mu & 0 \\ 0 & 0 & \mu \end{bmatrix} \begin{Bmatrix} \dot{\varepsilon}_{xx} \\ \dot{\varepsilon}_{yy} \\ \dot{\gamma}_{xy} \end{Bmatrix} \tag{3.5}$$

where λ and μ are Lame's constants. The value of Lame's constants is generally assumed to be 30 GPa (Fowler, 1990).

Aydan et al. (2000) proposed the use of maximum shear stress rate, mean stress rate and disturbing stress for identifying the potential locations of earthquakes. The maximum shear stress rate, mean stress rate and disturbing stress rate are defined below:

$$\dot{\tau}_{max} = \frac{\dot{\sigma}_1 - \dot{\sigma}_3}{2} \; ; \;\; \dot{\sigma}_m = \frac{\dot{\sigma}_1 + \dot{\sigma}_3}{2} \; ; \;\; \dot{\tau}_d = \left|\dot{\tau}_{max}\right| + \beta\dot{\sigma}_m \qquad\qquad (3.6)$$

Where β may be regarded as a friction coefficient. It should be noted that one (vertical) of the principal stress rates is neglected in the above equation since it cannot be determined from GPS measurements. The definition of disturbing stress rate is analogous to the well-known Mohr-Coulomb yield criterion in Geomechanics and Geoengineering. The concentration locations of these quantities may be interpreted as the likely locations of the earthquakes as they imply the increase in disturbing stress, Figure 3.6. If the mean stress has a tensile character and its value increases, it simply implies the reduction of resistance of the crust.

3.3   GPS Stations in Afghanistan and Its Vicinity

Compared to other countries, Afghanistan has only single GPS station located in Kabul. Aydan (2000, 2008, 2013, 2014) showed that crustal strains and stresses can be evaluated, and they may relate to seismicity of the region. However, it is almost impossible to analyze a detailed crustal strains and strains in Afghanistan. Nevertheless, the available data of GPS stations in Kabul and other GPS stations in the neighboring countries would be utilized in this section to evaluate the crustal deformation and straining in Afghanistan and its closed vicinity. Furthermore, the relations to the seismicity would be discussed.

3.3.1   GPS Stations and Deformation Rates

As pointed out previously, there is only one GPS monitoring station in Afghanistan. Table 3.1 gives the code, coordinate and annual horizontal deformation velocity of GPS stations. Figure 3.4 shows the locations of the stations and annual deformation velocities at the respective stations. The velocities given in Table 3.1 are computed with respect to that Euro-Asian plate.

Table 3.1 The code, coordinate and annual horizontal deformation velocity of GPS stations in Afghanistan and its vicinity used in this study.

Site	Lon.	Lat.	E(mm)	N(mm)	Reference
YAZT	61.034	36.601	3.14	0.91	(Masson, et al., 2007)
BAKH	60.36	35.02	0.08	-0.01	(Walpersdorf, et al., 2014)
DESL	59.297	31.96	1.33	6.24	(Walpersdorf, et al., 2014)
ZABO	61.57	31.049	1.72	0.91	(Walpersdorf, et al., 2014)
BAZM	60.18	27.865	5.22	3.77	(Walpersdorf, et al., 2014)
JASK	57.767	25.636	2.78	14.56	(Masson, et al., 2007)

Table 3.2 cont.. The code, coordinate and annual horizontal deformation velocity of GPS stations in Afghanistan and its vicinity used in this study.

Site	Lon.	Lat.	E(mm)	N(mm)	Reference
CHAB	60.694	25.3	1.14	7.96	(Masson, et al., 2007)
KCHI	67.113	24.931	5.6	28	(Mohadjer, et al., 2010)
QTAG	66.991	30.166	1.4	18.8	(Mohadjer, et al., 2010)
BAHAWALPUR	71.6833	29.4	5.04	28.6	(Walpersdorf, et al., 2014)
S2004	72.45	32.59	6.82	36.27	(Walpersdorf, et al., 2014)
RSCL	77.6	34.128	-5.7	20.3	(Mohadjer, et al., 2010)
NCEG	71.487	34.004	-0.8	29	(Mohadjer, et al., 2010)
MANM	71.68	37.542	-10.7	15.8	(Mohadjer, et al., 2010)
GARM	70.317	39.006	-1.2	2.4	(Mohadjer, et al., 2010)
SHTZ	68.123	37.562	22.7	3.9	(Mohadjer, et al., 2010)
KIT3	66.885	39.135	0.1	-1.4	(Mohadjer, et al., 2010)
KBUL	69.13	34.574	-0.1	10	(Mohadjer, et al., 2010)
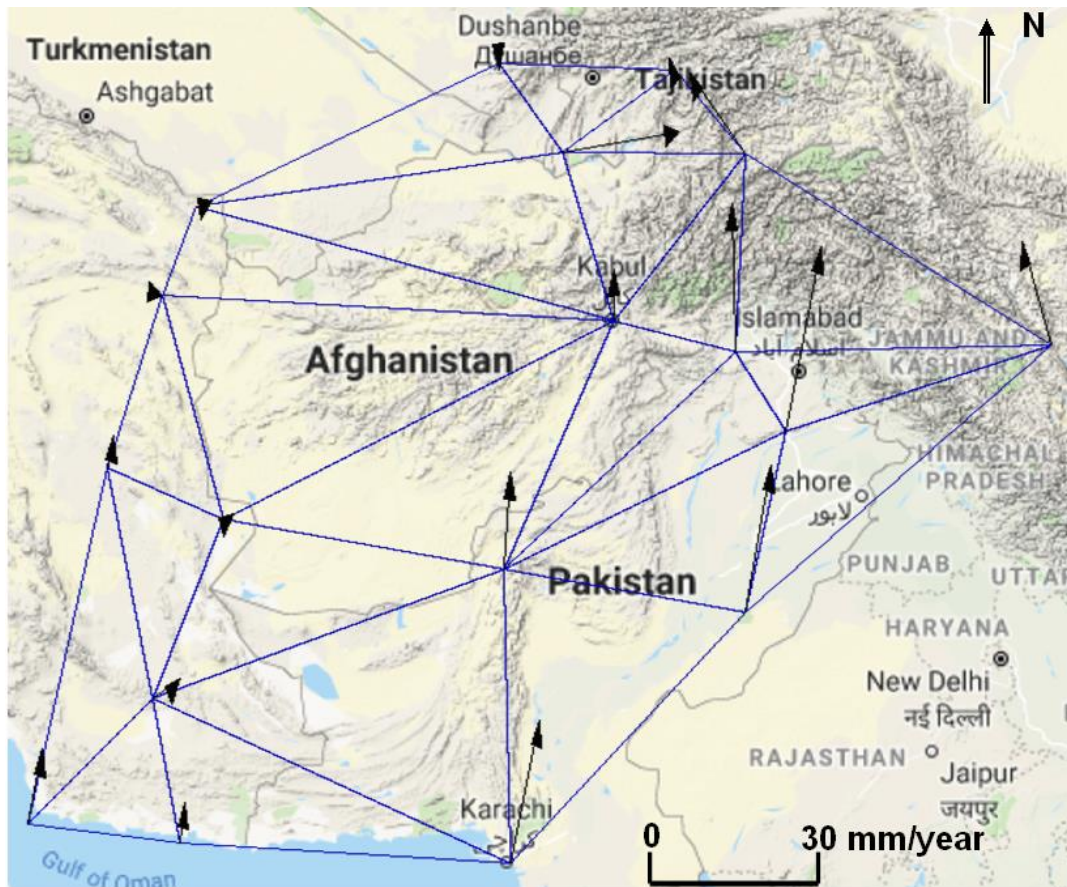
Figure 3.4 Annual deformation rates of GPS stations in Afghanistan and its vicinity.

3.3.2   Strain Rates

The method presented in Sub-section 3.2 is utilized to compute the strain rates. Figure 3.5 shows the annual strain rates in Afghanistan and neighboring regions (blue: compression; red: extension). The crustal straining is high along the major tectonic structures such as Pamir and Hindu-Kush Subduction zone, Chaman Fault, Makran subduction zone and Sistan Suture Zone (SSZ) while the annual strain in the central Afghanistan (Helmand Block) is quite small.

As noted from Figure, compressive principal strain rates are perpendicular to the plate boundary between Indian plate and Euro-Asian plate. It is interesting to note that the principal strain rates in the vicinity of Kabul are high and are close the strain rate variations in the vicinity of sinistral faults. Furthermore, the strain rate to the north of Hari-rud (Herat) fault implies dextral type straining in accordance with deformation sense of this fault.
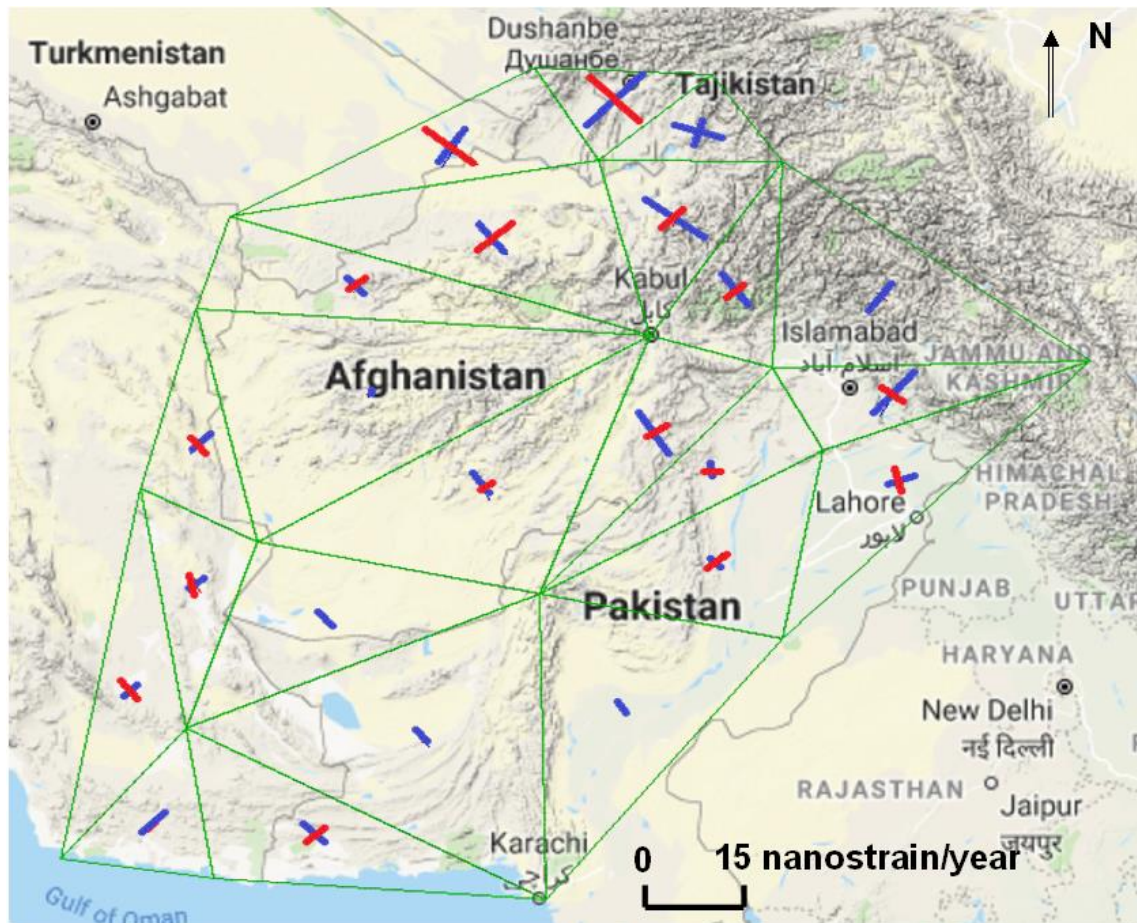
Figure 3.5 Annual strain rates in Afghanistan and its vicinity.

3.3.3   Stress Rates

The method presented in Sub-section 3.2 is utilized to compute the principal stress, maximum shear stress, mean stress and disturbing stress rates. Figure 3.6, Figure 3.7 and Figure 3.8 show the annual maximum shear stress, mean stress and disturbing stress rates in Afghanistan and neighbouring regions. The crustal stresses are high along the major teconic structures such as Pamir and Hindu-kush Subduction zone, Chaman Fault, Makran subduction zone and Sistan Suture Zone (SSZ) while the annual stress rates in the central Afghanisan (Helmand Block) is quite small. Furthermore, both the contours of maximum shear stress and disturbing stress rates have a striking similarity to the seismic zoning map of Shareq Abdullah (1993).

Figure 3.6 Maximum shear stress rate variations in Afghanistan and its neighboring countries

Figure 3.7 Mean stress rate variations in Afghanistan and its neighbouring countries

Figure 3.8 Disturbing stress rate variations in Afghanistan and its neighbouring countries

3.3.4   Interrelation between Strain Rates and Seismicity

Aydan et al. (2011) showed that the strain rates are closely related to the regional seismicity. Figure 3.9 and Figure 3.10 compare the computed strain, stress rates and seismicity of Afghanistan and its vicinity. Seismicity is quite high in Hindu-Kush, Kashmir Quetta and Sistan Suture Zone. It is interesting to note that high seismicity is observed particularly in the regions undergoing high extension type straining rate. There is no doubt that the GPS instrumentation in relation to the main tectonic features would yield better crustal straining and stress variations in Afghanistan and its relation to the regional seismicity. Nevertheless, the strain rates computed in this study are enough to have a clear image of crustal straining and stress changes in Afghanistan.

The recurrence parameters of the 9 seismotectonic zones of Afghanistan are calculated in section 4.2.2. Although the parameters are also based on the seismicity, they also represent the activity range of the faults in the corresponding zones. The activities of these zones are illustrated in Figure 4.6. As seen the faults in the vicinity of Hindu Kush and SE parts of Afghanistan are more active. The faults in the northern West and southern West Afghanistan are less active. In general, it is seen that the faults located in the regions with high strain rate has higher activity rate and they are less active where the strain rate is small.
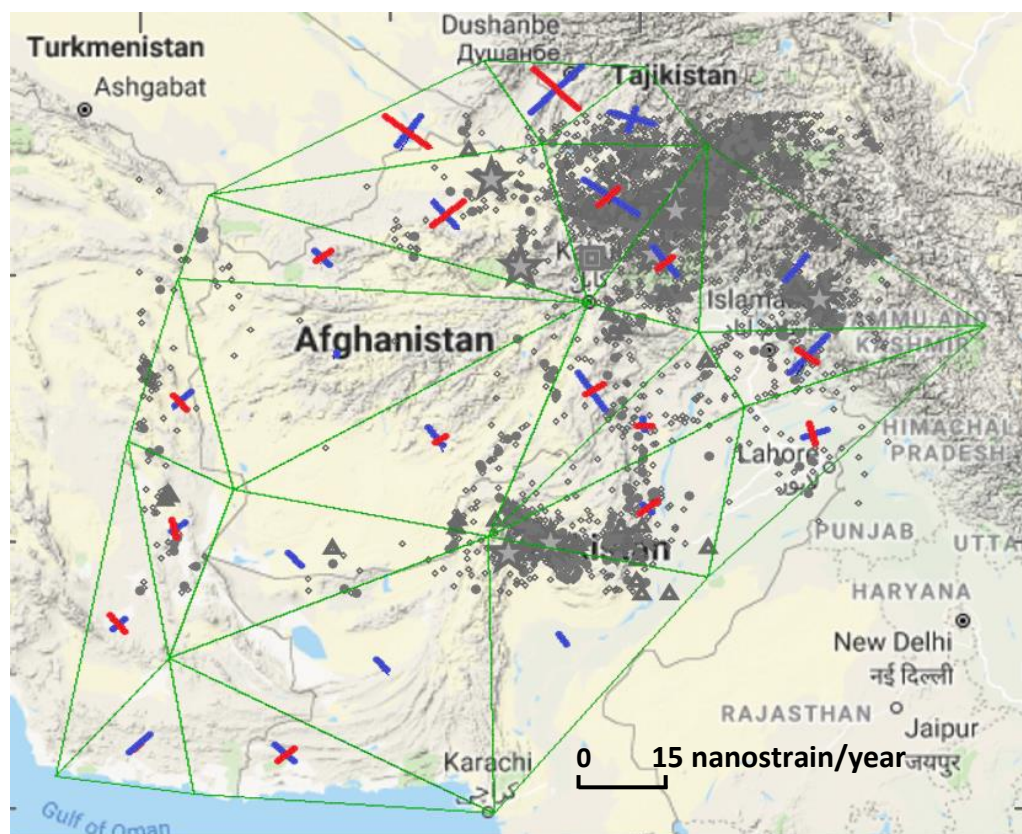
Figure 3.9 The relation of annual strain rates in Afghanistan and its vicinity to its seismicity.
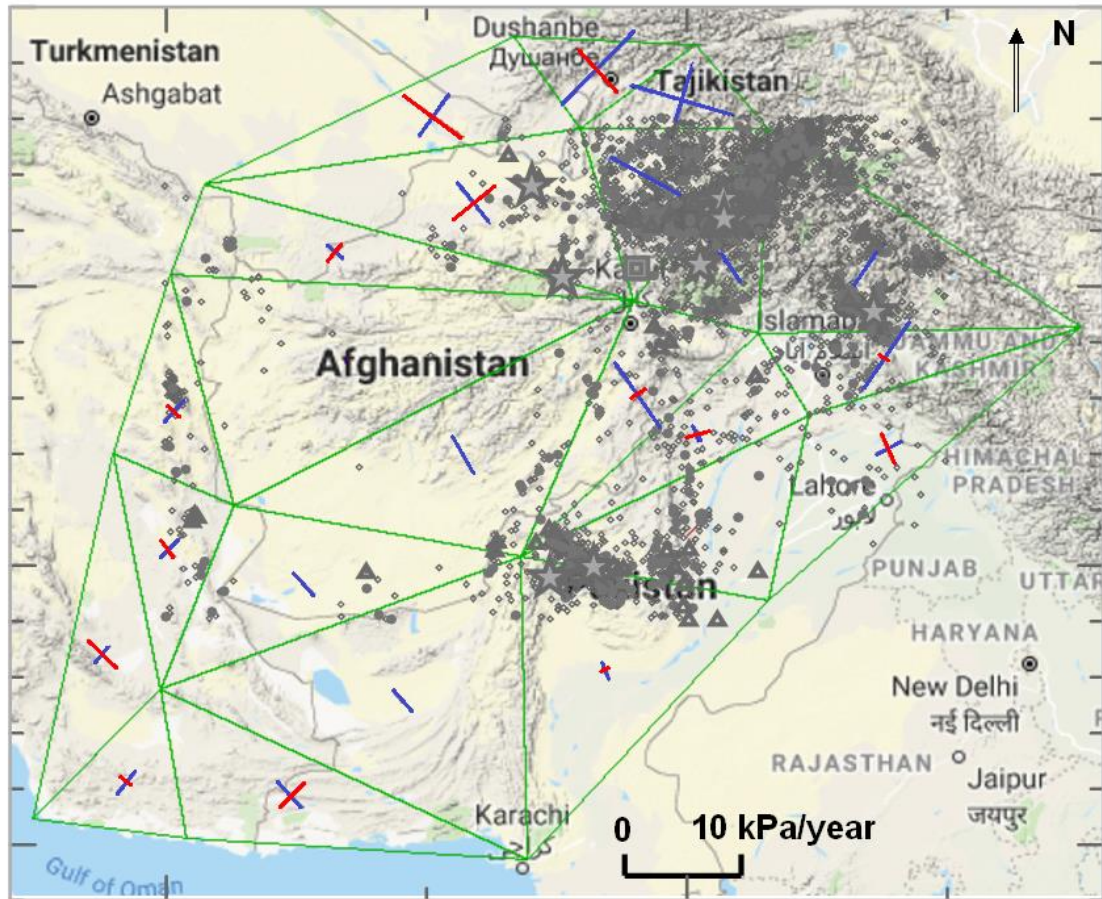
Figure 3.10 The relation of annual stress rates in Afghanistan and its vicinity to its seismicity.

CHAPTER 4   SEISMIC HAZARD ANALYSIS AND SEISMIC RISK ZONING

4.1 General

Afghanistan is in one of the active seismic belts of the world. Every few years, earthquakes take the lives of thousands of people in this country. It is amongst the regions about which the documented records of historical earthquakes are almost nil, making it challenging to give a clear guide about its earthquake risk. Decades of violence have left the country with few scientists and limited resources to address earthquake hazard. Afghanistan is divided into 4 earthquake regions (Wheeler, et al., 2005); among which the southern-east earthquake region where lifelines like Kabul, Jalalabad, Baghlan, Faizabad and some other big cities also exist, is the most severe earthquake region in the country. This region is close to the Eurasia- India global plates' convergence boundary, Figure 4.1. Most of the damage is caused not only by the strong ground motion and surface rupture, but also from liquefaction and extensive and successive landslides (Benz, et al., 2005). Considering the regional seismic activity, probability of potential for a devastating earthquake along Chaman fault near Kabul is unavoidable

This chapter presents the results of the evaluation of the seismic risk of Afghanistan using probabilistic seismic hazard analysis approach and the earthquake risk zonation of Afghanistan. The conventional PSHA method is augmented by modeling faults as line sources in addition to the area sources. We calculated earthquake parameters form instrumental and historical earthquakes explained in Chapter 2 and used them in the probabilistic seismic hazard analysis. We used a cumulative *b*-value calculated for each of the earthquake catalogues. We also calculated *b*-value for all the earthquake zones respectively which is used for the calculations in this study. We compared the results with some of the previous studies. The results are matching for some regions whereas it is either low or higher for other regions according to the calculated *b*-values. Effects from the earthquakes of the neighboring countries are also included. The computer program R-CRISIS2015 is used for hazard calculations. The analysis methods as well as their application to specific cases to Afghanistan earthquakes are explained in the following sections.

4.2 Probabilistic Seismic Hazard Analysis (PSHA)

In order to assess risk to a structure from earthquake shaking, we must first determine the annual probability of exceeding some level of earthquake ground shaking at a site, for a range of intensity levels. If one was willing to observe earthquake shaking at a site for thousands of years, it would be possible to obtain this entire curve experimentally. That is the approach often used for assessing

flood risk, but for seismic risk this is not possible because we do not have enough observations to extrapolate to the low rates of interest. In addition, we must consider uncertainties in the size, location, and resulting shaking intensity caused by an earthquake, unlike the case of floods where we typically only worry about the size of the flood event. Because of these challenges, our seismic hazard data must be obtained by mathematically combining models for the location and size of potential future earthquakes with predictions of the potential shaking intensity caused by these future earthquakes. The mathematical approach for performing this calculation is known as Probabilistic Seismic Hazard Analysis, or PSHA. PSHA is flexible enough to accommodate a variety of users' needs, and quantitative so that it can incorporate all knowledge about seismic activity and resulting ground shaking at a site. Rather than ignoring the uncertainties present in the problem, this approach incorporates them into calculations of potential ground motion intensity. While incorporation of uncertainties adds some complexity to the procedure, the resulting calculations are much more defensible for use in engineering decision-making for reducing risks.

With PSHA, we are no longer searching for an elusive worst-case ground motion intensity. Rather, we will consider all possible earthquake events and resulting ground motions, along with their associated probabilities of occurrence, in order to find the level of ground motion intensity exceeded with some tolerably low rate. At its most basic level, PSHA is composed of the following five steps.

1. Identification of all earthquake sources capable of producing damaging ground motions.
2. Characterization of the distribution of earthquake magnitudes (the rates at which earthquakes of various magnitudes are expected to occur).
3. Characterization of the distribution of source-to-site distances associated with potential earthquakes.
4. Prediction of the resulting distribution of ground motion intensity as a function of earthquake magnitude, distance, etc.
5. Combination of uncertainties in earthquake size, location and ground motion intensity, using a calculation known as the total probability theorem.

We have applied this method in the following sections to evaluate the exceedance of probability of and ground motion intensities from the sources that are believed to be producing earthquakes in Afghanistan.

4.2.1 Earthquake Data

The earthquakes used here for PSHA analysis are established from catalogues and reports of various international agencies that are in operation over a long period of time. The catalogues for instrumental earthquakes consist of International Seismological Center (ISC, 2016) and United

States Geological Survey (USGS). For the historical earthquakes, we used the only catalogue of (Ambraseys & Bilham, 2003). The catalogues include earthquakes of a broader area bounded by 27.0≤Latitude≤39.5, 58.5≤Longitude≤75.0, and M≥4.0. All catalogues were combined, and the duplicate events were removed. As the new GMPEs use moment magnitude scale (M_w), we used the relationships of (Scordilis, 2006) to convert the M_S and mb to M_w using equations, *1*, *2* and *3*, *and* the relationship of (Zare, 2014) was used to convert M_L to M_w using equation *4* from Chapter 2, to create a homogenized earthquake catalogue, Figure 4.1.
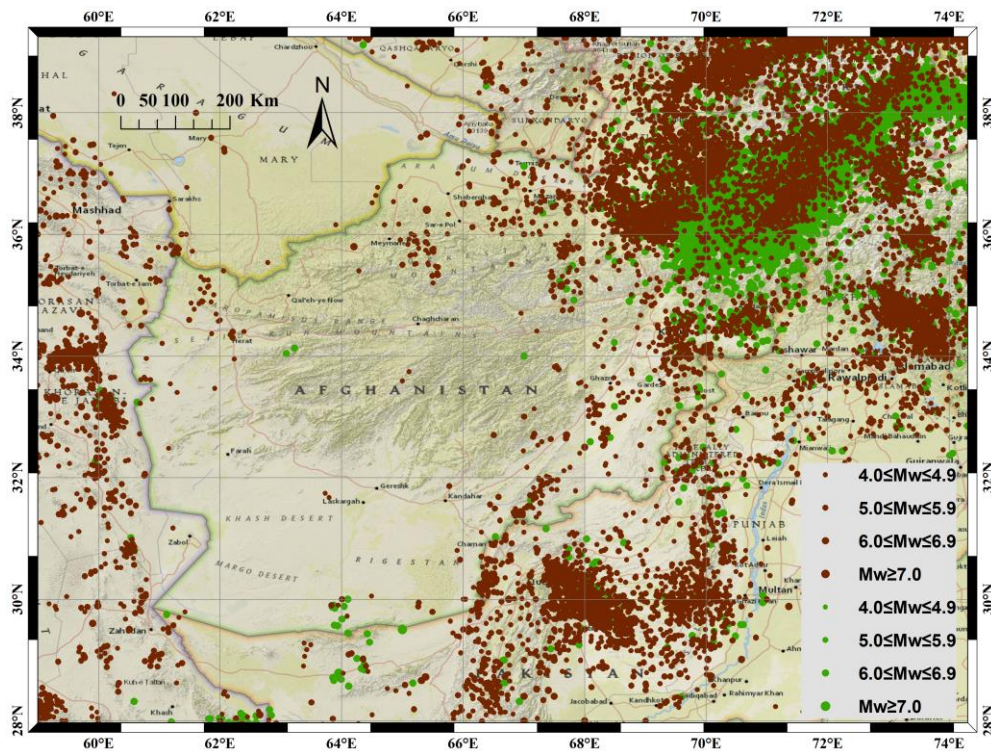
Figure 4.1 Homogenized earthquake catalogue for Afghanistan region. Red dots are the shallow earthquakes (depth≤50km) and the green dots are deep earthquakes (depth>50).

Many events in the homogenized catalogue are retrieved from the International Seismological Centre (ISC, 2016) and the United States Geological Survey (USGS) global catalogues. We analyzed the data of these three catalogues in time domain to identify the duration of data completeness. The catalogue of (Ambraseys & Bilham, 2003) is the only available catalogue for the historical events of Afghanistan, Figure 4.2. In this catalogue, only 56 events have been reported in about 11 centuries (734 to 1900) and is quite a small number. The earthquake record for the historical events of Afghanistan is almost nil. The USGS catalogue is complete for the events of M_w≥4.4 in the period of 1973-2019, and its complete for M_w≥5.5 from 1950-2019 and it is complete for the events of M_w≥6.0 in the period of 1900-2019. Some events of 4.0≤M_w≤4.5 have been reported in the period of 2015-2018, Figure 4.3.
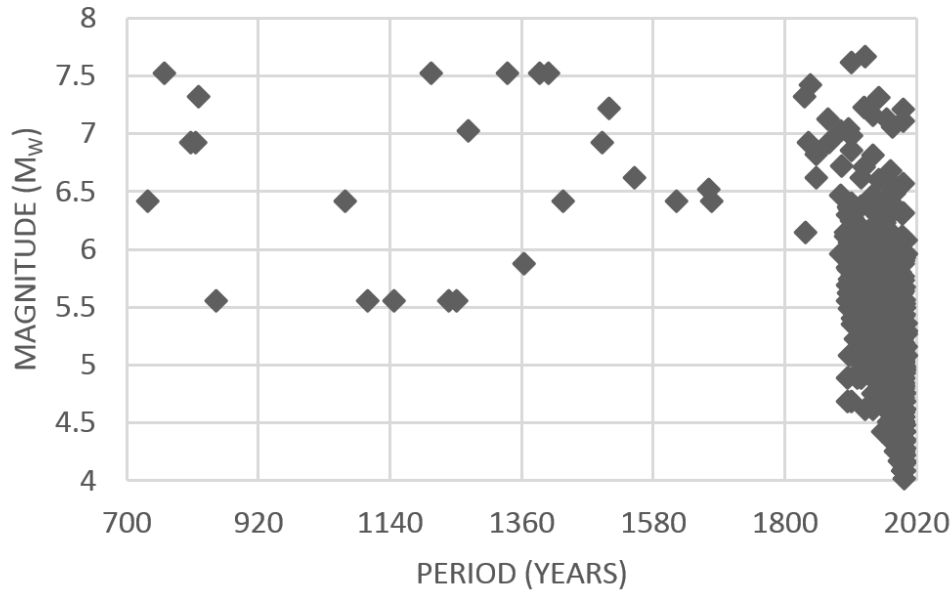
Figure 4.2 Distribution of historical and instrumental earthquakes in time domain from 734-200, catalogue of (Ambraseys & Bilham, 2003).

The ISC catalogue is complete for the events of $M_w \geq 6.0$ in the period of 1900-1900. It is complete for the events of $M_w \geq 5.5$ in the period of 1935-2019. It is complete for the events of $M_w \geq 4.0$ for the period of 1960-2019 with a gap of these events between 1970-2000, Figure 4.4. The preference begins with the ISC catalogue as it is the most complete of these three catalogues and follows USGS and then historical catalogue of Ambraseys and Bilham 2003.
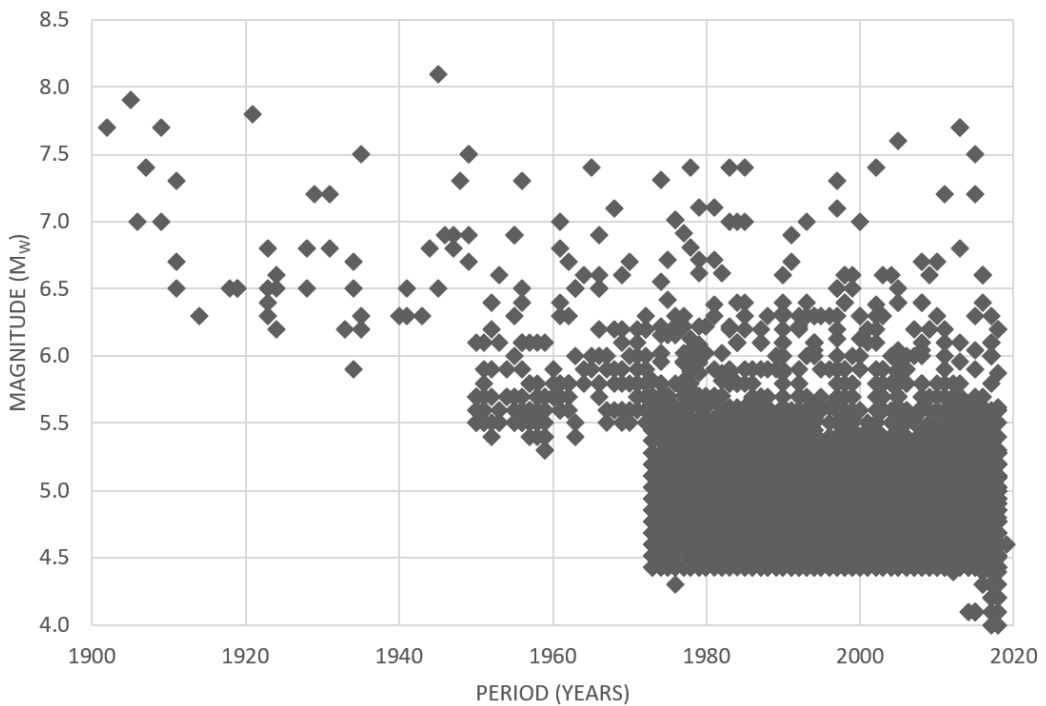
Figure 4.3 Distribution of instrumental earthquakes in time domain, USGS catalogue
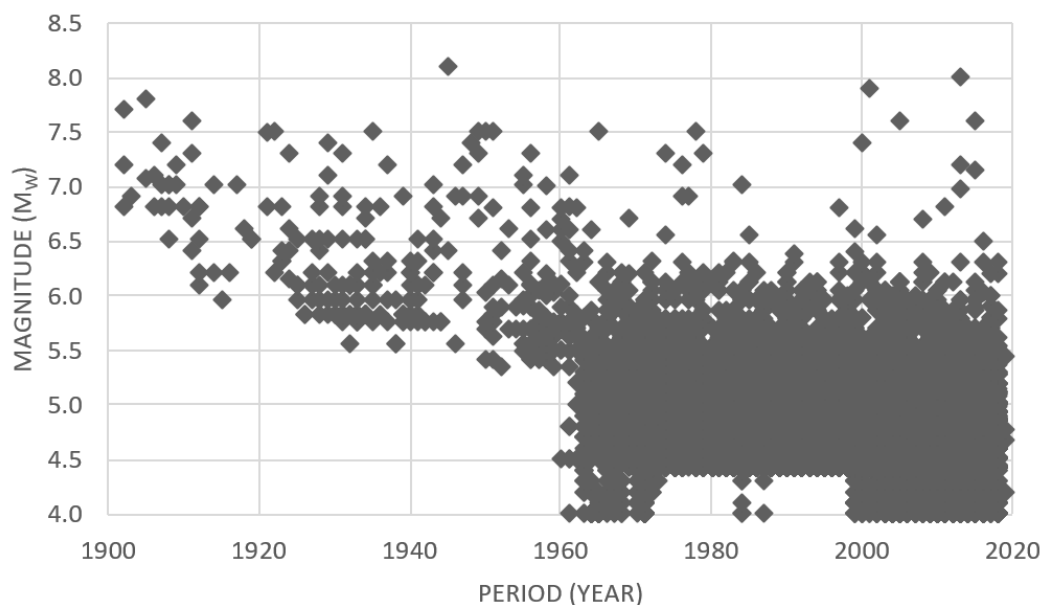
Figure 4.4 Distribution of instrumental earthquakes in time domain, ISC catalogue

4.2.2 Recurrence Parameters

We conducted the regression analysis using the Gutenberg-Richter relationship (Gutenberg & Richter, 1994) in equation *4-1* on the ISC and USGS catalogues of the broader area, respectively to obtain a cumulative *b*-value. The result yields log(*N*)=*6.0-1.02M* for the ISC catalogue, and it yields log(*N*)=*5.65-0.97M* for the USGS catalogue. We also calculated it for the catalogue of (Ambraseys & Bilham, 2003). It yields a *b*-value of 0.517 which is quite small and implies the incompleteness of the historical earthquake record of Afghanistan. It is observed that an average *b*-value of 1.0 is well established throughout both the catalogues and the Gutenberg-Richter relationship will be log(*N*)=*5.86-1.0M*, Figure 4.6. The average *b*-value of "1" is equal to the *b*-value of a previous study (Boyd, et al., 2007). We did not exclude the foreshocks and aftershocks due to the risk of removing too many earthquakes; hence, it accounts for any temporal uncertainty. Where *N* is the number of events per year having magnitudes greater than *M*, *a* and *b* are Gutenberg-Richter parameters.

$$\text{Log}(N_{(M)}) = a - b*M \tag{4-1}$$

Pamir and Hindu Kush of Afghanistan is where continental earthquakes as deep as 250 km and more occur frequently. We evaluated the casualties and damages of these earthquake to the buildings. The record is probably not documented well or not available. For most of the events the detailed record does not exist; however, for some of the main events we retrieved damage and casualties details from (NGDC/WDS), presented in Table 4.1. We found a relationship between the depth and casualties as well as depth to destruction, Figure 4.5.
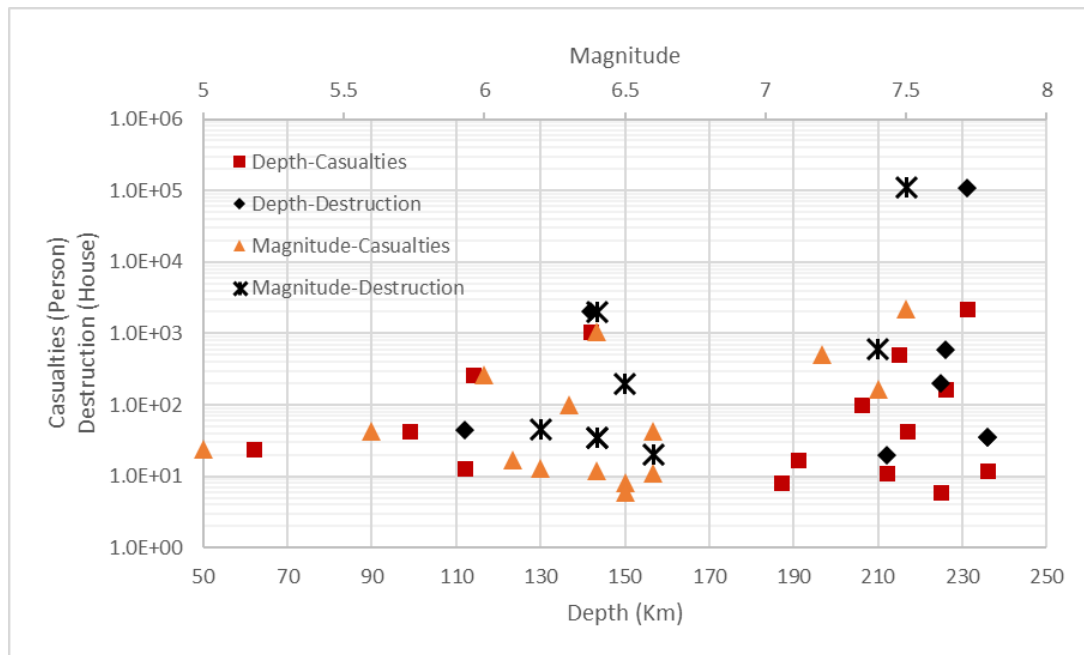
Figure 4.5 Magnitude-depth-destruction-casualty relationship for the Hindu Kush earthquakes. Earthquakes beyond 240 km seem not to damage structures and do not threaten lives in the nearby lifelines. This figure is developed based on data in Table 4.1.
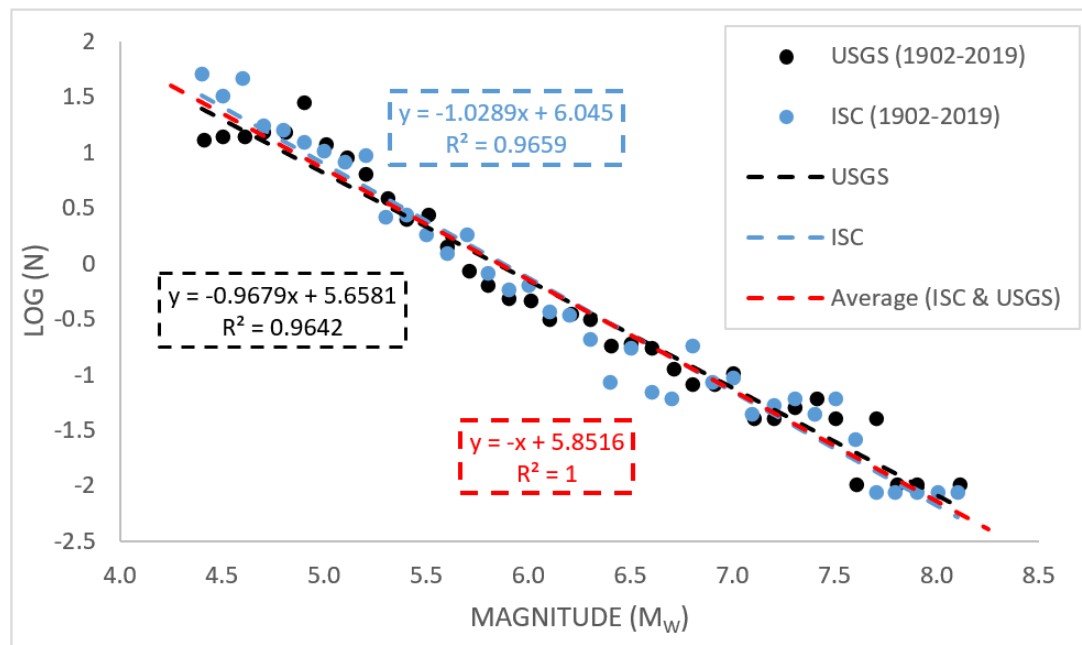
Figure 4.6 Regression analysis for the ISC and USGS catalogues

The deepest earthquake with casualties and damages so far recorded in Hindu Kush and Pamir region is 240 km. Considering this depth, we removed earthquakes deeper than 250 km. As the earthquake record for Afghanistan is not very well documented, particularly the historical earthquake record, *b*-value has been considered equal to 1 in a previous study of (Boyd, et al., 2007) for all areas of Afghanistan. However, the seismicity in NW and SW of Afghanistan seems quite small.
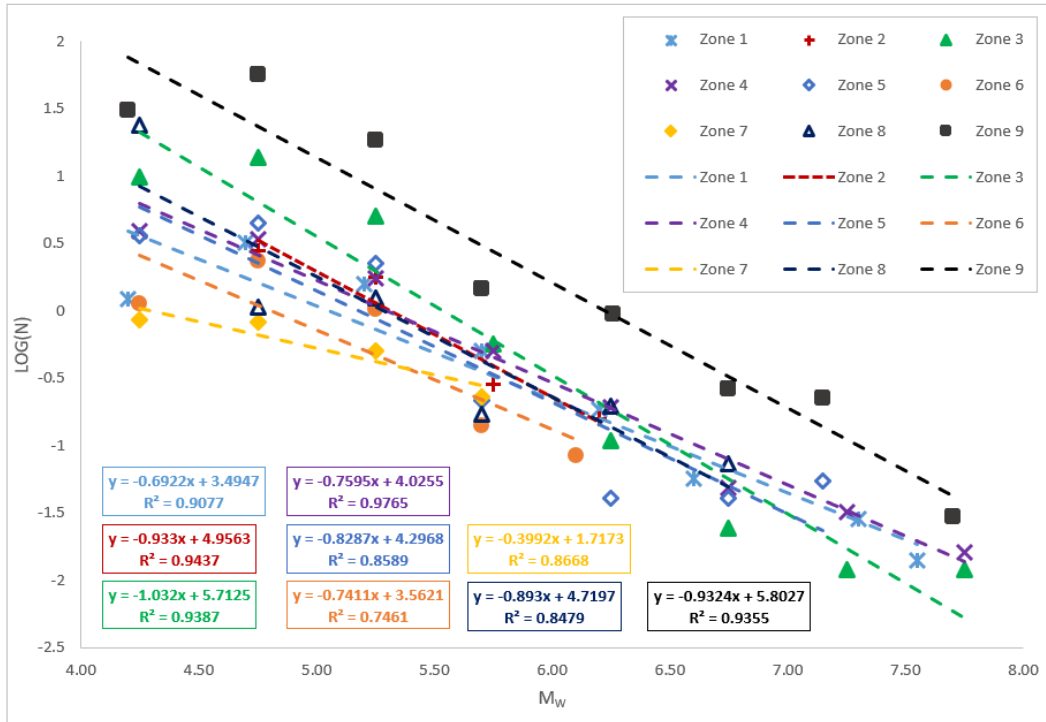
Figure 4.7 Regression analysis for the 9 earthquake area sources in Afghanistan

For earthquake hazard calculations, we used the 9 seismotectonic domains of (Ruleman, et al., 2007) as the area sources and are namely, Zone 1, Zone 2, …., and Zone 9. In order to include the effects of the earthquakes near the borders of Afghanistan, we used areas and line sources on the western border of Afghanistan (Zone 10- Zone 14, line sources 47, 50, 51, 52, 77, 79, 80, 82, 83, 87 and 92) from (Mahsuli, et al., 2019), and area sources in the northern border of Afghanistan (Zone 16- Zone 19) from (Ischuk, et al., 2018), and area sources on the southern and eastern border of Afghanistan (Zone 20- Zone 25) from (Rafi, et al., 2012), Figure 4.8. We clipped parts of the area sources outside the border of Afghanistan where they were overlapping the nine area sources inside Afghanistan. We calculated the *b*-value for the nine earthquake areas in Afghanistan, respectively. The *b*-value is equal to 1.03 for seismic zone 3 where most of seismic activity takes place and it is 0.93 for seismic zone 9 which is a zone of deep earthquakes. For rest of the earthquake zones, *b*-value is less than 1, Figure 4.7. Earthquake zone 7 is the least seismically active zone with a *b*-value of 0.4. From the magnitude-depth-destruction-casualty relationship in Figure 4.5, we considered earthquakes with depths equal to or less than 250km only for seismic zone 9 which is in Pamir and Hindu Kush region.

For the sources near the Afghanistan borders, we used the seismic parameters calculated for the corresponding sources in the original manuscripts. The major faults that are believed to be contributing to the seismicity of Afghanistan consists of the Chaman fault and the Central Badakhshan fault systems.

Table 4.1 Record of the deep earthquakes in Pamir and Hindu Kush region which is used as seismic area source 9 in this study, death toll and damages. Data retrieved from (NGDC/WDS).

Year	Month	Day	Hour	Minute	Sec	Place	Latitude	Longitude	Focal depth	Magnitude	MMI Intensity	Deaths	Injuries	Houses Destroyed	Houses Damaged
1832	1	22				Afghanistan	36.5	71							
1896	9	23	23	20		Afghanistan	37	71	160	7.5	6				
1908	10	23	20	14	6	Afghanistan: Hindu Kush	36.5	70.5	220	7					
1909	7	7	21	37	50	Afghanistan: Hindu Kush	36.5	70.5	230	8.1	7				
1911	7	4	13	33	26	Afghanistan: Hindu Kush	36	70.5	190	7.6					
1921	11	15	20	36		Afghanistan: Hindu Kush	36.5	70.5	215	7.8					
1922	12	6	13	55		Afghanistan: Hindu Kush	36.5	70.5	230	7.5					
1929	2	1	17	14		Afghanistan: Hindu Kush	36.5	70.5	220	7.1					
1937	11	14	10	58	12	Afghanistan: Hindu Kush	36.5	70.5	240	7.2	7				
1939	11	21	11	2		Afghanistan	36.3	70.6	220	6.9					
1949	3	4	10	19	25	Afghanistan: Hindu Kush, West Punjab	36	70.5	230	7.5	8				
1965	3	14	15	53	6	Afghanistan	36.3	70.7	219	7.3	7				
1976	11	27	21	42	12	Afghanistan; Tajikistan; Khorog	36.51	71.04	190	6.1	5				
1983	12	30	23	52	39	Afghanistan: Hindu Kush: Kabul, Samangan; Pakistan	36.37	70.73	215	7.2	7	26	483		
1985	7	29	7	54	44	Afghanistan: Hindu Kush: Chitral, Swat	36.19	70.89	99	6.6	8	5	38		
1990	7	13	14	20	43	Afghanistan: Hindu Kush: Pik Lenina	36.41	70.78	217	5.6	4	43			

Table 4.2 Con.. Record of the deep earthquakes in Pamir and Hindu Kush region which is used as seismic area source 9 in this study, death toll and damages. Data retrieved from (NGDC/WDS).

Year	Month	Day	Hour	Minute	Sec	Place	Latitude	Longitude	Focal depth	Magnitude	MMI Intensity	Deaths	Injuries	Houses Destroyed	Houses Damaged
1990	10	25	4	53	59	Afghanistan: Hindu Kush: Chitral, Mardan, Malakand	35.12	70.48	114	6	4	11	250		
1991	1	31	23	3	33	Afghanistan: Badakhshan, Baghlan, Laghman, Nangarhar	35.99	70.42	142	6.4	7	848	200	0	2000
1997	5	13	14	13	45	Afghanistan: Hindu Kush, Malakand, Peshawar	36.41	70.94	196	6.4		1		0	
1998	2	20	12	18	6	Afghanistan-Tajikstan: Yar Husain, Astor	36.47	71.08	236	6.4		1	11	35	0
2001	6	1	14	0	43	Afghanistan: Hindu Kush: Parvan	35.16	69.38	62	5		4	20	0	0
2002	3	3	12	8	19	Afghanistan: Hindu Kush: Samangan, Kabul, Rustaq	36.50	70.48	226	7.4		166		300	300
2002	12	25	19	13	42	Afghanistan: Jalalabad	35.70	69.86	91	5.5				0	0
2004	4	5	21	24	4	Afghanistan: Hindu Kush: Samangan; Pakistan	36.51	71.02	187	6.5		3	5	0	0
2005	12	12	21	47	46	Afghanistan: Tili, Jalalabad, Badakhshan	36.35	71.09	225	6.5		5	1	100	100
2008	12	29	3	37	41	Afghanistan; Pakistan; Mansehra, Shangla	36.40	71.07	158	5.8				0	0
2015	10	26	9	9	56	Afghanistan: Hindu Kush	36.52	70.36	231	7.5	7	399	1770	29230	79893
2015	12	25	19	14	19	Afghanistan; Pakistan	36.49	71.12	206	6.3	5	4	97	0	0
2016	4	10	10	29	12	Afghanistan: Khyber Pakhtunkhwa	36.47	71.13	212	6.6	5	6	5	0	20
2018	1	31	7	7		Afghanistan; Pakistan; Baluchistan	36.54	70.81	191	6.1		2	15	0	0
2018	5	9	10	41	45	Afghanistan: Takhar; Pakistan	36.99	71.36	112	6.2			13	0	45
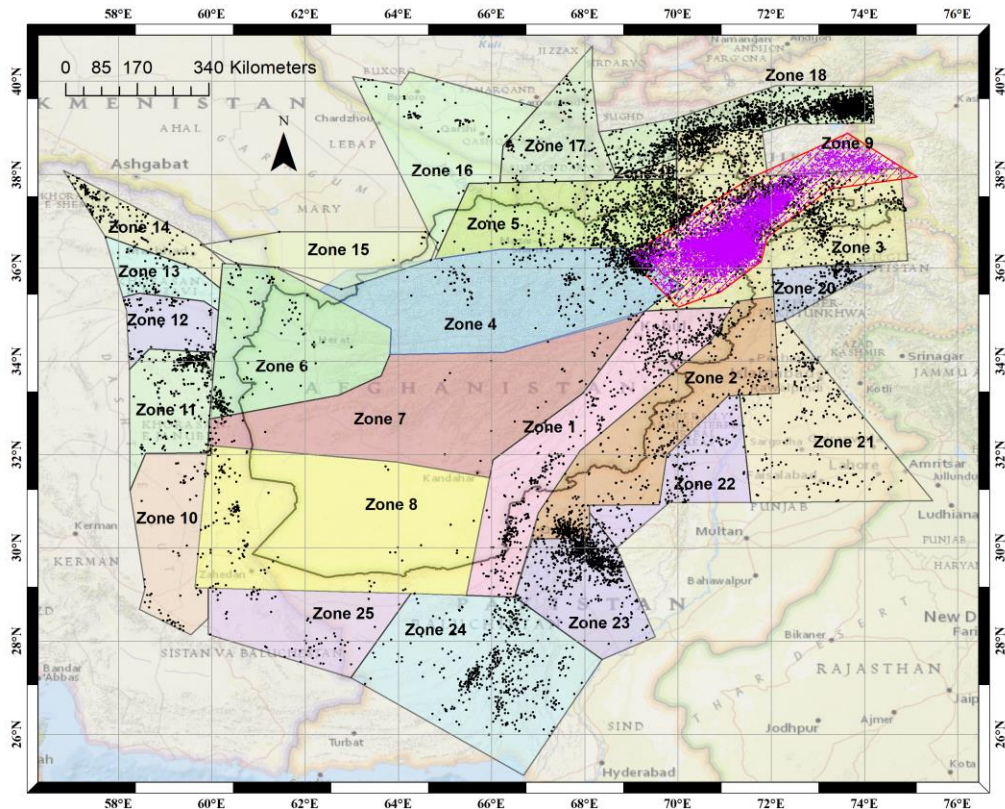
Figure 4.8 Area sources in Afghanistan region. The sources outside the border of Afghanistan are retrieved from other studies conducted for the neighboring countries.
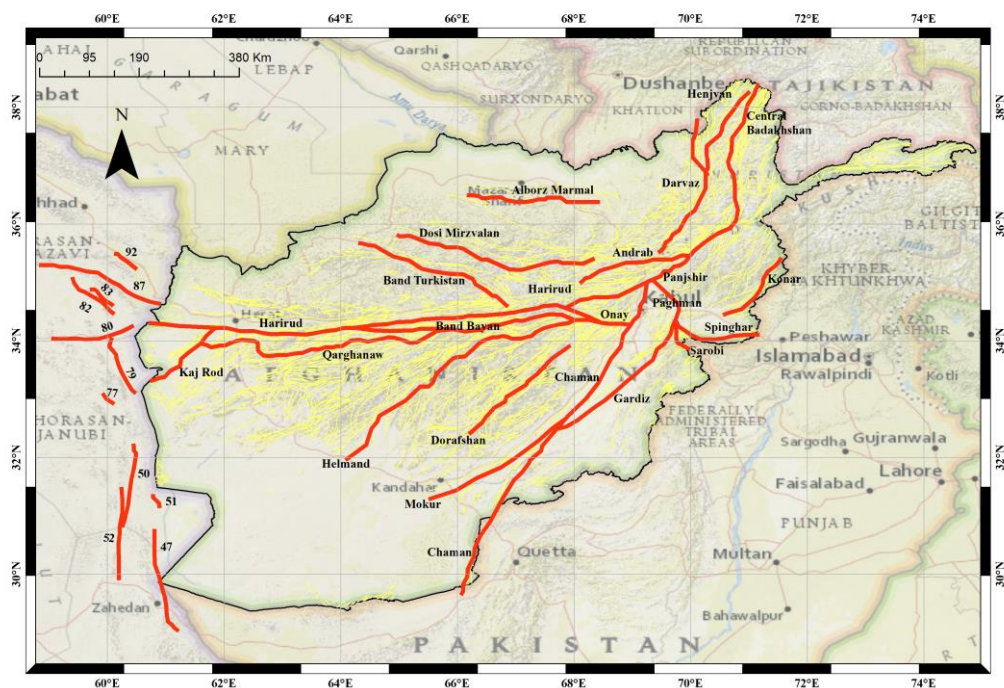
Figure 4.9 Faults modeled as line sources in this study. The faults inside Afghanistan are modified from (Wheeler, et al., 2005). The yellow lines in the background represent the many faults in Afghanistan with unknown earthquake activity. The faults on left of the western border of Afghanistan are modified from (Mahsuli, et al., 2019).

The Chaman fault system includes main Chaman fault meeting the Hari-rud fault at its North end near Kabul, Gardiz, Konar and Sarobi faults as its branches. The main Chaman fault is a left-lateral strike slip fault (Ruleman, et al., 2007) and has not released a high earthquake activity in recent history. This fault system absorbs most of its deformation from the Eurasia- India global plates' boundary and a 300-400km segment of this fault between 31-33.5°N has big similarity with the Balakot Bagh (B-B) fault of Pakistan where the 2005 M7.6 Kashmir earthquake took place. The Central Badakhshan fault makes the upper western margin of the Transpressional Plate Boundaries and the main Chaman fault comprises its other half of the lower West margin. We modeled all the faults in Afghanistan that are believed to be active Figure 4.9. using the earthquake parameters of the area sources in which the corresponding fault is located. We used the Gutenberg-Richter recurrence law in 4-2 to calculate the seismic parameters for modeling the area sources (Zone 1 – Zone 9) and line sources (faults) in the computer program RCRISIS2015. The seismic parameters for the sources inside Afghanistan are given in Table 4.3.

$$\lambda_m = \nu \frac{exp[-\beta(m-m_0)]-exp[-\beta(m_{max}-m_0)]}{1-exp[-\beta(m_{max}-m_0)]} \qquad (4.1)$$

Where $\nu = exp\ (\alpha - \beta m_0)$, $m_0 \leq m \leq m_{max}$, $\alpha = a*2.303$ and $\beta = b*2.303$.

For the area and line sources outside Afghanistan borders, the seismic parameters were used as calculated in the original manuscripts. For area sources (Zone 10, Zone 11, Zone 12, Zone 13 and Zone 14, and line sources 47, 50, 51, 52, 77, 79, 80, 82, 83, 87 and 92) seismic parameters were retrieved from (Mahsuli, et al., 2019), and for the area sources in the northern border of Afghanistan (Zone 16, Zone 17, Zone 18 and Zone 19) seismic parameters from (Ischuk, et al., 2018) were used, and for the area sources on the southern and eastern border of Afghanistan (Zone 20, Zone 21, Zone 22, Zone 23, Zone 24 and Zone 25), seismic parameters from (Rafi, et al., 2012) were used to model these sources in RCRISIS2015, Figure 4.10.
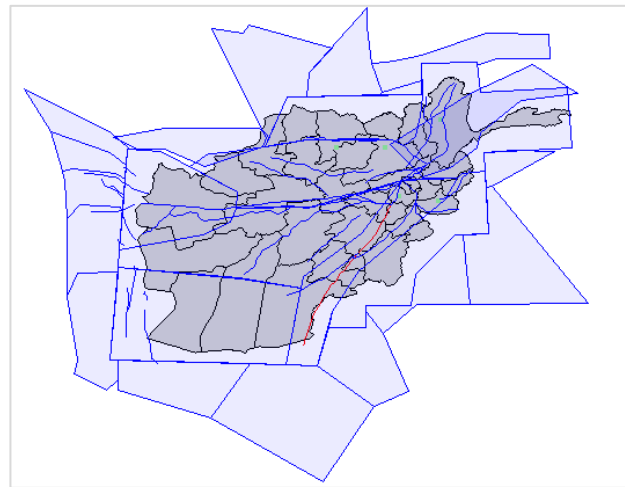
Figure 4.10 Modeling of the area and line sources in the RCRISIS2015 computer program.

Table 4.3 Seismic source model parameters for area and line sources in Afghanistan

Source Name	a	b	m	m_0	m_{max}	α	β	λ
Zone 1	3.49	0.69	4	4	7.5	8.05	1.59	5.321460
Zone 2	4.96	0.93	4	4	6.4	11.41	2.15	16.769519
Zone 3	5.71	1.03	4	4	7.6	13.16	2.38	38.440189
Zone 4	4.03	0.76	4	4	7.3	9.27	1.75	9.720261
Zone 5	4.30	0.83	4.5	4.5	7.3	9.90	1.91	3.696173
Zone 6	3.56	0.74	4	4	6.2	8.20	1.71	3.961026
Zone 7	1.72	0.40	4	4	5.8	3.95	0.92	1.319841
Zone 8	4.72	0.89	4.4	4.4	6.9	10.87	2.06	6.175078
Zone 9	5.80	0.93	4	4	7.8	13.36	2.15	118.433225
Alburz Maraml	4.30	0.83	4.5	4.5	7.3	9.90	1.91	3.696173
Andrab	4.03	0.76	4	4	7.3	9.27	1.75	9.720261
Bande Bayan	4.30	0.83	4.5	4.5	7.3	9.90	1.91	3.696173
Bande Turkistan	4.30	0.83	4.5	4.5	7.3	9.90	1.91	3.696173
Chaman	3.49	0.69	4	4	7.5	8.05	1.59	5.321460
Central Badakhshan	5.71	1.03	4	4	7.6	13.16	2.38	38.440189
Dorafshan	1.72	0.40	4	4	5.8	3.95	0.92	1.319841
Darvaz	5.71	1.03	4	4	7.6	13.16	2.38	38.440189
Dosi Mirzavalan	4.30	0.83	4.5	4.5	7.3	9.90	1.91	3.696173
Gardiz	3.49	0.69	4	4	7.5	8.05	1.59	5.321460
Hari Rud	4.30	0.83	4.5	4.5	6.2	9.90	1.91	3.696173

Table 4.4 Cont.. Seismic source model parameters for area and line sources in Afghanistan

Source Name	a	b	m	m_0	m_{max}	α	β	λ
Helmand	4.72	0.89	4.4	4.4	5.8	10.87	2.06	6.175078
Henjvan	5.71	1.03	4	4	7.6	13.16	2.38	38.440189
Kaj Rod	3.56	0.74	4	4	6.2	8.20	1.71	3.961026
Konar	4.96	0.93	4	4	6.4	11.41	2.15	16.769519
Mokur	3.49	0.69	4	4	7.5	8.05	1.59	5.321460
Onay	3.49	0.69	4	4	7.5	8.05	1.59	5.321460
Paghman	3.49	0.69	4	4	7.5	8.05	1.59	5.321460
Panjshir	3.49	0.69	4	4	7.5	8.05	1.59	5.321460
Qarghanaw	4.30	0.83	4.5	4.5	6.2	9.90	1.91	3.696173
Sarobi	3.49	0.69	4	4	7.5	8.05	1.59	5.321460
Spinghar	4.96	0.93	4	4	6.4	11.41	2.15	16.769519

4.2.3   Attenuation Relationship and Input Parameters

Attenuation relations specific to Afghanistan are not available; however, the tectonic settings in Afghanistan has similar geologic and climatic setting with faults elsewhere in the world (the San Andreas fault in the western U.S., the Wasatch fault, Utah and Karakoram fault of western China), (Ruleman, et al., 2007). Therefore, we used relations from the United States of America for hazard calculations. We applied a set of ground motion prediction equations for shallow earthquake zones and another set of ground motion prediction equation for deep earthquake zones. For shallow zones we used the relations of (Boore & Atkinson, 2008) for thrust and reverse faults. This set of equations are derived by empirical regression of an extensive strong-motion database and are for average horizontal-component ground motions as a function of earthquake magnitude, distance from source to site, local average shear-wave velocity, and fault type. They are for peak ground acceleration (PGA) and 5%-damped pseudo-absolute-acceleration spectra (PSA) at periods between 0.01 s and 10 s. The primary predictor variables are moment magnitude (M), closest horizontal distance to the surface projection of the fault plane (RJB), and the time-averaged shear-wave velocity from the

surface to 30 m (V_{S30}). The equations are applicable for M=5–8, R_{JB}<200 km, and V_{S30}=180–1300 m/s.

Table 4.5 Seismic source model parameters for area and line sources
outside the borders of Afghanistan

Source	b	m_{max}	β^*	λ
Zone 10	1.59	7.2	3.66	0.055
Zone 11	1.48	7.7	3.41	0.117
Zone 12	2.20	7.8	5.07	0.153
Zone 13	1.83	7.2	4.21	0.115
Zone 14	2.28	7.7	5.25	0.053
Zone 15	0.40	5.8	0.92	1.320
Zone 16	1.26	8.0	2.90	0.147
Zone 17	1.26	8.0	2.90	0.793
Zone 18	1.20	8.0	2.75	3.837
Zone 19	1.2 6	8.0	2.90	2.479
Zone 20	0.95	6.3	2.19	0.210
Zone 21	0.95	5.3	2.19	0.450
Zone 22	0.95	6.0	2.19	0.460
Zone 23	0.95	7.0	2.19	2.300
Zone 24	0.95	6.6	2.19	1.380
Zone 25	0.95	6.6	2.19	0.170
47	1.40	8.1	3.22	0.195
50	1.40	8.1	3.22	0.046
51	1.40	8.1	3.22	0.009

Table 4.6 Cont.. Seismic source model parameters for area
and line sources outside the borders of Afghanistan

Source	b	m_{max}	β^*	λ
52	1.59	7.2	3.66	0.064
77	1.48	7.7	3.41	0.009
79	1.48	7.7	3.41	0.126
80	1.48	7.7	3.41	0.333
82	2.20	7.8	5.07	0.009
83	2.20	7.8	5.07	0.009
87	2.20	7.8	5.07	0.166
92	2.30	7.2	5.25	0.054

*We calculated β from b-value ($\beta = b*2.303$)

$$\ln Y = F_M(\mathbf{M}) + F_D(R_{JB}, \mathbf{M}) + F_S(V_{S30}, R_{JB}, \mathbf{M}) + \varepsilon \sigma_T. \tag{4-2}$$

In this equation, F_M, F_D, and F_S represent the magnitude scaling, distance function, and site amplification, respectively. **M** is moment magnitude, R_{JB} is the Joyner-Boore distance (defined as the closest distance to the surface projection of the fault, which is approximately equal to the epicentral distance for events of M<6), and the velocity V_{S30} is the inverse of the average shear-wave slowness from the surface to a depth of 30 m. The predictive variables are **M**, R_{JB}, and V_{S30}; ε is the fractional number of standard deviations of a single predicted value of ln Y away from the mean value of ln Y (*e.g.,* ε=−1.5 would be 1.5 standard deviations smaller than the mean value). All terms, including the coefficient σ_T, are period dependent. Where σ is the intra-event aleatory uncertainty and τ is the inter-event aleatory uncertainty (this uncertainty is slightly different for cases where fault type is specified and where it is not specified; we distinguish these cases by including a subscript on τ).

For strike slip normal and reverse/thrust faulting, we used the equations of (Sadigh, et al., 1997). These relationships are for peak acceleration and response spectral accelerations from shallow crustal earthquakes. The relationships are based on strong motion data primarily from California earthquakes. Relationships are presented for strike-slip and reverse-faulting earthquakes, rock and deep firm soil deposits, earthquakes of moment magnitude M4 to M8+, and distances up to 100 km.

For deep earthquake zone, and for the faults that fall in this zone, we used empirical relations of (Atkinson & Boore, 2003) for deep interface. This set of ground-motion relations predict the pseudo acceleration (PSA) and peak ground acceleration, 5% damped, horizontal component on soil sites over a very large area of about 300 km wide by 500 km long and more. The relation by (Youngs, et al., 1997) was also used for subduction zone earthquakes. The later set of attenuation relationships are for peak ground acceleration and response spectral acceleration for subduction zone interface and intra-slab earthquakes of moment magnitude M 5 and greater and for distances of 10 to 500 km. We used logic three method and combined these relations with each weighing 50%. Site condition is rock with an average shear-wave velocity in the upper 30 meters of the crust equal to 760m/s.

4.2.4   Computer Program for Simulation

The computer program R-CRISIS2015 (Ordaz & M.A., 2017) is used for calculating the seismic hazard. RCRISIS is a powerful PSHA tools used in many earthquake-assessment projects worldwide (Tromans & Iain J., 2019; Aguilar-Meléndez A., et al., 2018; Hale, et al., 2018). It is a Windows based software with the capability of performing probabilistic seismic hazard analysis (PSHA) using a fully probabilistic approach allowing the calculation of results in terms of outputs with different characteristics (i.e., exceedance probability plots, set of stochastic events). The first version of the program was launched in 1986 and since then, almost thirty years ago, several and continuous updates and improvements have been included to keep the program as a state-of-the-art tool. Originally developed using FORTRAN as programming language (Ordaz, 1991) without a GUI, it developed later into CRISIS99 (Ordaz, 1999) which was a tool that first introduced a GUI written in Visual Basic but with the computation engine using a FORTRAN dynamic link library. Since 2007 the program was upgraded in view of the advantages offered by the object-oriented technologies (i.e. Visual Basic.NET). In that version, called CRISIS2007, both the GUI and the computation engine were written in the same programming language. R-CRISIS2015 is the latest version and provides a friendly environment to perform seismic hazard calculations within a fully probabilistic framework. The program computes seismic hazard by considering earthquake occurrence probabilities, attenuation characteristics and the geographical distribution of earthquakes. Seismic hazard results are mainly obtained, for each computation site, in terms of probabilities of exceeding a given intensity value within different time frames, whereas it is also possible to obtain the results in terms of both, non-exceedance probabilities and equivalent annual exceedance rates.

4.2.5   Earthquake Hazard

In this section, result of the analysis is presented. The northeastern part of Afghanistan has a higher ground motion comparing to other parts. The ground motion at the NW and SW is quite small and negligible. Probabilistic ground motions for 2% and 10% probability of exceedance in 50 years, resulted from this study for the five big cities located within the high seismic areas are presented in Table 4.7, respectively. To validate our findings, we compared the ground motions of this study with some other studies conducted previously. The ground motion for five cities from (Boyd, et al., 2007) is presented under column (1), and the ground motion from (Waseem, et al., 2019) is presented under column (2) and the results of this study is presented under column (3) highlighted in light gray color, Table 4.7. We calculated b-value from the earthquake in each of the nine earthquake zones, respectively. In the study of (Boyd, et al., 2007), the b-value has been considered equal to 1 for the entire Afghanistan. The b-value of this study is close to 1 for earthquake source zones 1, 3, and 9. For rest of the earthquake zones, it is lower than 1. The lowest b-value is 0.4 corresponding to Zone 7. The ground motion resulted from this study are lower from the results of (Boyd, et al., 2007) except for Faizabad and it is almost considerably lower than the results of (Waseem, et al., 2019) except for Badakhshan which is almost matching. The ground motion from (Waseem, et al., 2019) are considerably higher than the results of (Boyd, et al., 2007) and the results of this study. The lower ground motion of this study may be attributed to the varying b-value used in this study. The ground motion for NW and SW of Afghanistan is very low implying that those areas are seismically inactive as it also seems in instrumental and historical earthquake catalogues.

Table 4.7 Probabilistic ground motion (%g) for 2% and 10% probability of exceedance in 50 years

Period	Baghlan			Balkh			Faizabad			Jalalabad			Kabul		
(sec)	1	2	3	1	2	3	1	2	3	1	2	3	1	2	3
(2%) Probability of Exceedance															
0.0	55	64	45	33	68	20	75	107	69	40	75	35	48	83	32
0.2	131	144	121	78	154	47	149	199	204	104	172	91	113	182	82
1.0	37	53	49	22	40	26	89	79	74	33	54	41	53	62	38
(10%) Probability of Exceedance															
0.0	28	38	26	16	37	11	38	66	42	23	42	19	25	48	19
0.2	78	83	62	37	82	25	89	148	107	57	93	44	57	104	42
1.0	21	31	25	11	19	13	36	45	39	19	30	19	22	44	19

1. (Boyd, et al., 2007), 2. (Waseem, et al., 2019), 3. This study

The annual exceedance rate and earthquake hazard curves for 2% and 10% PE in 50 years is presented in Figure 4.11 and Figure 4.12; respectively. Faizabad, the capital of Badakhshan province has the highest ground motion (69%g at 0-sec, 2% PE and 42%g at 0-sec, 10% PE in 50 years, respectively) and Balkh the capital of Mazar-e-Sharif has the lowest (20%g at 0-sec, 2% PE and 11%g at 0-sec, 10% PE in 50 years, respectively) ground motion.
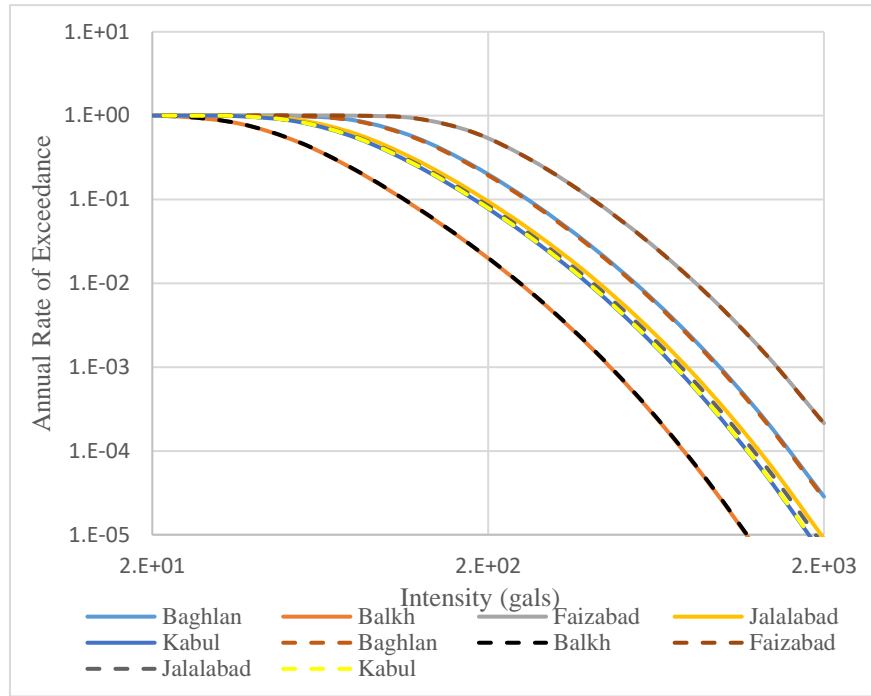
Figure 4.11 Probability of exceedance (PE) for five big cities of Afghanistan. The solid lines are representing 2% PE in 50 years and the broken lines represent the 10% PE in 50 years.
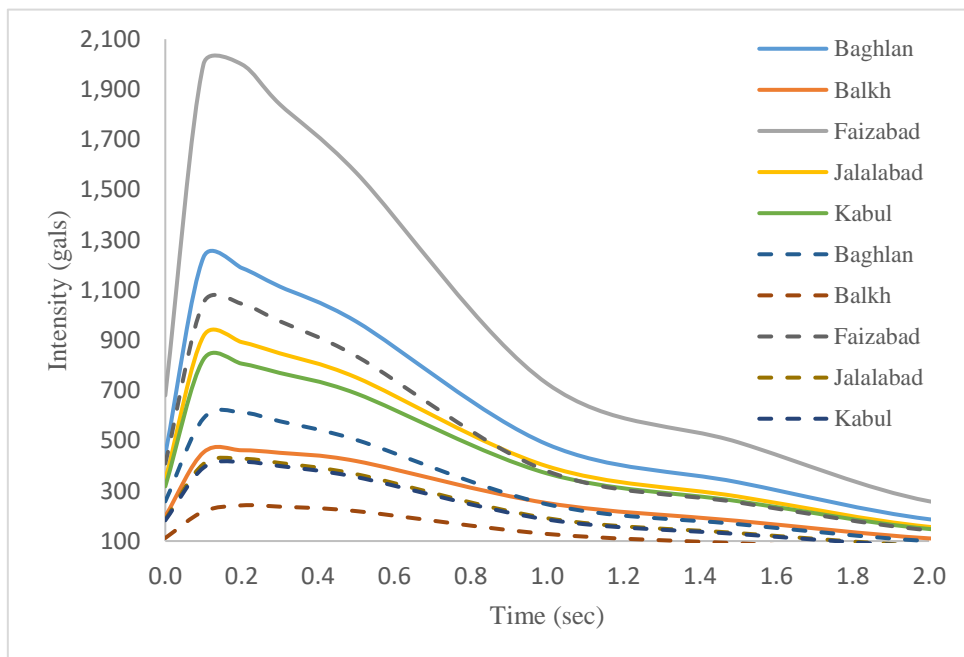
Figure 4.12 Ground motion for five big cities of Afghanistan. Solid lines represent ground motion for 2% (PE) in 50 years and the broken lines represent 10% (PE) in years.

Seismic hazard contour maps for PGA, 0.2-sec and 1.0-sec spectral acceleration corresponding to 2% and 10% exceedance probability in 50 years, are presented in Figure 4.13 Earthquake hazard map (PGA) with 2% PE in 50 years., Figure 4.14, Figure 4.15, Figure 4.16, Figure 4.17, and Figure 4.18.
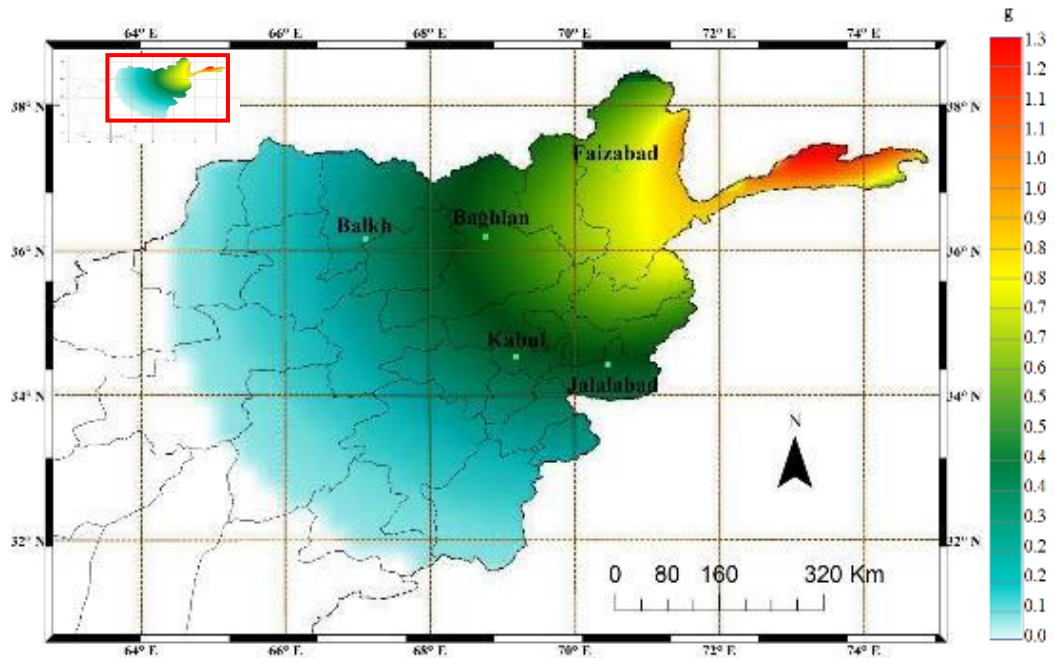
Figure 4.13 Earthquake hazard map (PGA) with 2% PE in 50 years.
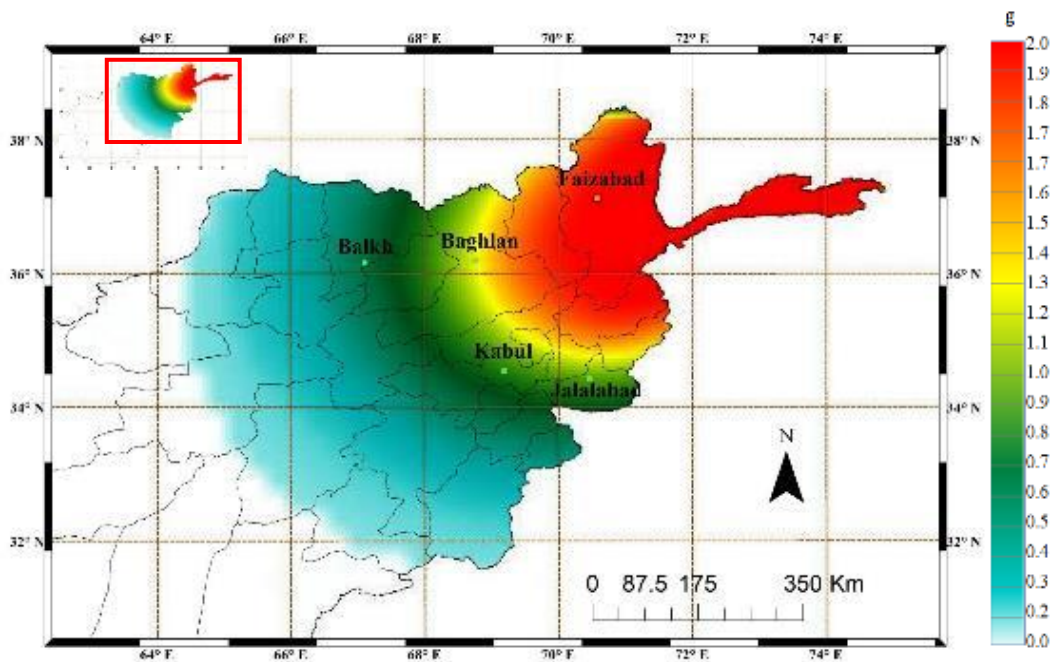
Figure 4.14 Earthquake hazard map (0.2-sec) with 2% PE in 50 years.
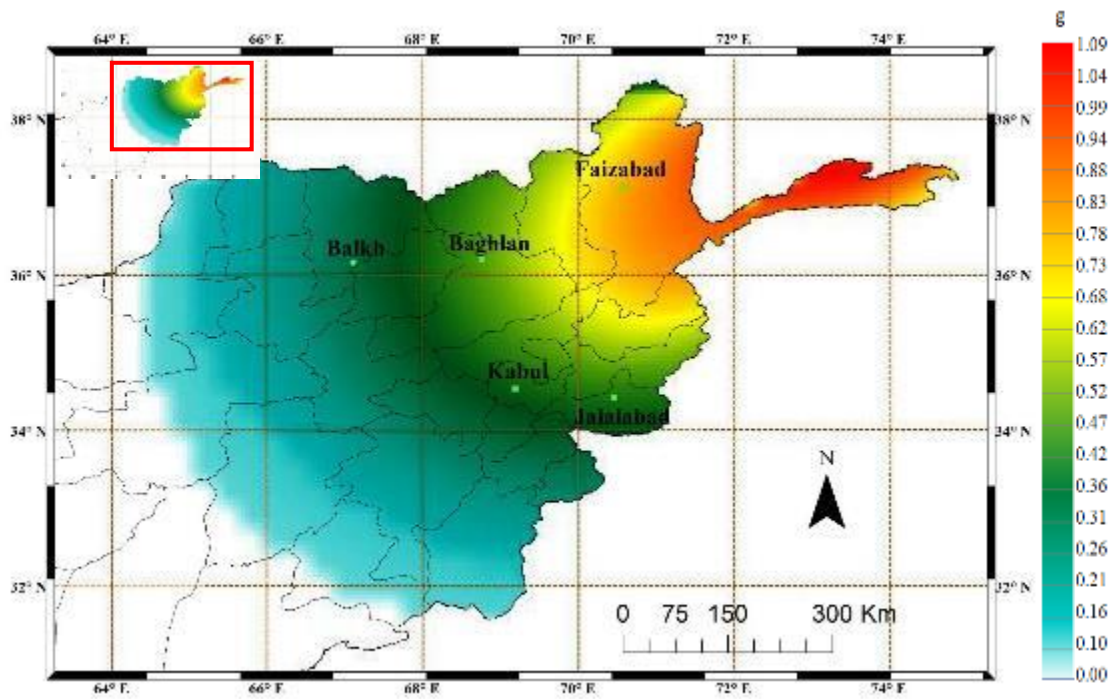
Figure 4.15 Earthquake hazard map (1-sec) with 2% PE in 50 years.
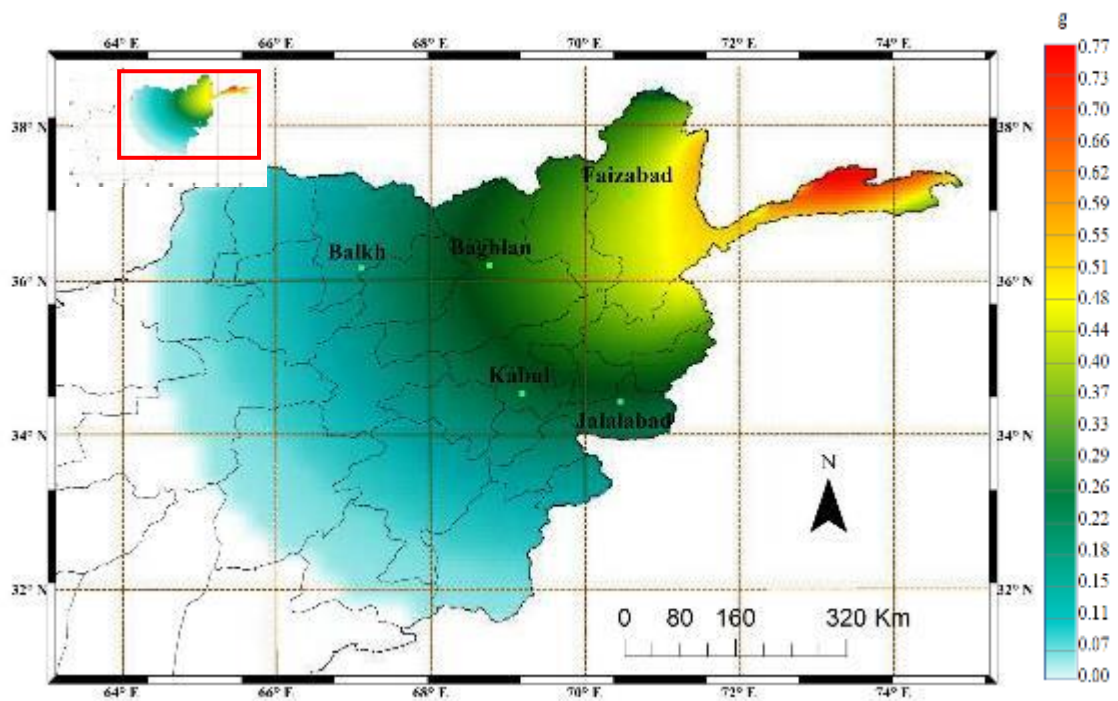
Figure 4.16 Earthquake hazard map (PGA) with 10% PE in 50 years.
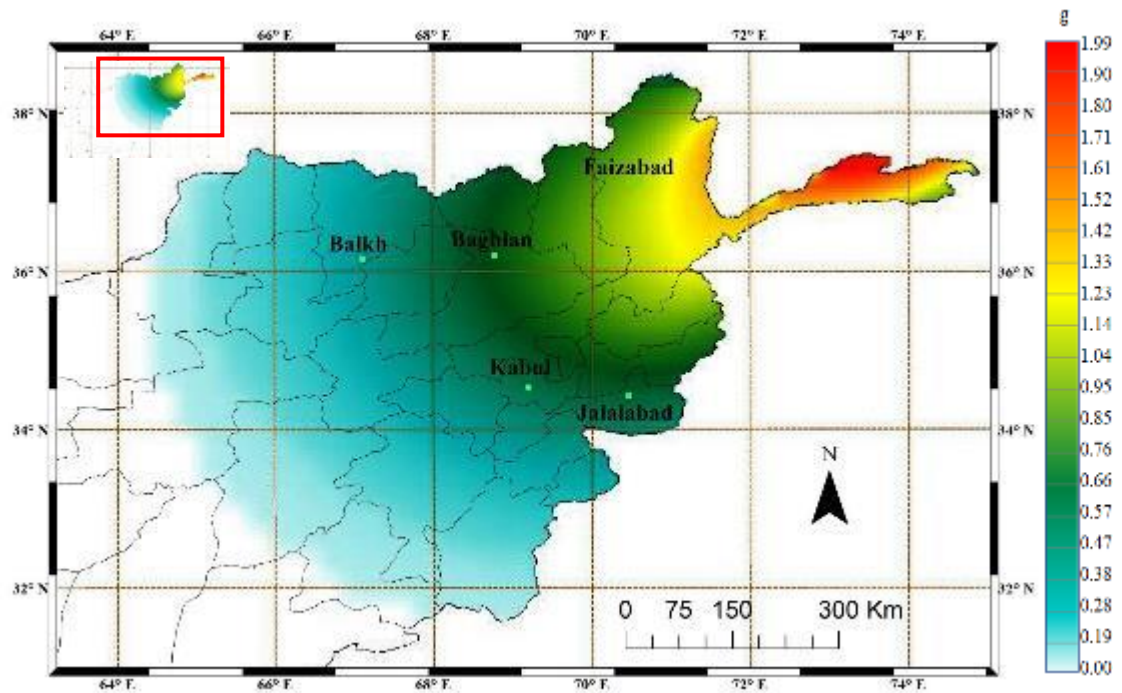
Figure 4.17 Earthquake hazard map (0.2-sec) with 10% PE in 50 years.
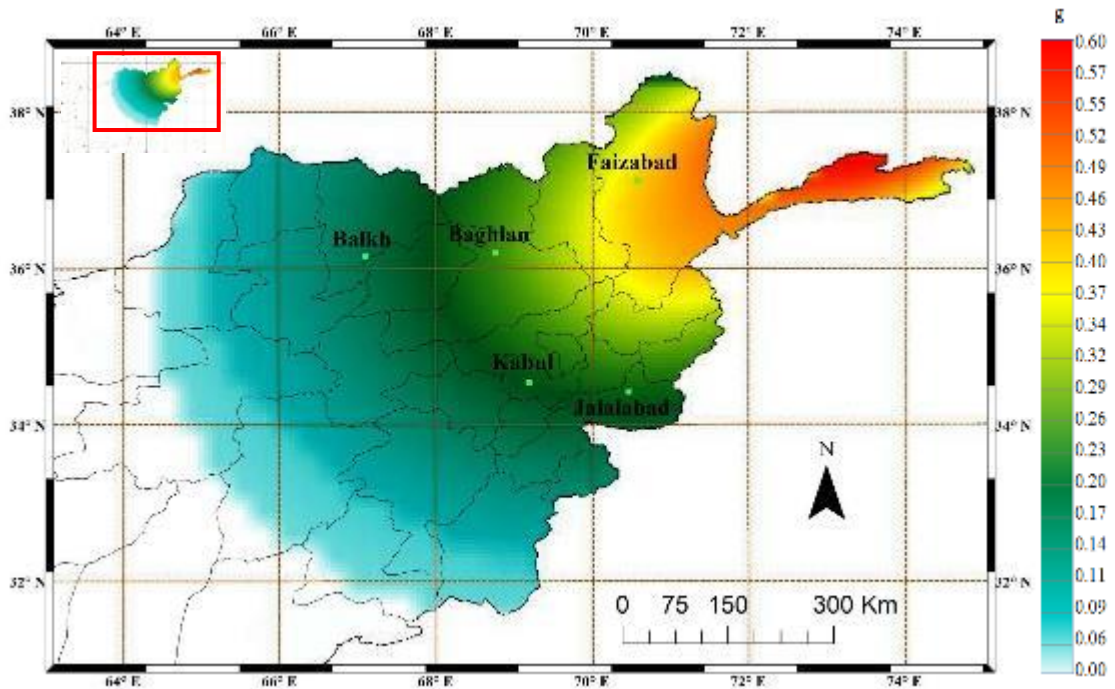
Figure 4.18 Earthquake hazard map (1.0-sec) with 10% probability of exceedance in 50 years.

4.3 Earthquake Risk Analysis

Several $M_w \geq 7.0$ earthquakes have occurred within 300 km or more of the Hindu Kush and Pamir region and In Mazar-e-Sharif, Figure 4.20 Active faults and location of $Mw \geq 7.0$ earthquakes both instrumental and historical earthquake in Afghanistan region.. The most recent being a $M_w7.6$ on 26 October 2015 that killed about 400 people. Another earthquake in this region occurred in 2002 just 20 km to the west of the 26 October 2015 event, and with a similar depth and thrust fault orientation (Hayes, 2017). The 2002 event caused more than 150 fatalities and the damage or destruction of over 400 houses in relation to an associated landslide. A $M_w7.4$ event in December 1983 at a similar depth just 8 km to the south of the October 26, 2015 earthquake resulted in 26 fatalities, hundreds of injuries and extensive damage in the region. The deadliest recent event ($M_w7.5$) in the region occurred 330 km to the southeast of the 26 October 2015 earthquake in the Kashmir region of Pakistan on October 8, 2005. This event killed at least 86,000 people and caused extensive damage. The 2005 event was a shallow event (26 km) and was caused by geologic forces that are distinctly different than those driving deep earthquakes in the Hindu Kush and Pamir region. An event of $M_w7.0$ in 819 in Faryab and $M_w7.0$ in 1505 in Kabul both with unidentified depths but less than 40 km has been reported in the historical catalogue of (Ambraseys & Bilham, 2003), and $M_w7.0$ in 1842 in Konar, and $M_w7.0$ 1956 in Bamiyan are reported in instrumental earthquake catalogues (ISC, 2016) & (USGS). All these earthquakes caused considerable damage and fatalities. We evaluated the seismic activity of the 8 shallow earthquake source zones in Afghanistan using the Gutenberg-Richter recurrence law given in equation 4-1 and the parameters provided in Table 4.3.
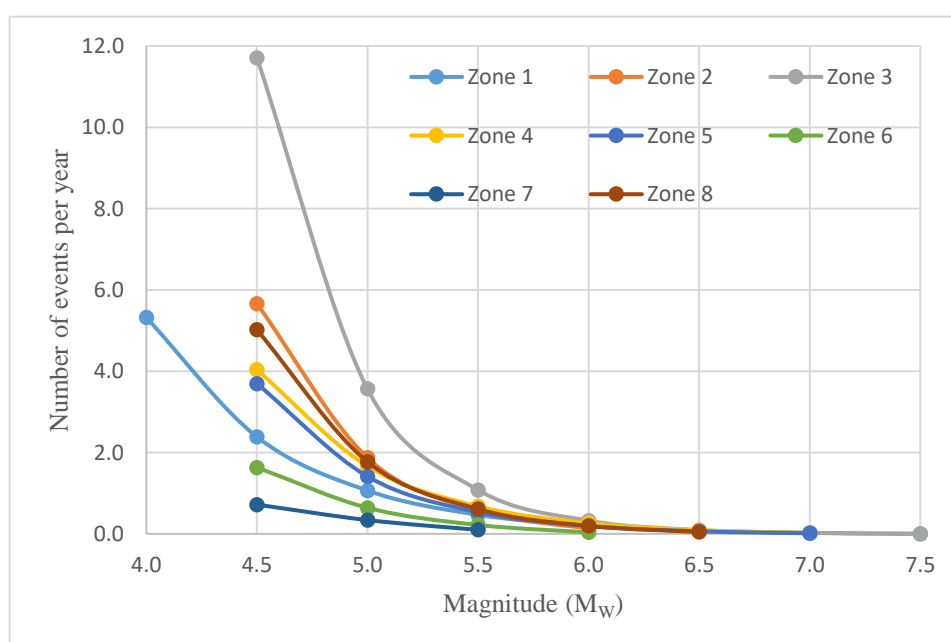
Figure 4.19 Seismic recurrence rate of the 8 shallow earthquake sources zones.
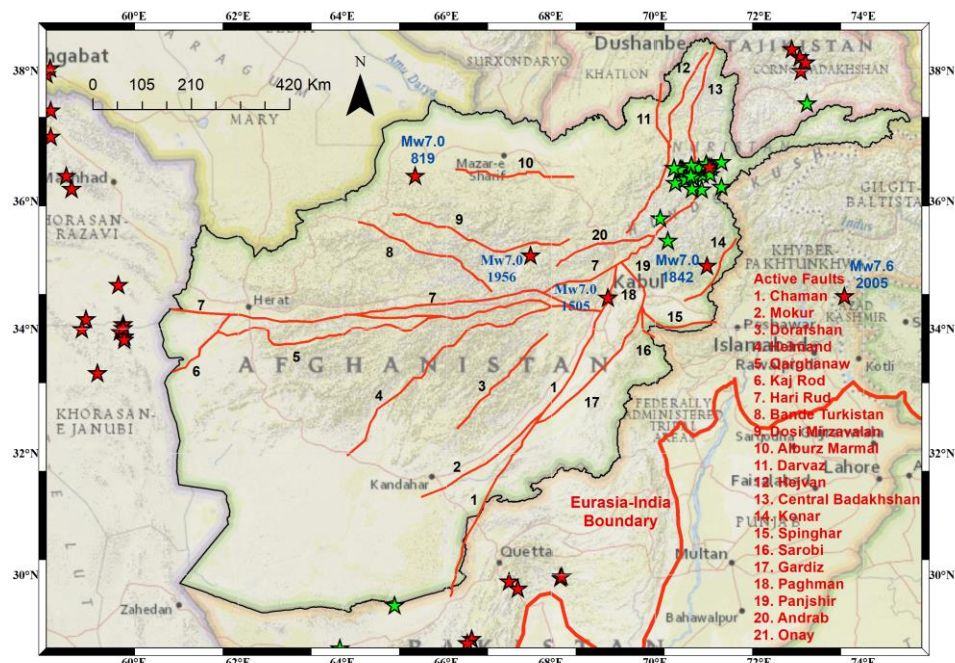
Figure4.20 Active faults and location of Mw≥7.0 earthquakes both instrumental and historical earthquake in Afghanistan region.

Seismic source zone 3 has the highest recurrence rate followed by source zone 2 and source zone 1, Figure 4.19. Seismic zone 8 has also a high recurrence rate but most of the events are outside Afghanistan border, effects of which may decrease to negligible amount when at the distances inside Afghanistan. The earthquake recurrence rate of the 8 shallow earthquake zones presented before is based on the distribution of the earthquakes only, regardless of the fault slip rates, location and orientation of the earthquake sources. The Chaman fault system has a reported slip rate of 2-20mm/year and higher rate where it enters western Pakistan (Lawrence, et al., 1992). The Indian plate has a 20-40mm/year slip rate where it comes close to a 300-400km segment of Chaman fault between (31°N-33.5°N), suggesting that $M_w>7.0$ could occur at 200 years interval along this segment (Ambraseys & Bilham, 2003). The main Chaman fault has not produced big earthquakes in historical and instrumental seismicity; however, its location near the Eurasia-India global fault, slip rate, and the potential of producing earthquakes as high as 2005 Kashmir earthquake, make seismic zone 1 and seismic zone 2 more having a higher risk factor comparing to other earthquake zones in Afghanistan Figure 4.20.

The historical earthquake catalogue of Afghanistan is quite incomplete making it difficult to predict future seismicity. The $M_w≥7$ historical earthquakes reported in the catalogue of (Ambraseys & Bilham, 2003) in the areas of Kabul and Mazar-e-Sharif remarks the need of some deterministic seismic hazard studies for those specific areas. Considering the faults' slip rates and locations, regional geological activities, earthquake recurrence rates in Figure 4.19, considerations from

(Ambraseys & Bilham, 2003), results of PSHA in this study and judgement of the authors, we divided Afghanistan into 4 earthquake activity zones, Figure 4.21.

The Chaman fault in the South-East Boundary Zone has a higher slip rate. The fault is near the Eurasia-India global fault boundary and seems to be accommodating most of the deformation of this global fault, and the high slip rate (20-40mm) of Eurasia-India plate when it comes near to this zone put it at higher risk comparing to other parts of Afghanistan. Existence of the Eurasia-India global plate and the slip rate increase the occurrence probability of a devastating earthquake. The North-East Zone is mostly a zone of deep earthquakes where shallow events also occur. It has the highest recurrence rate of earthquake occurrence and is a zone of higher risk in a second order.

The North Afghanistan Zone does not have big events in instrumental seismicity. However, two historical shallow earthquakes of $M_w=7.0$ have been reported and we gave it a risk of order 3 but almost near to North-East unless some deterministic studies are conducted corresponding to those earthquakes. The remaining part of Afghanistan is Southern-west Afghanistan that has the least active faults and the minimum earthquake recurrence rates, hence is subjected to comparatively to a lower earthquake risk.
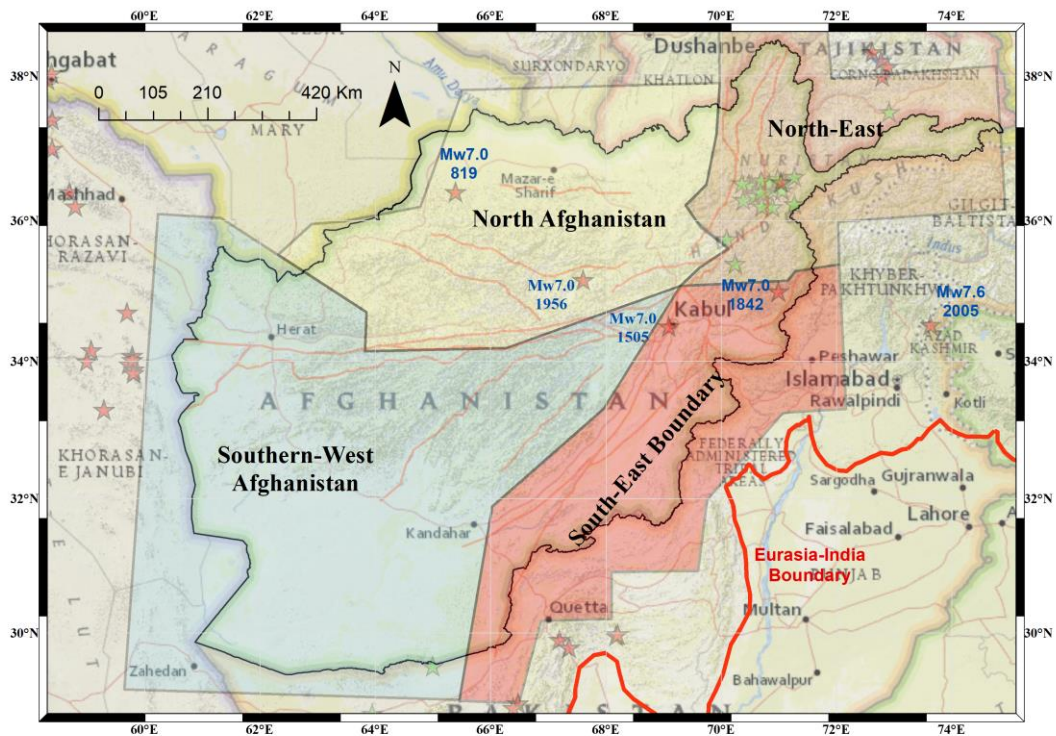
Figure 4.21 Earthquake risk zoning of Afghanistan resulted from this study. The South-East Boundary has the highest risk followed by North-East Afghanistan. North Afghanistan had few historical earthquakes, hence is in a risk of equal and close to the North-East seismic risk zone. Remaining part is the Southern-West Afghanistan where ground motion is low, hence it is the least risk zone.

4.4 Summary

Intermediate shallow earthquakes and high magnitude deep earthquakes have had considerable fatalities and damages in Afghanistan region. Shallow earthquakes of $M_w \geq 7.0$ occurring in the Pamir and Hindu Kush region or along the Chaman fault near Kabul or other lifelines could be a disaster, affecting a large portion of Afghanistan and adjacent Pakistan. The strong motion records are almost nil for the region making it difficult to precisely understand the actual phenomenon of the earthquakes happening in future. In the absence of such instrumental data, we used probabilistic earthquake hazard analysis approach to find out the anticipated ground motions in Afghanistan. The historical data from 8th century and instrumental data is used to define the seismic sources and source parameters. We augmented the conventional PSHA practice of using area sources by modeling faults as line sources. We calculated *b*-values corresponding to each source zone. The estimated 10% exceedance probability in 50 years of PGA at Kabul city is 19%g and the maximum spectral acceleration is 42%g corresponding to 0.2 second time period.

Results of this section are also presented in the form of contour maps and earthquake hazard curves. Estimated ground motion are close to some of the previous studies conducted for the region. It is a little high or low for some other areas which may be attributed to the varying *b*-value calculated based on available actual scenarios in this study. We also calculated the earthquake recurrence rate for the shallow earthquake source zones of Afghanistan. It is high for the north-east corner as well as for the southern-east boundaries of Afghanistan. We also assessed the geological activities in the region and proposed four earthquake activity zones. Although the simulated results for the southern-east Afghanistan is smaller compared to the northern-east, other geologic activities from global faults might also contribute to the earthquake activity of southern-east earthquake region and seems to be the severe earthquake zone in the country. The North-East of Afghanistan is a zone of both shallow and deep earthquakes induced from the displacements of faults inside Afghanistan only. Few historical events of $M_w = 7.0$ with little characteristics of the earthquake understood are reported in North Afghanistan. This signifies the importance of a thorough assessment on those earthquakes. The remaining Afghanistan is the southern-west part and seems to be free of significant earthquake events both in historical and instrumental eras as well as the geologic activity seems to be comparatively low.

The results presented here can be used in seismic analysis and design of infrastructural facilities in Kabul or other parts of Afghanistan. Nevertheless, the most important aspect is to be well-prepared against the worst scenarios such as the possibility of a great earthquake on the Chaman fault. The strong ground motions can be quite high, and these would have an important implication in the earthquake preparedness of Afghanistan with a hope that the devastating 2005 Mw7.6

Kashmir earthquake would not repeat. Although the strong motion instrumentation of Afghanistan is none, this study might be an important contribution for the seismic vulnerability of major settlements in Afghanistan.

CHAPTER 5   STRONG GROUND MOTION ESTIMATION FOR KABUL CITY

5.1 General

In this section, we estimate the strong ground motion using deterministic earthquake hazard approach for some of the specific earthquakes in Afghanistan with effects on Kabul. Kabul is the capital province of Afghanistan (34.55° N, 69.20° E), and the most populated (about 4.6 million people, (Kabul, 2017)) and the fastest growing city of the country. Kabul is also one of the largest cities (64th) in the world. Kabul city is at the southern east earthquake region of Afghanistan, a region with severe seismicity (Wheeler, et al., 2005). Three main faults meet and form a junction at the North of Kabul province. Main Chaman fault is passing west of Kabul in about 16 km from the City, Figure 5.1. The Transpressional Plate Boundary of Afghanistan is at the North-West of the Eurasia-India global plates boundary. This region has experienced devastating earthquakes and has caused immense damage to life and properties. Pamir and Hindu Kush where continental deep earthquakes take place is in about 300 km in the North-East of Kabul from where earthquakes usually create shocks in Kabul city. The $M_w7.5$ Hindu-Kush earthquake of October 26, 2015 with the epicenter 45 km north of Alaqahdari-ye Kiran wa Munjan of Badakhshan of Afghanistan at a depth of 210-212 km and death toll of approximately 400 is an example of the earthquakes that affects structures in Kabul city.

This earthquake was recorded at several regional accelerograph strong ground motion stations in Pakistan. The earthquake caused tremendous shake to the crowded city of Kabul. Damages to the old and new structures due to this earthquake in Kabul city has been unofficially reported. Building damage due to foundation failures due to liquefaction were also reported in several parts of the city. The MMI intensity of this event at Kabul city has been estimated to be VI. Although, Kabul city is located far away from the epicenter of this event and other large earthquakes, non-structural damage from the earthquakes in Pamir and Hindu Kush region of Afghanistan are usually and unofficially reported.

With the fast-increasing density of population and large industrial establishments in recent times, the occurrence probability of a high-magnitude earthquake from the regional geologic activities exists. The 2005 Mw 7.6 Kashmir earthquake was an example of such events. Occurrence of a great earthquake in or near Kabul, can be highly devastating. Therefore, it is of great need to have a reliable estimation of earthquake ground motion to construct earthquake-resistant structures. This requires good regional coverage of strong motion observations as well as detailed micro zonation studies for urban planning and design of infrastructures. There is lack of information on

ground motion data of strong earthquakes as its application in engineering is concerned. The available quantified information on seismic hazard in Afghanistan is sparse that earthquake engineers face problems in estimating the design ground motion at Kabul city. The lack of strong motion data can be remedied up to some extend by using analytical source mechanism models.
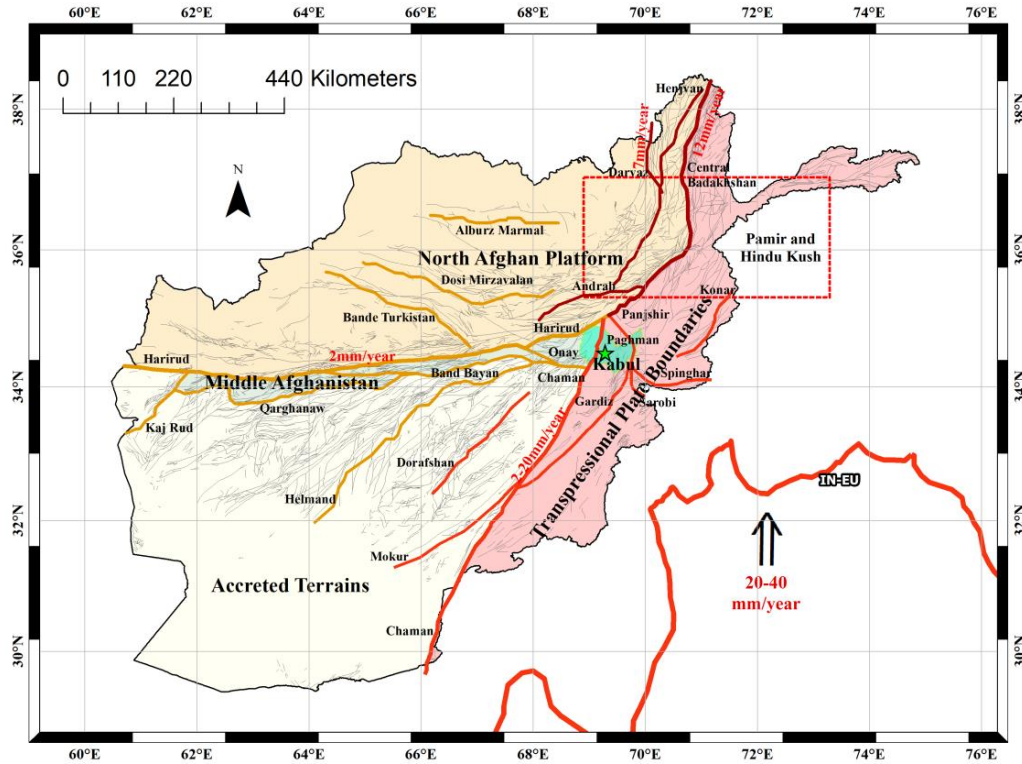
Figure 5.1 Active faults in Afghanistan, location of Kabul city, and M_w7.5 Hindu Kush earthquake. The line in grey are the many seismically unidentified faults. Faults map modified from (Wheeler, et al., 2005).

In this chapter, we evaluate the effects of earthquakes happening in Hindu Kush area by simulating the M_w 7.5 Hindu Kush earthquake of 26, October 2015 and a hypothetical earthquake anticipated to be taking place on a Main Chaman fault segment near Kabul city using different deterministic earthquake analysis approaches. The fault location and source parameters are retrieved from different international agencies that operate in the region for a long time. We used a modified version of stochastic point source model of (Boore, 1983), the method of (Aydan, 2012), (Aydan, et al., 2009a; Aydan, et al., 2009b) and a method proposed by (Sugito, et al., 2000) for simulating strong ground motion. The results are presented in the form of contour maps, time histories and Peak Ground Acceleration (PGA). In the following sections we explain these methods and their application to specific earthquakes in Afghanistan.

5.1.1   Strong Motion Simulation (SMSIM)

The Strong Motion Simulation or Stochastic Model Simulation method for simulating ground motions is based on the assumption that the amplitude of ground motion at a site can be specified in a deterministic way, with a random phase spectrum modified such that the motion is distributed over a duration related to the earthquake magnitude and to distance from the source. This method of simulating ground motions often goes by the name "the stochastic method." It is particularly useful for simulating the higher-frequency ground motions of most interest to engineers, and it is widely used to predict ground motions for regions of the world in which recordings of motion from damaging earthquakes are not available. This simple method has been successful in matching a variety of ground-motion measures for earthquakes with seismic moments spanning more than 12 orders of magnitude. One of the essential characteristics of the method is that it distills what is known about the various factors affecting ground motions (source, path, and site) into simple functional forms that can be used to predict ground motions. SMSIM is a set of programs for simulating ground motions based on the stochastic method. The programs are based on modifications made by David M. Boore to the stochastic method first introduced by (Hanks & McGuire, 1981). The source codes are written in Fortran, and executables that can be used on a PC.

5.1.2   Strong Motion Prediction on Rock Surface by Superposed Evolutionary Spectra

This method is a prediction model for strong ground motion on rock surface with the shear wave velocity of $v_s=500\sim600$ m/sec. It is developed based on strong motion dataset consisting of 118 components of major Japanese accelerograms including the records from the 1995 Hyogoken-nambu Earthquake. The model incorporates the effect of direction of successive faulting relative to site using the superposing technique of evolutionary power spectra in time domain. The program incorporates two types of prediction models: the Model-I for given earthquake magnitude and hypo-central distance, and the Model-II for given fault parameters, such as fault length and width, seismic moment of fault, rupture pattern and rupture velocity , and propagation velocity of seismic waves. The Model-II incorporates the effect fault size, successive fault rupture, and rupture direction, on characteristics of ground motion. We used Model-II to estimate the ground motion for a hypothetical earthquake taking place near Kabul city. The model is explained in the following sections.

5.1.2.1   *Prediction Model for Given Fault Parameters (Model -II)*

The basic ground motion prediction Model-I is extended into the model which incorporates size of the fault, fault rupture direction and its velocity, and seismic moment as a parameter of

earthquake scale, Figure 5.2. A fault is divided into several small events. In this extended model, the arriving time lag resulted from rupture on the fault and difference of propagation distance of ground motions for each individual unit event are considered. Consequently, the evolutionary power spectra for great earthquakes are given from the superposition of those from each unit event on the time domain. The steps for estimating strong ground motion for a specific earthquake is explained below.

(1) Calculation of the number of superposition N_G, for given seismic moment, M_0, and identification of the integral numbers along both axes, N_x and N_y, by which the given fault can be divided properly according to the fault dimension.

(2) Calculation of the hypo-central distance, R_{ij}, and mean arrival time lag, $t_{a_{ij}}$, of seismic motion for each unit event considering the fault dimension, rupture velocity, and propagation velocity of seismic waves, as well as the geometrical condition between a specific site and a fault.

(3) Calculate the evolutionary spectra, G_{ij}, for each distance, R_{ij}, and M=6.0 using the Model-I, and superpose the evolutionary power spectra, G_{x_0}, considering the arrival time lag of each unit event; and

(4) Generation of the ground motion time history.
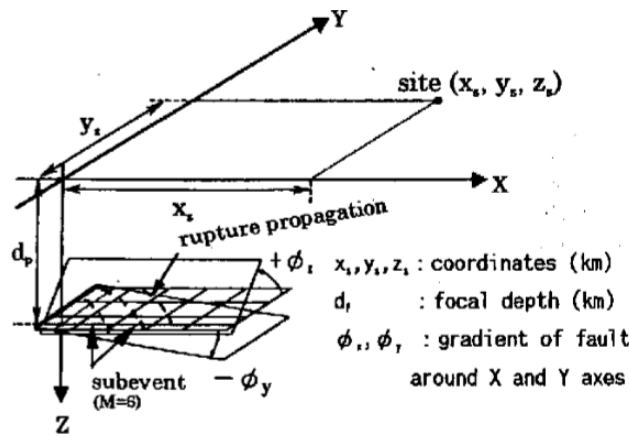
Figure 5.2 Illustration of fault modelling with multiple fault rupture, EMPR-II (Sugito, et al., 2000).

5.2 Applications

In the following sections, we apply each of the methods explained before to specific earthquakes in Afghanistan. There earthquake from Hindu Kush and Pamir region usually create big shocks in Kabul city. Although, damage to structures have not been reported, however, unofficial reports

imply that these earthquakes create damage to structural and non-structural members of buildings. We have estimated the ground motion from the 2015 Mw 7.6 Hindu Kush earthquake using Stochastic Simulation (SMSIM) at Kabul city and is presented in the following section. The potential for an earthquake Mw≥7.0 along Chaman Fault near Kabul is probably very high. We simulated a hypothetical earthquake along Chaman fault near Kabul using the Superposed Evolutionary Spectra method of (Sugito, et al., 2000).

5.2.1 Simulation of 2015 M$_w$ 7.5 Hindu Kush Earthquake,

The tectonic setting of Afghanistan involves fundamentally the northward motion of the Indian plate sub-ducting beneath Eurasia plate in the Tibet. Movement of the Indian plate is accommodated in Afghanistan and Pakistan by the Chaman fault through mainly sinistral faulting, Figure 5.3.
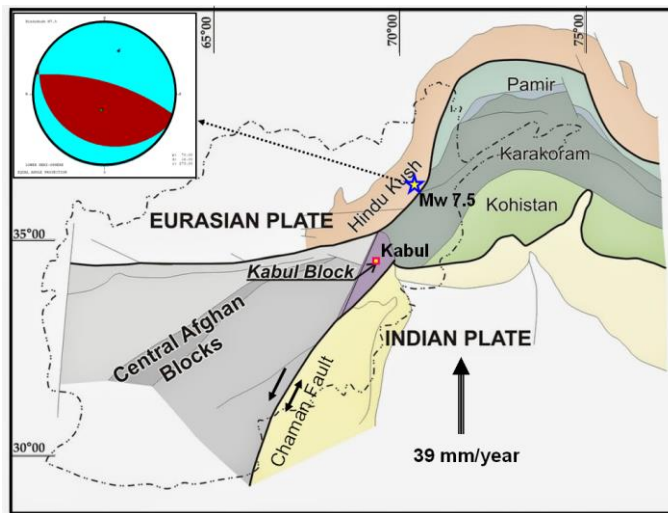
Figure 5.3 Illustration of Kabul block near Eurasia-India global fault.

However, the tectonic setting is more complex in the vicinities of Hindu Kush Mountains. Figure 5.4 shows a cross-section depicting the subduction of the Indian plate beneath the Eurasia plate in the vicinity of the Hindu Kush Mountains. It is noted that the Indian plate is steeply bended, and it is probably in the process of detachment from the Indian Plate and sinking into the upper mantle, which would affect the seismicity of the region for decades from now on.

The M$_w$ 7.5 Hindu Kush earthquake of Afghanistan took place on 26 October 2015 and the instrumental data of the earthquake is presented in Table 5.1 together with some estimations. The focal mechanism of the earthquake was due to thrust faulting with a dip direction and dip angle of 16° and 70°, respectively (USGS). The rake angle was 273°, which implies almost thrust faulting with a slight sinistral component. The hypocenter depth of the earthquake was 210-213 km.
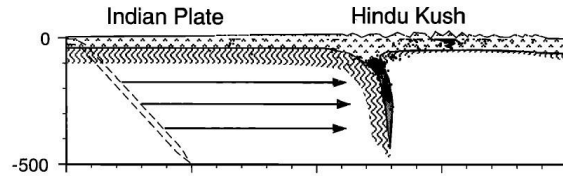
Figure 5.4 Subduction of Indian Plate beneath Hindu-Kush Mountains. Modified from (Pavlis & Das, 2000).

Table 5.1 Instrumental and estimated data for 2015 M_w 7.5 Hindu Kush earthquake

Institute	Strike/dip/rake	Slip (cm)	Rupture Duration (s)	Fault length (km)
USGS	106/70/87	615	20+5	40
HARVARD	104/69/91		27.2	
GFZ	106/65/95			
This study*	-	380	31.5	88

* Based on (Aydan, 2012) empirical formulas for Mw 7.5

The earthquake was widely felt in north-eastern Afghanistan, north-western Indian, and northern Pakistan. It killed at least 115 people in Jalalabad and destroyed more than 4,000 homes in Jarm, Badakhshan of Afghanistan. The event was more strongly felt in Pakistan and killed at least 289 people and destroyed more than 29,230 houses there. The Intensity of this event was (VI) at Bagrami and Jalalabad, (V) at Kabul and Mahmud-e-Raqi, (VII) at Abbottabad and Wah of Pakistan; (VI) at Rawalpindi, (V) at Amritsar, Badambagh and Palwal of India and at Dushanbe of Tajikstan. It was felt (III) at Tashkent, Uzbekistan. It was also felt (II) at Ghorahi and Kathmandu, Nepal, Doha of Qatar (USGS). The intensity and inferred strong motions data of this event are presented in Table 5.3. Although there is no acceleration data taken in Kabul for this earthquake, we used some records from Peshawar, Nilore (Islamabad) and Dera-e-Ismail Khan of Pakistan. The acceleration at these stations are listed in Table 5.2 and the acceleration record and response spectra are presented in Figure 5.5, Figure 5.6 and Figure 5.7.

The epicentral distance of Peshawar in Pakistan is quite like the epicentral distance of Kabul city from the location of the 2015 M_w Hindu Kush earthquake. The earthquake caused damage to mudbrick and stone masonry with earthen mortar in Peshawar and Kabul Cities. The analyses of collapsed structures imply that the acceleration might be up to 0.158g in Kabul city, which may correspond to spectral acceleration rather than the base acceleration. The heavy damage in Peshawar also support the high spectral accelerations shown in Figure 5.5. It should be also noted that the hypocenter of the earthquake is very deep. It is expected that high frequency waves would attenuate, and long-period components would be more dominant. As the earthquake was felt at far-distant locations, the observations support this conclusion.

Table 5.2 Strong motions for2015 M_w 7.5 Hindu Kush earthquake, retrieved from (Ahmad, 2015).

Institute	Epicentral distance (km)	EW	NS	UD
Peshawar	280	0.05g	0.053g	0.038g
Nilore	430	0.021g	0.020g	0.017g
D.I. Khan	514	0.026g	0.036g	0.015g

Table 5.3 Intensities and inferred strong ground motion for 2015 M_w 7.5 Hindu Kush earthquake[*].

Locality	Network	Intensity (MMI)	PGA (cm/s^2)	PGV (cm/s)	Distance (km)
Charikar	DYFI	V	43	5.44	277
Kabul	DYFI	VI	70	9.74	306
Kabul	DYFI	V	51	6.77	309
Kabul	DYFI	V	42	5.44	316
Kabul	IU	VI	22	1.7	315
Dushanbe	DYFI	V	42	5.44	303
Garm	TJ	IV	53	1.9	315
Tashkent	DYFI	III	4	-	540
Peshawar	DYFI	V	45	5.85	339
Peshawar	DYFI	VI	70	9.74	341
Islamabad	DYFI	VII	139	21.71	391
Srinagar	DYFI	V	54	7.28	489
Islamabad	DYFI	VI	108	16.22	393
Islamabad	DYFI	V	37	4.7	384

[*]Data in this table is retrieved from USGS website.
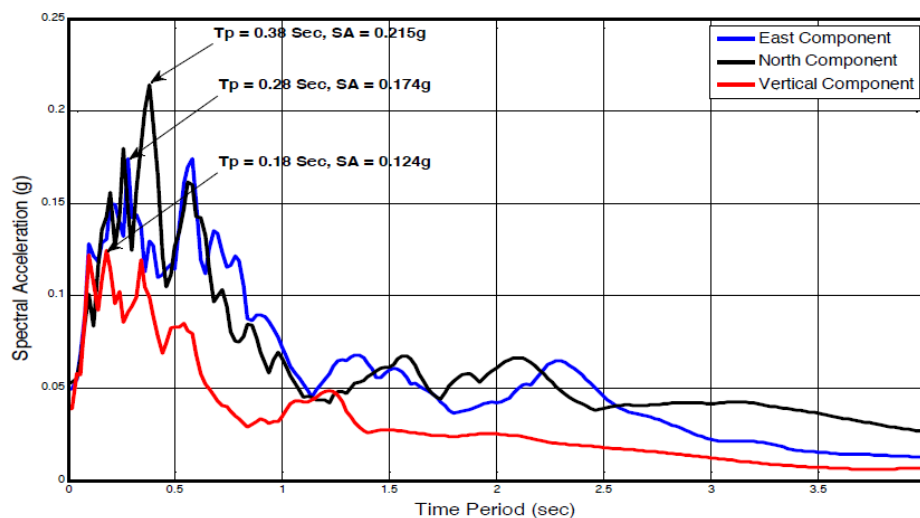
Figure 5.5 Response spectra of acceleration records at Peshawar (Ahmad, 2015)
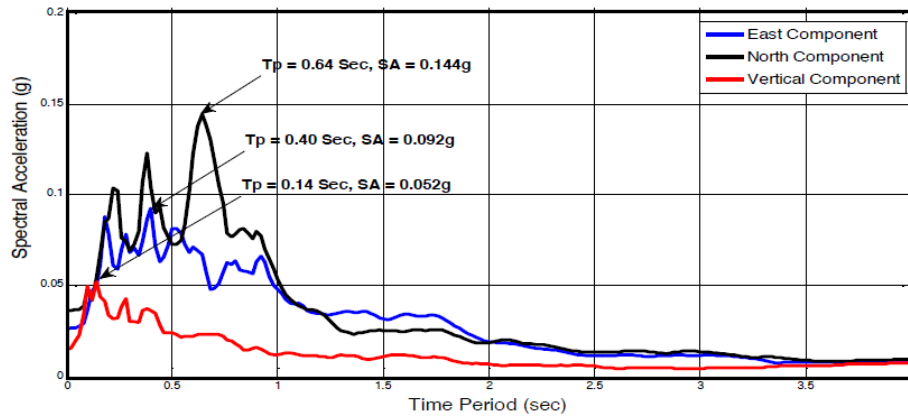
Figure 5.6 Response spectra of acceleration records at DI Khan (Ahmad, 2015)

(Horizontal East Component)

PGA = 0.05g, Bracketed Duration = 61.12sec

(Horizontal North Component)

PGA = 0.053g, Bracketed Duration = 58.05sec

(Vertical Component)

PGA = 0.038, Bracketed Duration = 73.47sec
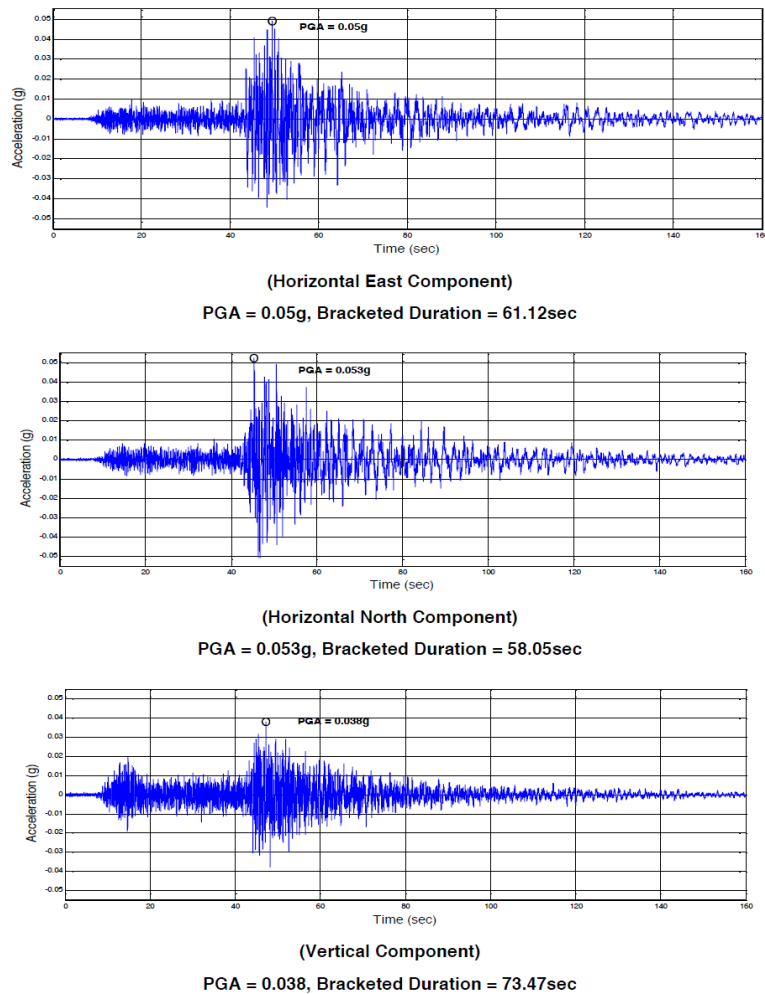
Figure 5.7 Acceleration records at Peshawar (Ahmad, 2015).

5.2.1.1 *Simulation Method and Model Parameters*

We used the stochastic seismological model originally proposed by (Hanks & McGuire, 1981) and later generalized by (Boore, 1983) for simulating synthetic acceleration time histories. This model is a good alternate for simulating synthetic acceleration time histories with few known source and medium parameters. Here, ground motion is modelled as a band limited finite duration

Gaussian white noise in which the radiated energy is assumed to be distributed over a specified duration.

In this method, various factors affecting ground motion source, path, and site factors are put together into a physically determined algorithm and is used to predict ground motion. The model parameters used for simulation are given in Table 5.4. The distance between Kabul city and location of this earthquake is about 300km. The simulated acceleration, velocity and displacement time series are presented in Figure 5.8. The PGA at Kabul city is about 7 gals. This number is quite small comparing to those recorded in similar distances of Pakistan. Accelerations reported in Kabul is between 22 gals to 70 gals. The results show a smaller number comparing to the minimum recorded acceleration in Kabul city. The simulated response spectra for Kabul city at bedrock is presented in Figure 5.9, and the response spectra for Kabul city at ground surface is presented in Figure 5.10. The acceleration response spectra flat up to 2-seconds.

Table 5.4 Model parameters used in simulation

Acceleration Fourier Amplitude Spectrum	$A(f,M_0,R)=S(f,M_0)D(f,R)P(f)$
Source Spectrum-*Brune Source Spectrum*	$S(f,M_0)=C(2\pi f)^2 M_0 * 1/(1+f/f_c)^2$
	$C=R_\varnothing FV/(4\pi\rho\beta^3 R_1)$
	$R_\varnothing=0.55$, $F=2$, $V=\sqrt{2}$
	$\rho=2.8 g/cm^3$
Corner Frequency	$F_c=4.9*10^6 \beta\Delta_\sigma/M_0^-$
	$\beta=3.5$ km/s
	$\Delta_\sigma=100$ bars
Attenuation	$D(f,R)=Dg(f,R)D(f)$
Geometric spreading	$Dg(R)=1/R$ (R<70 km)
	$Dg(R)=1/70; 70<R<130$ km
	$Dg(R)=1/70(130/R)^{0.5}$ R>130 km
Q model-Anelastic Attenuation	$Q(f)=220f^{0.52}$
Low-Cut Filter	$P(f)=\exp(-\pi\kappa f)$
	Kaapa (κ)=0.006 hard rock
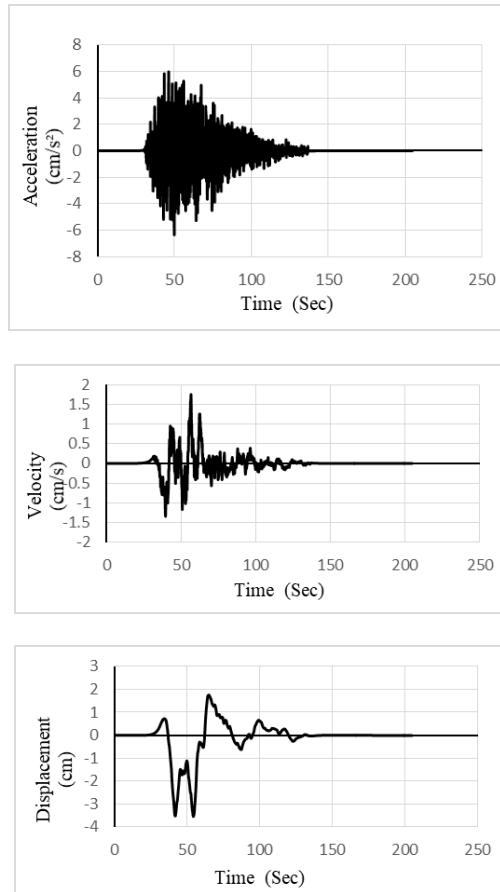
Figure 5.8 Acceleration, velocity and displacement time series, M_w=7.5, R=300 km.
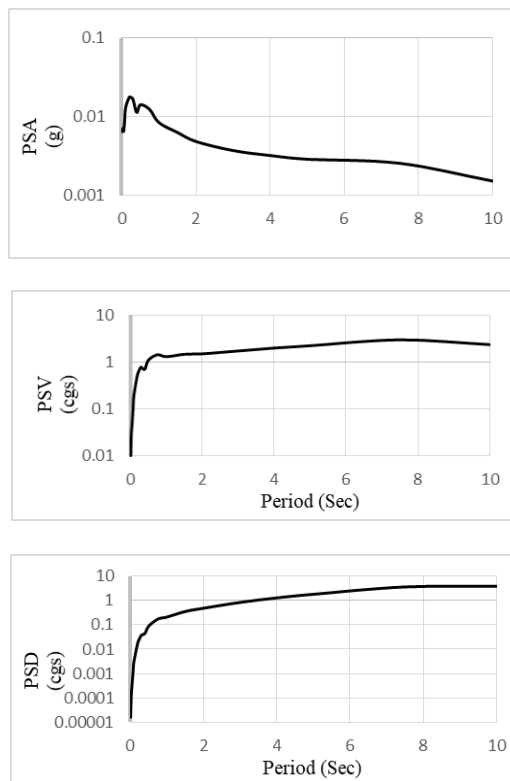
Figure 5.9 Response spectra at bedrock, M_w 7.5, R 300 km
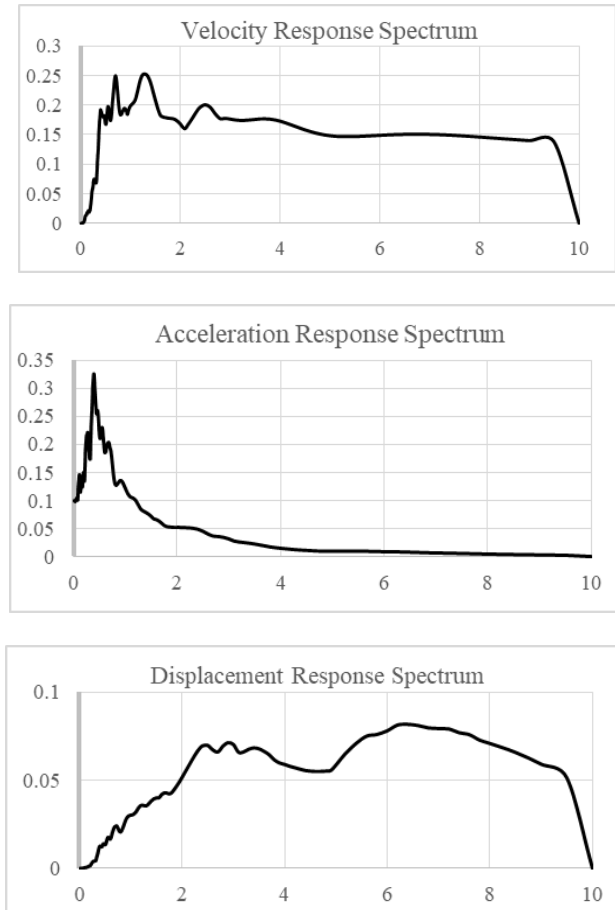
Figure 5.10 Surface level response at 5% damping, M$_w$7.5, R 300 km

The method presented previously utilizes Green Function Method while its parameters are based on some empirical relations. Here, we utilize a method proposed by (Aydan, 2012; Aydan, et al., 2009a; Aydan, et al., 2009b) to estimate the distribution of maximum strong motions for Kabul city. The method itself here is used for estimating the maximum ground acceleration using the empirical relations for inter-plate earthquakes as the 2015 M$_w$7.5 Hindu Kush earthquake occurred at the plate boundary between the Indian plate and Eurasia plate. The source parameters presented before are used in this method. The estimations of the maximum ground acceleration at the ground surface at the epicenter is only 95 gals and it attenuates to 4 gals beyond 250 km, Figure 5.11. Nevertheless, the directional effects in the attenuation of maximum ground acceleration are well evaluated. Results of the above two methods are almost matching, they are quite small to the values reported in Kabul, although.
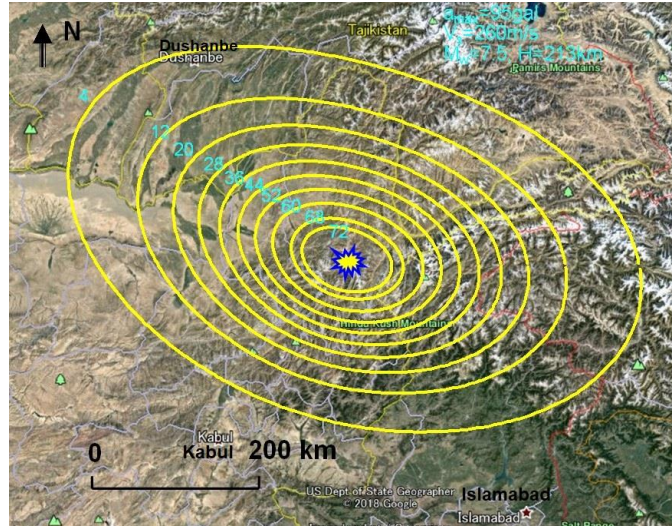
Figure 5.11 Estimated maximum ground accelerations for the Mw 7.5 earthquake using the method of (Aydan, 2012; Aydan, et al., 2009a; Aydan, et al., 2009b).

5.2.2 Strong Motion Estimation by Empirical Approaches

Although, the damaging effects of the 2015 Hindu Kush earthquake was felt widely, the strong motions in Kabul city due to larger earthquakes are much more important. The major fault near Kabul city is the famous Chaman fault, which passes at about 16 km NW of the city. This fault joins the Hari-Rud fault at the north of Kabul city. We segmented the Chaman fault and the nearest segment to Kabul city is 100 km long, Figure 5.12. A historical earthquake of M_w=7.0 1505 has also been reported in the catalogue of (Ambraseys & Bilham, 2003), Figure 5.13. Additionally, as the main Chaman fault absorbs most of the Eurasia-India global fault movement, occurrence probability of high-magnitude earthquakes along this fault cannot be denied. We considered a hypothetical earthquake along the 100km long segment of Main Chaman fault and simulated the ground motion using the method proposed by (Aydan, et al., 2009a; Aydan, et al., 2009b; Aydan, 2012). We calculated the characteristics of the hypothetical earthquake which are presented in Table 5.5. Figure 5.14 and Figure 5.15 show the estimated contours of maximum ground acceleration and maximum ground velocity for bedrock by assuming that the fault has a strike, dip and rake angle with a hypocenter depth of 20 km as given in Table 5.5. The shear wave velocity of bedrock is taken as 760 m/s.

Table 5.5 Characteristics of anticipated earthquake

Length (km)	Strike/dip/rake	Mw	Slip (cm)	Rupture Duration (s)
90	206/90/0	7.24	274	23
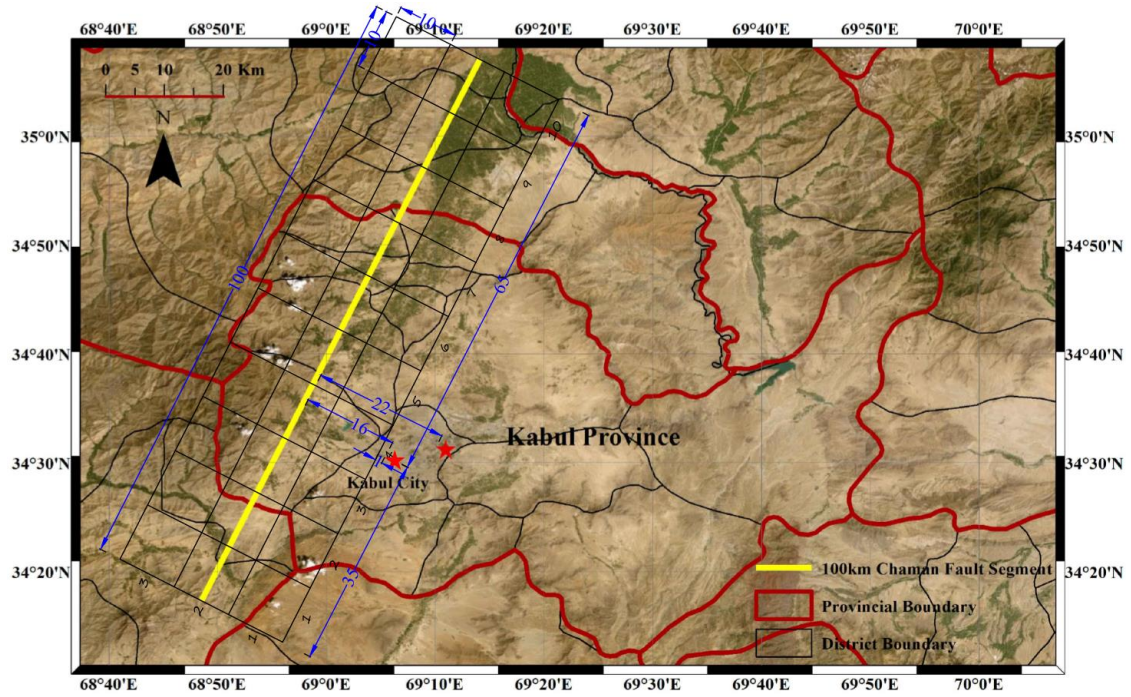
Figure 5.12 100 km segment of Main Chaman fault at the vicinities of Kabul city.
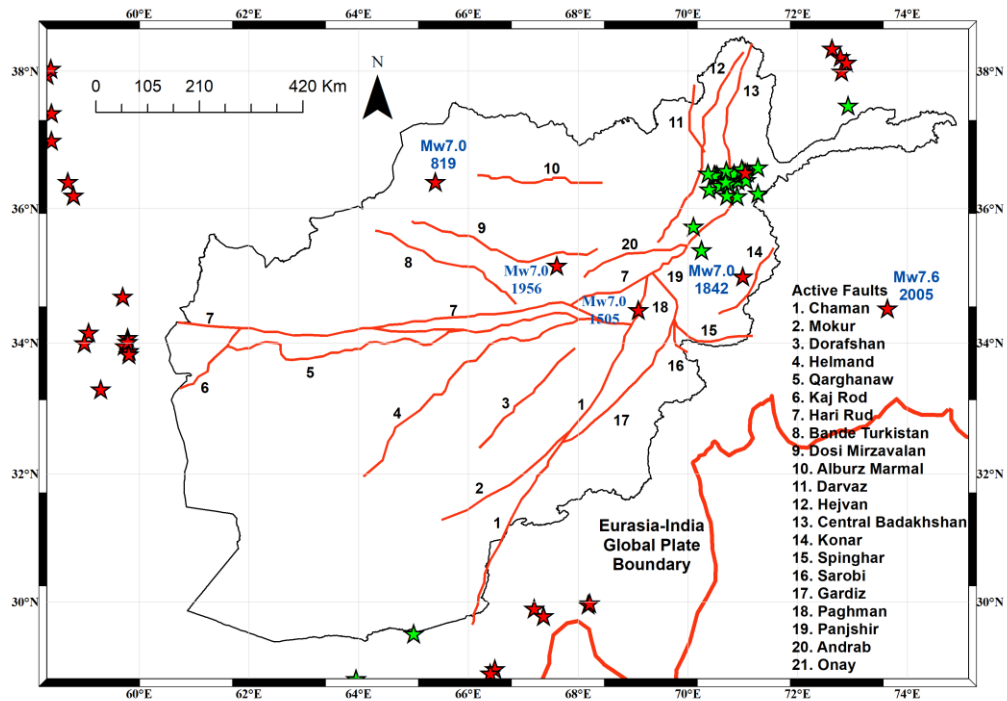
Figure 5.13 Mw≥7.0 earthquakes in Afghanistan, active faults and location of Eurasia-India global plate boundary. Red stars represent shallow earthquakes (M_w≤50km) and blue stars represent deep earthquakes (M_w>50km).
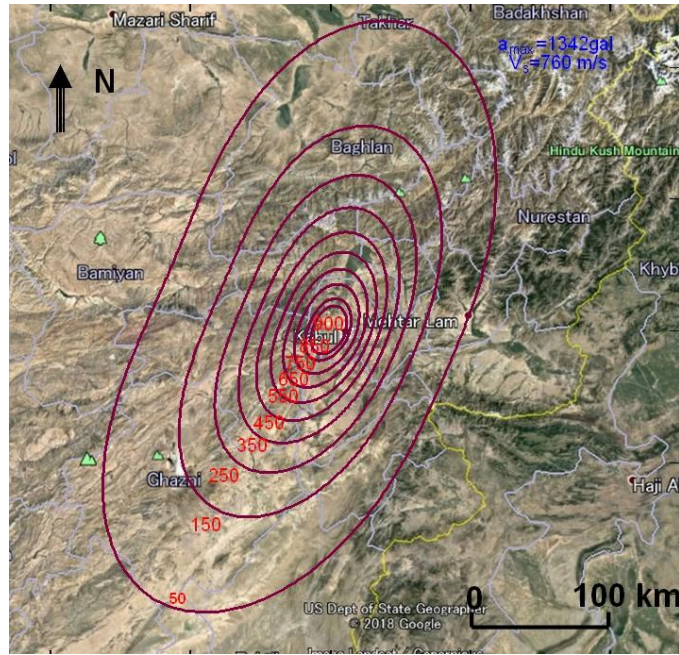
Figure 5.14 Estimated maximum ground acceleration contour for the hypothetical earthquake of M_w 7.24 on the Chaman Fault near Kabul city.
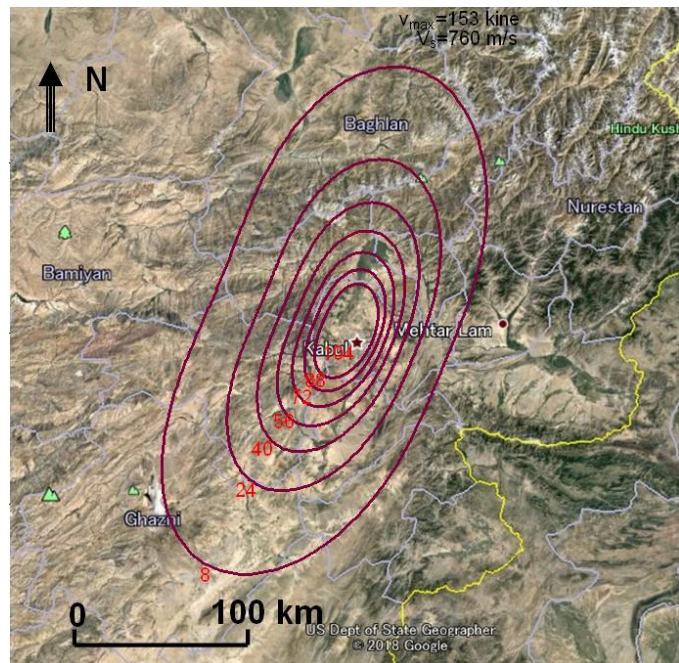
Figure 5.15 Estimated maximum ground velocity contour for the hypothetical earthquake of M_w 7.24 on the Chaman fault near Kabul city.

5.2.3 Strong Motion Estimation of a Hypothetical Earthquake along Chaman Fault using the Superposed Evolutionary Spectra (Model -II)

We used the method of ground motion estimation proposed by (Sugito, et al., 2000) to simulate the hypothetical earthquake along the 100 km long Main Chaman fault segment near Kabul city. We used the EMPR-II model of this method which is used for simulating earthquakes with given

fault parameters. We considered a fault area of 100 km by 30 km and divided it into a grid of elements (10 x 10) km, assuming that the rupture could initiate at the center of each of these elements Figure 5.16. We used three different asperity locations and simulated for all the 30 scenarios of each of these three cases, Figure 5.17. The green bold line represents the fault, hatched cells with red line border represents asperity locations and the numbers in each cell represents the asperity ratio for every element. Red star is the rupture initiating point which varies with each element. The simulated ground motions corresponding to the 90 scenarios is presented in Table 5.6. The ground motions are maximum when rupture occurs at 8-1, case 1. We also calculated the ground motion at the vicinity of the epicenter at element 4-1 which has the least distance from Kabul city. The time history series, Fourier amplitude and Pseudo Velocity with 5% at Kabul city for case-1 when the rupture initiates at 8-1 and at the vicinity of the epicenter of element 4-1 is presented in Figure 5.18 and Figure 5.19.
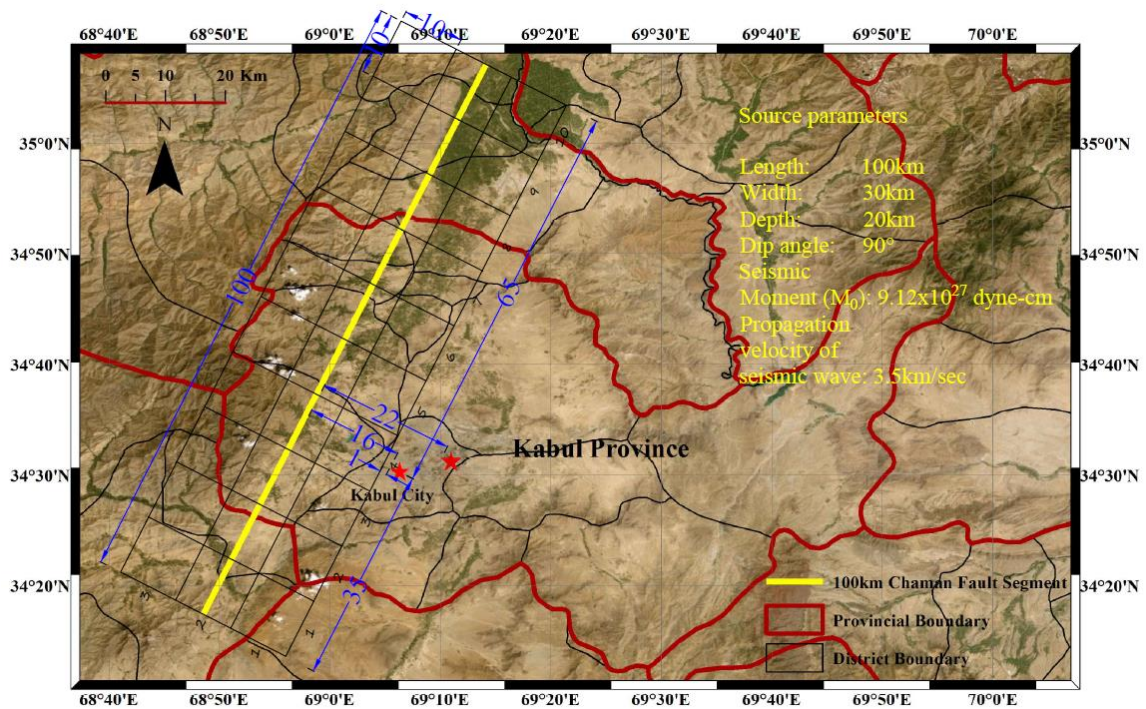
Figure 5.16 Location of Kabul and distribution of fault area into equal elements and source parameters.

The ground motion at Kabul city is maximum when rupture occurs at element 8-1, case 1. Maximum acceleration, velocity and displacement are 513 gal, 42 kine and 10 cm corresponding to 16.74 seconds, respectively. The acceleration, velocity and displacement are 953 gal, 98 kine and 30 cm corresponding to 10.92 seconds respectively at the epicenter when the rupture start at 4-1, case 1. The acceleration time history for these two scenarios is presented in Figure 5.18 and the velocity and displacement time series, Pseudo velocity and Fourier amplitude for these two

scenarios are presented in Figure 5.19. Results of the method used before is close to the results presented in this section.

Kabul is small city with a high population density. There are structures built and people living at the vicinities of the fault. For calculations, we selected a specific point representing Kabul city; however, the city itself is distributed in several kilometer radius from the location of Kabul city indicated by star below the 4-1 element of the fault in Figure 5.17. It implies that the epicenter of the anticipated earthquake can be a lifeline and as noted from the figures, the ground acceleration could be about 953 gal for Kabul city. Similarly, the maximum ground velocity would be about 100 kine.
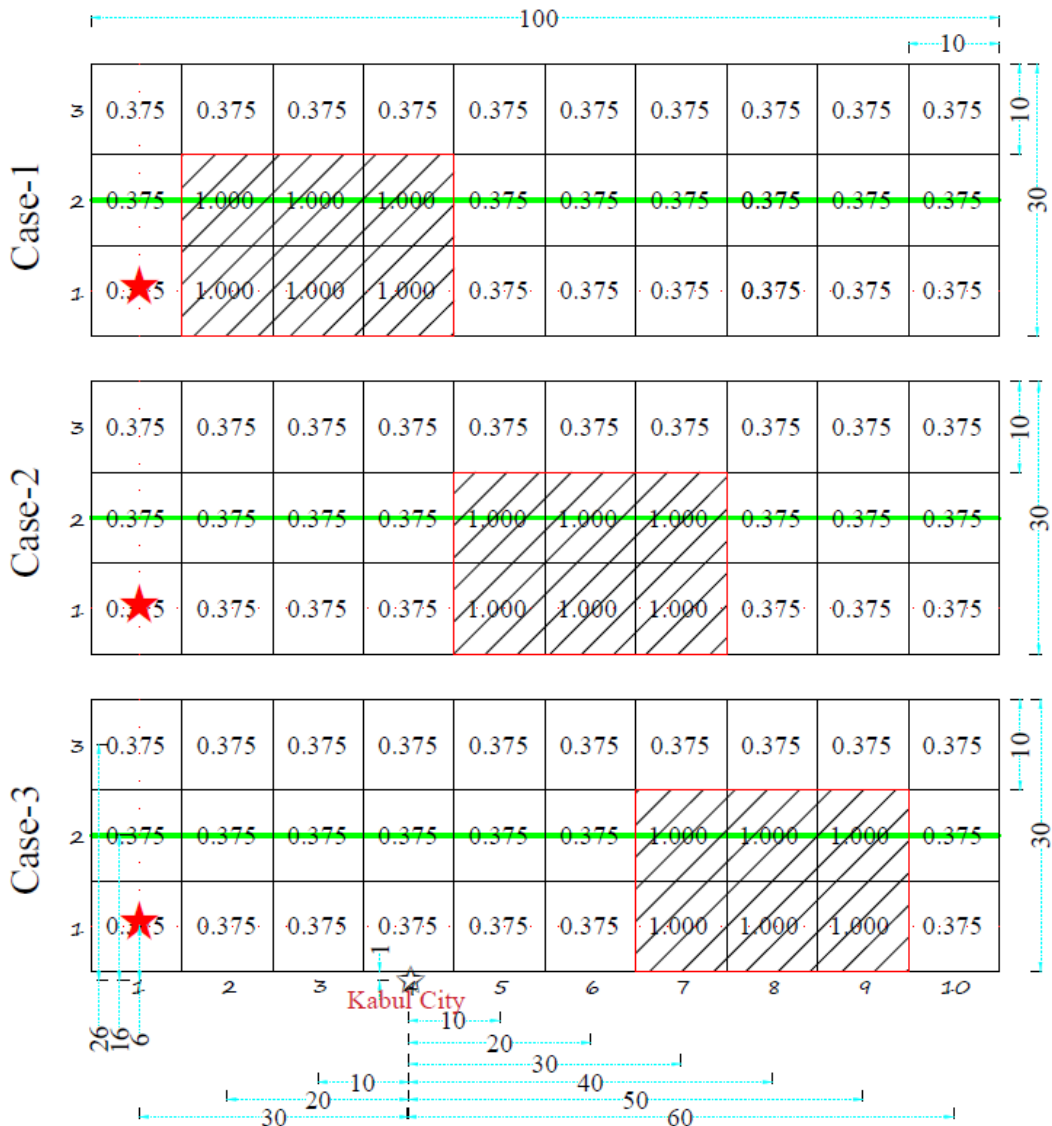
Figure 5.17 Asperity location and ratios for three cases. Kabul city is located 16km beneath element 4-1 and is the target site. Site location is indicated by measurements at the bottom and left of Case-3 which is the same for cases 1 and 2.
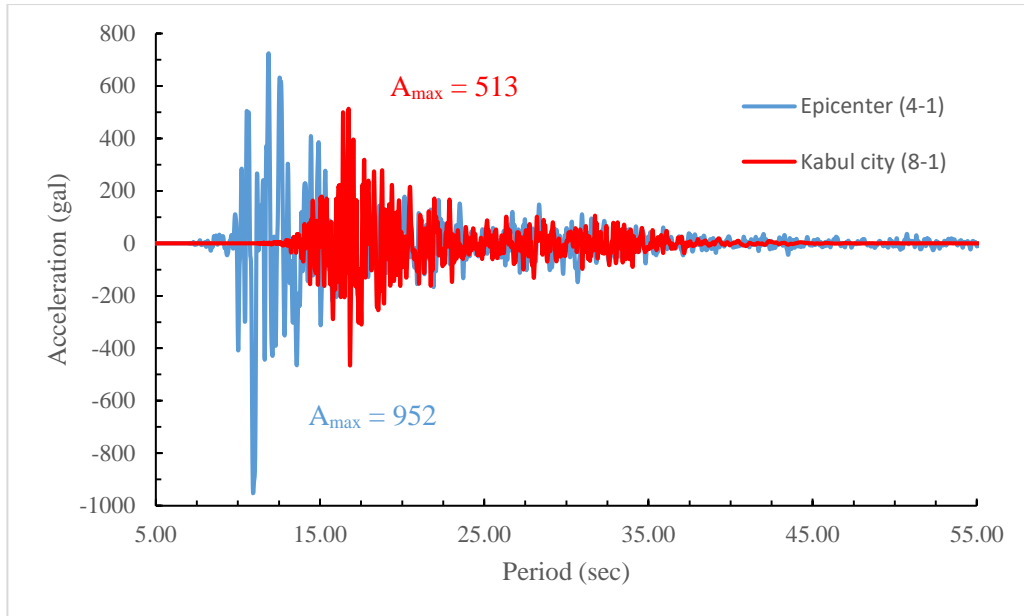
Figure 5.18 Acceleration time series. Red line represents the acceleration at Kabul city when the rupture starts at 8-1, Case 1 and the blue line represents the acceleration series at the vicinities of the epicenter when the rupture starts at 4-1, Case 1.

In this section, we simulated strong ground motion induced at the vicinity of Kabul city by the 2015 M_w7.5 Hindu Kush earthquake and source to site distance of 300 km using SMSIM, a FORTRAN program that account for attenuation and local site conditions. The response spectra at base and surface level is calculated for Kabul city. The simulated spectral pseudo-acceleration with 5% damping is presented. The maximum ground acceleration at the surface level is quite small. To confirm the results, we simulated the same earthquake using another method that gives almost similar results. Damage to structures in Kabul city from Hindu Kush earthquakes are usually and unofficially reported. Although the simulated results are smaller compared to the reported numbers, other construction factors might also contribute to the damage of structures in Kabul city. Additionally, strong motion records taken in Peshawar and D.I. Khan induced by the 2015 M_w 7.5 Hindu Kush earthquake have been summarized. They are higher than the results of this study. These results may be also of great significance to check the estimations. This signifies the importance of a thorough multi-hazard assessment on structures in Afghanistan.

The Chaman fault near Kabul is seismically inactive both in instrumental as well as historical seismicity; however, some historical events have been reported as well as the potential for occurrence of earthquakes Mw≥7.0 exists as the fault is absorbing most of its deformation from Eurasia-India global fault in the region. The 2005 Mw7.6 Kashmir earthquake was also because of the Eurasia-India plates' deformation in the region. To account for the effects of a similar earthquake near Kabul city, we estimated ground motion for a hypothetical earthquake along a 100 km long segment of main Chaman fault near Kabul city.
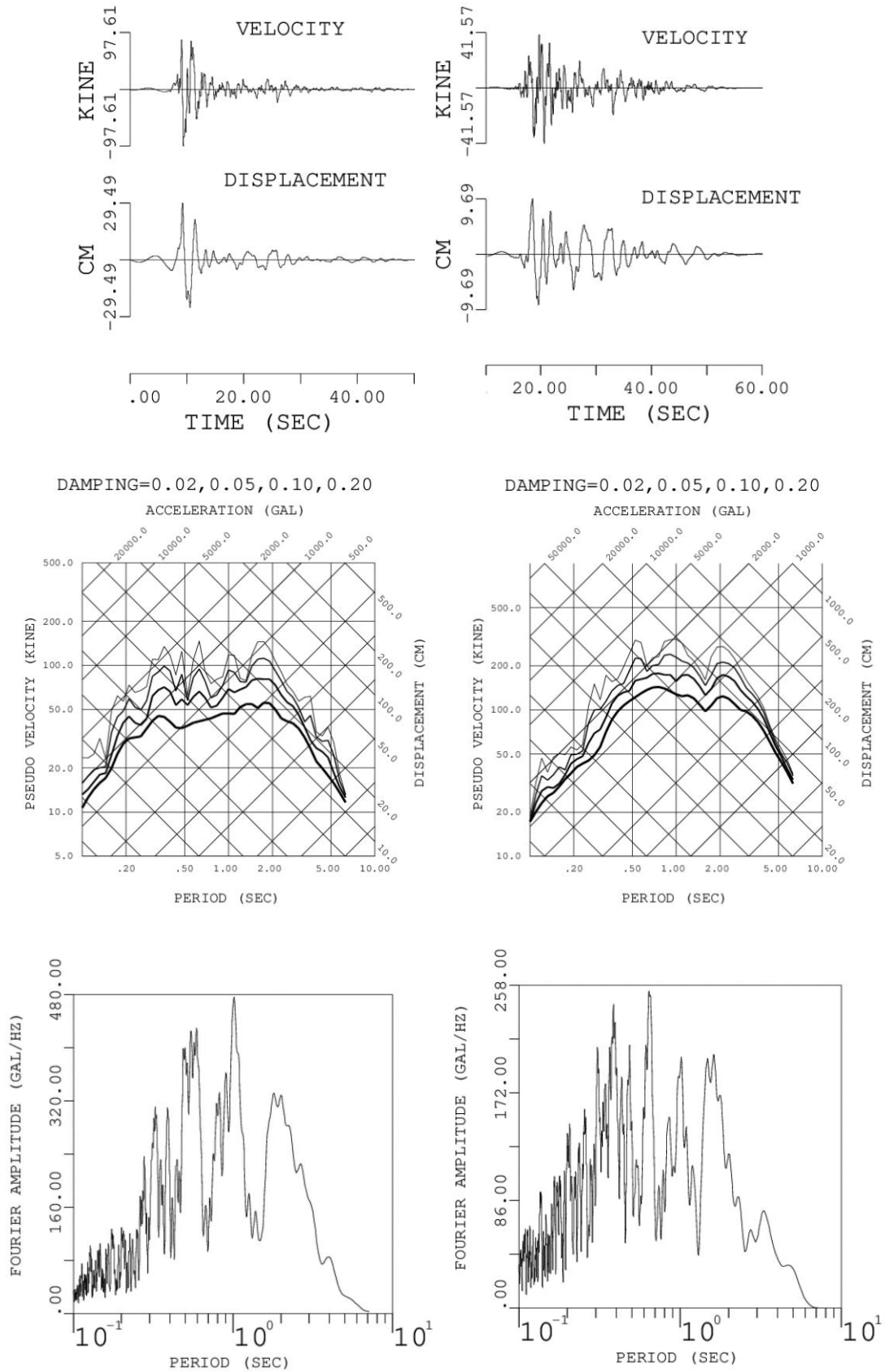
Figure 5.19 Velocity and Displacement time series, 5% dumping Pseudo Velocity and Fourier Amplitude at the epicenter (Left 3 figures in column order) if the rupture take place at 4-1, Case 1; and at Kabul city (Right 3 figures in column order) if the rupture start at 8-1, Case 1.

78

Table 5.6 Acceleration, velocity and displacement at Kabul city generated from the simulation of the 90 scenarios

S/N	Initiation of Rupture	Site (Kabul city) x	y	Case-1 Asperity Ratio	Result Amax (gal)	Vmax (kine)	Dmax (cm)	Case-2 Asperity Ratio	Result Amax (gal)	Vmax (kine)	Dmax (cm)	Case-3 Asperity Ratio	Result Amax (gal)	Vmax (kine)	Dmax (cm)
1	1-1	30		0.375	443.9	47.7	15.7	0.375	343.8	35.8	12.2	0.375	375.1	41.3	14.6
2	2-1	20		1.000	365.3	48.0	16.1	0.375	299.5	35.4	11.5	0.375	341.7	45.2	14.5
3	3-1	10		1.000	347.7	46.5	15.2	0.375	301.7	29.5	9.4	0.375	298.8	40.2	12.8
4	4-1	0		1.000	388.6	49.6	15.7	0.375	348.9	31.6	9.9	0.375	407.6	53.0	15.7
5	5-1	-10	-6	0.375	408.6	**54.5**	17.2	1.000	304.6	32.2	10.8	0.375	369.7	32.2	8.8
6	6-1	-20		0.375	411.1	54.4	**17.8**	1.000	319.4	42.1	13.7	0.375	335.1	32.1	10.6
7	7-1	-30		0.375	459.1	50.8	16.8	1.000	348.6	38.7	13.7	1.000	322.7	34.2	11.9
8	8-1	-40		0.375	**512.7**	**41.6**	**9.7**	0.375	391.6	33.7	10.6	1.000	357.7	32.3	9.1
9	9-1	-50		0.375	447.8	47.7	7.7	0.375	380.3	35.4	9.0	1.000	339.7	34.8	8.8
10	10-1	-60		0.375	446.5	43.6	8.4	0.375	342.9	33.9	6.9	0.375	323.5	34.8	8.1
11	1-2	30		0.375	170.8	15.5	4.3	0.375	139.0	16.8	4.2	0.375	154.6	17.7	4.3
12	2-2	20		1.000	190.3	17.2	4.7	0.375	176.7	16.1	4.3	0.375	151.1	15.7	4.3
13	3-2	10		1.000	209.4	21.0	5.0	0.375	194.8	18.0	4.5	0.375	184.8	17.9	4.1
14	4-2	0		1.000	157.0	20.5	4.6	0.375	222.9	20.3	5.2	0.375	212.1	18.5	4.9
15	5-2	-10	-16	0.375	151.9	21.2	4.3	1.000	218.3	20.8	4.6	0.375	201.6	19.1	5.0
16	6-2	-20		0.375	169.3	16.5	4.1	1.000	144.8	20.9	4.7	0.375	197.6	19.5	5.0
17	7-2	-30		0.375	181.9	16.6	4.4	1.000	161.2	23.3	4.9	1.000	184.1	20.2	5.1
18	8-2	-40		0.375	201.0	18.0	4.8	0.375	174.0	24.1	4.7	1.000	206.6	22.0	5.1
19	9-2	-50		0.375	220.5	18.9	4.9	0.375	189.1	22.1	4.4	1.000	174.0	22.6	5.0
20	10-2	-60		0.375	191.7	19.0	5.2	0.375	186.4	19.3	4.7	0.375	172.6	23.3	4.9
21	1-3	30		0.375	110.4	15.3	3.0	0.375	128.2	14.1	2.9	0.375	108.6	15.2	2.9
22	2-3	20		0.375	142.8	15.8	3.4	0.375	127.7	14.5	3.1	0.375	109.7	15.7	3.2
23	3-3	10		0.375	154.9	18.0	3.7	0.375	137.7	17.1	3.4	0.375	140.6	16.5	3.4
24	4-3	0		0.375	135.6	19.3	3.7	0.375	159.3	18.8	3.9	0.375	149.4	16.6	3.7
25	5-3	-10	-26	0.375	128.0	17.3	3.3	0.375	139.3	20.0	3.8	0.375	138.2	18.7	3.6
26	6-3	-20		0.375	126.9	14.7	3.1	0.375	143.3	20.1	3.8	0.375	148.2	18.8	3.7
27	7-3	-30		0.375	137.4	15.9	3.2	0.375	143.3	19.5	3.7	0.375	146.5	19.8	3.8
28	8-3	-40		0.375	154.5	16.2	3.5	0.375	136.2	17.1	3.3	0.375	140.3	19.3	3.8
29	9-3	-50		0.375	154.4	15.7	3.5	0.375	140.9	14.2	3.3	0.375	131.0	18.1	3.7
30	10-3	-60		0.375	148.0	16.6	3.5	0.375	143.3	14.8	3.3	0.375	131.9	18.3	3.6

The results indicate that the ground motion near Kabul city could be up to 953 gal and the velocity could be up to 100 kines. Although the strong motion instrumentation of Afghanistan is none, the results presented here can be used in seismic analysis and design of infrastructure facilities in the vicinity of Kabul city. In view of recent earthquakes with dense strong motion coverage in Japan, USA, Italy and Turkey, these values should be such that they must be the basis for the earthquake-resistant design of structures in Afghanistan. Nevertheless, the most important aspect is to be well-prepared against the worst scenarios such as the possibility of a great earthquake on the Chaman fault. The strong ground motions can be quite high, and these would have an important implication in the earthquake preparedness of Afghanistan with a hope that the devastating 2005 Mw 7.6 Kashmir earthquake would not repeat. Furthermore, it is no need to say that the establishment of a strong motion network in Afghanistan is a must in order to check the assumptions as well as to have instrumental data of strong ground motions for the seismic design of structures.

CHAPTER 6   BUILDING STOCK AND ITS CHARACTERISTICS

6.1 General

The choice of building materials and construction methods depend upon the social living pattern, economic affordability, accessibility of the site, yearly and daily temperature variations and the rainfall in the area. Before the 20th century, mud and mud bricks were the main construction material for buildings in Afghanistan. Mud bricks with mud mortar were used in the cities for construction of buildings and in the rural areas on-site soil in the form of dense mud was used for this purpose. These two are still a widely used material for construction in rural areas due to ease in construction, reduction in cost and increase efficiency and sustainability. In early 20th century, the modernization started rapidly and then followed a somewhat slow process of development in which the Capital Kabul and main cities of the province witnessed implementation of infrastructures. The half-dried bricks were the first use of modern material for construction. During that time, government buildings were constructed using reinforced concrete and burnt bricks and in some parts of the country the international community implemented infrastructure projects using reinforced concrete. Except very few cities and few international donors, construction in Afghanistan is carried out using the very conventional methods barely meeting the minimum requirements of international codes. In contemporary construction industry, for most of the owners of residential buildings, design means a simple Plan Drawing. They never ask the contributions of structural, architecture, mechanical, electrical engineers to do their respective designs for a building. However, they give the plan to the contractors who are in most of the cases unprofessional builders letting them decide orientation of structural elements. The first national engineering code in Afghanistan was developed in 2012; however, necessary work to grow its usage has not taken place. Major part of the code is not based on the actual construction and material of Afghanistan as there are insufficient economic capacity for identifying the actual strength and weakness of material and methods. Here, we shed light on type of the buildings currently used to be built in different parts of Afghanistan, methods and the material characteristics and assess the different aspects considering their stability against earthquake threats. Concrete mix design seldom take place, and if so, deriving parameters are typical considered same as those used in the USA, India and/or UK.

6.2 Afghanistan Building Code (ABC 2012)

The Afghanistan Structural Code is developed by the Afghanistan National Standard Authority (ANSA) in 2012. It is the first code developed for construction purpose in Afghanistan. Decades of violence in the country always caused the construction industry to receive little attention of the governments. The code so far doesn't have major application in practical or theoretical application. I have been working as Junior Teaching Assistant in one of the Higher Education Institutions of Afghanistan and had not have a hard copy of the code in our institute. It implies that enough work has not taken place to publicize the document and work for its usage in the country. From the citations and reference, it seems that the code is not developed based on the minimal actual construction situation in Afghanistan. Section 311.4 (page 116 of 496) of the code is discussing the earthquake ground motion values for design of structures in Afghanistan.

6.3 Common Building Types in Afghanistan

Currently, the common type of buildings in Afghanistan include reinforced concrete buildings, burnt brick masonry, mud brick masonry buildings and on-site soil dense-mud building. The massive influx of dollars to Afghanistan between 2002 to present changed the socio-economic situation of people living in urban regions of the country, particularly those who live in big cities which is an obvious attribution to the urban appearance of these cities. In Afghanistan 95% of construction is with mud. Only in urban areas, contemporary modern building materials are used. In a classification by Ministry of Urban Development and Housing (Guidelines, 2003), following main types of houses are used in Afghanistan.

1. Brick (Sun dried) wall with wooden roof (use of wood logs)
2. Brick (Sun dried or burned) with timber roof (use of sawn timber)
3. Wooden wall/Nuristan houses
4. Stone wall with wooden roof
5. Brick (Sun dried or burned) wall and Dome roof
6. Contemporary modern building materials like burnt-brick, cement concrete, R.C.C frame structure etc.

The many commercial and private buildings sparkling like glass palaces in the mud–brown landscape of Kabul and is deemed a result of the money that came to this country in recent decades. Moving to the outskirts of the big and small cities, this effect is decreasing and finally the people in remote villages still use the mud brick masonry houses for dwelling. Considering this aspect, the common type of residential houses in Afghanistan can be classified to three categories; namely, reinforced concrete house, burnt-brick masonry house, mud-brick masonry house and dense-mud

house. In this chapter, characteristics of materials and methods used for these types of houses is discussed. Reinforced concrete and burnt-brick masonry houses are common in the cities and later types are common in the rural areas. Here, we give the priority to reinforced concrete structures as by its failure the casualty is higher and the later will be discussed following.

6.4 Building Material

The contemporary building material in most of the cities of Afghanistan is composed of concrete. The people with the first-class economy in the country use to build reinforced concrete structures. Those with the second-class economic situation still use to build burnt-brick cement structures with steel or concrete precast beams for the roof construction. And those with lower-class economy use to build concrete block masonry with cement. In the rural areas and remote provinces, the later one is dominating the construction industry. In the villages, mud-brick masonry is still commonly used. The wet earth as the construction material is almost not used; however, in some of the area with bad economic situation, one cannot avoid it usage as it is the freely available material with low construction skills. In the sections coming, different type of material used for construction in Afghanistan, the workmanship, skills will be discussed.

6.4.1 Reinforced Concrete

Concrete is relatively cheap and strong, and most of its ingredients are readily available in natural forms in nearly every area of the world. They are one of the common and readily available building materials in Afghanistan also. Afghanistan is a mountainous country making availability of crushed aggregate easy for use in concrete; however, it is rarely used because of its higher cost and difficult production process comparing to river gravel readily available. In most of the construction works river gravel is used which includes soil contents and round gravel affecting concrete strength. Use of concrete for construction was still little before 2000 as the socioeconomic situation was not good. It became common in last two decades. Concrete is yet produced with conventional methods. Concrete is prepared on sites through mixer for slabs and foundations that need much concrete comparing to columns and footings. Concrete is made by hand mixing for columns and beams as they need little concrete for which people do not pay for mixer, Figure 6.3. Concrete plants are very rare even in big cities like Kabul, Herat, Kandahar etc. and if there is, it is very expensive for which neither the people for their private buildings nor government for their projects can afford. Concrete mix design rarely take place. Regardless of the ingredients' properties, a typical mix ratio of 1:2:3 (cement, sand, stone) is proposed to achieve the minimal strength (Manual of Building Construction for Afghanistan). Different material, their production and properties are discussed in the following sections.

6.4.1.1 *Water*

Good water is essential for quality concrete. Portable water is recommended in most of the international codes. Water for concrete should be free of trash, organic matter and excessive chemicals and minerals. However, there are no standards and/or government control set in Afghanistan to examine the water used in concrete. In cities, almost all water used for preparing concrete is from deep wells which are almost satisfactory. But for projects where either deep wells do not exist or are not allowed to be dig, river or stream water is used which has a lot of organic matter and chemical minerals. As concrete mix design does not take place, so the water-cement ratio is not respected. The team operating the concrete mixer are kind of the technical people to control the mix in the mixer drum. The workability of concrete is a measure of water content. Of course, all standards are met for infrastructure projects implemented by USAID and/or other donors when they monitor the projects directly.

6.4.1.2 *Cement*

There were three cement manufacturing factories in Afghanistan. At present only one at Pul-e Khomri city, the capital of Baghlan province is producing Ordinary Portland Cement (OPC). Production capacity is 1000 bags (50 kg each) per day. The quality of cement is good (MUDH, 2003). The remaining requirement of cement is met through import from Pakistan and Iran. In rural areas as most of the construction is made using mud, the use of cement is nil, but in the case of community structures there is some use of cement. The use of cement is predominantly in the urban areas, where close to 40% of construction activities calls for use of cement. About 60% of the remaining construction in urban areas uses mud (MUDH, 2003). There are problems with the way cement is stored in the private stores. Enough precautions to protect cement from moisture is almost nil. Sometimes small consolidated particles exist in the bags.

6.4.1.3 *Sand and Coarse Aggregate*

River sand for construction is available across all regions of Afghanistan. There is a shortage of coarse aggregate for construction activities. Stone quarries are found in all major provinces, but lack of working stone crushing units is causing the lack of aggregate. Almost all the stone crushing units have been destroyed in the war. River pebbles are used as a substitute for coarse aggregate for construction activities.

6.4.1.4 *Steel*

In recent decades, some companies started fabrication of construction bars; however, the production capacity is less than demand and a general ideology that the imported products have better quality is very common among all Afghans. Majority of these companies operate in Kabul.

They can supply to some percentage the required steel in the whole country. Remaining need is met through imports from Russia, Pakistan and Iran. Unfortunately, there is no government quality control neither on steel production inside the country, nor on those imported. Testing of steel in structural laboratories is not common except for the infrastructure projects funded by USAID and other donors. They sent sample of the material abroad for testing. The workmanship of placing steel reinforcement in structural elements is low. In order to save time, the bar benders tie/fasten alternate joint instead of fastening them in every joint.

6.4.2 Sun Dried Brick (Adobe)

The Sun-dried brick (Khesht-e-Kham/Woma Khashta) is the primary form of the burnt-brick. It is almost of the same size and larger sizes of 38cm x 38cm x 8cm and 25cm x 12cm x 6cm is also available. Mud bricks are human made easily constructed from on-site soil and available almost all over the country. Its making does not need special skill, but everyone can make it with very simple wooden frame that makes several small size bricks at once, Figure 6.1. Mud brick construction is kind of a small business for some of the families to find money for their daily life and the whole family work together even children. Compressive strength data is generally not available but if it is thrown on its flat bottom from half-height of an average person, it most of the time splits in the middle. Samples from Nahrin of Badakhshan and Kabul gave a dry compressive strength of 70 kg/cm2 and a density of 1650 kg/m3 (Guidelines MUDH, 2003). Mud mortar is used for mud brick masonry. Quality of masonry is average. Two layers of burnt brick are put on the wall once and the wall is raised to full height to prevent planks to prevent the mud from washing out the rains. As of 2003, MUDH has reported that 95 percent of the construction in Afghanistan is with mud and it the most affordable. They also have recommended development of new Code/Guidelines with high consideration of mud construction for construction activity in Afghanistan.
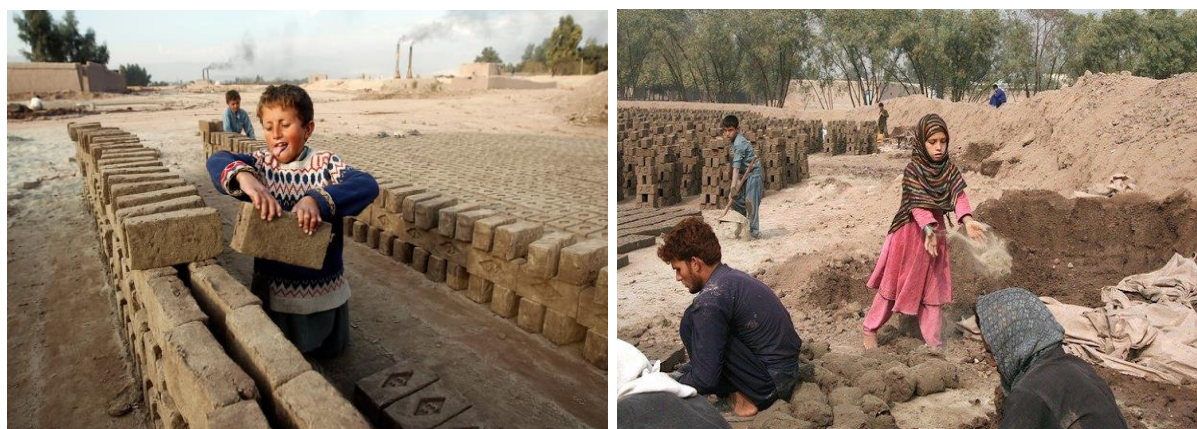
Figure 6.1 Making of mud bricks. Left: children are exposing bottom of the half-dried bricks to atmosphere for drying. Right: Children prepare mud for making of bricks

6.4.3 Stone and Stone Masonry

Afghanistan is a mountainous country except the southern west region. Random rubble stones are available almost everywhere except in the desert areas and some plains. Usually hard compacted stone is used in construction. Traditionally, stone is used for foundation and plinth. In hilly region where good clayey soil is not available, hard compacted stone is used for super structures. In stone construction, wooden logs are used for strengthening of corners and wooden band is used at lintel. Sometimes even at sill level wooden band is used. In foundation the general practice is to use rubble masonry with sand packing or mud mortar, Figure 6.3.
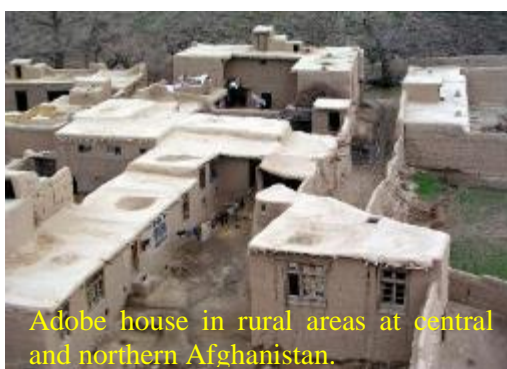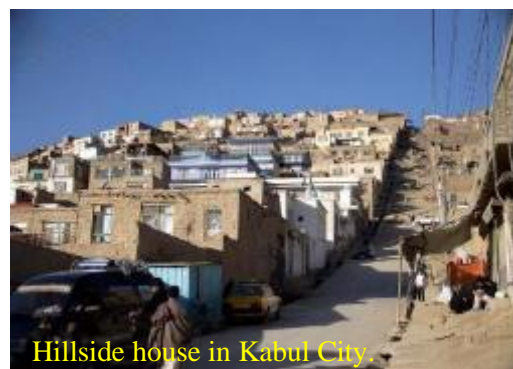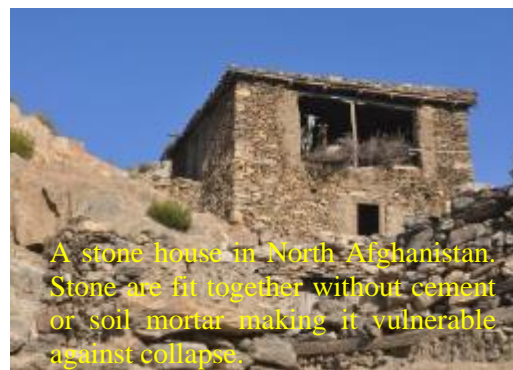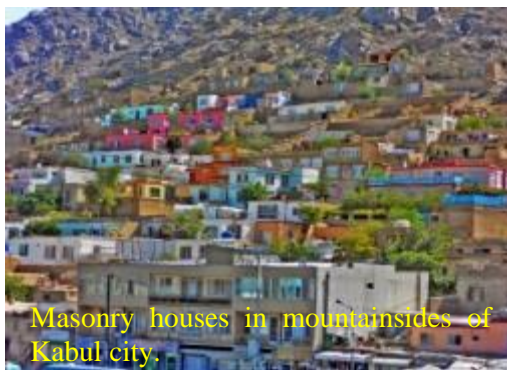
Figure 6.2 Sample of houses constructed by the lower economy class people in central and northern parts of Afghanistan.

Figure 6.3 Concrete ingredients and hand mixing take place on a ground where the water and cement paste can penetrate. The reinforcement bending is in most of the cases poor. The bars are not wire-tied or welded on every joint. The wood panels and supports used for formwork is usually of poor quality resulting in wasting of cement water paste and insufficient space between the forms and reinforcement. The steel is exposed to atmosphere and the concrete is weak against water penetration.

Figure 6.4 Stone masonry, Left to right: Continuous footing between concrete columns, foundation of an old structure in the outskirts of a hill in a central area of Kabul city, near Shah-e-du shamshira Masjid, dry stone masonry work which are still taking place on large scale, a stone masonry work for foundation of a residential building in a hillside in central Kabul, a view of relatively new built houses in hillside in Kabul and abandoned rocks available in a mountain.

The general practice in plinth construction is use of mud mortar or dry masonry. The capital of Afghanistan Kabul has a high population density and is a mountainous area. Most of the people live in the mountains. They use hand drills and explosive to split rock pieces from mountain body and then make their own houses. This is taking place in a big scale whereas there does not exist basic community facilities. They do not use mortar; however, when there is possibility of collapse, some households use cement mortar, but it is very rare as the economic situation of the households cannot afford it, Figure 6.2 and Figure 6.4. They are severely vulnerable to earthquakes and if an event close in size to the 2005 Kashmir earthquake happen, it will have far more devastating consequences.

6.4.4   Brick Walls

Normally good quality burnt-brick is available near urban areas and main centers of provinces like Jalalabad, Kabul, Kandahar, Herat and Mazar-e-Sharif. Bricks are usually good quality with almost even size (not bent), giving metallic sound when struck with each other. The common size of brick is 20cm x 10cm x 5-6cm, but the size varies city to city. Most of the burnt-brick plants think of the size with highest demand in the market. In Kandahar the mostly liked brick size is 22cm x 11cm x 7cm. It is understanding that in Afghanistan the compressive strength of burn bricks ranges from 50 kg/cm2 to 80 kg/cm2. Regularity of the bricks depend company to company. One can hardly find bricks all solid and straight on edges. Almost none of the supplies sell whole-solid bricks but they give at least about 50 bricks in pieces and bricks into pieces at the time of transportation. Placing of the bricks in the wall depend on the skill of the mason. Very few masons can weave whole wall look straight and nice unless otherwise they work very slow which raised cost of the construction.

Figure 6.5 Brick masonry work with poor alignment of brick rows. A regular brick masonry work with high workmanship; however, this is not affordable by private owners and in government projects. (Gohar Khaton Girls School in Kabul).

6.4.5   Stack Wall (Pakhsa Wall)

Stack wall are made from on-site soil locally available without any additives. The mud after removal of the gravel and small stones, is mixed with water, puddled and left for 24 hours. With this preparation, mud lumps are made and stacked in order to construct a mud wall. The wall is constructed in layers and each layer has a thickness of 70 to 80 cm and layer height of 70 to 80 cm. One layer is put in a day and the next is put on the dried-up layer next day. Sometimes, a stone or sun-dried brick is inserted at the edges and the junctions between two layers of stacked wall. A locally made tool known as Pakhsa Taras is used to dress the wall. Wooden pools are placed on top of the window and door opening working as a lintel. The final finish of the wall is done with mud plaster. The mud plaster is made from mud, water and rice or wheat husk. No scaffold is used for constructing the wall. Usually the mason sites on the wall itself while constructing. Normally the brick masonry work is also executed in the similar fashion. As in Adobe walls, two layers of burnt brick are put on top once the wall is raised full height to prevent washing of the mud in rains or grass or wooden planks are used for rain protection of the mud. This type of houses is preferred a lot because of its thermal efficiency and economic affordability but are very rare in urban areas by now; however, it still has a huge use in rural areas, Figure 6.6 .

Figure 6.6 Houses made of stack wall: Left: Room ready for roof construction. Majority of the houses in Nahrin of Baghlan province has the same structure with some recent addition of wooden pools within the walls. Right: Mud preparation for plastering of stack walls.

6.4.6   Wood

Wood is used in doors/windows, for corner strengthening and for roof construction. Poplar poles are used a lot in regions with climate condition suitable for its growth. Chinare Sokat, a local species is cultivated across Afghanistan for wood, but it is good enough to be used only the roof. Of late due to increasing demand for construction activities, wood is imported from Pakistan. The wood is not treated before being used in construction as they do not face any problems due to termites. Sawn wood is also available in all regions.

6.4.7   Cement Concrete (CC) Blocks

The scarcity of cement and coarse aggregate will make the possibility of using CC block technique for reconstruction a difficult proposition. There is also a lack of advance manufacturing systems and skills required for using CC blocks, Figure 6.7. In few school projects implemented in northern Afghanistan and adjacent parts of Tajikistan, some charity foundation and humanitarian aid organizations have used it in building schools. They have produced the block as part of the same project. Usage demand looks still little so that investments have not been taken place yet.

6.5   Construction Skills and Mechanization

Traditionally, manpower is available for construction activity. The level of mechanization in construction activity is insignificant. Only in areas around big cities like Kabul, Herat, Mazar-e-Sharif, Jalalabad and Kandahar could one see some signs of mechanization. For small scale construction Site-mixers are used for construction activity. For very few infrastructure projects, concrete from concrete plants is provided. For private and government constructions, there is no economic affordability for concrete from plant and pumps. The training facilities and quality control on construction are almost nil in Afghanistan.

Figure 6.7 Producing and usage of CMU for a school building in northern parts of Afghanistan adjacent to the border with Tajikistan.

6.5.1   Construction Methods of Concrete Frame Structures

Use of reinforced cement concrete became very common in urban areas of Afghanistan particularly in big cities from the year 2000. The complete construction usually includes RCC for the structural elements and burnt-brick masonry for walls. In most of the cases the bricks are not embedded into the concrete as of the case for school buildings constructed under the direct inspection of Ministry of Education. Previously, the concept of constructing the partitions walls first and then filling the columns was seen more; however, in most of the government works, now one can see that the frame is constructed first, and then the walls raised. The deriving factor in

opting one of these methods is the cost, not the resistance against lateral loads. In the following section, the different ideology in selecting either of these two methods is described in detail.

6.5.1.1 *Frame First*

In major cities, residential mansions and high-rise buildings are mostly built using this method. One can rarely find a mansion and/or a high-rise building owner be an ordinary person. They are either high rank person in the government or one that unexpectedly got money in some ways. The aesthetic aspect of the building is much more important than the internal design, comfortability or structural safety. As a general role, in every community, things develop according to the demand of dominating layer of people in a society. Therefore, in major cities where rich people surplus others class, the frame is built first Figure 6.8.
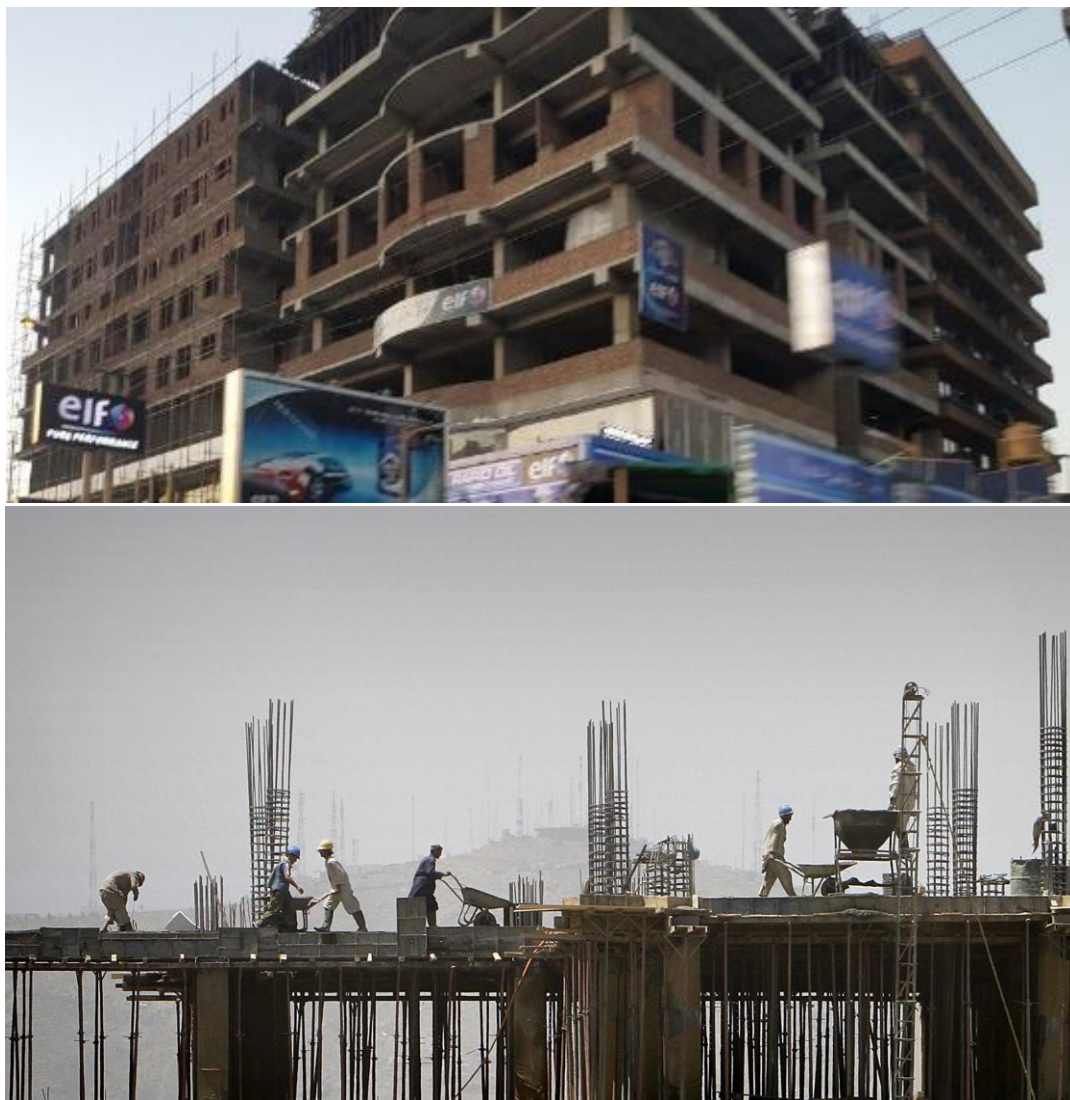
Figure 6.8 Construction photo of a high rise building in Quwa-e-Markaz area of Kabul city.

In the case of commercial buildings, this is the case in all situations as they look for rapid construction. As the first story frame is built, the masonry work for this and the framework for the following story take place simultaneously. In this case the brick masonry walls are not inter-locked with the frame and the possibility of crack development in moderate earthquakes exist, particularly the walls that are built on the overhanging end of the slabs.

6.5.1.2 *Partitions First*

Most of the people with average economy prefer this method of construction. The contractors of the average scale projects also prefer it as they don't need to fix formwork for bottom of the beams and 2/3 side of the columns, Figure 6.9. Once again, the concept of lateral stability of the walls is not the deriving factor. Most of the schools constructed by Ministry of Education is built using this method. In this method of construction one can rarely see the back and forth placement of bricks at the ends of the walls where it connects to the column, Figure 6.10 . In this the walls are constructed first and once they are raised to the full height, forms to one side of the external columns, two side of the columns on the corner of the building. The columns at the interior does not need side formwork.

Figure 6.9 Example of construction of brick masonry walls in Afghanistan.

Figure 6.10 Formation of a rough surface to the end of the masonry so that it integrates well with the column.

6.6 Typical Seismic Damage of Common Buildings in Afghanistan and Elsewhere

If earthquakes only moved the ground vertically, buildings might suffer little damage because all structures are designed to withstand vertical forces those associated with gravity to some extent. But the rolling waves of an earthquake, especially Love waves, exert extreme horizontal forces on standing structures. These forces cause lateral accelerations, which scientists measure as g-forces. A magnitude-6.7-quake, for example, can produce an acceleration of 1 g and a peak velocity of 40 inches (102 centimeters) per second. Such a sudden movement to the side (almost as if someone violently shoved you) creates enormous stresses for a building's structural elements, including beams, columns, walls and floors, as well as the connectors that hold these elements together. If those stresses are large enough, the building can collapse or suffer crippling damage. Buildings constructed on bedrock often perform well because the ground is firm. Structures that sit atop soft or filled-in soil often fail completely. The greatest risk in this situation is a phenomenon known as liquefaction, which occurs when loosely packed, waterlogged soils temporarily behave like liquids, causing the ground to sink or slide and the buildings along with it.

Afghanistan is in a high-seismic activity zone. Given the rugged and mountainous nature of the country and the location of villages, towns and cities, there is always a high propensity for widespread death and destruction whenever an earthquake, landslide, mudslide, avalanche, or flooding occurs, due to 2002 estimation that since the early 1980s, natural disasters in Afghanistan have killed an estimated 19,000 people and displaced 7.5 million people. Since 1954, there have

been about 30 earthquakes resulting to about 11,302 deaths, 10,554 injuries, 95,855 homeless and 514,125 people affected. The deadliest of these earthquakes were the 1998 twine earthquakes of Rustaq in Takhar province, 2002 in Nahrin of Baghlan, 2015 of Hindu Kush in Afghanistan and Pakistan. In the following section, we explain effects of some of the deadly earthquake on buildings in Afghanistan.

6.6.1   1998 Rustaq and 2002 Nahrin Earthquakes of Afghanistan

Following the earthquake (magnitude 6.1 on the Richter scale) on 4 February, affecting the Rustaq district in Takhar province about 50 km from the border with Tajikistan, several aftershocks continue, causing additional damage. The aftershock affected up to 28 villages, out of which 6 to 7 were destroyed. The earthquakes killed about 2,300 and 4000 people, respectively and destroyed about 8,100 houses and making 8,000 homeless. The shock triggered extensive landslides adding to the damage and killing more than 6,000 livestock. Another set of 3 earthquakes (6.0, 5.1, 5.8) with the same source occurred in 2002 centered in Old City of Nahrin (Shahr Kona) and killed about 1200 people. Most of the houses in both regions are adobe, mudbrick and stone masonry construction. Collapse mechanism of the houses in both earthquakes are explained in Figure 6.11.

The earthquakes destroyed almost all the adobe-constructed houses. Those build by mud-brick masonry and mud-brick masonry work with lateral poplar poles' reinforcement have partially withstand the shocks. In most of the houses, abundant mountainous stones were used in the foundation and walls. Stone masonry walls with earth mortar have also collapsed. The mud-brick walls reinforced with poplar poles have provided better response comparing to the stone masonry walls that were used with earth mortar.

6.6.2   2005 Mw 7.6 Kashmir Earthquake

The 2005 Mw 7.6 was the deadliest of its type in 21st century. It killed about 85,000 people and destroyed more than 150,000 houses and other structures. Effect of this earthquake was not felt in Afghanistan as it was quite far, and the earthquake was a shallow event having major local impact. The destruction of the event was widespread and devastating. Many masonry bearing wall structures completely collapsed in the affected areas. The frame element such as columns in a small percentage of buildings in the area were collapsed. In some case, the infill walls have prevented total collapse of the buildings. School and hospital buildings that have had poor construction quality and lack of seismic design had been affected. Brick masonry, stone masonry and adobe houses were destroyed because of the big shock of the earthquake, Figure 6.12.
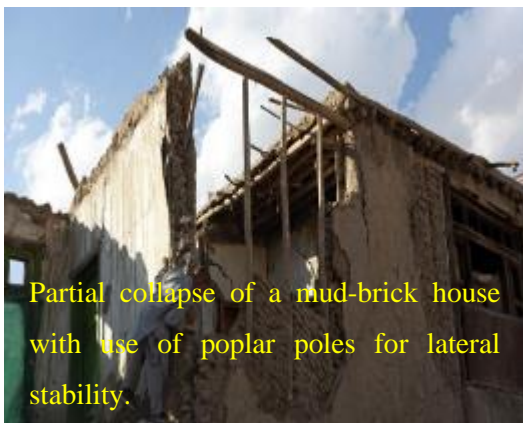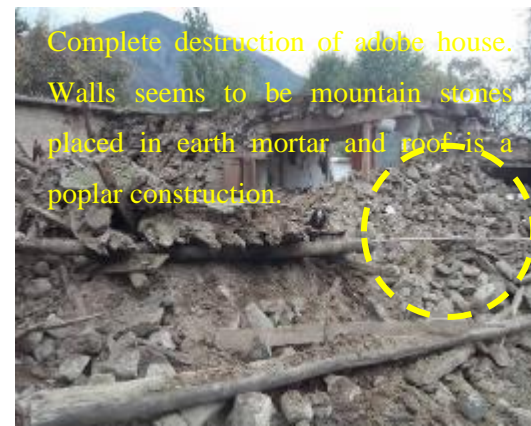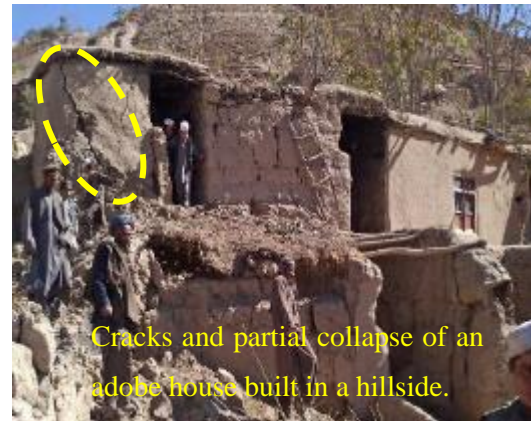
Figure 6.11 Illustration of collapse mechanism of the adobe, mud-brick and stone masonry structures in Nahrin and Rustaq earthquakes of Afghanistan.

6.6.3   2015 Mw 7.5 Hindu Kush Earthquake of Afghanistan and Pakistan

This epicenter of this event was about 210 km deep. The earthquake shocked Kabul and resulted into minor damages. It resulted more damage in Pakistan side. The shock was felt India, Tajikistan and nearby countries also. The earthquake killed about 400 people in Afghanistan and Pakistan with

many victims in Pakistan. The damage mechanism to adobe structures included corner damage, delamination, partial wall collapses and total structural collapse, Figure 6.14.

The earthquake caused minor damages to reinforced concrete and burnt-brick masonry buildings in Afghanistan and Pakistan. The damages in Afghanistan included mainly removal of the plasters and in certain cases the ceramics. Cracks were also reserved in the partition wall. There are unofficial reports that some of the high-rise buildings had undergone partial foundation settlements also. I believe there have been damage to structures in Kabul; however, since the official reporting of these events are against the interests of the private sector holders, they seriously avoid investigation in the cases of such events. Few types of damage to buildings is presented in Figure 6.15, only as a sample. The damages in Pakistan included the flexural cracking under-designed RC structures, pounding at the expansion joints, in-plane shear damages in masonry infill and horizontal cracking at roof diaphragm movement (Ahmed, 2015). Some parts of this chapter are reflected in **"Tokashiki, N., Ö. Aydan, N. Z. Nasiry, T. Ito & M. Geniş (2018). Dynamic response and stability of some historical masonry structures subjected to ground shaking. The 3rd Int. Symp on Rock Dynamics, RocDyn3, Trondheim (Editors: Charlie C. Li, Xing Li, Zong-Xian Zhang), 533-539".**

Figure 6.12 Destruction of reinforced and masonry structures in 2005 Mw 7.6 Kashmir earthquake

Figure 6.13 2015 Mw 7.5 Hindu Kush earthquake damage to reinforced concrete and masonry structures in Pakistan (Ahmed, 2015)

Figure 6.14 Collapse mechanisms of adobe structures in 2015 Hindu Kush earthquake of Afghanistan and Pakistan.

Figure 6.15 2015 Mw 7.5 Hindu Kush earthquake damage to reinforced concrete and masonry structures in Afghanistan

CHAPTER 7   PHOTO-ELASTICITY TESTS AND THEIR FINITE ELEMENT ANALYSIS AND PHYSICAL MODEL TESTS

7.1 Photo-elasticity Tests and Their Finite Element Analysis

7.1.1 Introduction

Photo-elasticity used in various engineering fields in the past to investigate the stress concentrations since its invention in 1815 by Brewster and it is formulated by (Fresnel, 1820) to establish relation between phase difference of lights and maximum shear stress acting within the object subjected to some tractions along its boundaries. This is the only method to visually observe stresses and it served well in various field of engineering e.g. (Frocht, 1965). However, this technique receives less attention nowadays due to the advances of numerical techniques as well as computational technology. However, the computational results from numerical techniques may still require some validation by this technique particularly in fracturing and/or dynamic problems. Furthermore, the validation of computational codes for simulating the behavior of discontinuum is especially necessary. The remote-sensing techniques of airborne or space are also fundamentally based on the principles of photo elasticity although the laser beams such as SAR, LIDAR, DInSAR are used.

This technique was utilized to study the stress variations and distributions by considering typical conditions of slip of faults, masonry structures, frame structures and buildings of frame type.

7.1.2 Principle of Photo Elasticity, Devices and Materials

The invention of photo-elasticity technique is attributed to (Brewster, 1815) while (Fresnel, 1820) was the person to formulate the phase delay to the maximum shear stress acting in a stressed body with a given thickness t, which related to the phase retardation (Figure 7.1). This relation is given in the following form:

$$\Delta = \frac{2\pi t}{\lambda} C(\sigma_1 - \sigma_3) \qquad\qquad (7.1)$$

where C is photo-elasticity coefficient, λ is vacuum length and σ_1, σ_3 are principal stress components. A fringe pattern appears due to optical inference of waves. The number of fringe order N is related to retardation factor as

$$N = \frac{\Delta}{2\pi}$$
(7.2)

One can determine the state of stress at various points in the material from fringe patterns.

The actual photo-elasticity devices are quite large and expensive requiring a light-source with well-known characteristics. However, it is quite difficult to find light sources commercially available in Japan while one can easily get them from some other countries such as India, China and USA in nowadays.
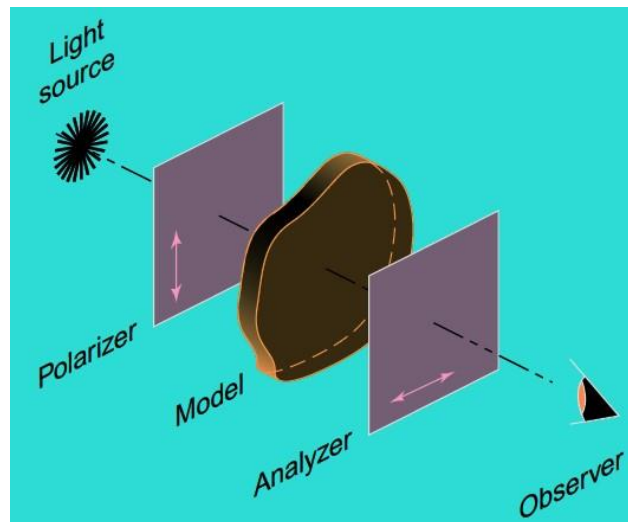
Figure 7.1 Principle concept of photo-elasticity devices

Originally polariscopes, which are based on photo-elasticity principle, are developed for showing the stress distributions and concentrations in relation to educational purposes. It is also possible to produce hand-made polariscopes utilizing LED lights, polarizer films while digital cameras with circular polar lenses can be used as an analyzer and to take static and dynamic images (Figure 7.2). Such a system for photo-elasticity experiments is shown in Figure 7.2 (Aydan, 2020) and the outcomes of these studies are presented in the next sections.

Figure 7.2 Implementation of photo-elasticity principle in practice, from (Aydan, 2020)

The models tested in this study were made of polyurethane. Polyurethane material has different stiffness, namely denoted as 20, 30, 50 and 70 degrees by the producer. These models allow to investigate elastic stress distributions in various model tests reported in this section.

7.1.3   Photo-Elasticity Tests on the Stress State of Faults

7.1.3.1   *Slit-like Faults*

Samples having slit-like faults are often used to study the effect of distributed cracks on the overall behavior of faults. For this purpose, samples having a slit having its longitudinal axis oriented to 0, 45, 90 degrees from horizontal prepared and subjected to different loading regimes as shown in Figure 7.3. As noted from the figure, stress distributions in samples are quite different depending upon the orientation of the longitudinal axis of the slit. While the effect of 90-degree slit is less, the stress concentrations occur at the tip of the slit and tensile stresses occur near the central part of the slits for samples having 0 and 45 slits.
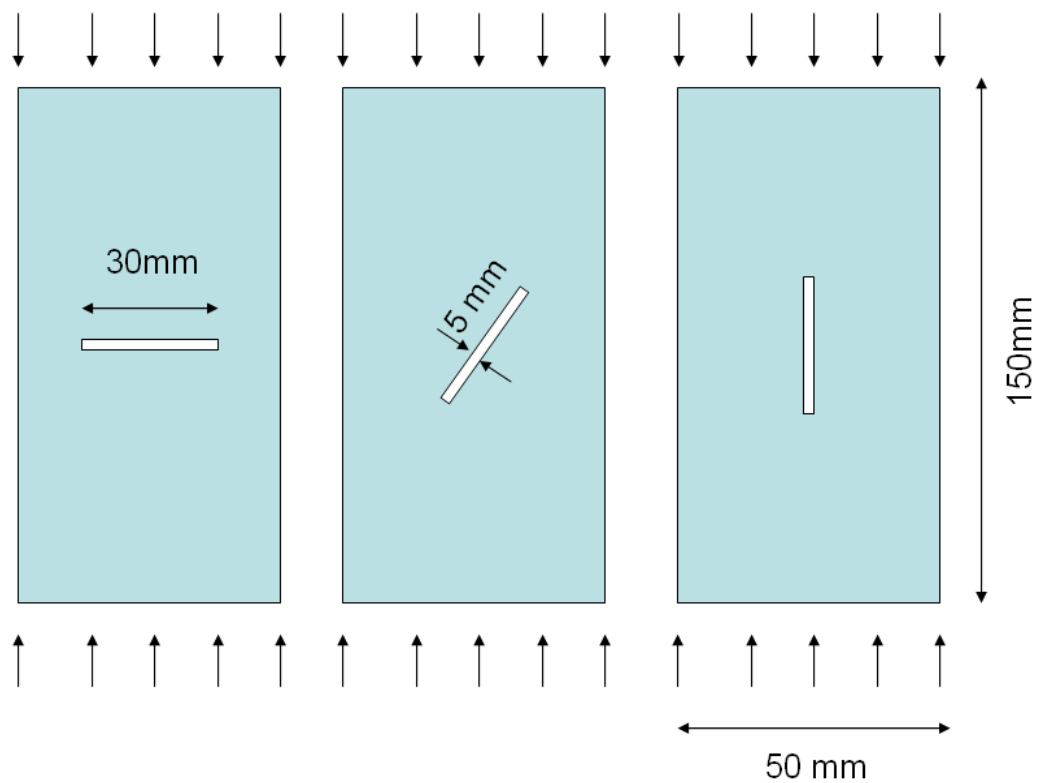
Figure 7.3 Dimensions and loading conditions of slit-like fault models
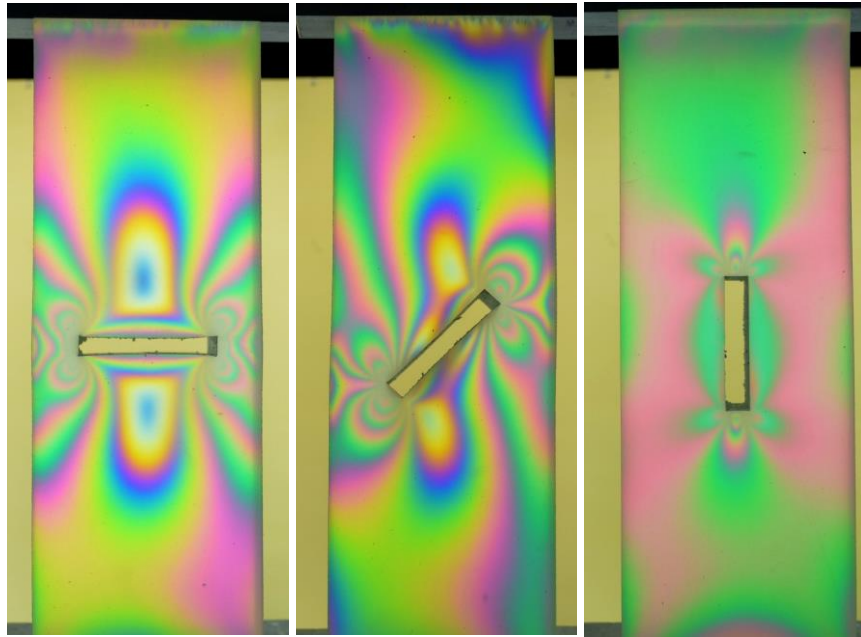
(a) 0 degree slit   (b) 45 degree slit   (c) 90 degree slit
Figure 7.4 Stress distribution in samples having slits with different orientations

Next, the same slit-like faults samples are subjected to normal and shear loads as illustrated in Figure 7.5, Figure 7.6, Figure 7.7 show the maximum stress distributions in the vicinity of slit-like faults under normal load only and normal and shear loads. As noted from the figures, the stress concentration occurs at the tips of the slits.
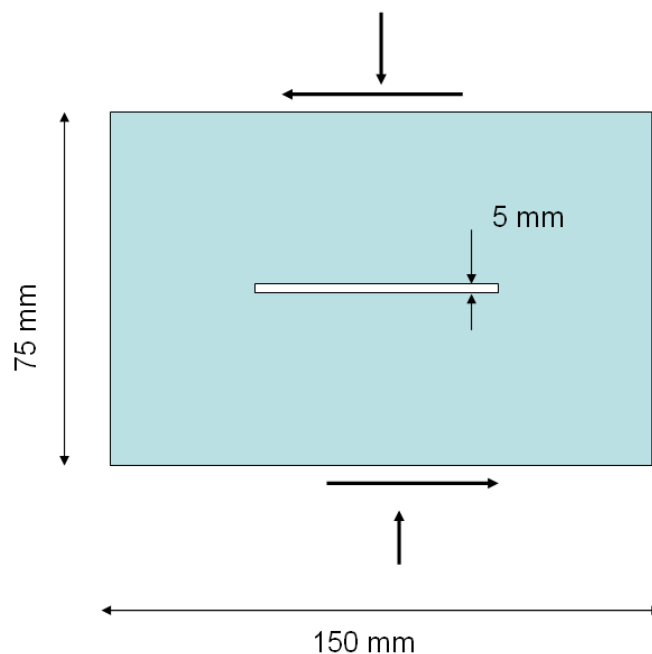
Figure 7.5 Illustration of normal and shear loads on the slit-like faults samples.
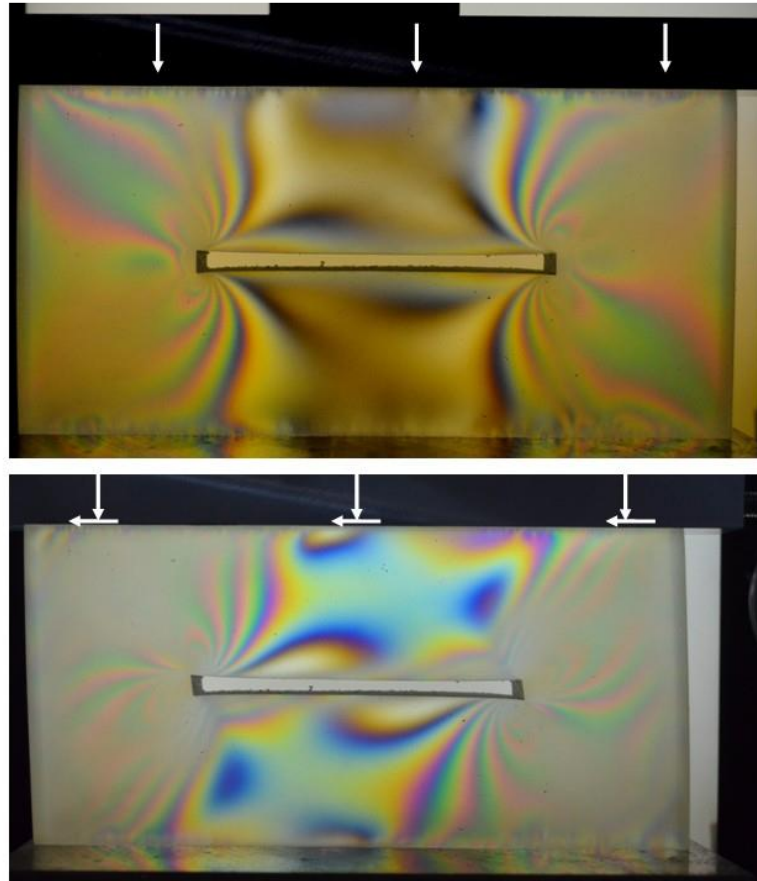
Figure 7.6 Maximum shear stress distributions under different loading regimes (90º).
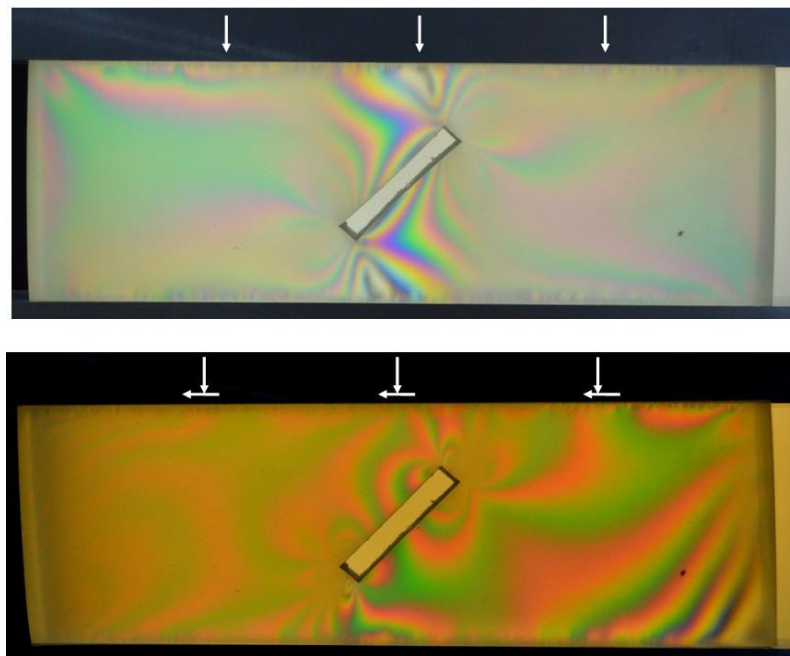
Figure 7.7 Maximum shear stress distributions under different loading regimes (45º).

7.1.3.2 *Faults with Regular Asperities*

Faults with asperities are considered to simulate strong motions. Such models assume that fault surface is flat. However, there are not flat and undulating. A sample having a discontinuity plane consist of regular asperities with a 15 degrees inclination as illustrated in Figure 7.8 is used. Figure 7.9 and Figure 7.10 show the maximum stress distributions subjected to normal load only and a combined shear and normal loading together with a relative slip, respectively. As noted from Figures 7.9 and 7.10, the existence of discontinuity plane plays a great role on the overall stress distribution. Furthermore, the slip results in high compression on contact side and tensile stresses on separated side of asperities. This result may also important implications on the visualization of asperity models commonly used in earthquake science for simulating strong ground motions.
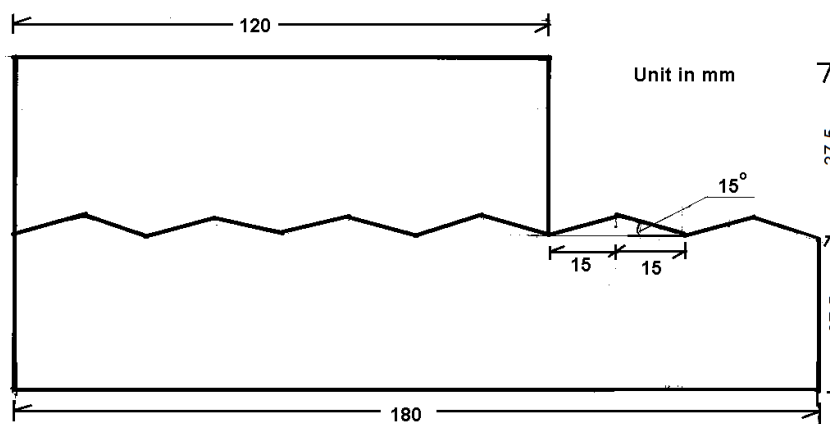
Figure 7.8 Dimensions of the fault model with regular asperities.
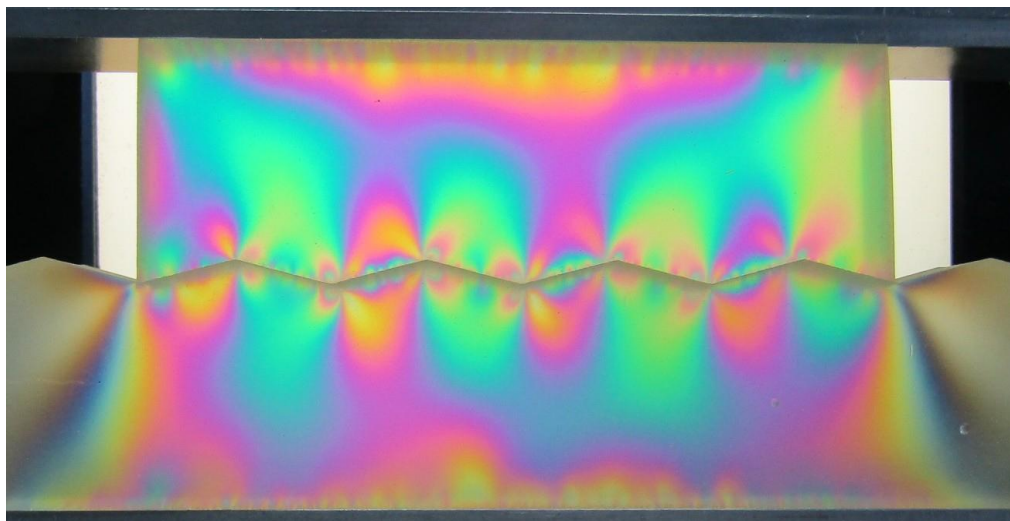
Figure 7.9 Stress distribution of a sample of regularly spaced asperities under normal loading only.
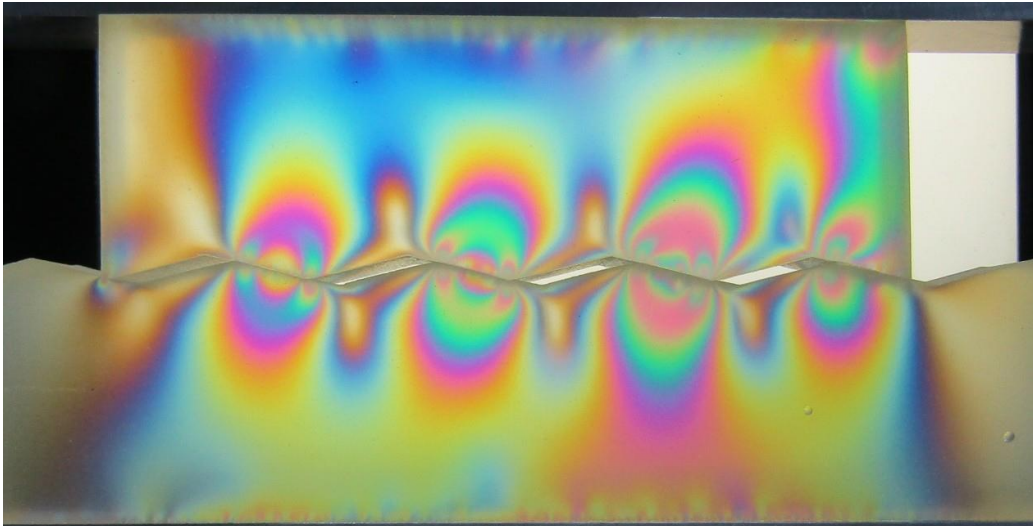
Figure 7.10 Stress distribution of a sample of regularly spaced asperities under combined normal and shear loading.

7.1.3.3   *Faults with Irregular Rough Asperities*

Stress distribution in the vicinity of fault-like discontinuity plane in a continuum model subjected to dextral fault type boundary conditions is studied as shown in Figure 7.11. The surface configuration of the fault-plane was relatively rough. As noted from the figure, stress concentrations occur at the tips of the fault plane while symmetric stress shadows occur in the central parts on both sides of the fault plane. Nevertheless, the stress distributions are quite complex as compared with those of well-shaped fault models.
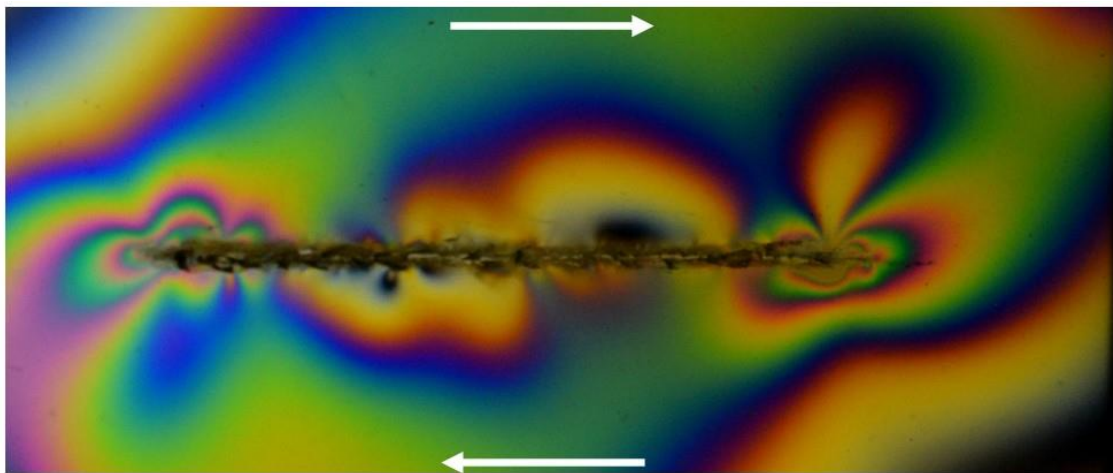
Figure 7.11 Stress distribution in the vicinity of a model fault plane subjected to dextral type fault boundary conditions.

7.1.4   Photo-Elasticity Tests on Structures

The tests reported in this section are concerned with some fundamental elements of masonry and framed structures.

7.1.4.1   *Masonry Structures*

Masonry structures generally consists of stones, bricks or mixed with or without mortar. Mortar itself may be soil with straws, lime-based or cement-based. The weakest masonry structure based on pure frictional resistance, which is also categorized as dry masonry structures. Figure 7.12 shows the maximum stress distribution in masonry wall models. As noted from the figure, the stress distributions are not uniform even they are subjected to uniform normal or normal and shear loads. Particularly vertical joints do not transfer stress laterally or very small stress transfer. The same situation is also valid for the masonry wall subjected to normal and shear loads.

(a) normal load only   (b) normal and shear loads
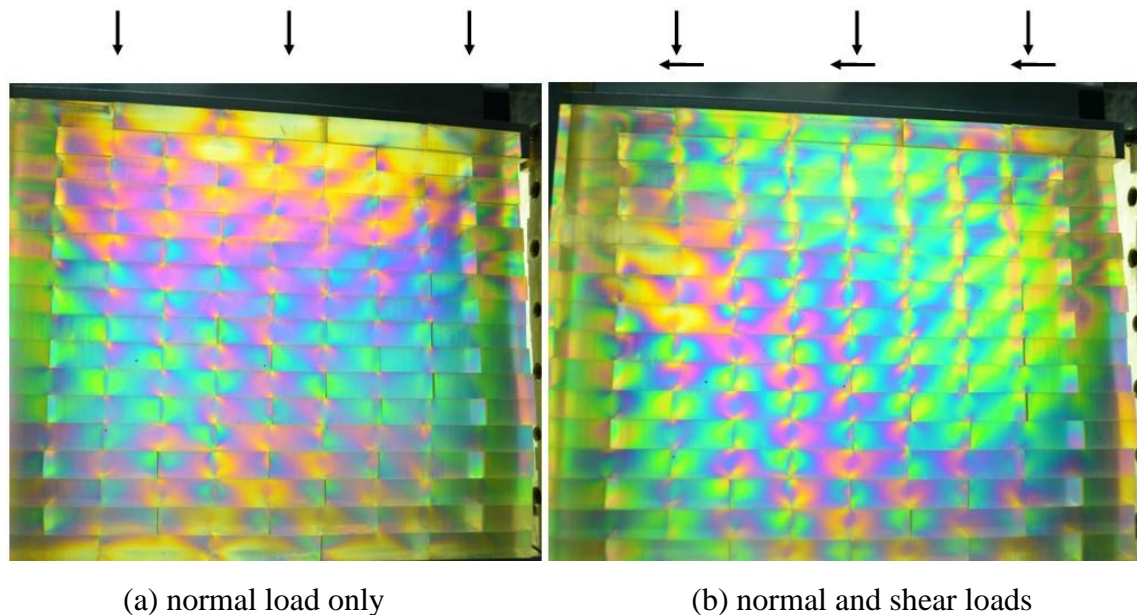
Figure 7.12 Stress distributions in masonry walls under (a) normal load only and (b) normal and shear load.

The lintels or slabs are known to be providing some resistance and ductility to masonry walls. However, this aspect of lintels and slabs is not investigated by experimental and numerical techniques in earthquake engineering. Some photo-elasticity model tests on masonry walls with lintels are carried in order to illustrate the effect of lintels on stress distributions in masonry walls as shown in Figures 7.13 and 7.14. As noted from Figures 7.13 and 7.14, lintels result in better stress distribution within the wall and decrease stress concentrations in individual masonry blocks.
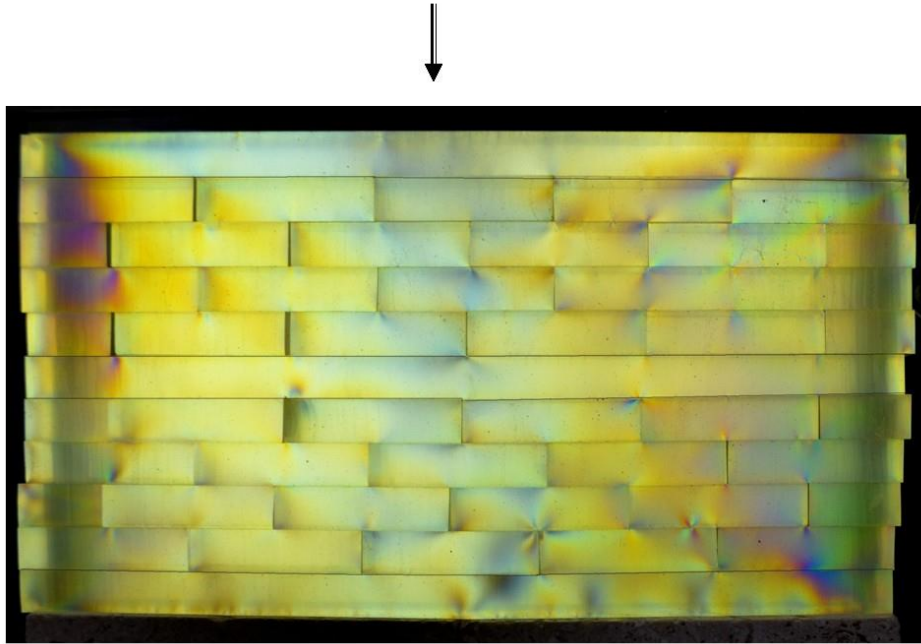
Figure 7.13 Stress distribution in a masonry wall with lintels under normal load only.
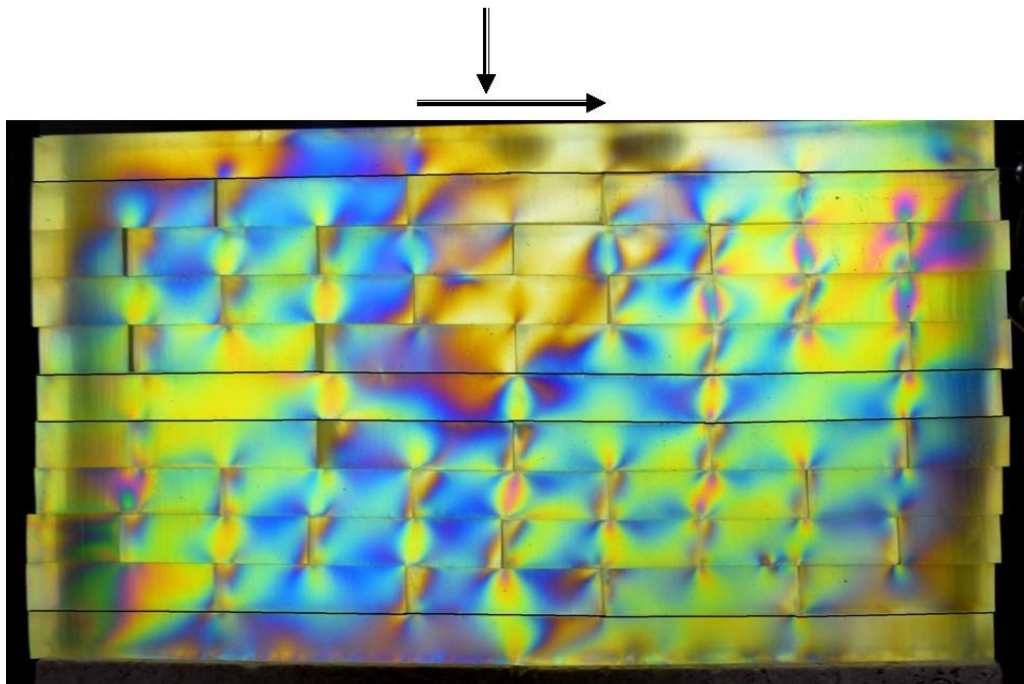
Figure 7.14 Stress distribution in a masonry wall with lintels under normal and shear loads.

7.1.4.2   *Frames*

Reinforced concrete or steel frame structures are generally designed as framed structures, in other words, they are moment resistant structures. Various photo-elasticity tests were carried out under different loading regimes.

7.1.4.2.1   Single Frame Structure with/without Infill Walls

A single frame is the most fundamental element for formed structures. Figure 7.15 and Figure 7.15 show the maximum stress distributions in frames with and without infill walls under normal load only and normal and shear load. As noted from the figures vertical columns carry out the normal loads and lateral beams are subjected to tensile stresses. However, the application of shear loads increases stress concentrations at the corners, particularly. When frames filled with walls, whose stiffness is about 1/3 of that of the frames, the stress concentrations decrease in amplitude and walls also carry some loads acting on the frames.

(a)   (b)
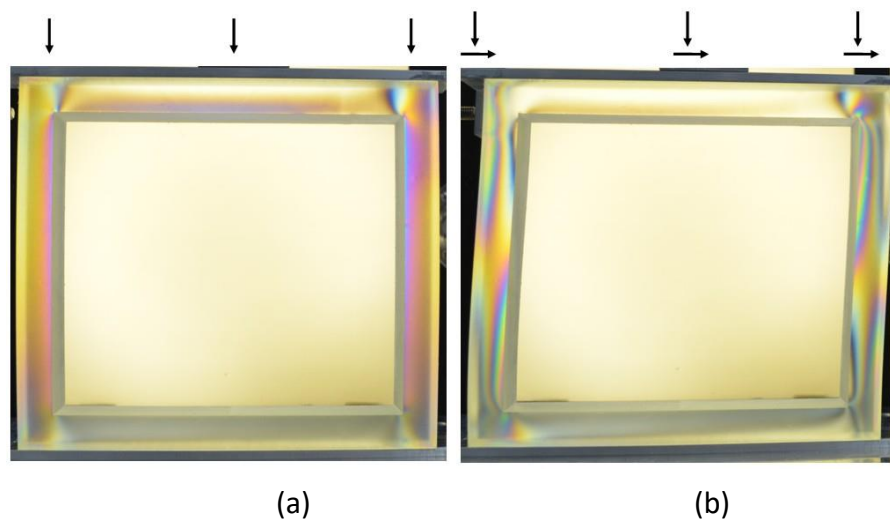
Figure 7.15 Stress distribution in single frame under (a) normal load only and (b) normal and shear load.

(a)   (b)
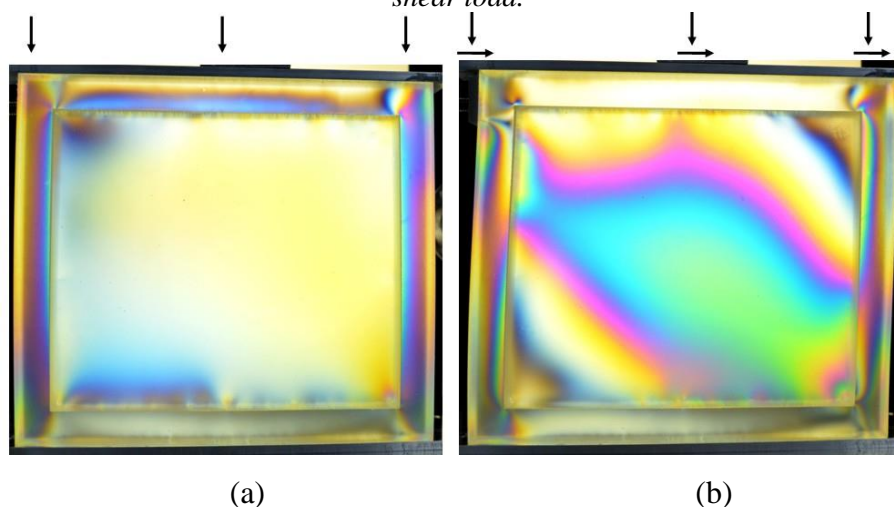
Figure 7.16 Stress distribution in single frame under (a) normal load only and (b) normal and shear load.

7.1.4.2.2   Frame Building Models

In this section, photo-elasticity tests on 4 story frame structures with/without infill walls and weak-floor conditions are carried out and stress distributions are investigated. Figure 7.17 shows the 4-story frame structure without infill walls under normal load only and normal and shear load conditions. As noted from the figure, stress concentrations are quite high at the column and beam connections. Furthermore, stresses are symmetric with respect to the middle of the structure. Particularly shear (horizontal) load causes high stress concentrations at the connections of columns and beams as expected. Concentrations at those connections causes cracking as often observed in earthquake reconnaissance.

(a)   (b)
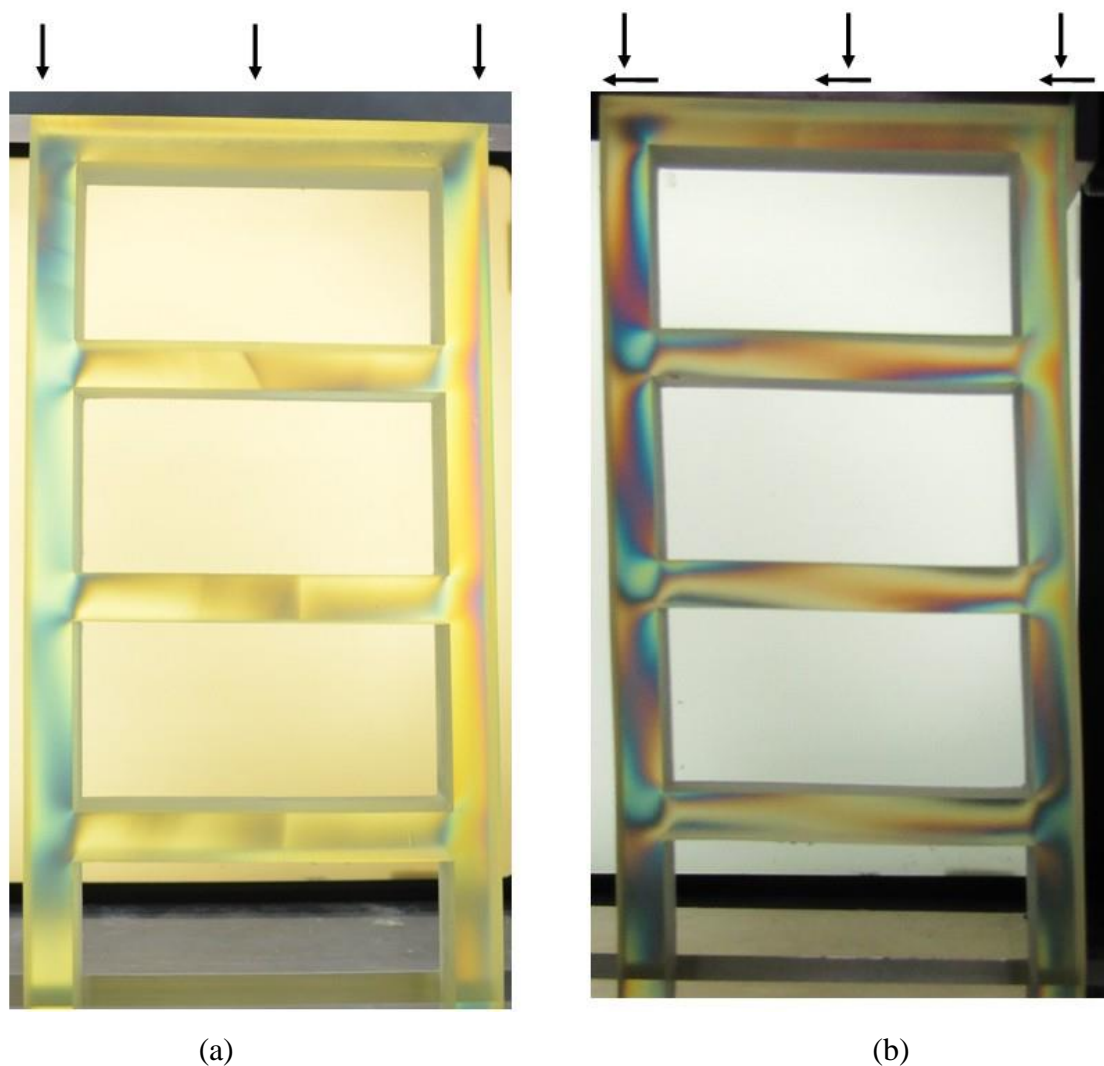
Figure 7.17 Stress distributions in 4 story frame structure under (a) normal load only and (b) normal and shear loads.

It is quite often observed that soft (weak) floor condition exist in frame structures due to shops, offices or parking area requirements. In other words, the ground floor consists of columns while upper floors generally have infill walls. Figure 7.18 shows the maximum shear stress distributions

in the 4-story frame structure with weak (soft) floor condition under normal load only and normal and shear load conditions. As noted from the figure the stress concentrations on columns at the ground floor are high and very high stress concentration occur at column-beam connection just below the first floor with infill wall. These results confirm that actual observations of earthquake damage at such locations.

(a)   (b)
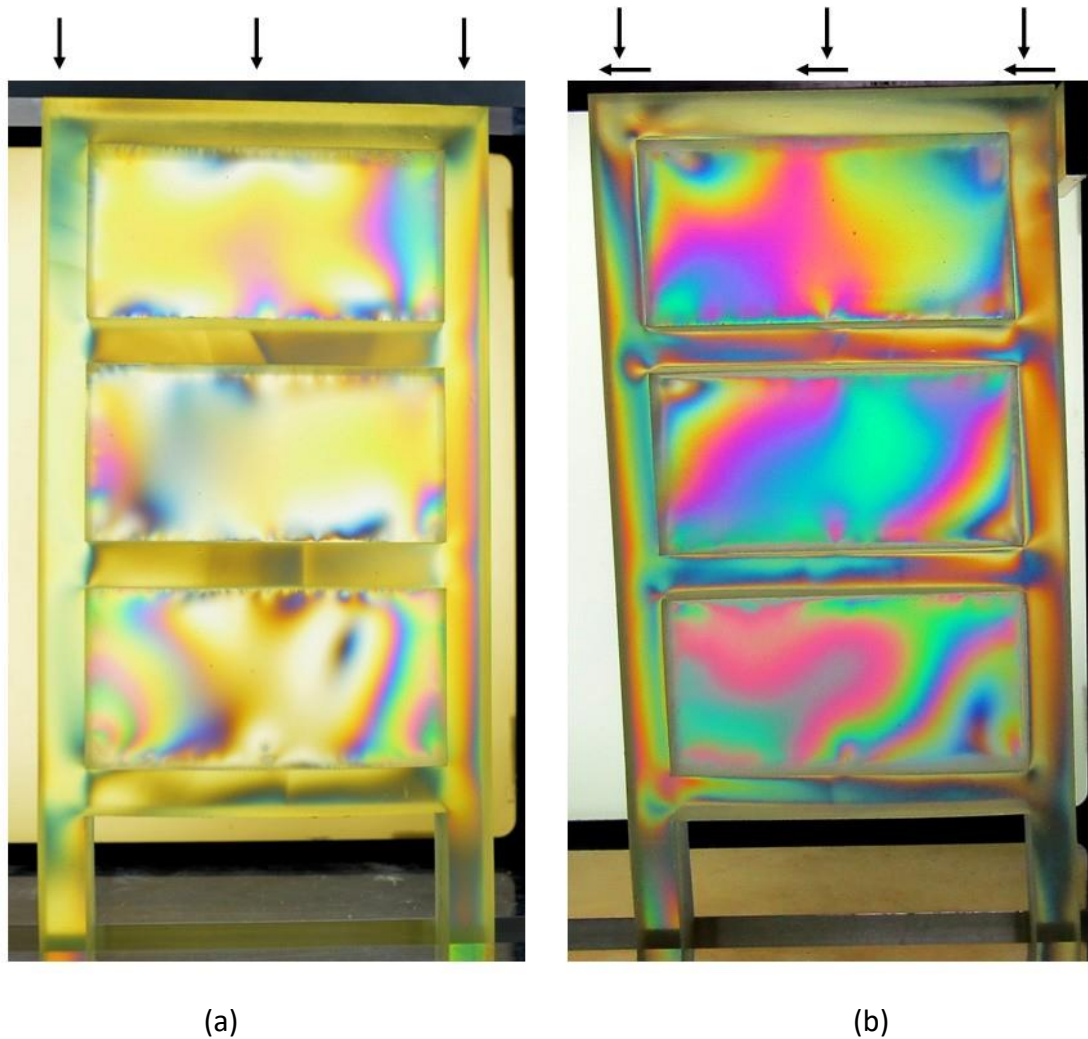
Figure 7.18 Stress distributions in 4 story frame structure with soft (weak) floor condition under (a) normal load only and (b) normal and shear loads.

When the frame structure has infill walls in each floor, loads on column decreases and stress concentrations tend to decrease at the column-beam connections. However, it should be noted that this conclusion is valid provided that frames and infill walls are in good contact.

Figure 7.19 shows the maximum shear stress distributions in the 4-story frame structure with infill walls under normal load only and normal and shear load conditions. As noted from the figure the stress concentrations on columns at the ground floor are drastically decreased as compared with high very high stress concentration at the ground floor columns in the case of framed weak floor structure.

(a)   (b)
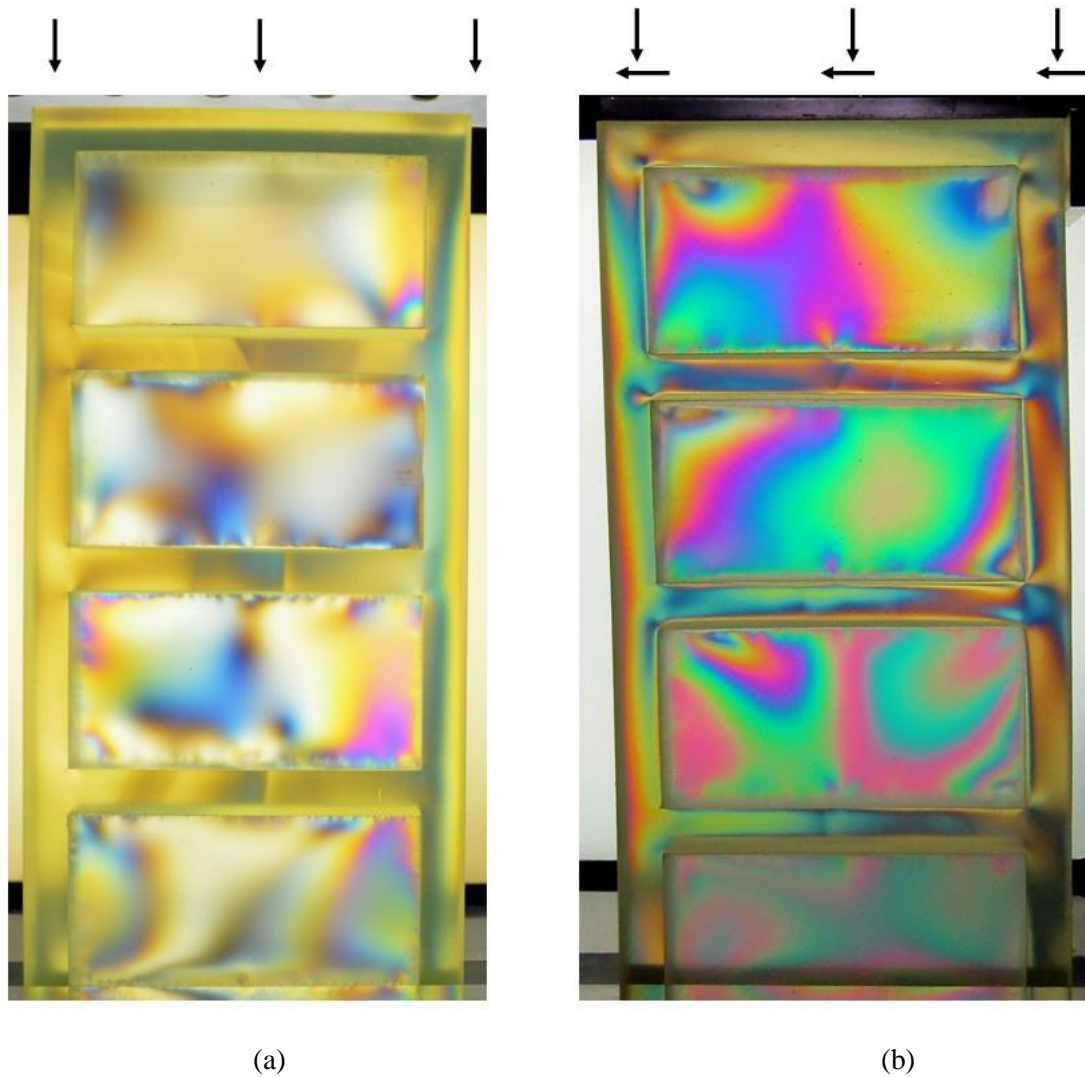
Figure 7.19 Stress distributions in 4 story frame structure with infill walls under (a) normal load only and (b) normal and shear loads.

7.1.5   Finite Element Analyses of Physical Models used in Photo-Elasticity Tests

7.1.5.1   *Material Properties*

Finite element analyses require data on mechanical properties of physical models. Some compressions experiments were carried out to determine the elastic modulus and Poisson's ratio. Figure 7.20 shows the strain-stress response of several polyurethane samples under uniaxial compression condition. Table 7.1 summarize the material properties several polyurethane samples. Polyurethane-20 used for faults, infill walls, layers and blocks while polyurethane-40 was utilized as materials of frame of single-frame and RC frame structures.

Table 7.1 The elastic modulus and Poisson's ratio of several polyurethane samples

Material	Elastic Modulus (MPa)	Poisson's ratio	Models used
Polyurethane-20	7.3	0.38	Faults, infill walls, layers and blocks
Polyurethane-40	15.8	0.20	Frames
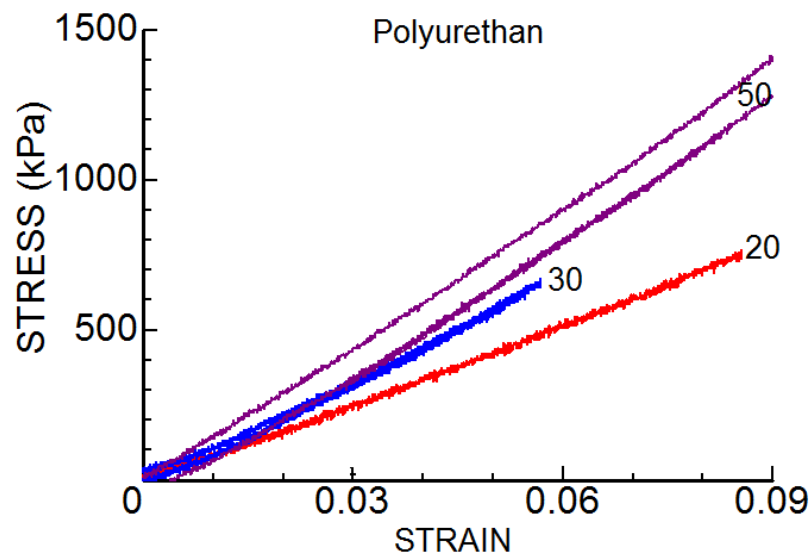
Figure 7.20 The strain-stress response of several polyurethane samples under uniaxial compression condition

7.1.5.2   Fault Models

7.1.5.2.1   Slit-like Fault Models under Uniaxial Compression

Finite element analyses were carried out for slit -like faults with an inclination of 0 and 90 degrees subjected to uniaxial loading condition were analyzed. The bottom side of the models was fully fixed. Figure 7.21 and Figure 7.22 show the maximum shear stress distributions. As noted from the figures, stress concentrations are quite high at the end of slits. However, the amplitude of maximum shear stress is much higher for the 0-degree slit-like fault.
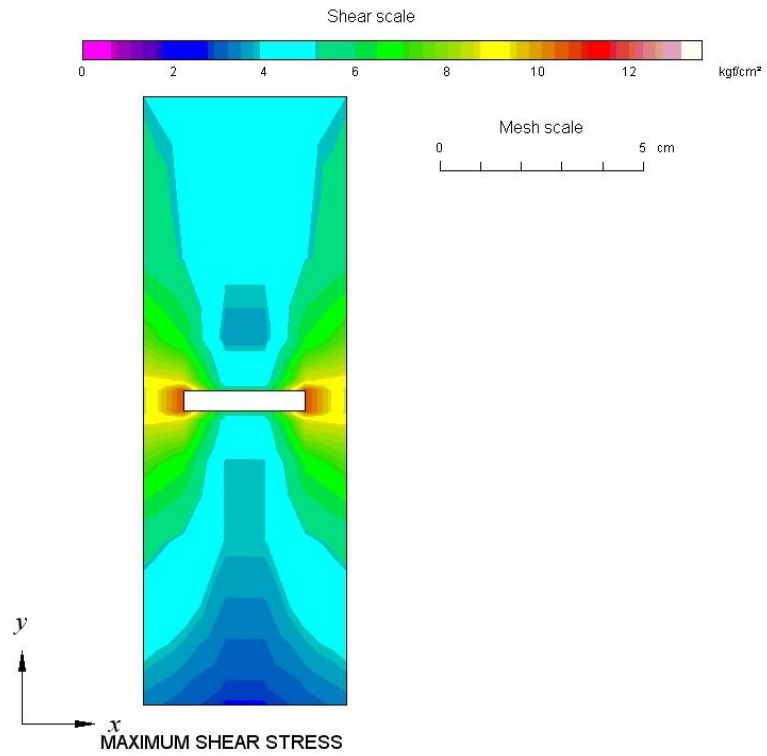
Figure 7.21 Maximum shear stress distribution for 0 degree slit-like fault
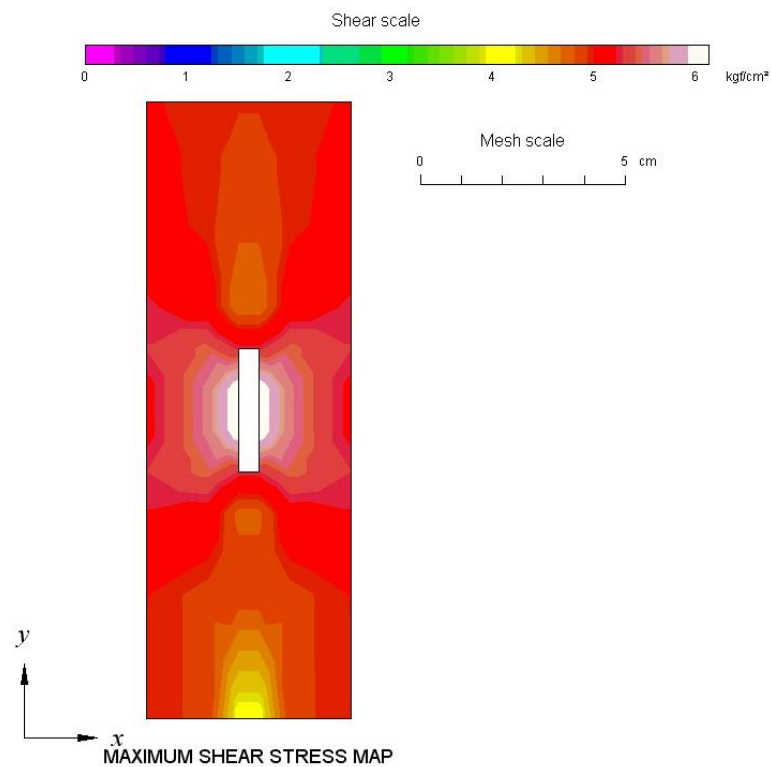
Figure 7.22 Maximum shear stress distribution for 90 degree slit-like fault

7.1.5.2.2   Fault Models under Shearing

Next finite faults with zero thickness were analyzed under no contact and frictional contact. Figure 7.23 to Figure 7.26 show minimum principal stress and maximum shear stress distributions for given contact conditions. The bottom of the models was fixed a subjected to uniform shear traction at the top of the model. The high stress concentrations occur in the vicinity of the tip of fault. The stress is much higher for under no contact or frictionless fault compared with frictional contact. Distribution of minimum principal stress distributions are quite close to those of the photo-elasticity tests.
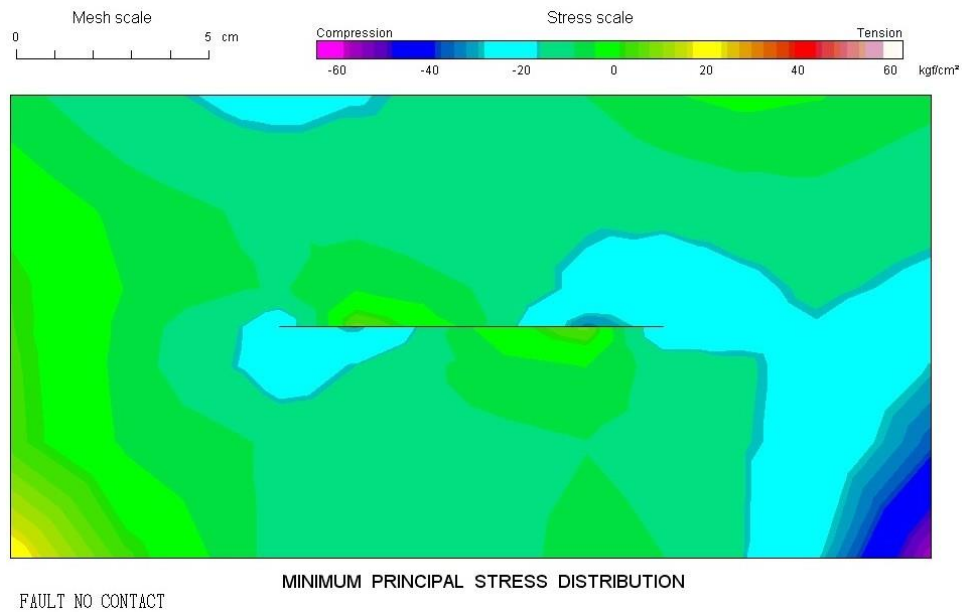
Figure 7.23 Minimum principal stress distribution (no-contact fault)
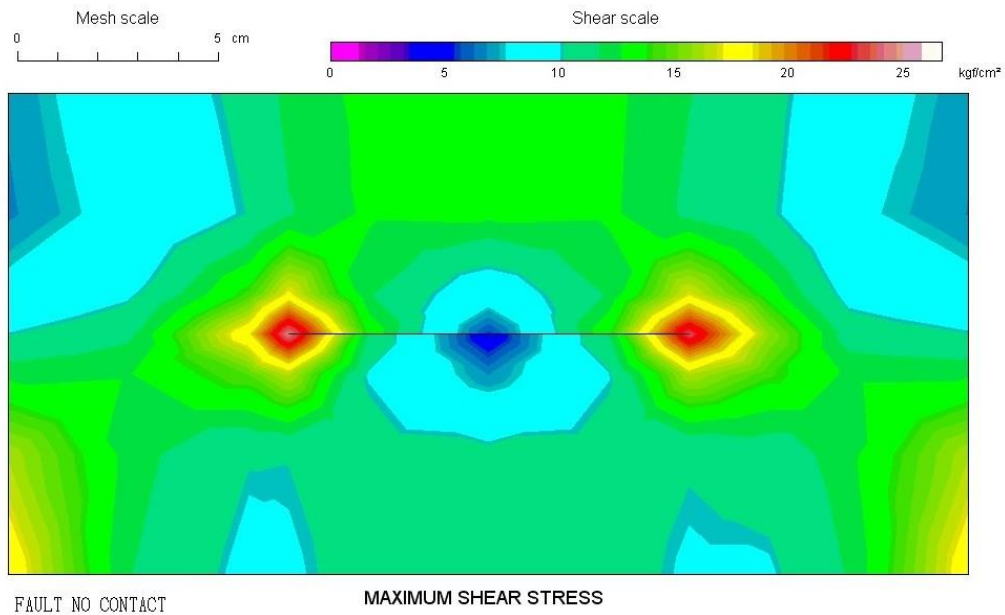
Figure 7.24 Maximum shear stress distribution (no-contact fault)
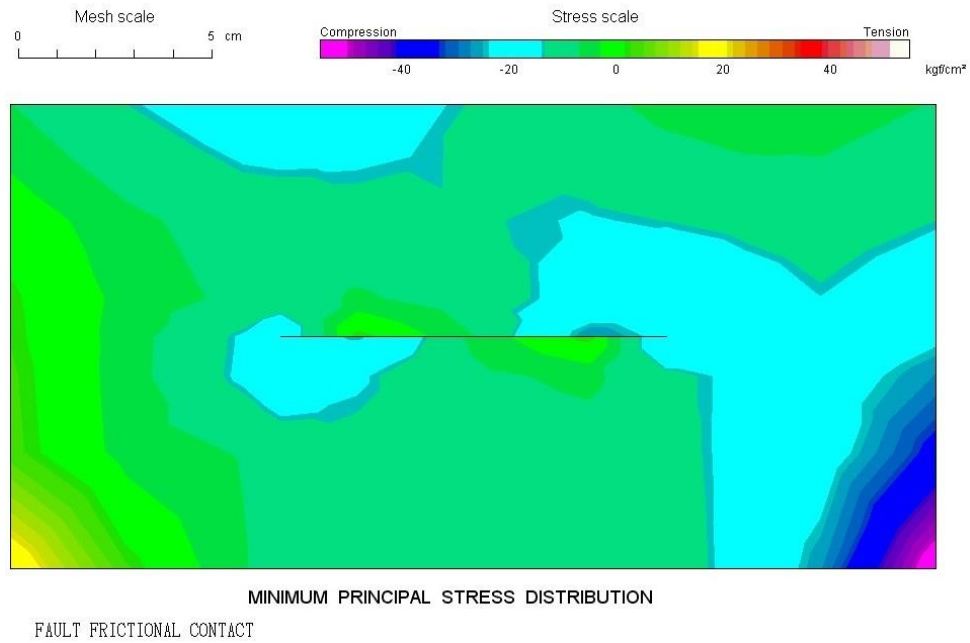
Figure 7.25 Minimum principal stress distribution (frictional fault)
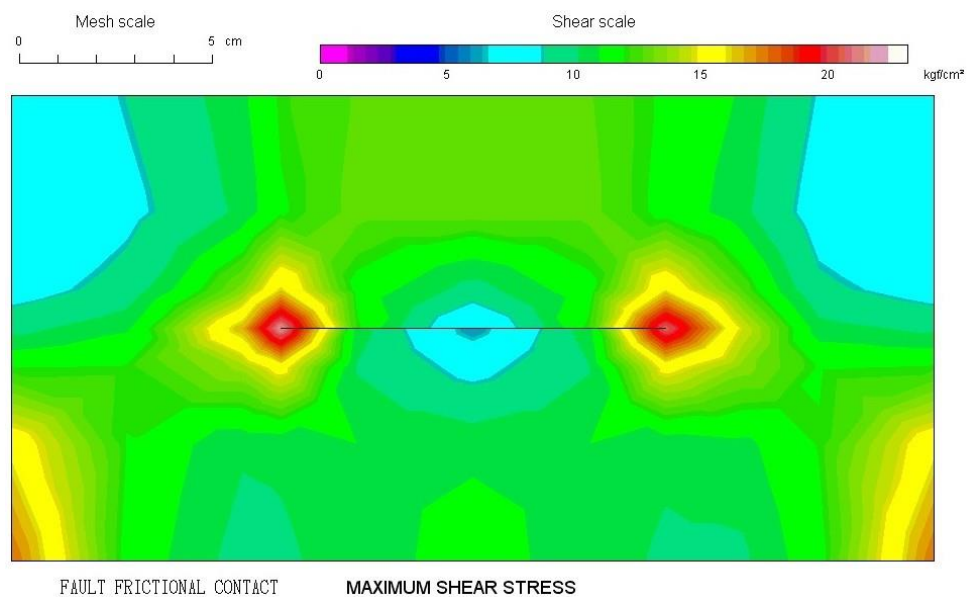
Figure 7.26 Maximum shear stress distribution (frictional contact fault)

7.1.5.3   *Single-frame Models under Combined Compression and Shearing*

Next the effect of infill walls on the response of single frame subjected to combined compression and shearing loads. Walls were considered to be in fully contact condition with while the bottom of the models were fixed. The results of computations are showed in Figure 7.27 to Figure 7.30. As noted from the figures, the infill walls increase the stiffness so that deformation of the models become smaller. Furthermore, the stress state is entirely different and less stress concentrations occurred when stress distributions for both cases are compared.
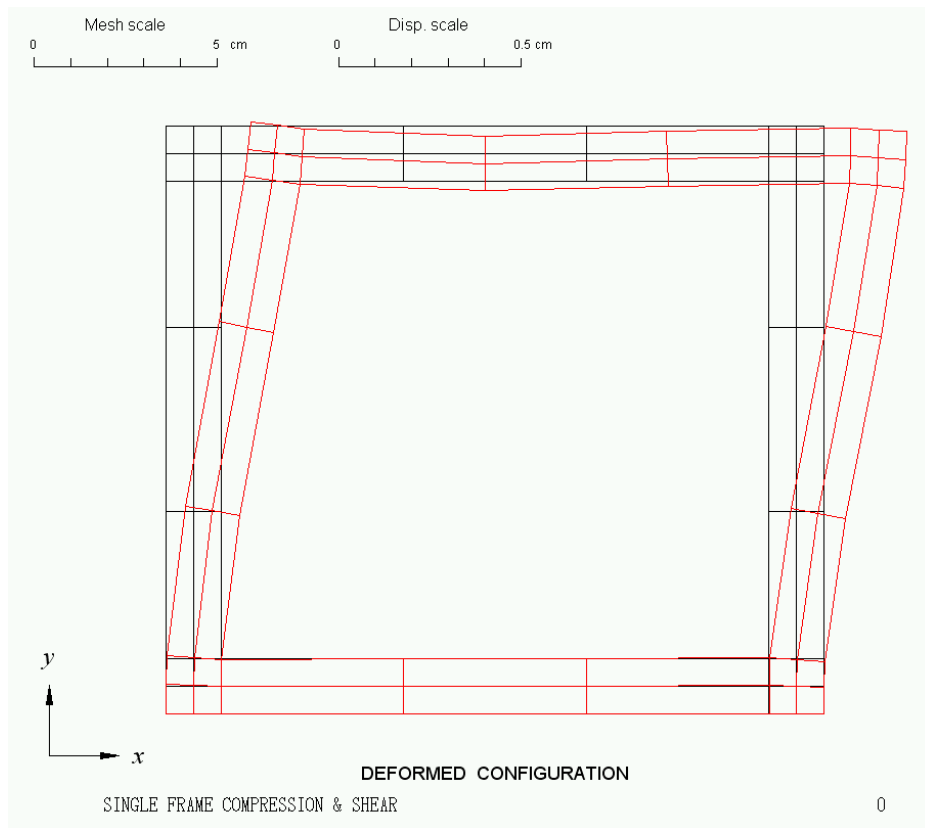
Figure 7.27 Deformed configuration (single bare frame)
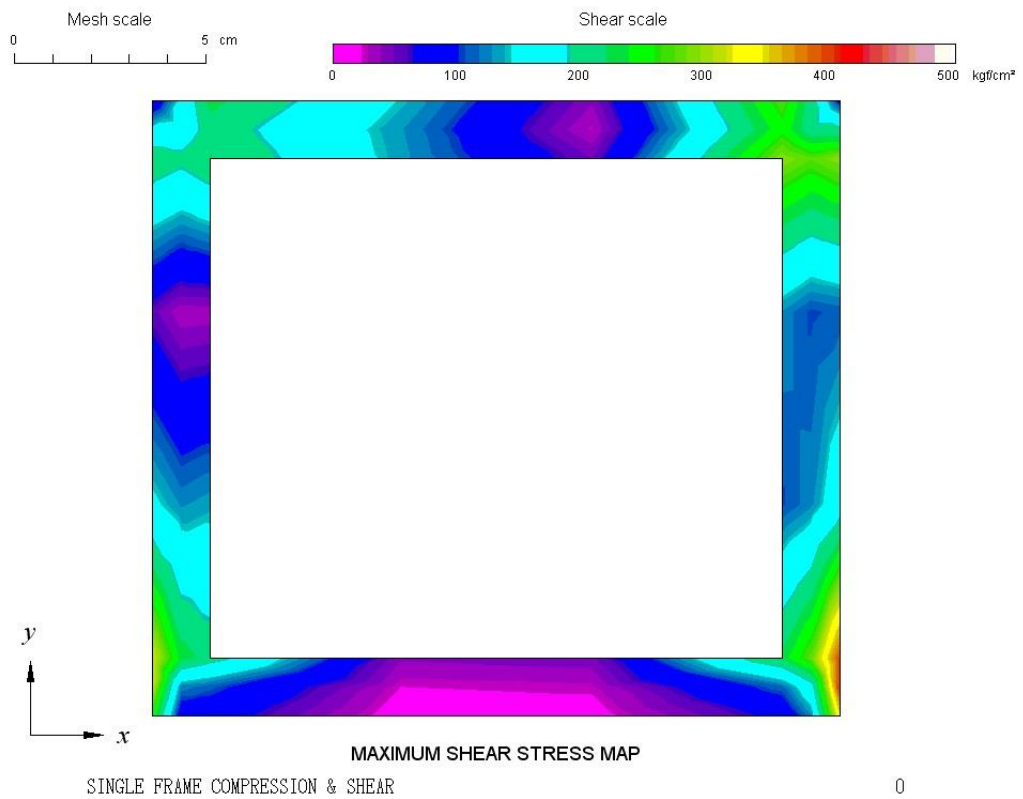
Figure 7.28 Maximum shear stress distribution (single bare frame)
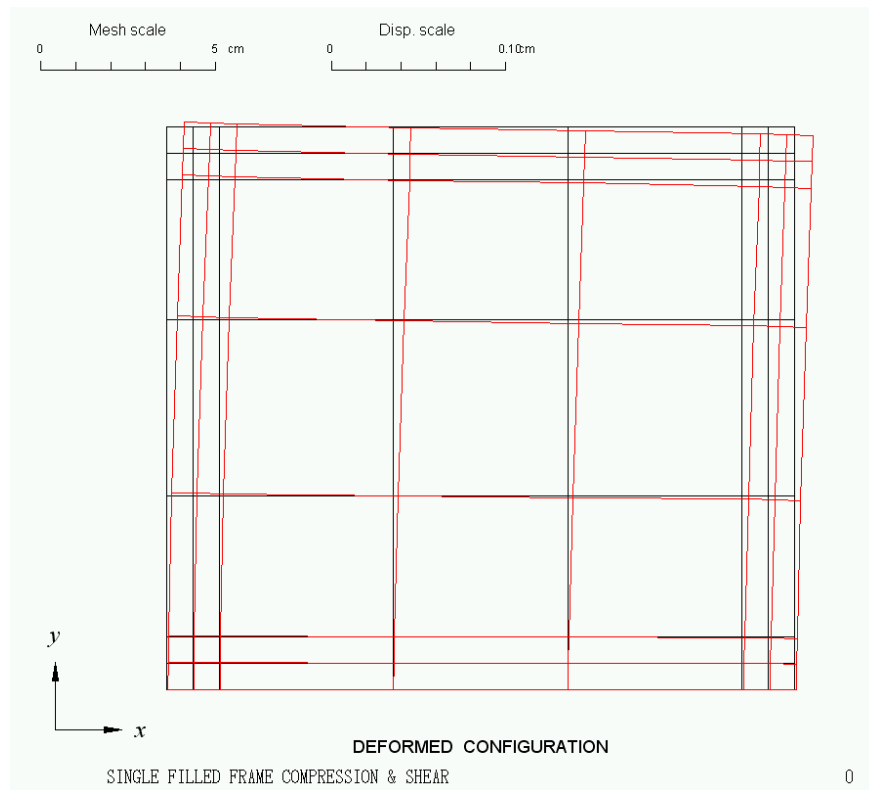
Figure 7.29 Deformed configuration (single frame with infill wall)
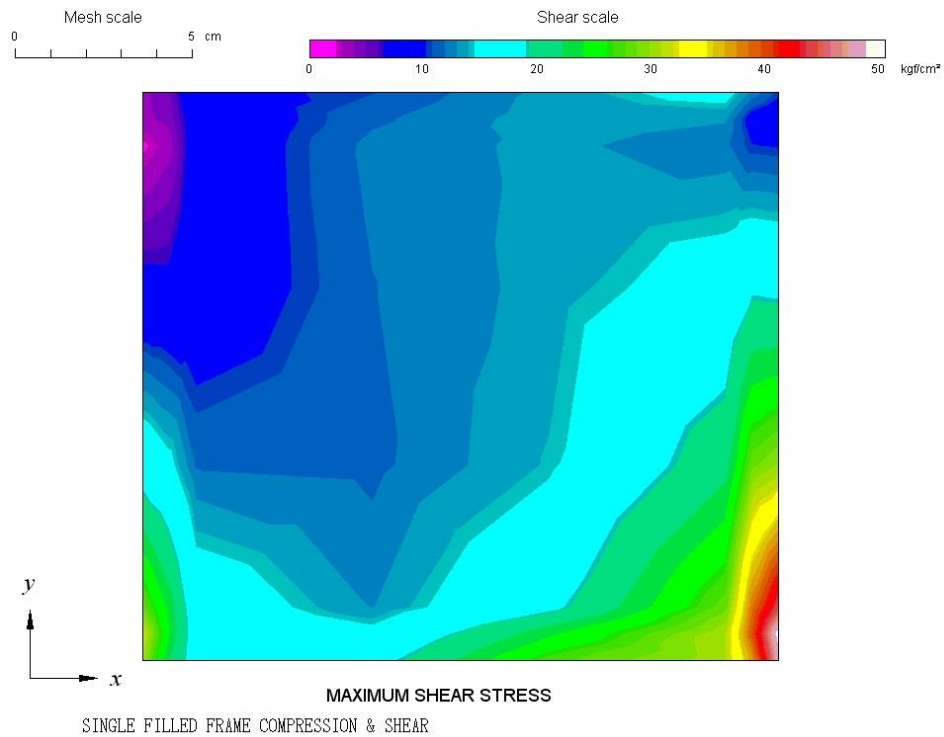
Figure 7.30 Maximum shear stress distribution (single frame with infill wall)

7.1.5.3.1   Four Story Frame Models under Combined Compression and Shearing

Finally, four story frame buildings were analyzed for bare, weak floor (soft story) and full infill walls under a combined compression and shearing. Deformed configurations and maximum shear stress distributions are shown in Figure 7.31 to Figure 7.33. The results are quite similar to those of photo-elasticity tests. Although the stiffness of the 4-story bare frame model is less stiff, the stress distribution is quite uniform (Figure 7.31). On the other hand, stress concentrations at the first floor of the 4-story frame model with weak floor is quite high (Figure 7.32). This shows that the structures having weak floor (soft story) are quite vulnerable to be damage at the first floor. The stress state of 4 story frame structure with full infill walls is more uniform, and the deformation is much less as seen in Figure 7.33.
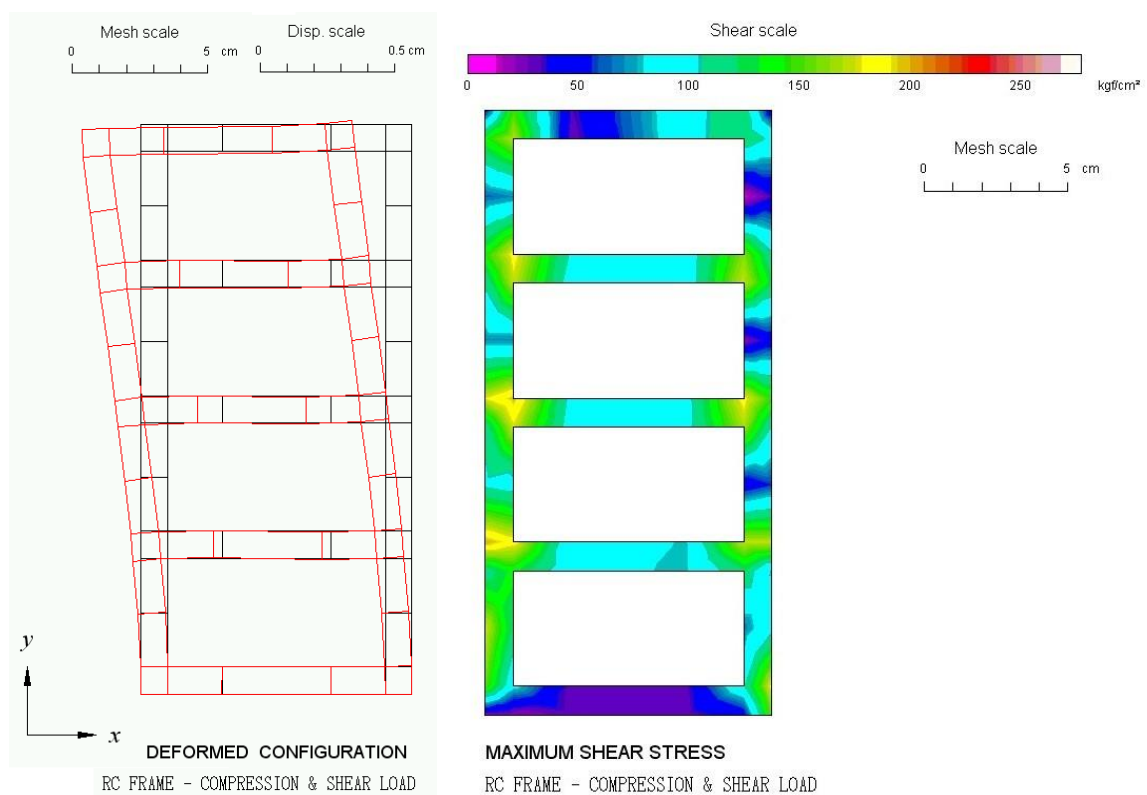
(a) Deformed configuration   (b) Maximum shear stress distribution

Figure 7.31 Computed deformed configuration and maximum shear stress distribution of 4 story bare frame structure subjected to combined compression and shearing
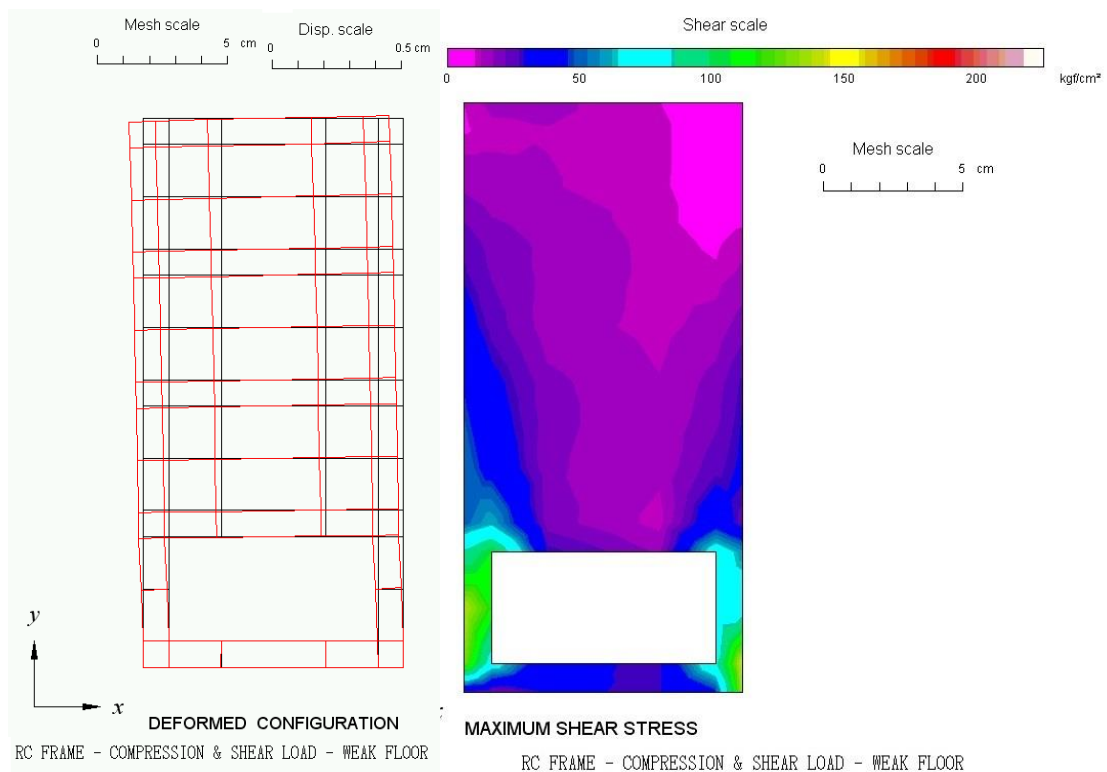
(a) Deformed configuration   (b) Maximum shear stress distribution

Figure 7.32 Computed deformed configuration and maximum shear stress distribution of 4 story frame structure with weak floor (soft story) subjected to combined compression and shearing
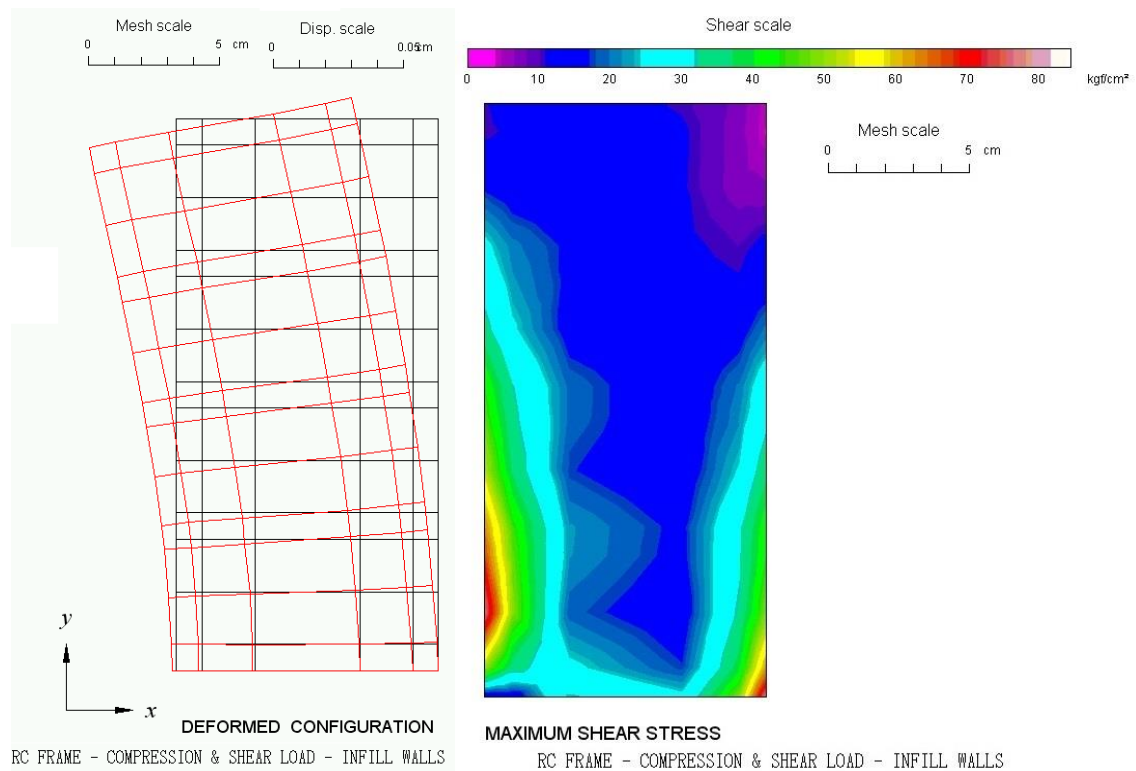
Figure 7.33 Computed deformed configuration and maximum shear stress distribution of 4 story frame structure with infill walls subjected to combined compression and shearing

119

7.2   Shaking Table Tests on Physical Model Tests of Masonry Walls

Some physical model tests have been also carried out to investigate the dynamic responses of masonry walls by varying the wall height and the number of lintels. Blocks were made of woods and they correspond to dry masonry condition. Some particular attention was given to the number of lintels on the overall stability and deformation responses of the masonry walls. Figure 7.34 to Figure 7.36 show views of the model walls before and after shaking for various height of the masonry walls.
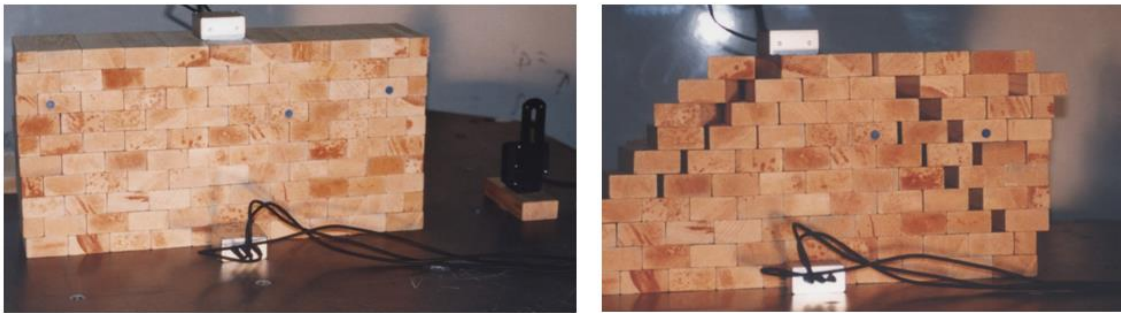
Figure 7.34 Views of the wall with 9 layers of wooden blocks before and after shaking
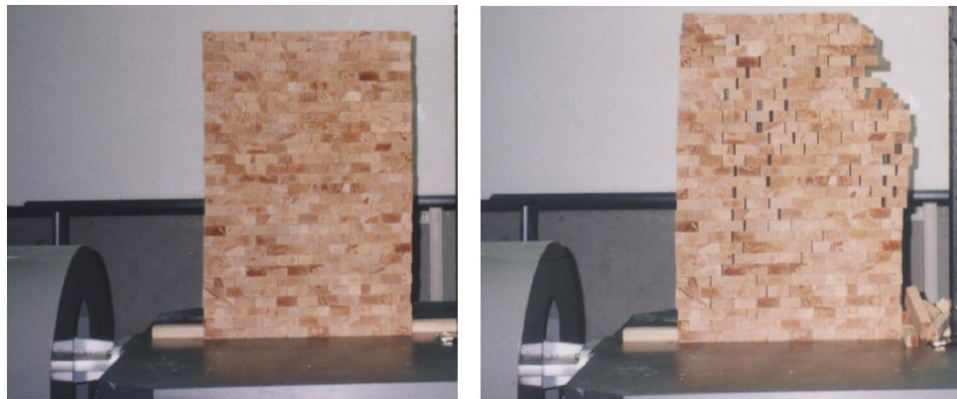
Figure 7.35 Views of the wall with 30 layers of wooden blocks before and after shaking
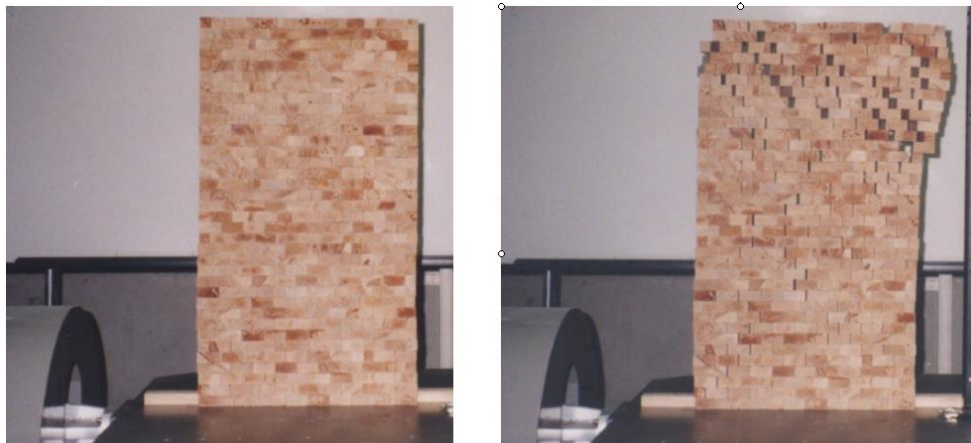
Figure 7.36 Views of the wall with 30 layers of wooden blocks before and after shaking

Figure 7.37 shows the wall with 48 layers of wooden blocks having different number of lintels. In this particular experiment, the lintel number was varied from 0 to 3. Figure 7.38 shows an example of input acceleration and acceleration response measured at the top of the wall with 48 layers of wooden blocks. The amplitude of the input wave was 50 gals and frequency was ranged from 4 to 14 gals. As noted from the figure, large amplification of the acceleration is noted. Figure 7.39 shows the Fourier spectrum of the response of the wall. The frequency of the wall was 6.56 Hz. Figure 7.40 shows the Fourier spectra of the top of the wall for different number of lintels. This result implies that the masonry walls with lintels may sustain larger ground motions subjected to in-plane (shear) loading.

Figure 7.37 Views of the wooden masonry walls with different number of lintels.
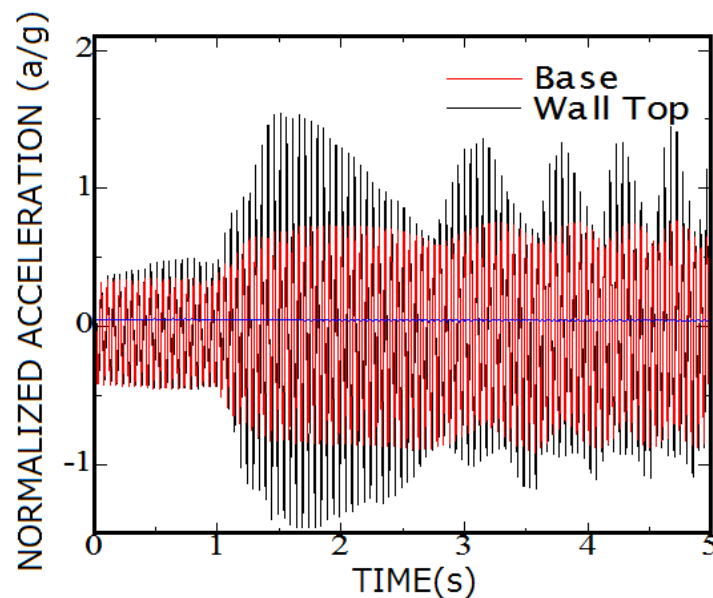
Figure 7.38 Acceleration records of the base acceleration and the acceleration response at the top of the wall.
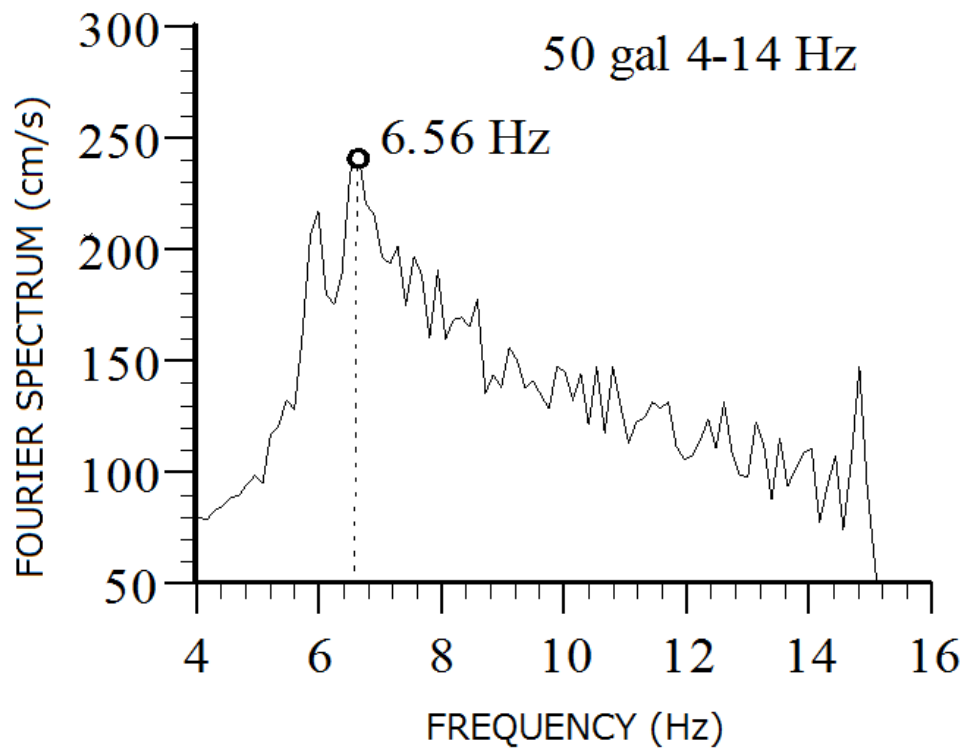
Figure 7.39 The Fourier spectrum of the acceleration response of the top of the wall.
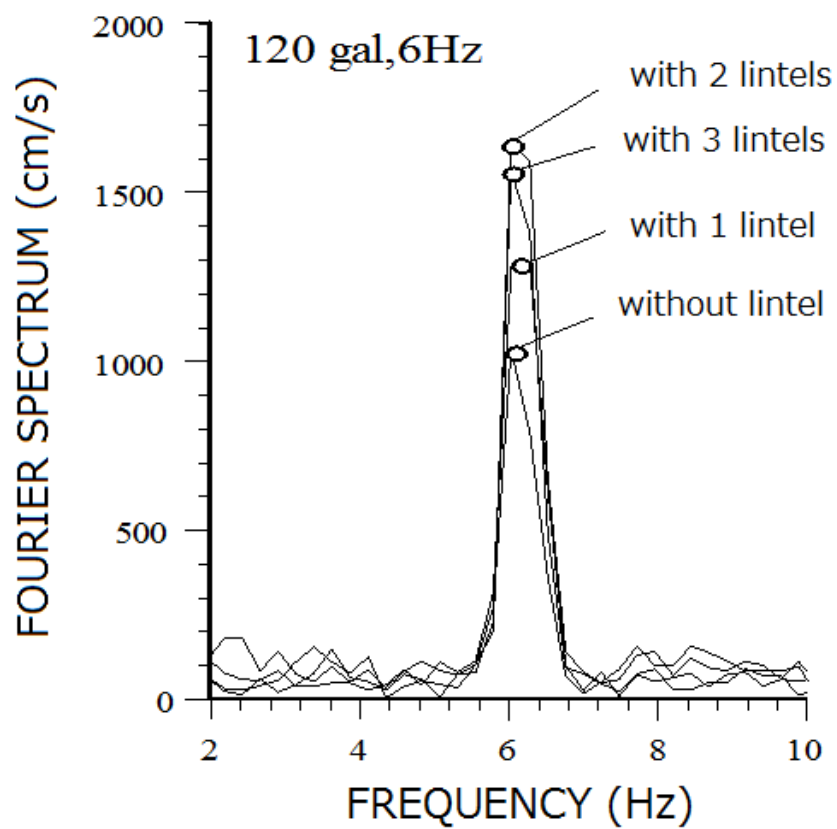
Figure 7.40 The Fourier spectrum of the acceleration response of the top of the wall with different number of lintels.

Figure 7.41 shows views of the wall with 2 lintels before and after shaking. It is interesting to note that slippage and opening of the blocks limited by the existence of lintels. In other words, lintels act as a restrainer of failure, which definitely increase the ductility of the masonry wall in-plane loading condition. Figure 7.42 shows the permanent displacement as a function of shaking duration. This figure clearly illustrates the ductility of the masonry walls with lintels when they are subjected to in-plane (shear) loading.

Figure 7.41 Views of the wooden masonry wall before and after shaking
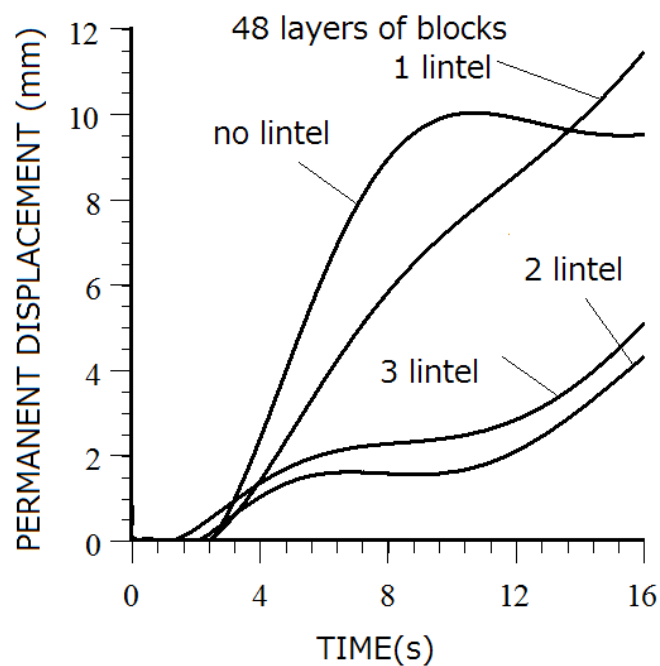
Figure 7.42 Permanent displacement responses of the masonry wall with 48 layers of wooden blocks and different number of lintels as a function shaking duration.

7.3 Shaking Table Tests on Masonry Structure Model

Finally, model experiments were carried out on a masonry building structure subjected to shaking and its failure modes presented. The experiments were concerned with single story houses having a heavy roof using plastic blocks with the dimensions of 50x50x20mm. The model houses were built in such way that two sidewalls would be parallel to ground shaking while two walls would be subjected to out-of plane loading. Figure 7.43 shows an example of input acceleration response measured at the top of the model masonry house. It is interesting to notice that slippage occur at the acceleration level of 220-225 gals. Figure 7.44 shows some views of the masonry house before and after shaking. experiments together with accelerations records. The experiments clearly showed that the walls, which are subjected to out-of plane loading, tend to collapse first while the side-walls parallel to shaking tend to fail by inter-block sliding. The ground shaking to cause total collapse of the side-walls parallel to the direction of shaking should be such that the total relative displacement of the inter-block sliding should exceed the half length of the block in the respective direction. The experiments are also showed that the corners of the buildings are quite prone to fail first due to the concentration of two modes at such particular locations. As concluded by Aydan et al. (2003), for ordinary masonry structures, toppling or overturning failure would take place at lower intensity of shaking as compared with that related to sliding failure.
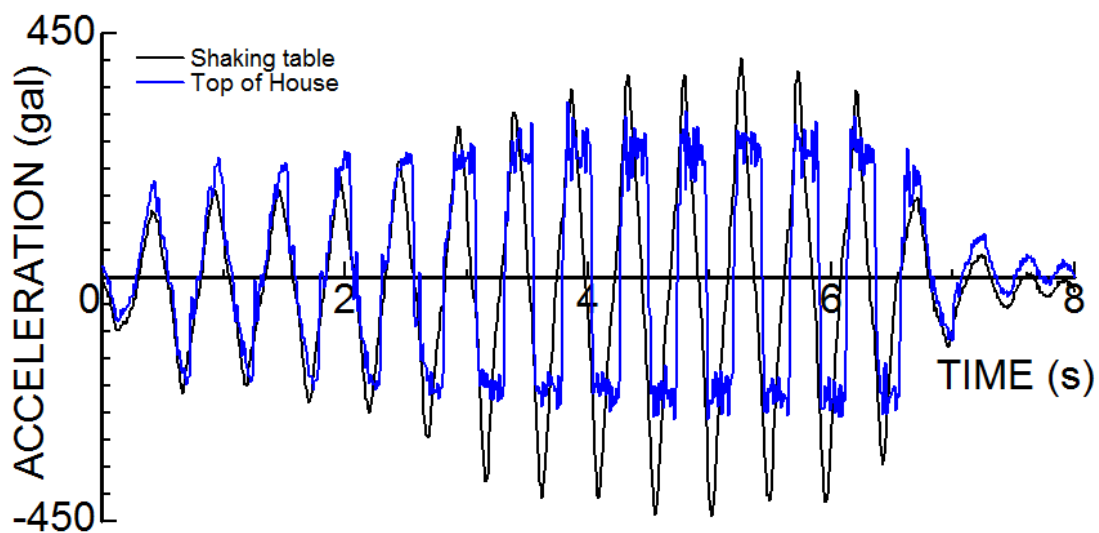
Figure 7.43 Records of acceleration on the shaking table and top of the model masonry house.
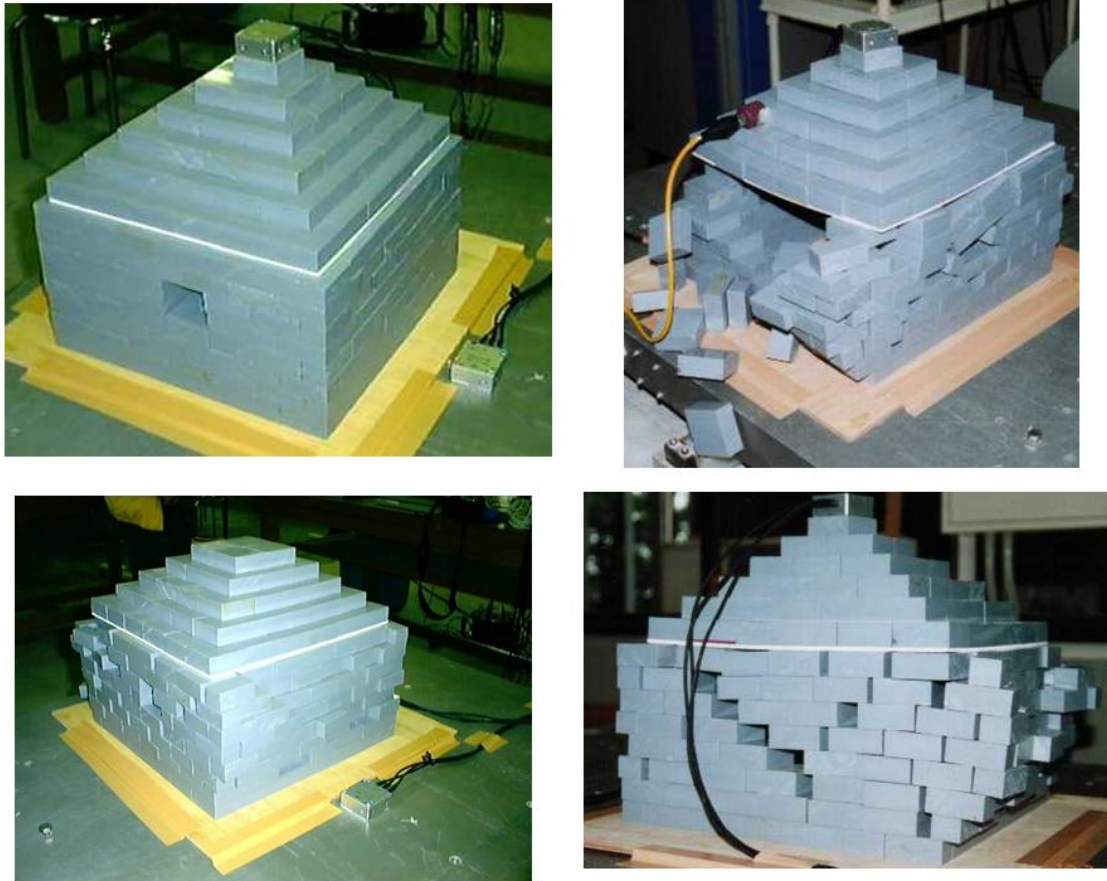
Figure 7.44 Views of the model masonry house before and after shaking

CHAPTER 8 EVALUATION OF VIBRATION CHARACTERISTICS OF STRUCTURES

8.1 Theory of Vibrations and Wave Propagation

8.1.1 Momentum Conservation Law

Any structure or continuum body subjected to motion, the momentum conservation law should hold. Momentum is defined in integral form as given below (e.g. (Eringen, 1980; Mase, 1970) and Aydan 2017).

$$\mathbf{p} = \int_{\Omega} \rho \mathbf{v} d\Omega \tag{8.1}$$

Preliminary relations

$$\int_{\Omega} \nabla \cdot \boldsymbol{\sigma} d\Omega = \int_{\Gamma} \boldsymbol{\sigma} \cdot \mathbf{n} d\Gamma \; ; \; \frac{d(d\Omega)}{dt} = = (\nabla \cdot \mathbf{x}) d\Omega \; ; \; \mathbf{t} = \boldsymbol{\sigma} \cdot \mathbf{n} \tag{8.2}$$

Conservation of momentum is written in the following form in view of Eq. (8.2), which is also known Reynolds transport Theorem (Figure 8.1)

$$\frac{d}{dt} \int_{\Omega} \rho \mathbf{v} d\Omega = \int_{\Gamma} \mathbf{t} d\Gamma + \int_{\Omega} \mathbf{b} d\Omega \tag{8.3}$$

Eq. (8.3) may be re-written as

$$\int_{\Omega} \left(\frac{d(\rho \mathbf{v})}{dt} + (\rho \mathbf{v}) \nabla \cdot \mathbf{v} \right) d\Omega = \int_{\Omega} \nabla \cdot \boldsymbol{\sigma} d\Omega + + \int_{\Omega} \mathbf{b} d\Omega \tag{8.4}$$

Carrying out the derivation in Eq.(4), we have the following

$$\int_{\Omega} \left(\left(\frac{d\rho}{dt} + \rho (\nabla \cdot \mathbf{v}) \right) \mathbf{v} \right) d\Omega + \int_{\Omega} \rho \frac{d\mathbf{v}}{dt} d\Omega = \int_{\Omega} (\nabla \cdot \boldsymbol{\sigma} + \mathbf{b}) d\Omega \tag{8.5}$$

The first term on left hand side disappears by virtue of mass conservation law takes the following form

$$\int_{\Omega} \rho \frac{d\mathbf{v}}{dt} d\Omega = \int_{\Omega} (\nabla \cdot \boldsymbol{\sigma} + \mathbf{b}) d\Omega \tag{8.6}$$

Eq. (6) may be re-written as

$$\int_{\Omega} \left[\rho \frac{d\mathbf{v}}{dt} - \left(\nabla \cdot \boldsymbol{\sigma} + \mathbf{b} \right) \right] d\Omega = 0 \tag{8.7}$$

To satisfy Eq. (8.7), the integrand should be zero so that we have the following relation

$$\rho \frac{d\mathbf{v}}{dt} = \nabla \cdot \boldsymbol{\sigma} + \mathbf{b} \tag{8.8}$$

Furthermore, the derivation on the left-hand side may be related to acceleration or displacement vectors as follow:

$$\frac{d\mathbf{v}}{dt} = \mathbf{a} \ \text{ or } \ \frac{d\mathbf{v}}{dt} = \frac{d^2\mathbf{u}}{dt^2} \tag{8.9}$$
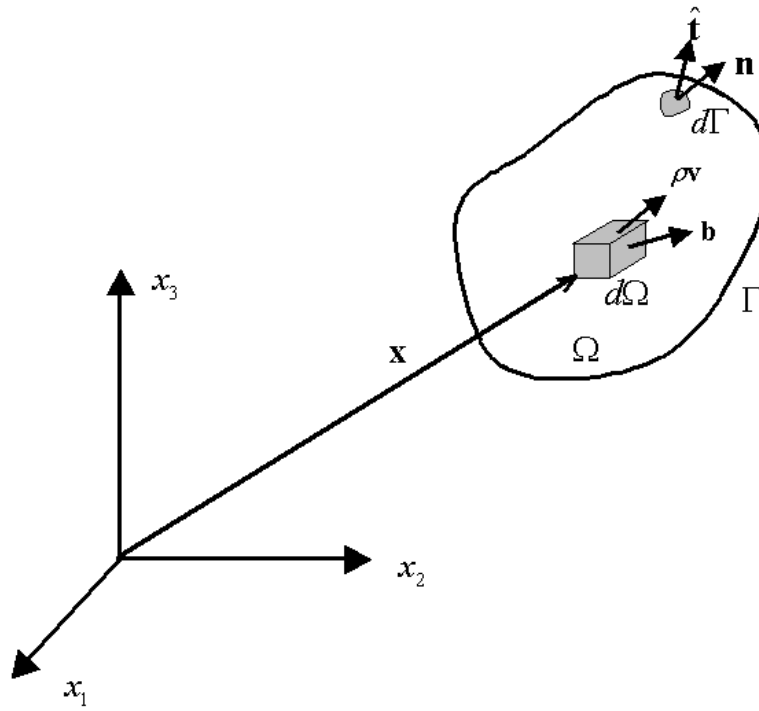
Figure 8.1 Illustration of momentum conservation law (from Aydan 2017)

8.1.2 Earthquake Induced Elastic Waves

It is known that earthquakes cause fundamentally two types of earthquakes (Figure 8.2). First type waves are called body waves and they are p-wave and s-wave. P wave or primary waves pass through every material. S-waves or secondary waves arrive the observation point after the p-wave. The second type waves are called surface waves and they are further subdivided into Rayleigh and Love waves. Figure 8.3 shows a record of 1939 Erzincan earthquake taken at Harvard University. It is known that shear waves are not transmitted through materials in liquid phase. As the outer

core of the earth is in liquid phase, no shear waves are observed beyond 143 degrees from the earthquake focus. Surface waves (Rayleigh and Love) are observed near the earth surface and they disappear as the depth increases.
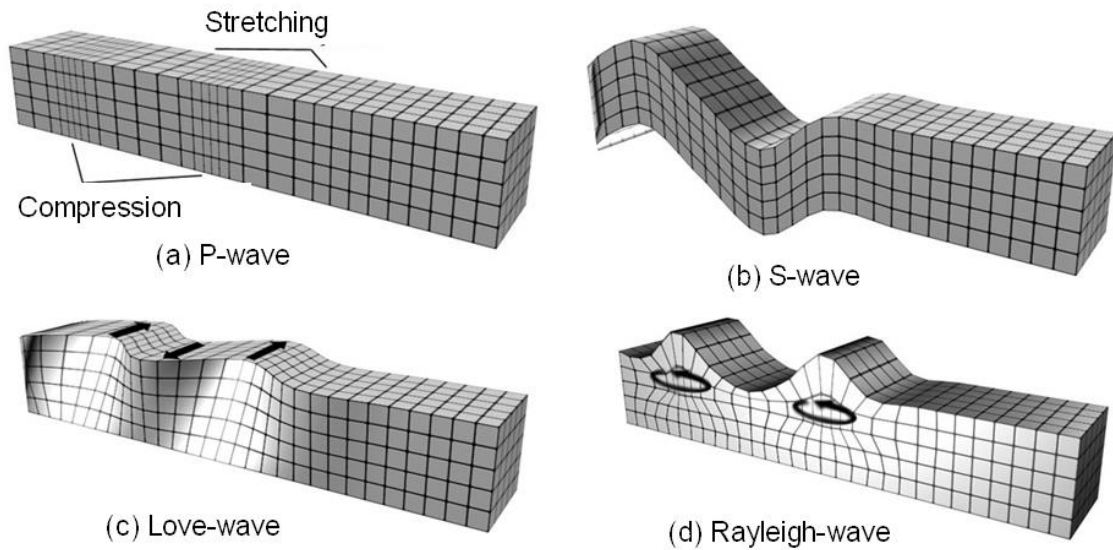
Figure 8.2 Illustration of wave types
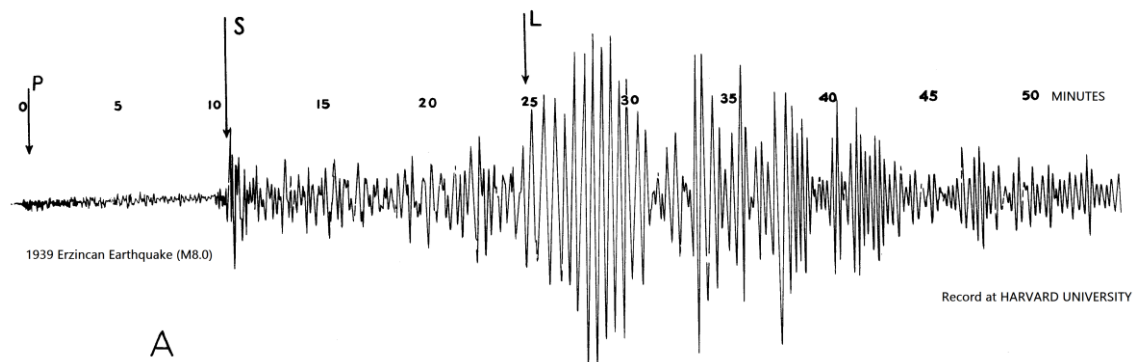
Figure 8.3 The seismogram of the 1939 Erzincan earthquake at Harvard University (from Ketin, 1970)

The equation of motion given by Eq. (8.8) can be re-written in the index notation as follow

$$\frac{\partial \sigma_{ij}}{\partial x_j} + b_i = \rho \frac{\partial^2 u_i}{\partial t^2}$$
(8.9a)

or specifically

$$\frac{\partial \sigma_{11}}{\partial x_1} + \frac{\partial \sigma_{12}}{\partial x_2} + \frac{\partial \sigma_{13}}{\partial x_3} + b_1 = \rho \frac{\partial^2 u_1}{\partial t^2} \tag{8.9b}$$

$$\frac{\partial \sigma_{12}}{\partial x_1} + \frac{\partial \sigma_{22}}{\partial x_2} + \frac{\partial \sigma_{23}}{\partial x_3} + b_2 = \rho \frac{\partial^2 u_2}{\partial t^2} \tag{8.9c}$$

$$\frac{\partial \sigma_{13}}{\partial x_1} + \frac{\partial \sigma_{23}}{\partial x_2} + \frac{\partial \sigma_{33}}{\partial x_3} + b_3 = \rho \frac{\partial^2 u_3}{\partial t^2} \tag{8.9d}$$

Normal strain components are related to components of displacement vector if infinitesimal strain approach is adopted

$$\varepsilon_{ij} = \frac{1}{2}\left(\frac{\partial u_i}{\partial x_j} + \frac{\partial u_j}{\partial x_i} \right) \tag{8.10a}$$

or specifically

$$\varepsilon_{11} = \frac{\partial u_1}{\partial x_1} \; ; \; \varepsilon_{22} = \frac{\partial u_2}{\partial x_2} \; ; \; \varepsilon_{33} = \frac{\partial u_3}{\partial x_3} \tag{8.10b}$$

Engineering shear strains are related to the components

$$\gamma_{ij} = 2\varepsilon_{ij} \text{ with } i \neq j \tag{8.10c}$$

or specifically

$$\gamma_{23} = \frac{\partial u_2}{\partial x_3} + \frac{\partial u_3}{\partial x_2} \; ; \; \gamma_{12} = \frac{\partial u_1}{\partial x_2} + \frac{\partial u_2}{\partial x_1} \; ; \; \gamma_{13} = \frac{\partial u_1}{\partial x_3} + \frac{\partial u_3}{\partial x_1} \tag{8.10d}$$

Rotational strains are defined as

$$\omega_1 = \frac{1}{2}\left(\frac{\partial u_3}{\partial x_2} - \frac{\partial u_2}{\partial x_3} \right) ; \omega_2 = \frac{1}{2}\left(\frac{\partial u_1}{\partial x_3} - \frac{\partial u_3}{\partial x_1} \right) ; \; \omega_3 = \frac{1}{2}\left(\frac{\partial u_2}{\partial x_1} - \frac{\partial u_1}{\partial x_2} \right) \tag{8.10e}$$

The constitute law between stress and strain can be expressed if material is isotopic elastic body as

$$\sigma_{ij} = \lambda \delta_{ij} \varepsilon_{kk} + 2\mu \varepsilon_{ij} \; ; \; \varepsilon_{kk} = \varepsilon_{11} + \varepsilon_{22} + \varepsilon_{33} \; ; \tag{8.11a}$$

or specifically

$$\begin{Bmatrix} \sigma_{11} \\ \sigma_{22} \\ \sigma_{33} \\ \sigma_{12} \\ \sigma_{23} \\ \sigma_{13} \end{Bmatrix} = \begin{bmatrix} \lambda+2\mu & \lambda & \lambda & 0 & 0 & 0 \\ \lambda & \lambda+2\mu & \lambda & 0 & 0 & 0 \\ \lambda & \lambda & \lambda+2\mu & 0 & 0 & 0 \\ 0 & 0 & 0 & \mu & 0 & 0 \\ 0 & 0 & 0 & 0 & \mu & 0 \\ 0 & 0 & 0 & 0 & 0 & \mu \end{bmatrix} \begin{Bmatrix} \varepsilon_{11} \\ \varepsilon_{22} \\ \varepsilon_{33} \\ \gamma_{12} \\ \gamma_{23} \\ \gamma_{13} \end{Bmatrix} \qquad (8.11b)$$

Where λ and μ are Lame coefficients are specifically given in the following form:

$$\lambda = \frac{E\upsilon}{(1+\upsilon)(1-2\upsilon)} \quad \text{and} \quad \mu = \frac{E}{2(1+\upsilon)} \qquad (8.12)$$

Let us introduce the followings

$$\Delta = \frac{\partial u_1}{\partial x_1} + \frac{\partial u_2}{\partial x_2} + \frac{\partial u_3}{\partial x_3} \qquad (8.13a)$$

$$\nabla^2 = \nabla \cdot \nabla = \frac{\partial^2}{\partial x_1^2} + \frac{\partial^2}{\partial x_2^2} + \frac{\partial^2}{\partial x_3^2} \qquad (8.13b)$$

Eq. (8.13a) corresponds to volumetric strain while Eq.(8.13b) is called Laplacian operator.

Inserting constitutive law given by Eq.(8.11) together with relations between strain and displacement components given by Eq. (8.10) into the equation of motion and differentiating Eqs. (8.10b, 8.10c, 8.10d) with respect to x_1, x_2 and x_3, respectively yields for each respective directions provided that elastic coefficients, density and body forces are constant as follow,

$$(\lambda+\mu)\frac{\partial^2 \Delta}{\partial x_1^2} + \mu\nabla^2 \frac{\partial u_1}{\partial x_1} = \rho\frac{\partial}{\partial x_1}\left(\frac{\partial^2 u_1}{\partial t^2}\right) \qquad (8.15a)$$

$$(\lambda+\mu)\frac{\partial^2 \Delta}{\partial x_2^2} + \mu\nabla^2 \frac{\partial u_2}{\partial x_2} = \rho\frac{\partial}{\partial x_2}\left(\frac{\partial^2 u_2}{\partial t^2}\right) \qquad (8.15b)$$

$$(\lambda+\mu)\frac{\partial^2 \Delta}{\partial x_3^2} + \mu\nabla^2 \frac{\partial u_3}{\partial x_3} = \rho\frac{\partial}{\partial x_3}\left(\frac{\partial^2 u_3}{\partial t^2}\right) \qquad (8.15c)$$

Summing up 10.32a, 10.32b and 10.32c results in the following equation

$$(\lambda + \mu)\nabla^2\Delta + \mu\nabla^2\Delta = \rho\frac{\partial^2\Delta}{\partial t^2} \quad \text{or} \quad V_p^2\nabla^2\Delta = \frac{\partial^2\Delta}{\partial t^2} \quad \text{or} \quad V_p^2\nabla^2\varepsilon_v = \frac{\partial^2\varepsilon_v}{\partial t^2} \qquad (8.16)$$

where

$$\lambda + 2\mu = \frac{E\upsilon}{(1+\upsilon)(1-2\upsilon)} + \frac{E}{1+\upsilon} = \frac{E(1-\upsilon)}{(1+\upsilon)(1-2\upsilon)} \qquad (8.17a)$$

$$V_p = \sqrt{\frac{E(1-\upsilon)}{\rho(1+\upsilon)(1-2\upsilon)}} \qquad (8.17b)$$

$$\varepsilon_v = \Delta \qquad (8.17c)$$

Eq. (8.16) is known as the governing equation of p-wave propagation in solids. As it is noted from this equation p-wave propagation is directly related to volumetric straining. During the propagation of p-wave, solid will undergo dilatational and compressive volumetric straining.

Similarly inserting constitutive law given by Eq.(8.11) together with relations between strain and displacement components given by Eq. (8.10) into the equation of motion takes the following form specifically for each respective direction

$$(\lambda + \mu)\frac{\partial\Delta}{\partial x_1} + \mu\nabla^2 u_1 + b_1 = \rho\frac{\partial^2 u_1}{\partial t^2} \qquad (8.18a)$$

$$(\lambda + \mu)\frac{\partial\Delta}{\partial x_2} + \mu\nabla^2 u_2 + b_2 = \rho\frac{\partial^2 u_2}{\partial t^2} \qquad (8.18b)$$

$$(\lambda + \mu)\frac{\partial\Delta}{\partial x_3} + \mu\nabla^2 u_3 + b_3 = \rho\frac{\partial^2 u_3}{\partial t^2} \qquad (8.18c)$$

Differentiating Eqs. (8.18b) (8.18c) with respect to x_3 and x_2 yields the followings provided that elastic coefficients, density and body forces are constant.

$$(\lambda + \mu)\frac{\partial^2\Delta}{\partial x_3\partial x_2} + \mu\nabla^2\frac{\partial u_2}{\partial x_3} = \rho\frac{\partial^2}{\partial t^2}\left(\frac{\partial u_2}{\partial x_3}\right) \qquad (8.19a)$$

$$(\lambda + \mu)\frac{\partial^2\Delta}{\partial x_2\partial x_3} + \mu\nabla^2\frac{\partial u_3}{\partial x_2} = \rho\frac{\partial^2}{\partial t^2}\left(\frac{\partial u_3}{\partial x_2}\right) \qquad (8.19b)$$

Subtracting (8.19a) from (8. 19b)   results in

$$(\lambda + \mu)\left(\frac{\partial^2 \Delta}{\partial x_2 \partial x_3} - \frac{\partial^2 \Delta}{\partial x_3 \partial x_2}\right) + \mu \nabla^2 \left(\frac{\partial u_3}{\partial x_2} + \frac{\partial u_2}{\partial x_3}\right) = \rho \frac{\partial^2}{\partial t^2}\left(\frac{\partial u_3}{\partial x_2} - \frac{\partial u_2}{\partial x_3}\right) \quad (8.20)$$

Using the rotational strain definition given by Eq. (8.10e) and dividing Eq. (8.20) gives

$$\frac{\mu}{\rho} \nabla^2 \omega_1 = \frac{\partial^2 \omega_1}{\partial t^2} \qquad\qquad (8.21a)$$

Using the same procedure for other directions together with rotation strain components given by Eq. (8.10e), one can easily derive the followings,

$$\frac{\mu}{\rho} \nabla^2 \omega_2 = \frac{\partial^2 \omega_2}{\partial t^2} \qquad\qquad (8.21b)$$

$$\frac{\mu}{\rho} \nabla^2 \omega_3 = \frac{\partial^2 \omega_3}{\partial t^2} \qquad\qquad (8.21c)$$

Eq. (8.21) is the governing equation of Rayleigh waves. The coefficient in Eq. (8.21) is interpreted as the propagation velocity of rotational waves

$$V_s = \sqrt{\frac{\mu}{\rho}} \text{ or } V_s = \sqrt{\frac{E}{2\rho(1+\upsilon)}} \qquad\qquad (8.22)$$

If Δ is 0 and body force is negligible, one easily gets the following expressions from Eq. (8.19)

$$\frac{\mu}{\rho} \nabla^2 u_1 = \frac{\partial^2 u_1}{\partial t^2} \text{ or } V_s^2 \nabla^2 u_1 = \frac{\partial^2 u_1}{\partial t^2} \qquad\qquad (8.23a)$$

$$\frac{\mu}{\rho} \nabla^2 u_2 = \frac{\partial^2 u_2}{\partial t^2} \text{ or } V_s \nabla^2 u_2 = \frac{\partial^2 u_2}{\partial t^2} \qquad\qquad (8.23b)$$

$$\frac{\mu}{\rho} \nabla^2 u_3 = \frac{\partial^2 u_3}{\partial t^2} \text{ or } V_s \nabla^2 u_2 = \frac{\partial^2 u_2}{\partial t^2} \qquad\qquad (8.23c)$$

Eq. (8.23) is known the fundamental equation of distortion (shear) waves known as S-waves. It should be noted that the propagation velocity of S-waves is the same as that of Rayleigh waves.

8.1.3 Numerical Solution of Equation of Motion and Natural Frequency and Damping Characteristics

The final forms of discretized form of equation of motion (8.9) irrespective of method of solution (FDM, FEM, BEM) and continuum or discontinuum, depending upon the character of governing equation, may be written in the following form:

$$[M]\{\ddot{\phi}\} + [C]\{\dot{\phi}\} + [K]\{\phi\} = \{F\} \qquad (8.24)$$

The specific forms of matrices [M], [C], [K] and vector {F} in the equation above will only differ depending upon the method of solution chosen and dimensions of physical space. Viscosity matrix [C] is associated with rate-dependency of geomaterials. However, in many dynamic solution schemes, viscosity matrix [C] is expressed in the following form using Rayleigh damping approach as

$$[C] = \alpha[M] + \beta[K] \qquad (8.25)$$

where α, β are called proportionality constants. This approach becomes very convenient in large-scale problems if central finite difference technique and mass lumping are used.

Natural frequencies of any structure or continuum body can be obtained from the following equation system by assuming that damping matrix [C] is nil and external force {F} are zero in Eq. (8.25).

$$[M]\{\ddot{U}\} + [K]\{U\} = \{0\} \qquad (8.26)$$

Eq. (8.26) is known as the equations system of free-vibration.

Requiring the variable vector {U} can be expressed as a harmonic function given as

$$\{U\} = \{\phi\}e^{iwt} \qquad (8.27)$$

If Eq. (8.27) is inserted in Eq. (8.26), one can easily obtains the following equation system

$$([K] - \omega^2[M])\{\phi\} = \{0\} \qquad (8.28)$$

Solution of equation (8.28) is known as Eigen value analyses yielding ω^2 and $\{\phi\}$. ω^2 is known Eigen values and $\{\phi\}$ Eigen value vector.

8.1.4 Simplification of Structures for Determination of Their Vibration Characteristics

Although the most appropriate method would be the solution of equation of motions under given boundary and initial conditions, the structural are often simplified to obtain their approximate responses and vibration characteristics. They are mostly simplified to single degree of freedom structures by assuming they may vibrate either in shear mode or bending mode.
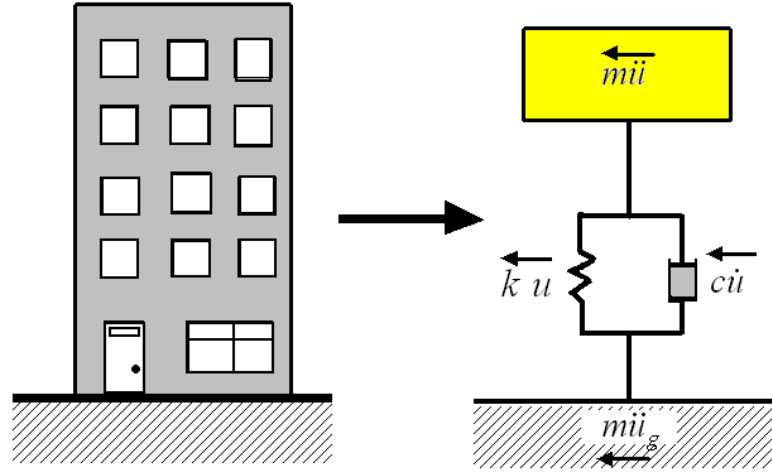
Figure 8.4 Simplification of structures as single-degree of freedom structure.

The force equilibrium of a simplified structure shown in Figure 8.4, may be give as

$$\sum_{K=1}^{n} F_i = F_{eq} - F_d - F_e - F_I = 0 \qquad (8.29)$$

where

$$F_d = c\frac{du}{dt} \;;\; F_e = k\,u \;;\; F_{eq} = -m\frac{d^2 u_g}{dt^2} \;;\; F_I = m\frac{d^2 u}{dt^2} \qquad (8.30)$$

Eq. (8.29) may be reduced to the following form by using relations given in Eq. (8.30) as

$$m\frac{d^2 u}{dt^2} + c\frac{du}{dt} + k\,u = -m\frac{d^2 u_g}{dt^2} \qquad (8.31)$$

Introducing the following relations

$$\omega_o = \sqrt{\frac{k}{m}} \;;\; 2h\omega_o = \frac{c}{m} \qquad (8.32)$$

Eq. (8.31) may be reduced to the following form

$$\frac{d^2u}{dt^2} + 2h\omega_o \frac{du}{dt} + \omega_o^2 u = -\frac{d^2u_g}{dt^2} \tag{8.33}$$

where ω_o is known as angular natural frequency and h is damping coefficient.

Free Vibration

If damping coefficient and base acceleration are zero, Eq. (8.33) reduces to the following form:

$$\frac{d^2u}{dt^2} + \omega_o^2 u = 0 \tag{8.34}$$

The solution of Eq. (8.34) is obtained as follows

$$u = C_1 e^{\lambda_1 t} + C_2 e^{\lambda_2 t} \tag{8.35}$$

where the roots are given specifically as

$$\lambda_1 = i\omega_o; \lambda_2 = -i\omega_o; i = \sqrt{-1} \tag{8.36}$$

Using the following relations

$$e^{i\omega_0} = \cos\omega_o t + i\sin\omega_o t \text{ and } e^{-i\omega_0} = \cos\omega_o t - i\sin\omega_o t \tag{8.37}$$

Thus, the final form of solution is

$$u = A\cos\omega_o t + B\sin\omega_o t \tag{8.38}$$

Introducing the following initial conditions

$$u(0) = u_0; \dot{u}(0) = v_0 \text{ at } t = 0 \tag{8.39}$$

yields the integration coefficients as

$$A = u_0; B = \frac{v_0}{\omega_0} \tag{8.40}$$

Thus, the exact solution takes the following form

$$u = u_0 \cos \omega_o t + \frac{v_0}{\omega_0} \sin \omega_o t \qquad (8.41)$$

Eq. (8.41) may be re-written by introducing the following identities

$$R \cos \theta = u_0 \,; R \sin \theta = \frac{v_0}{\omega_0} \,; R = \sqrt{\left(\frac{v_0}{\omega_0}\right)^2 + u_0^2} \qquad (8.42)$$

as

$$u = R \cos(\omega_o t - \theta) \qquad (8.43)$$

Finally, one obtains the vibration characteristics of the structure such as natural period, natural frequency in terms of natural angular frequency as

$$T_0 = \frac{1}{f_0} = \frac{2\pi}{\omega_0} \qquad (8.44)$$

Damped Free Vibration

If base acceleration is zero, Eq. (8.33) reduces to the following form:

$$\frac{d^2 u}{dt^2} + 2h\omega_o \frac{du}{dt} + \omega_o^2 u = 0 \qquad (8.45)$$

The solution of Eq. (8.45) can be obtained as follows:

$$u = C_1 e^{\lambda_1 t} + C_2 e^{\lambda_2 t} \qquad (8.46)$$

where roots are

$$\lambda_1 = -\omega_0 h + i\omega_d \,; \lambda_2 = -\omega_0 h - i\omega_d \,; i = \sqrt{-1} \,; \omega_d = \omega_0 \sqrt{1 - h^2} \qquad (8.47)$$

Thus, the general form of solution takes the following form

$$u = e^{-\omega_0 h t} \left(A \cos \omega_d t + B \sin \omega_d t \right) \qquad (8.48)$$

Introducing the following initial conditions

$$u(0) = u_0 \,; \dot{u}(0) = v_0 \text{ at } t = 0 \qquad (8.49)$$

136

yields the integration constants as

$$A = u_0 ; B = \frac{h\omega_0 u_0 + v_0}{\omega_d} \tag{8.50}$$

Inserting integration constants given by Eq. (8.50) into Eq. (8.48) results in

$$u = e^{-\omega_0 h t}\left\{ u_0 \cos \omega_d t + \frac{h\omega_0 u_0 + v_0}{\omega_d} \sin \omega_d t \right\} \tag{8.51}$$

Again, using the following identities,

$$R\cos\theta = u_0 ; R\sin\theta = \frac{h\omega_0 u_0 + v_0}{\omega_d} ; R = \sqrt{\left(\frac{h\omega_0 u_0 + v_0}{\omega_d}\right)^2 + u_0^2} \tag{8.52}$$

Eq. (8.51) takes the following form

$$u = e^{-\omega_0 h t} R \cos(\omega_d t - \theta) \tag{8.53}$$

where

$$T_d = \frac{1}{f_d} = \frac{2\pi}{\omega_d} = \frac{T_0}{\sqrt{1 - h^2}} \tag{8.54}$$

The value of damping coefficient h has the value of 0.02-0.05. To determine the value of damping coefficient h, the following procedure may be followed. The value of displacement response at given time step $t = t_{i+1}$ may be written as

$$u_{i+1} = e^{-\omega_0 h t_{i+1}} R \cos(\omega_d t_{i+1} - \theta) \tag{8.55}$$

Similarly, at a time step $t = t_i$, the displacement response may also be given as

$$u_i = e^{-\omega_0 h t_i} R \cos(\omega_d t_i - \theta) \tag{8.56}$$

Diving Eq. (8.56) by Eq. (8.55) yields the following

$$\frac{u_i}{u_{i+1}} = \frac{e^{-\omega_0 h t_i} R \cos(\omega_d t_i - \theta)}{e^{-\omega_0 h t_{i+1}} R \cos(\omega_d t_{i+1} - \theta)} \tag{8.57}$$

Introducing the following relations using the peak to peak values

$$T_d = t_{i+1} - t_i \,;\,; \quad \cos(\omega_d t_{i+1} - \theta) = 1\,; \quad \cos(\omega_d t_i - \theta) = 1 \qquad (8.58)$$

Eq. (8.57) may be re-written as

$$\ln\left(\frac{u_i}{u_{i+1}}\right) = \omega_0 h T_d = \frac{2\pi h}{\sqrt{1-h^2}} \qquad (8.59)$$

If $h \ll 1$, Eq. (8.59) may be further simplified so that damping coefficient h can be obtained as follow:

$$h = \frac{1}{2\pi} \ln\left(\frac{u_i}{u_{i+1}}\right) \qquad (8.60)$$

However, there will be a number of peak values. Therefore, if peak values are plotted in the space of u_{i+1} and u_i, a curve-fitting procedure will yield the value of damping coefficient h.

Forced Vibration subjected to sinusoidal vibration

Let us assume Eq. (8.33) is subjected to the base acceleration given as

$$\frac{d^2 u_g}{dt^2} = \alpha \sin \omega t \qquad (8.61)$$

The general solution of resulting differential equations can be written as

$$u = u_h + u_p \qquad (8.62)$$

where

$$u_h = e^{-\omega_0 h t}\left(A\cos\omega_d t + B\sin\omega_d t\right); \quad u_p = C\sin\omega t + D\cos\omega t \qquad (8.63a)$$

$$C = -\frac{\alpha}{\omega_0^2} \cdot \frac{1-(\omega/\omega_o)^2}{[1-(\omega/\omega_o)^2]^2 + 4h^2(\omega/\omega_o)^2} \,; \qquad (8.63b)$$

$$D = \frac{\alpha}{\omega_0^2} \cdot \frac{2h\omega/\omega_o}{[1-(\omega/\omega_o)^2]^2 + 4h^2(\omega/\omega_o)^2} \qquad (8.63c)$$

Non-homogenous part of the solution may be re-written as

$$u_p = R\sin(\omega_d t - \theta) \qquad (8.64)$$

138

where

$$R = \frac{\alpha / \omega_o^2}{\sqrt{[1-(\omega/\omega_o)^2]^2 + 4h^2(\omega/\omega_o)^2}} \; ; \; \theta = \tan^{-1}\left(\frac{2h\omega/\omega_0}{1-(\omega/\omega_o)^2}\right) \tag{8.65}$$

Thus, displacement response may be re-written in terms of base displacement or base acceleration as follows:

$$\left|\frac{u}{u_g}\right| = \left|\frac{u}{\alpha/\omega^2}\right| = \frac{(\omega/\omega_o)^2}{\sqrt{[1-(\omega/\omega_o)^2]^2 + 4h^2(\omega/\omega_o)^2}} \; ; \tag{8.66a}$$

$$\left|\frac{u}{\ddot{u}_g}\right| = \left|\frac{u}{\alpha}\right| = \frac{1/\omega_0^2}{\sqrt{[1-(\omega/\omega_o)^2]^2 + 4h^2(\omega/\omega_o)^2}} \tag{8.66b}$$

If $\omega = \omega_0$, the displacement response of non-homogenous part is

$$u_p = \frac{\alpha}{2h\omega_0^2}\sin \omega t \tag{8.67}$$

Introducing the initial conditions given as

$$u(0) = 0; \dot{u}(0) = 0 \text{ at } t = 0 \tag{8.68}$$

yields the integration coefficients as

$$A = \frac{1}{2h\omega_0^2} \; ; B = \frac{1}{2\omega_0\omega_d} \tag{8.69}$$

Thus the final form of solution is

$$u = -\alpha e^{-h\omega_0 t}\left[\frac{1}{2h\omega_0^2}\cos \omega_d t + \frac{1}{2\omega_0\omega_d}\cos \omega_d t\right] + \frac{\alpha}{2h\omega_0^2}\sin \omega t \tag{8.70}$$

If $h \ll 1$, we have

$$\omega_0 \approx \omega_d \tag{8.71}$$

Thus Eq. (8.70) takes the following form

$$u \approx \frac{\alpha}{2h\omega_0^2}(1 - e^{-h\omega_0 t})\cos\omega_d t \qquad\qquad (8.72)$$

Equation (8.72) is the displacement response of the structure in resonant mode.

Forced Vibration subjected to Arbitrary Vibration

When base acceleration is arbitrary such as those caused by earthquakes, Eq. (8.33) may be re-written for a given time step t_i as

$$\frac{d^2 u_i}{dt^2} + 2h\omega_o \frac{du_i}{dt} + \omega_o^2 u_i = -\left(\frac{d^2 u_g}{dt^2}\right)_i \qquad\qquad (8.74)$$

Eq. (8.74) can be solved using different integration techniques such as central difference technique, linear acceleration method or Newmark β method. For example, if the linear acceleration method is used,

$$v_{n+1} = v_n + \frac{1}{2}(a_n + a_{n+1})\Delta t \qquad\qquad (8.75a)$$

$$u_{n+1} = u_n + v_n \Delta t + \frac{1}{3}(a_n + \frac{1}{2}a_{n+1})\Delta t^2 \qquad\qquad (8.75b)$$

subjected to the following initial conditions:

$$v_{t=0} = a_{t=0}\Delta t \text{ and } u_{t=0} = u_0 \text{ at } t=0 \qquad\qquad (8.76)$$

8.2 Vibration Characteristics Measurement Techniques

8.2.1 Free Vibration

This technique is based on the measurement of acceleration responses of structures by subjecting to an initial displacement and velocity field. Such conditions may be introduced to the structure through some external forces such as passing vehicles, pulse-like impacts. Different accelerometers can be used for these purposes. These days there are both wired or wireless accelerometers, which can be easily used for monitoring vibrations and storage as well as for data-processing.

8.2.2   Forced Vibration

This technique utilizes dynamic forces such as shaking table or other types of vibration sources. The acceleration responses are measured as a function of induced vibration source using accelerometers attached to the structure and vibrator source. In this case, different accelerometers can be also used. They are both wired or wireless accelerometers, which can be easily used for monitoring vibrations and storage as well as for data-processing.

8.2.3   Micro-tremor Measurement Technique

Micro-tremor is a low amplitude ambient vibration of the ground caused by man-made or atmospheric disturbances. Observation of micro-tremors can give useful information on dynamic properties of the site as well as the structures. Micro-tremor observations are easy to perform. There are different micro-tremor devices. In this study, SPC-51A micro-tremor device produced by Tokyo Sokushin Company is used.

8.2.4   Fourier Spectra Analysis

Fourier transformation is generally used to simulate real wave forms by numerical approximate functions (e.g. Aydan 2017). Let us consider the actual acceleration form is given by the following function.

$$a = a(t) \tag{8.77}$$

Fourier transform of Function (8.77) is replaced by the following function

$$a(t) = \sum_{k=0}^{\infty} \left[A_k \cos(kt) + B_k \sin(kt) \right] \tag{8.78}$$

If Eq. (8.78) is approximated by a finite number (N) of data with a time interval (Δt), Eq. (8.78) can be re-written as

$$\tilde{a}(t) = \frac{A_o}{2} + \sum_{k=1}^{N/2-1} \left[A_k \cos(2\pi f_k t) + B_k \sin(2\pi f_k t) \right] + \frac{A_{N/2}}{2} \cos 2\pi f_{N/2} t \tag{8.79}$$

where

$$f_k = \frac{k}{N\Delta t} \tag{8.80}$$

If time (t) is represented by $m\Delta t$, coefficients A_k and B_k in Eq. (8.78) would be expressed as

$$A_k = \frac{2}{N}\sum_{m=0}^{N-1} a_m \cos\frac{2\pi km}{N} \quad k = 0,1,2,....,\frac{N}{2}-1,\frac{N}{2} \qquad (8.81a)$$

$$B_k = \frac{2}{N}\sum_{m=0}^{N-1} a_m \sin\frac{2\pi km}{N} \quad k = 1,2,....,\frac{N}{2}-1 \qquad (8.81b)$$

For k th frequency, the maximum amplitude, phase angle and power would be obtained as

$$C_k = \sqrt{A_k^2 + B_k^2} \;\; ; \quad \phi_k = \tan^{-1}\left(-\frac{B_k}{A_k}\right) \; ; \quad P_k = \frac{C_k^2}{2} \qquad (8.82)$$

It should be noted that, the amplitude of Fourier coefficient C_k is multiplied by the half of the period of the record (T/2) in Fast Fourier Transformation (FFT). Therefore, Fourier spectra explained above differs from the FFT spectra in the value of amplitudes and its unit.

8.3 Applications

8.3.1 Tower Models

Three simple tower models, which are 6, 14 and 36 cm high and made of plastic material and fixed to the base with a rigid 4 cm high clamps, were prepared and tested under free and forced vibration models. Figure 8.5 shows model towers on a shaking table equipped with wired or wireless accelerometers. Figure 8.6, Figure 8.7, Figure 8.8 show the acceleration response of towers subjected to free-vibration condition.

(a) Towers with wire-less accelerometers   (b) Towers with wired accelerometers

Figure 8.5 Experimental setup of tower models equipped with different type accelerometers.
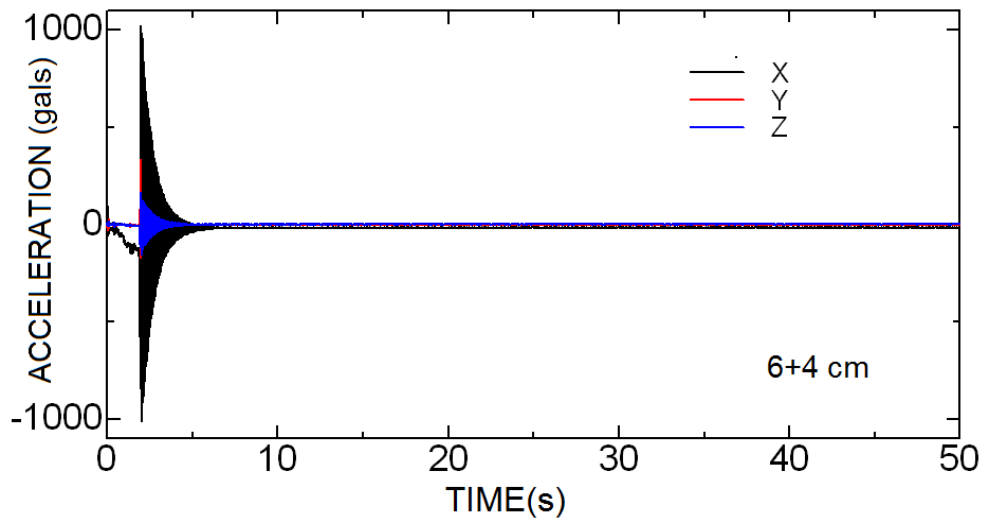
Figure 8.6 Free vibration response of (6+4) cm tower model.
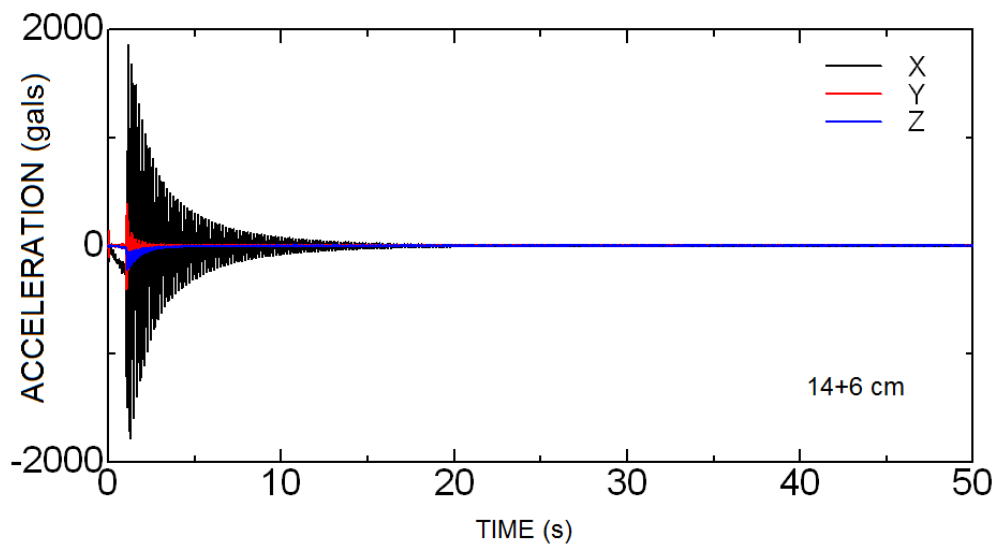
Figure 8.7 Free vibration response of (16+4) cm tower model.
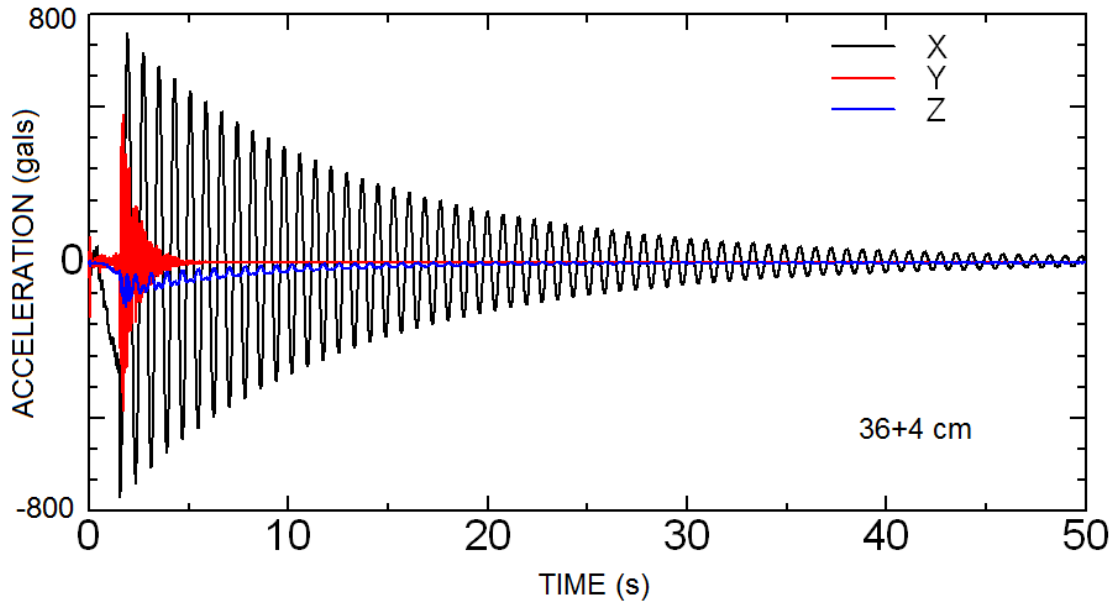
Figure 8.8 shows the Fourier spectra of the records shown in Figures 8.5, 8.6 and 8.7.

As noted from the Figure 8.8, the natural frequency of (36+4) cm tower is much lower than the (6+4) cm tower. This simple example illustrates that the natural frequency of the higher structures would be smaller than those of shorter structures.
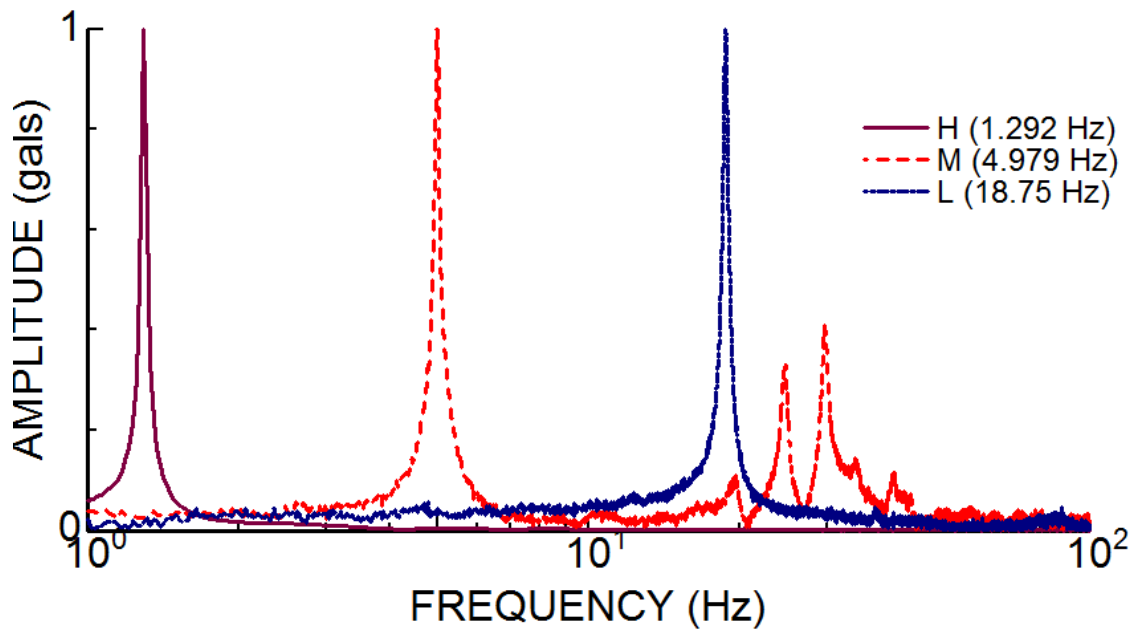
Figure 8.9 Normalized Fourier spectra of tower models subjected to free vibration.

Next towers were subjected to a sweeping experiment was carried out and the records are shown in Figure 8.9. The amplitude of waves was about 100 gals with a frequency range between 1 to 70Hz. As noted from the figure, the tall tower starts to shake at lower frequencies and its vibration is almost nil at higher frequencies.
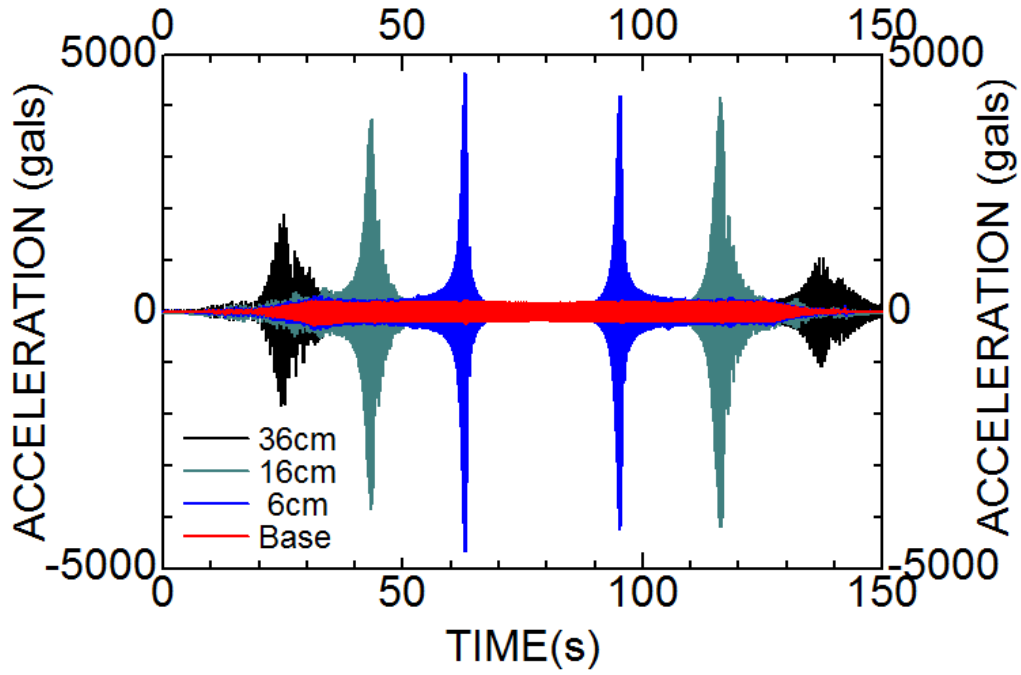
Figure 8.10 Acceleration responses of tower models during a sweeping test.

The Fourier spectra of the records shown in Figure 8.10 are shown in Figure 8.11. When Figure 8.11 compared with Figure 8.9, the results are almost the same. It is interesting to notice that the vibration characteristics of towers can be easily obtained from free-vibration tests.
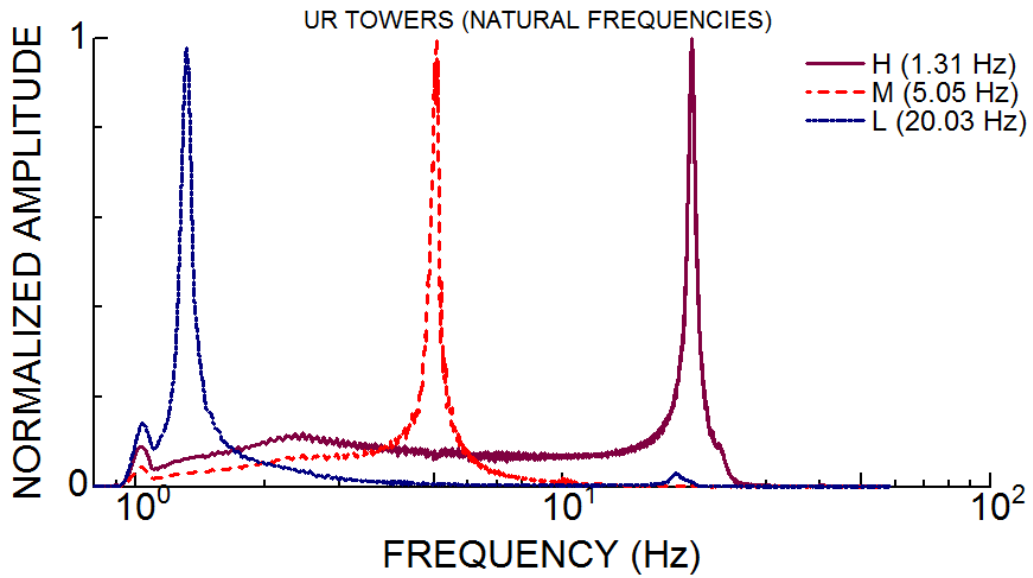
Figure 8.11 Normalized Fourier spectra of tower models subjected to forced vibration.

8.3.2   Building Models

As the building models are more rigid than the towers models, the results of a sweeping experiment are explained herein. Three building models with 4, 8 and 12 stories made of plastic material and fixed to the base were prepared and tested under forced vibration condition. Figure 8.12 shows model towers on a shaking table equipped with wired or wire-less accelerometers. Figure 8.13 shows the acceleration response of building models subjected to a sweeping test with a frequency ranging between 1-70 Hz.
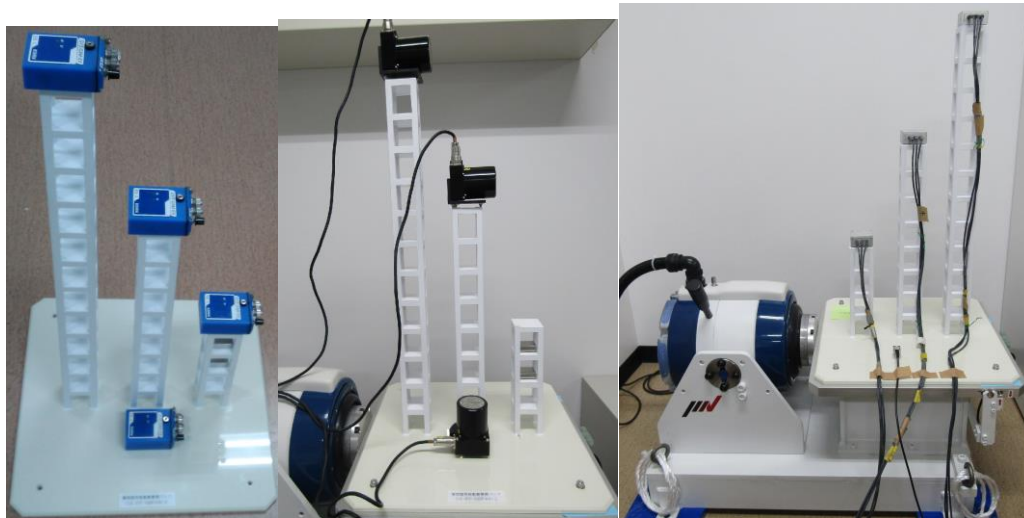
Figure 8.12 Instrumentation of building models.
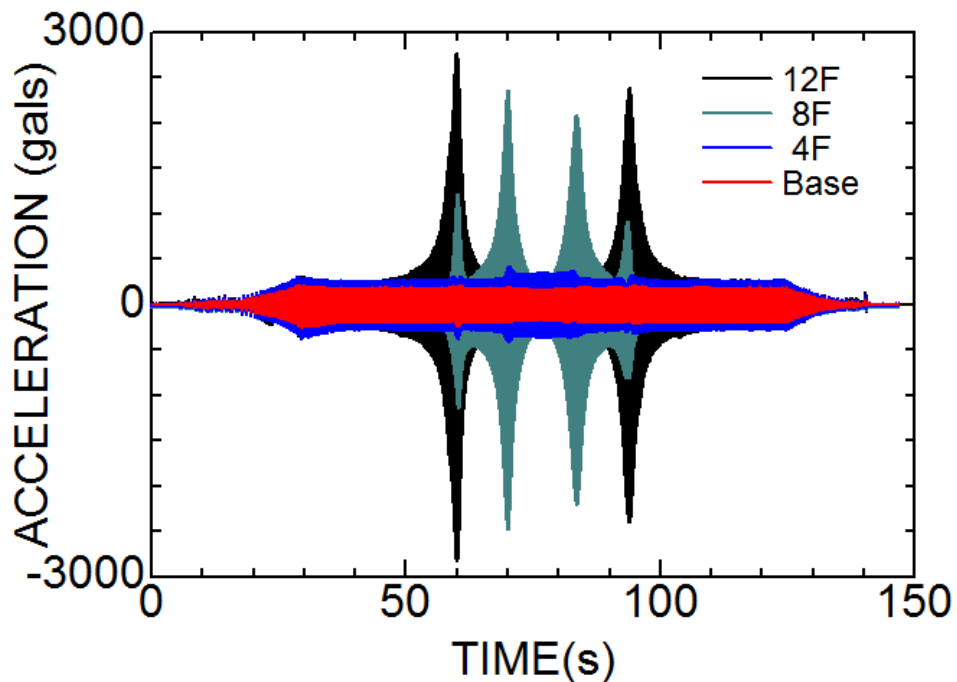
Figure 8.13 Acceleration responses of building models during a sweeping test.
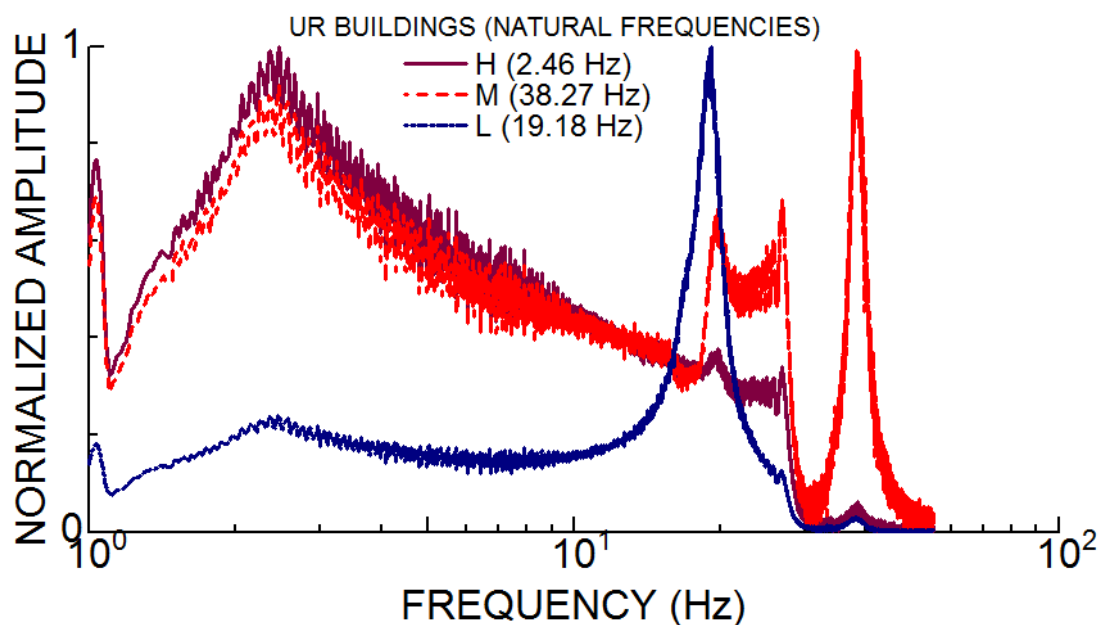
Figure 8.14 Normalized Fourier spectra of building models subjected to forced vibration.

8.3.3   Photo-Elastic Frame Models

8.3.3.1   *Frame Only*

To understand the vibration characteristics of single frames used in Photo-elasticity tests described in Chapter 7, some free-vibration tests were carried out as shown in Figure 8.15. Wireless accelerometers set to triggering mode were used for this purpose.
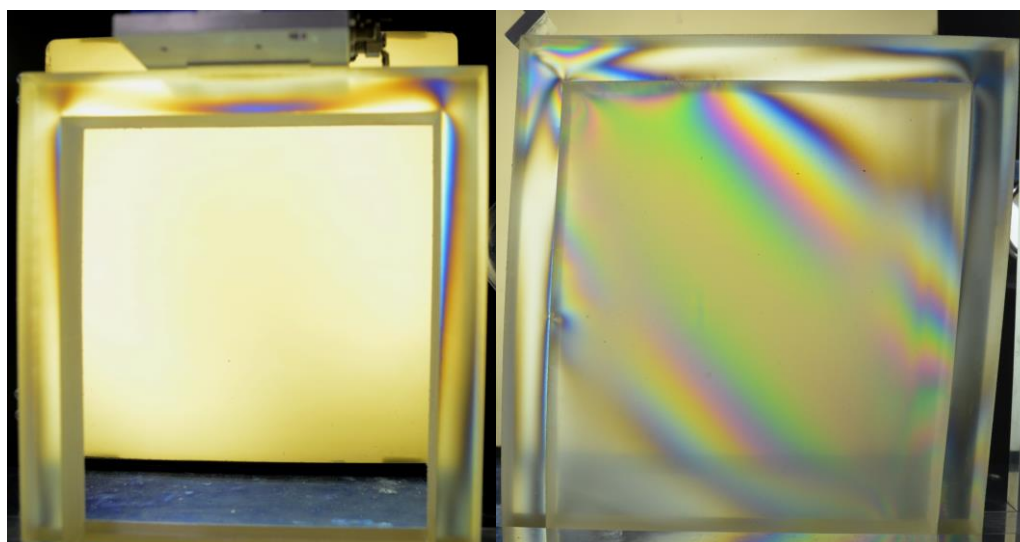
Figure 8.15 Views of set-up of single frames with/without infill walls for free-vibration tests.

Tests on frames with or without infill walls were carried out and the Fourier spectra of records are shown in Figure 8.16. As expected, the dominant natural frequency of the frame with infill wall

is greater than that for the frame without infill wall. This is due to the increased rigidity of the frame with infill wall.
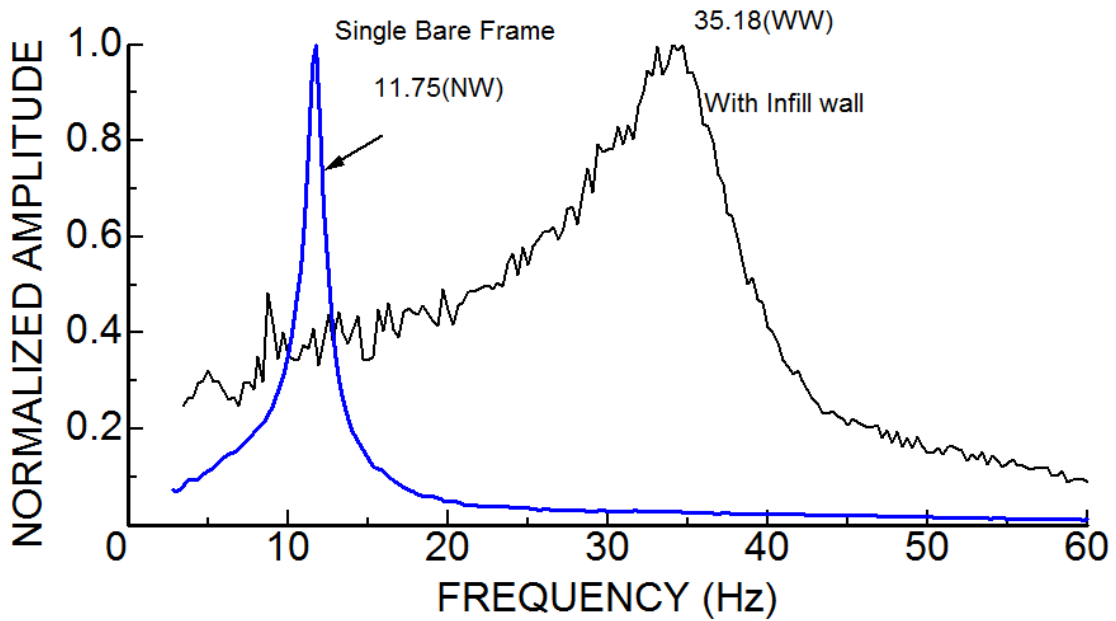
Figure 8.16 Fourier spectra of frames with/without infill wall subjected to the free-vibration.

Eigen value analyses of the single frames bare and with infill wall utilizing finite element method were carried out. Figure 8.17 shows the FEM models. Figure 8.18 shows the deformation response for Mode 1 and computed Eigen values for the single frame are given in Table 8.1. The computed results are somewhat different from measured values and they are higher from the measured results. One of the main reasons might be mechanical properties and constraint conditions. Nevertheless, the computational results confirm the frequency of the frame with infill wall would be greater than that of bare single frame.

#1   #2

(a) Bare frame   *(b) Frame with infill wall*
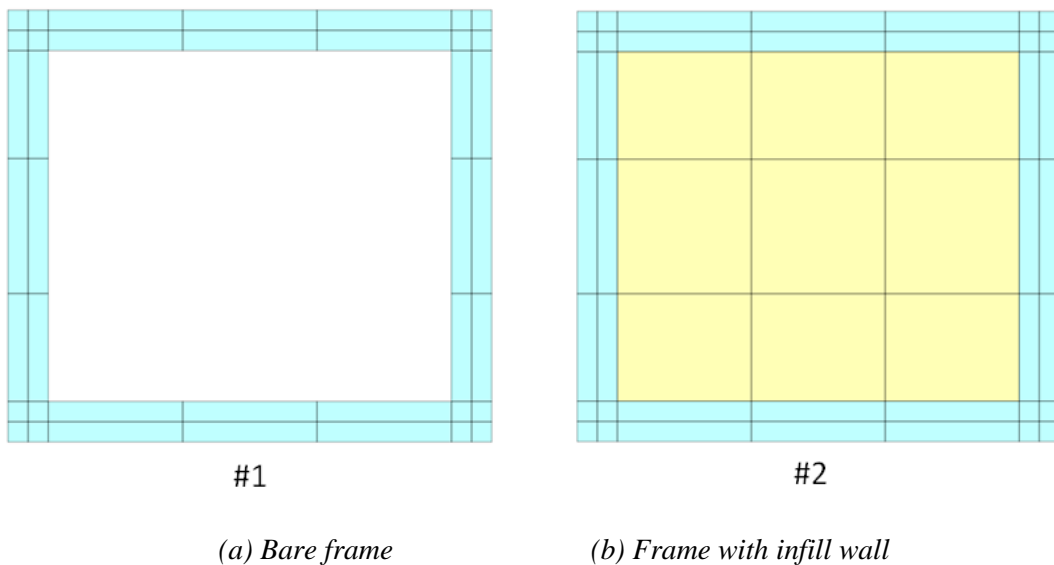
Figure 8.17 FEM models for Eigen value analyses

(a) Bare frame   (b) Frame with infill wall
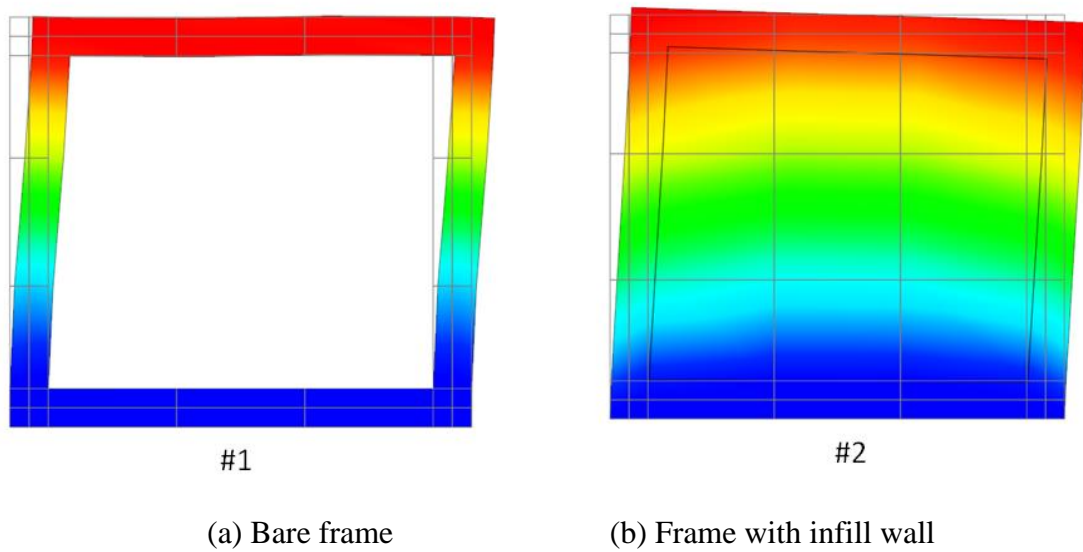
Figure 8.18 Deformation response for Mode 1

Table 8.1 Computed frequency and period of single frame structures

Model	Frequency	Period
#1	11.923	0.083
#2	57.345	0.017

8.3.3.2 *Four Story Frame Models*

Four story framed structures used in Photo-elasticity tests described in Chapter 7 were subjected to free-vibrations and their acceleration responses were measured using the wire-less accelerometers set to triggering mode. The four-story framed structures are shown in Figure 8.19 and were.

a) Framed structure without any infill wall

b) Framed structure with soft (weak) floor (without any infill wall at the ground floor),

c) Framed structure with infill walls.

Figure 8.20 shows the Fourier spectra of four-story framed structures. As expected, the dominant natural frequency of the structure with soft(weak) floor condition is the middle among all structures. The structure with infill walls has the greatest natural frequency. It is also interesting to note that the dominant natural frequency of the framed structure without infill walls is slightly lower than that for the structure with soft(weak) floor condition.
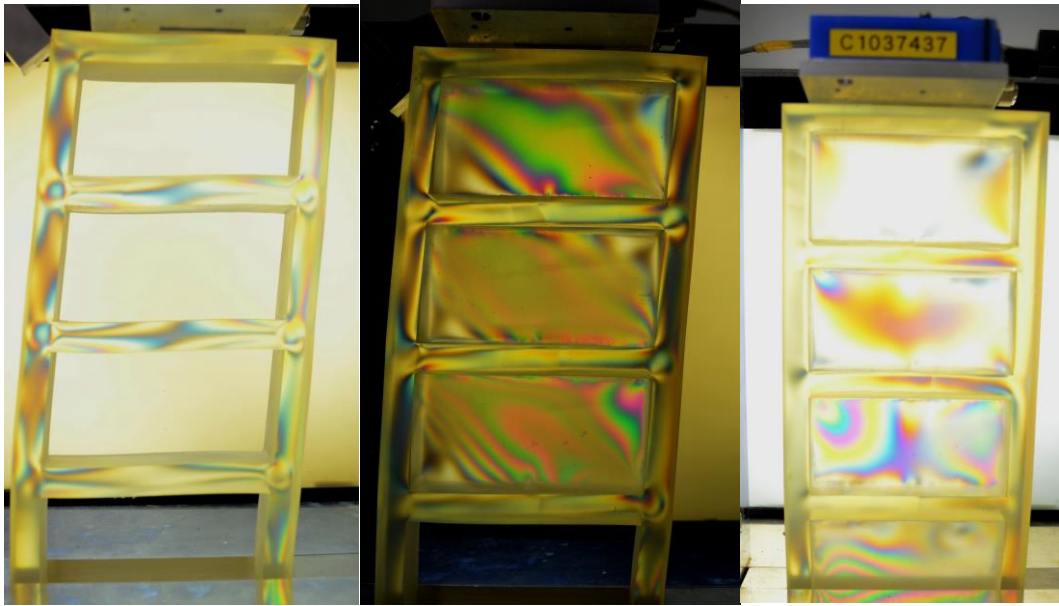
(a) Without any infill wall   (b) Soft(weak) floor condition   (c) With infill walls

Figure 8.19 Four story framed structure models subjected to free-vibration.
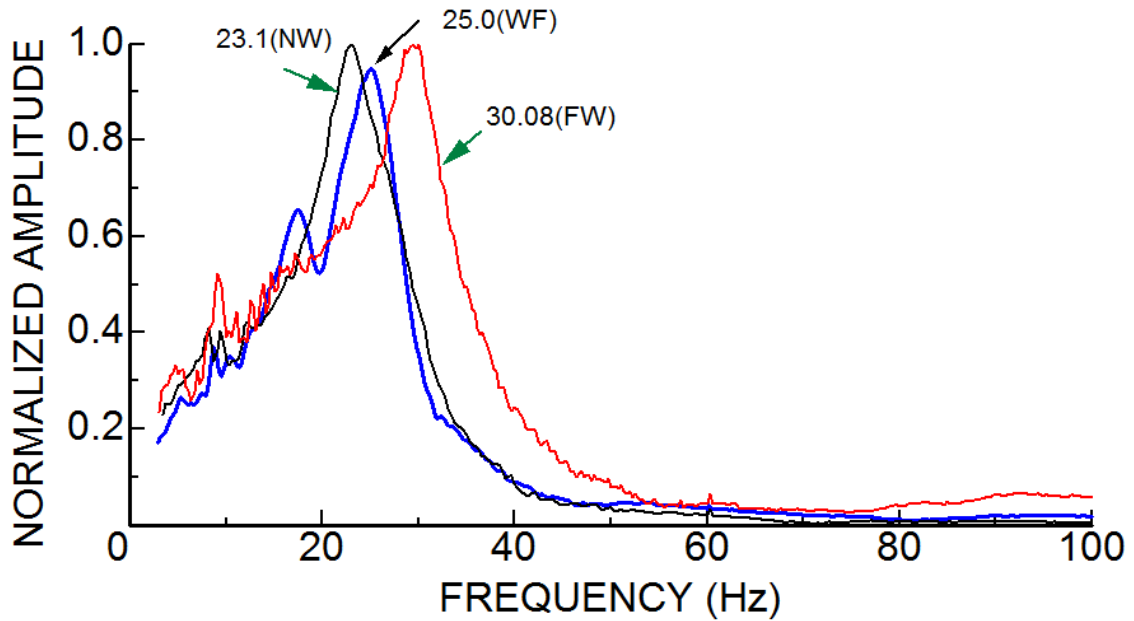
Figure 8.20 Fourier spectra of four-story framed structures subjected to free-vibration

A series of Eigen value analyses using the finite element method were carried using the models shown in Figure 8.21. Figure 8.22 shows the deformation response for Mode 1 and computed Eigen values for the 4 story frame structures are given in Table 8.2. The computed results are somewhat different from measured values and they are higher from the measured results. One of the main reasons might be mechanical properties and constraint conditions. Nevertheless, the computational results confirm the frequency of the frames with infill wall would be greater than that of bare frame.

Table 8.2 Computed frequency and period of frame structures

Model	Feature	Frequency	Period
#1	Bare	12.035	0.083
#2	Weak Floor	15.882	0.063
#3	Infilled	29.054	0.034
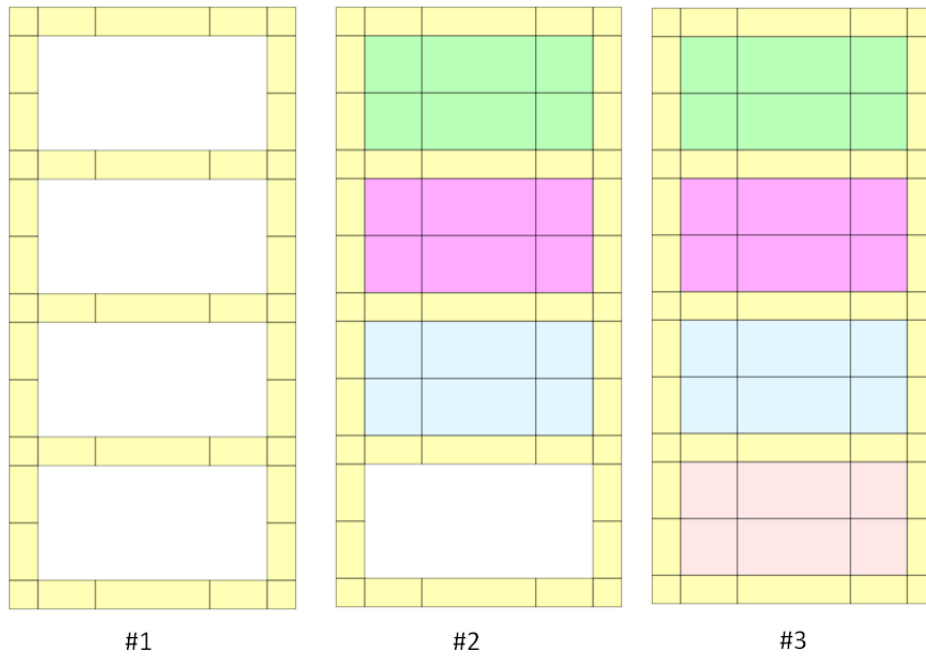
Figure 8.21 Finite element models for Eigen value analyses
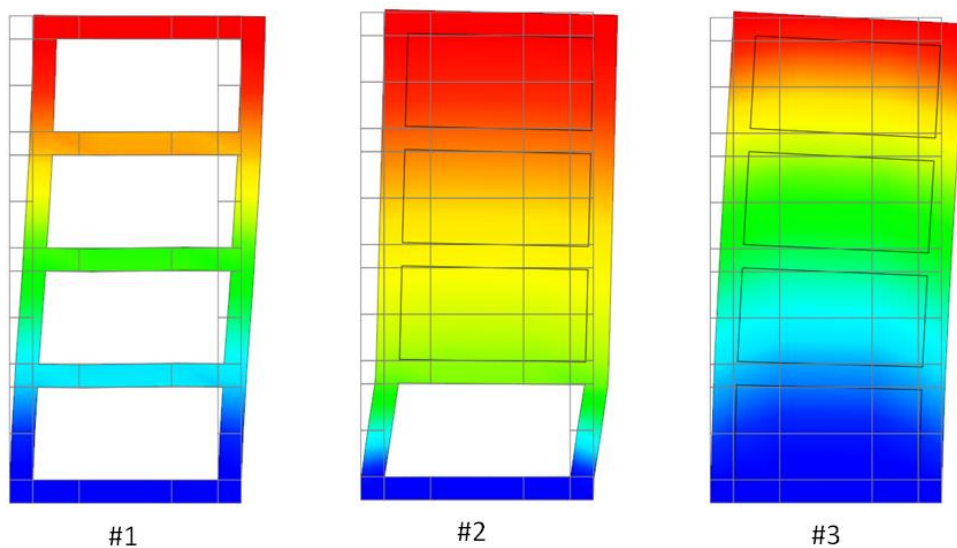
Figure 8.22 Computed deformation response for Mode 1

8.3.4 Beam Models

The natural frequency of a beam 170 cm long, 20 cm thick and 11.5cm wide, reinforced with two steel bars was determined using wire-less accelerometers in drop-weight tests and by micro-tremor device with the ambient induced vibration. The beam was cracked during drop-weight tests. SPC-51A micro tremor device was also used to determine the natural frequency of cracked beam as shown in Figure 8.23. Thus, the natural frequencies of un-cracked and cracked beam are determined and compared as shown in Figure 8.24. As noted from the figure, the natural frequency of cracked beam decreases as compared with that of the un-cracked beam. In the same figure, the H/V spectra obtained from the micro-tremor measurements is also plotted. It is interesting to note that the micro-tremor method distinctly yielded natural frequencies of the beam for cracked and un-cracked states. However, the amplitude for the un-cracked state is slightly lower than that for the cracked state.
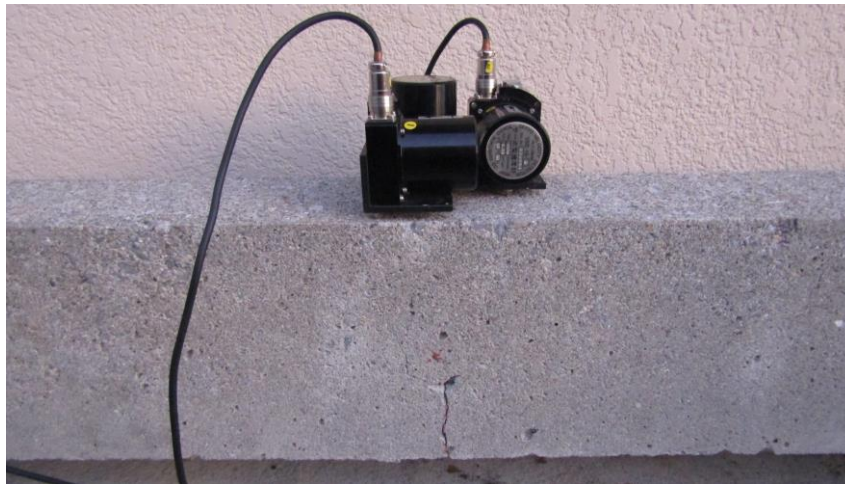
Figure 8.23 Monitoring of cracked beam using a SPC-51A micro-tremor device.
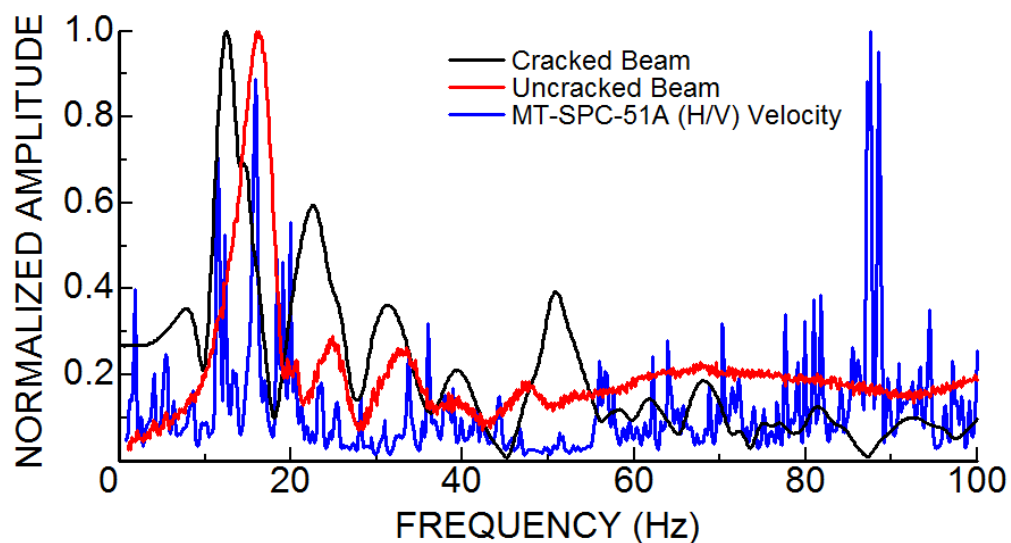
Figure 8.24 Comparison of Fourier spectra of un-cracked and cracked beams.

A beam of a pipe type having an external diameter of 50mm and length of 5600mm was subjected to free vibration. In the first experiment, the beam was subjected to distributed mass over its entire length (Figure 8.25). In the second experiment, an additional concentrated mass was added at the center of the beam. Figure 8.26 compares the Fourier spectra of the acceleration records for both cases. As noted from the figure, the natural frequency of the beam with concentrated load decreases as compared with that of the beam with distributed mass only. In view of theoretical considerations, the natural frequency should be affected by the total mass of the beam and the increase in the total mass would result in lower value natural frequencies.

Figure 8.25 A view of the measurement set-up.
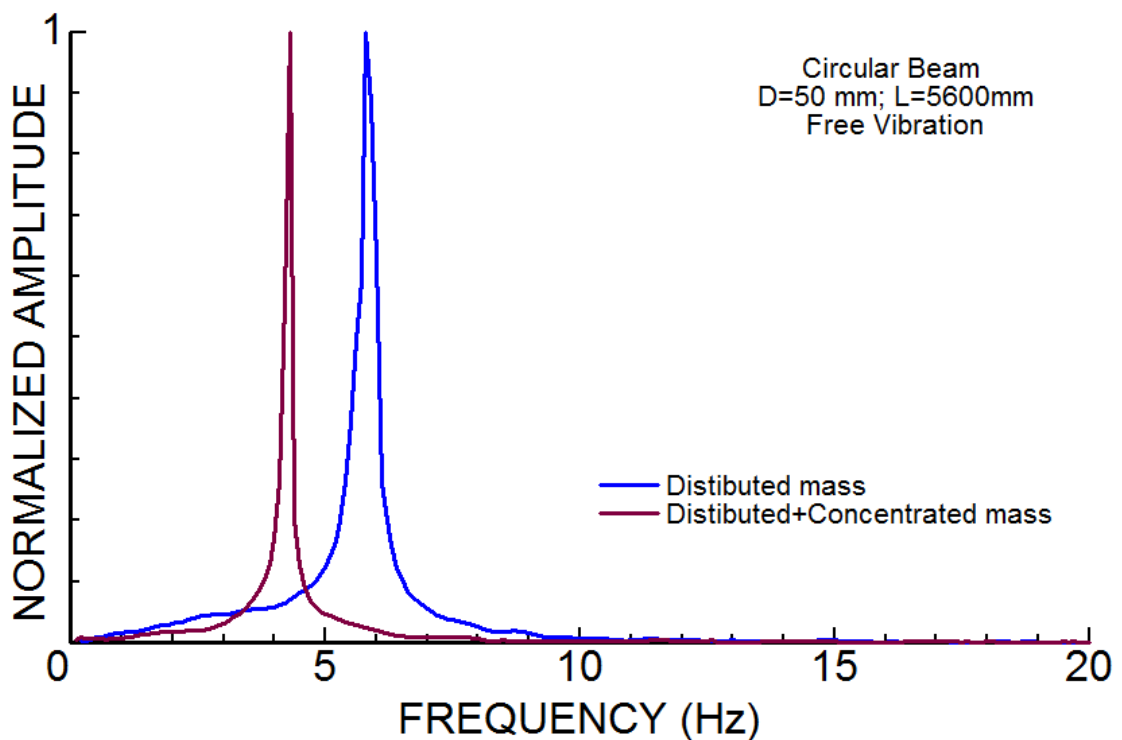
Figure 8.26 Comparison of Fourier spectra of beams with different masses.

8.3.5   Actual Structures

8.3.5.1   *Bridge of the University of the Ryukyus*

There is a reinforced concrete bridge spanning over the reservoir of an earth-fill dam in the Senbaru Campus of the University of the Ryukyus (Figure 8.27). The bridge is 85m long, 3m wide (Figure 8.28). This bridge was suffering the alkali-silica reaction (ASR) problem and it was repaired recently. Natural frequencies of this bridge were measured using drop-weight test and micro-tremor method. The measurements before and after the repair indicated there was almost no major differences in natural frequencies as seen in Figure 8.29. Furthermore, the different techniques yielded almost the same results. As the micro-tremor device is most costly compared with the drop-weight test, the drop-weight test may be quite effective and cheaper technique to determine the vibration characteristics of the structures.
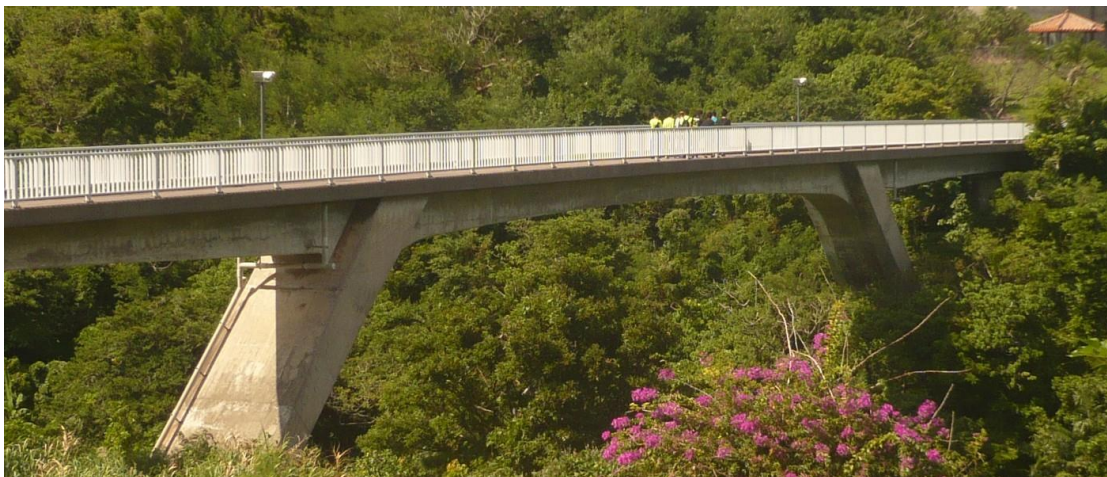
Figure 8.27 A view of the bridge of the University of the Ryukyus.
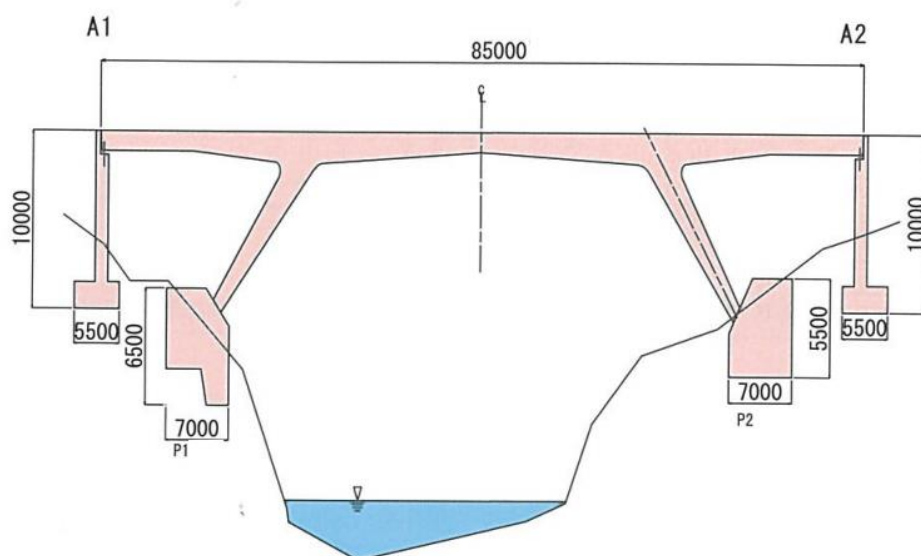
Figure 8.28 A view of the bridge of the University of the Ryukyus.
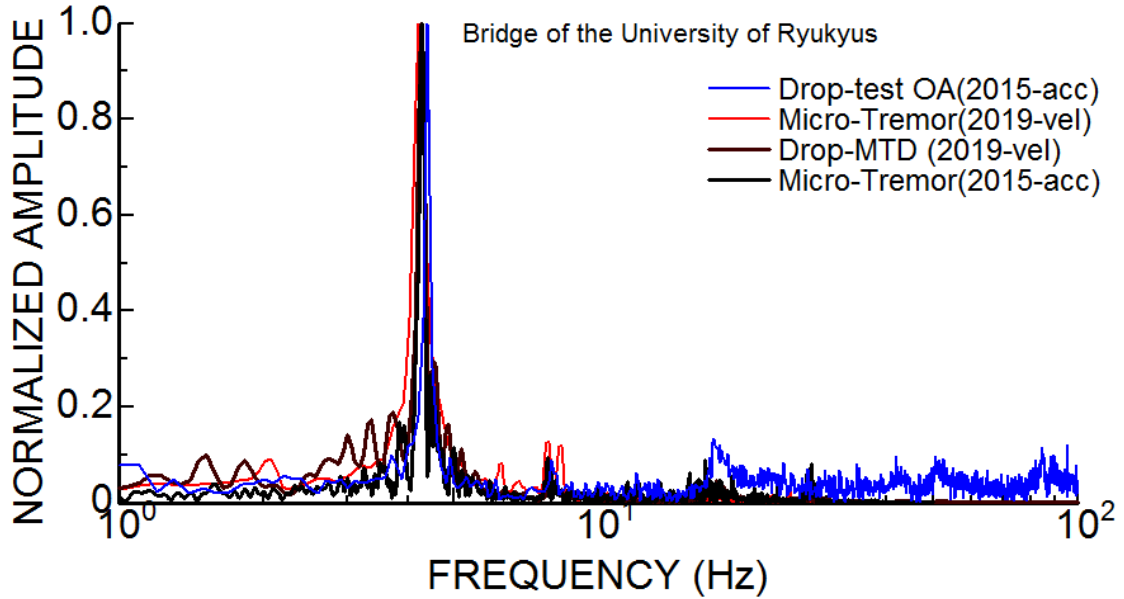
Figure 8.29 Comparison of Fourier spectra of the bridge of the University of the Ryukyus using different measurement techniques.

8.3.5.2 *Vibration of Yofuke Bridge due to Passing Trucks*

As pointed out in Subsection 8.2.1, passing vehicles may also induce the vibration of structures. The vibrations of Yofuke bridge due to passing trucks (about 10 tonf) were measured using wireless stand-alone accelerometers set to trigger mode (Figure 8.30). Figure 8.31 shows the Fourier spectra of measured acceleration wave forms. Despite measurements were done in 2015 and 2017, the results indicate that the dominant natural frequency of the bridge remains the same. nevertheless, some additional frequencies are noted, and these may imply that some degradation of the bridge has been taking place.

Figure 8.30 Views of Yofuke bridge and instrumentation.
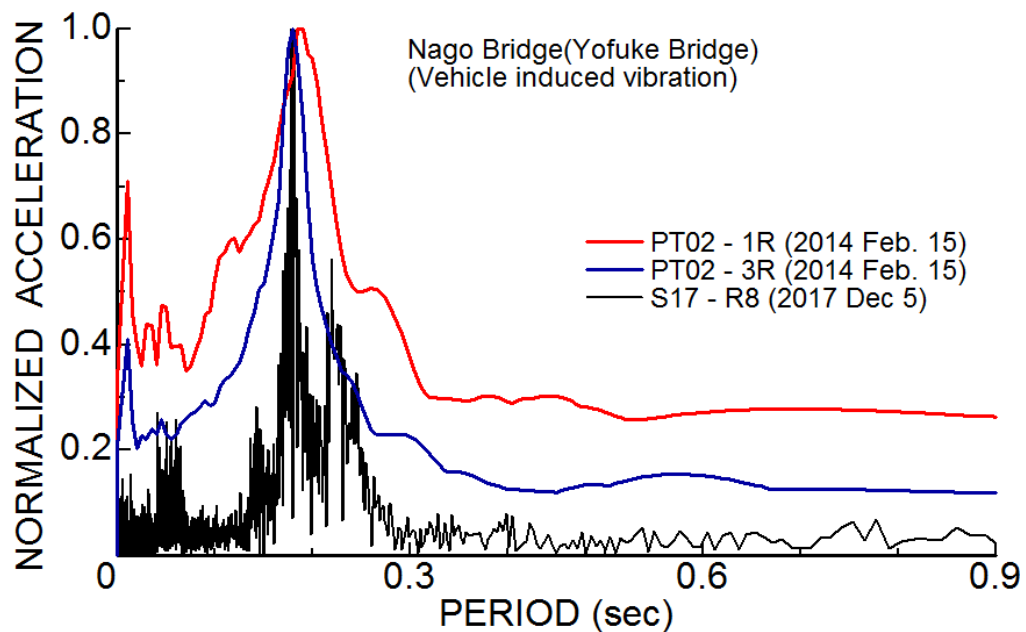
Figure 8.31 Comparison of Fourier spectra of truck-induced vibrations measurements at the Yofuke bridge in Nago City at different times

8.3.5.3 *Bridges in Kandahar (Afghanistan)*

The author has implemented vibration measurements at Helmand Bridge in Helmand Province and Bag-e-Pul and Tarnak Bridges in Kandahar Province for the first time in Afghanistan. Figure 8.32 shows the Bag-e-Pul bridge and measurement at Tarnak Bridge in Kandahar Province. The vibrations induced by passing vehicles were utilized to evaluate the vibration characteristics of the reinforced concrete bridge with a similarity to the measurements at Yofuku Bridge in Nago City of Okinawa Island shown in

Figure 8.30. It is interesting to note that the frequency of this bridges between 5.04 and 5.59 Hz, which is quite close to that (5.56 Hz/0.18s) of the Yofuke Bridge.

(a) Bag-e-Pul Bridge   (b) Measurement at Tarnak Bridge
Figure 8.32 Views of the bridges and measurements (girder length is 14m)
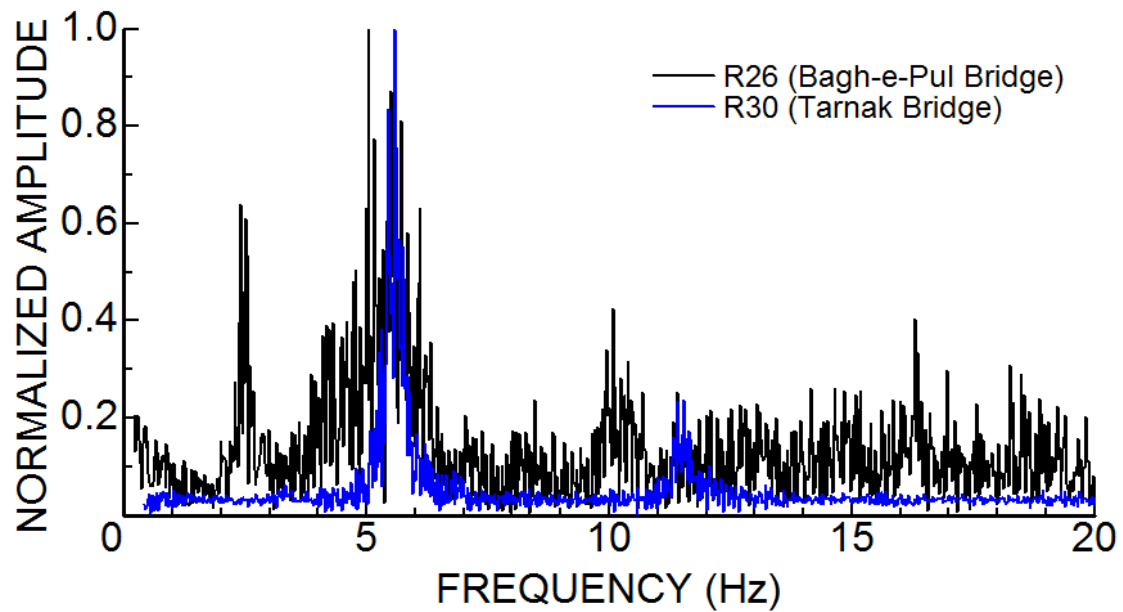
Figure 8.33 Comparison of Fourier spectra of vibrations of bridges in Kandahar Province (Afghanistan)

8.3.5.4   *Pole for Hybrid Energy of Wind and Solar*

A unique pole has a wind turbine and solar panel to produce a combined renewable-energy in the campus of the University of the Ryukyus. The rotation axis of the wind turbine coincides with the vertical axis of the pole. Figure 8.34 show a view of the pole and instrumentation. Two accelerometers are attached to the pole. One of the accelerometers was attached to the pole at about 130 cm from the base plate and the other one was attached to the base plate. Micro-tremor sensors were directly put upon the base plate. Figure 8.35 compare the Fourier spectra of acceleration records obtained from the wire-less accelerometer and micro-tremor sensor. Despite slight difference, the dominant natural frequency of the pole is almost the same. The noise-like components may be due to the interaction between the base plate and base-concrete foundation.

Figure 8.34 View of the pole and instrumentation
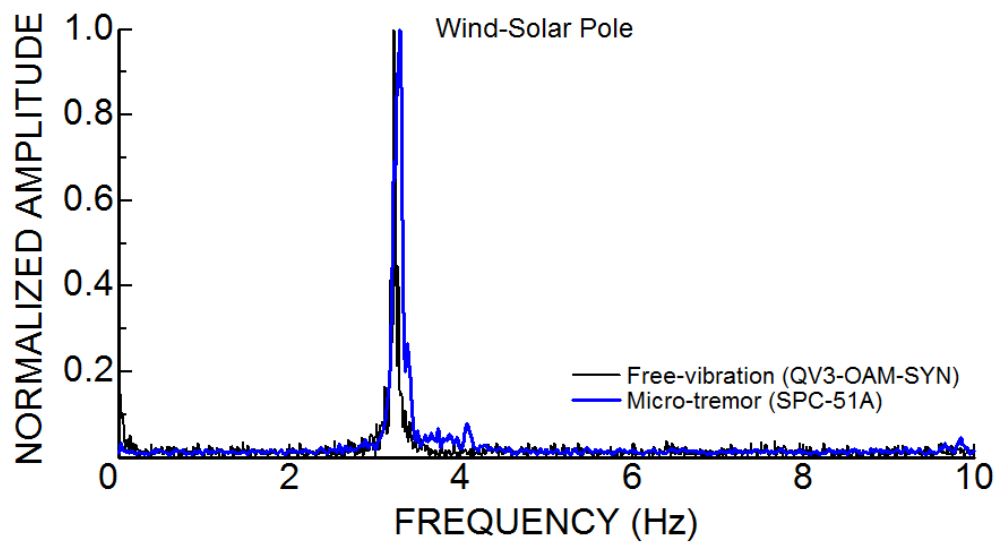
Figure 8.35 Comparison of the Fourier spectra of acceleration records obtained from the wireless accelerometer and micro-tremor sensor.

8.3.5.5   *Wooden Houses*

The natural frequencies of old and new wooden two-story buildings were measured using SPC-51A micro-tremor device. The new building was built over the site of the old building. The old

building was built about 36 years at the time of demolition. Figure 8.36 compares the natural frequencies of the wooden house using H/V spectra technique. While the natural frequency of the new building is about 10.39 Hz (0.96s), the old building has the dominant natural frequency at 6.13 Hz (0.163s). This result implies that the old building which was built about 36 years ago underwent some degradation.
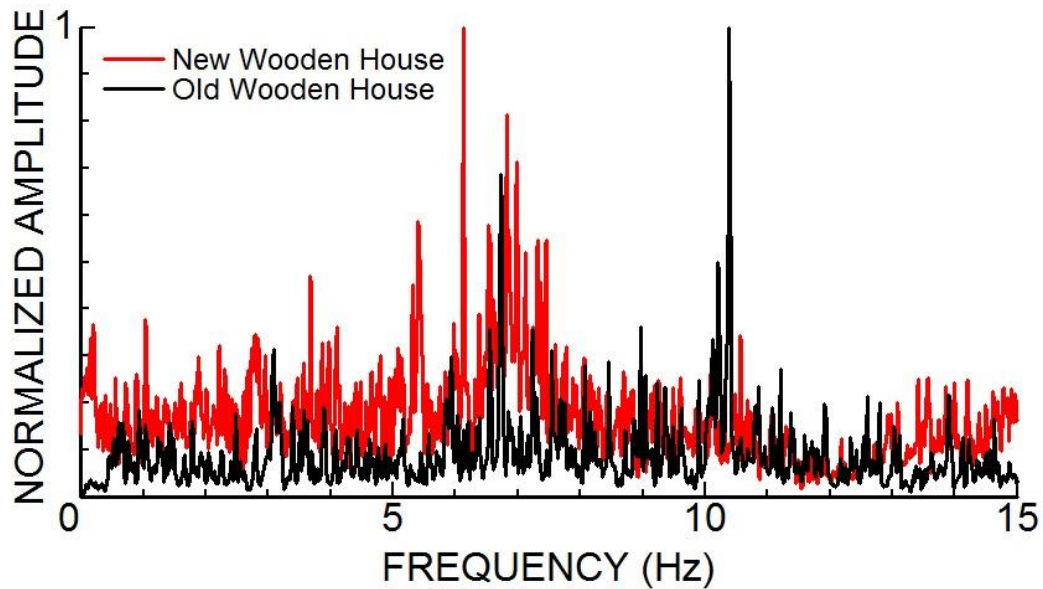
Figure 8.36 Comparison of the H/V Fourier spectra of acceleration records for old and new wooden two story buildings.

8.3.5.6 Reinforced Concrete Building

Reinforced concrete building was a five-story building and it was built about 35 years ago and it is located in Shimashi district of Ginowan City. The dominant natural frequency of this building is about 4.09 Hz (0.244s), Figure 8.37.
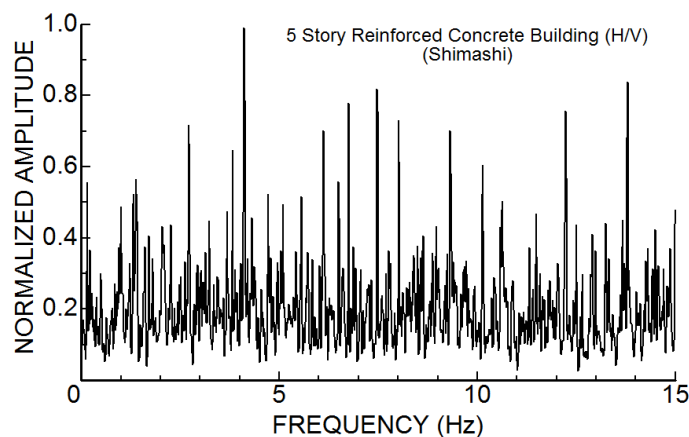
Figure 8.37 Comparison of the H/V Fourier spectra of acceleration records for reinforced concrete five story building.

8.4 Past Studies on Natural Frequency of Buildings

There are some past studies on the natural periods of buildings. These results were compiled by (Aydan, et al., 2000a; Aydan, et al., 2000b). The results are shown in Figure 8.38. In the same figure, some empirical estimations by Aydan et al. (2000b) and seismic codes of Turkey and United States are plotted. (Aydan, et al., 2000b) concluded that most of the data implies that the natural frequencies of various type buildings obey the following relation as a function of number of floors:

$$T_n = 0.065N \qquad\qquad (8.1)$$

Nevertheless, it is strongly recommended to utilize the actual data whenever it is possible.
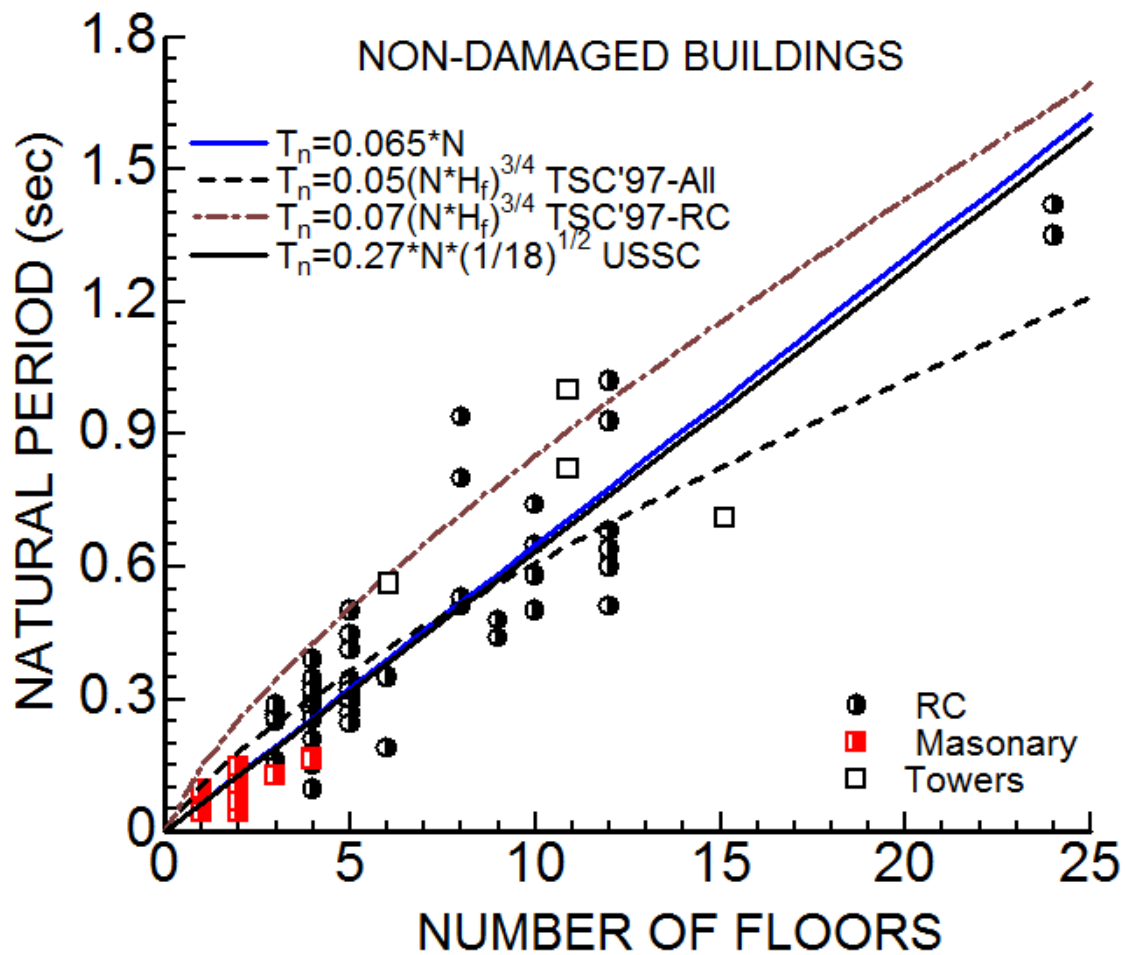
Figure 8.38 The natural frequencies of various type buildings as a function of floor number (Aydan, et al., 2000b).

CHAPTER 9   PROPOSALS AND RECOMMENDATIONS

9.1 General

Most of the civil structures in Afghanistan are lacking the necessary earthquake resistant measurements because of the relatively low workmanship and unavailability of modern building codes based on actual conditions. The construction methods in Afghanistan are yet very old and conventional. Decades of interval war and violence were major problems for the scientists to explore the earthquake hazard. In last few decades when Afghanistan started to develop, the corruption made it more difficult considerably adding to the low quality of construction in the country. In this chapter, some proposals are made and changes in the workmanship are recommended based on the results of the previous chapters to increase the safety of life and property in Afghanistan from future earthquakes. The risk zoning, strong motion zoning, seismic design spectra and some retrofitting methods applicable to buildings in Afghanistan are discussed in the following sections.

9.2 Seismic Risk Zoning

The Afghanistan region has experienced devastating earthquakes in the past. The potential for recurrence of such earthquakes is high considering the past seismicity as well as the regional geologic activities. Although the historical earthquake record is almost nil, few earthquakes as high as Mw≥7.0 is documented by (Ambraseys & Bilham, 2003). These events are serious alarms to the safety measurements of life and property in Afghanistan. The 2005 Mw7.6 Kashmir earthquake was a real-life experience with a death toll of 85,000 people and property damage of about 150,000 houses. The Kashmir earthquake occurred on a blind thrust fault between the Hindu Kush region and the Eurasia-India global plate boundary. The source for the earthquake was the energy released by the global plate boundary. Although, the fault was recognized inactive by the geologists in Pakistan, the event was devastating. This has a big similarity with the Chaman fault as in Afghanistan. The northeastern is subjected to earthquakes from Hindu Kush region and the southeastern Afghanistan has a higher risk factor from the Eurasia-India global plate boundary. The major earthquake source in the later region is the main Chaman fault. The fault is seismically inactive both in historical as well as the instrumental earthquake eras; however, evidence exist that the fault has the potential of releasing energy for big earthquakes. We divided Afghanistan into four seismic risk zones presented in Figure 9.1. The zones and possible earthquake damage are explained in brief in the following section and the criteria for classifying the risk severity of each zone is based on the following facts.

1. Geographic location of the zone from global plate boundaries with high annual slip rate.

2. Density of past earthquake distribution, particularly those with high impact on life and property loss.

3. Results of the earthquake risk analysis of Afghanistan and ground motion estimation for Kabul City in Chapter 4 and Chapter 5 of this study. and

4. The results of the study of (Ambraseys & Bilham, 2003). Each of these zones and the extent of earthquake risk is explained in the following sections.
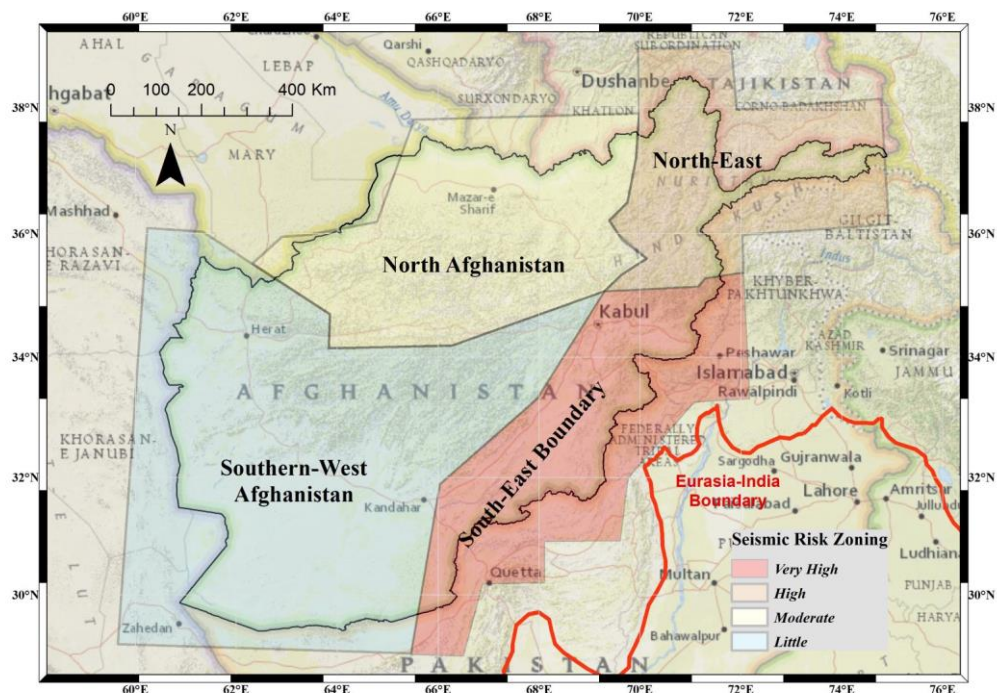
Figure 9.1 Earthquake risk zoning of Afghanistan

9.2.1 South-East Boundary Zone

This seismic zone has the highest possible earthquake risk. The major earthquake source in this zone is the main Chaman Fault entering Afghanistan at the west from Pakistan. The sub-fault of this system released earthquake of Mw 7.7 in 1970 in Quetta City of Pakistan with a death toll of 35,000 people. Other devastating earthquakes are the Mw 7.0 historical earthquake of 1505 near Kabul City of Afghanistan. The earthquake being a historical one has little know about it. It was a shallow earthquake with the probable depth of less than 40 km. Another earthquake in this region has happened in 1842 in Konar of Afghanistan yet very little known about the characteristics as well as the impact. And the major factor for this zone being the highest in risk is the fact that the main Chaman fault did not release energy of big earthquakes in near future and that the historical

earthquake catalogue is quite incomplete. This makes the main Chaman fault be very similar to the Balakot-Bagh fault of Pakistan where the 2005 Mw 7.6 Kashmir earthquake took place. The fault was identified as inactive by geologists in Pakistan and the focal mechanism of the event remarks a blind thrust fault. Considering all these facts, the possibility of a devastating earthquake along Chaman fault is has the highest possibility. In addition, Kabul and Nangarhar are the cities with highest population and buildings construction density, hence the death and damage toll may be very high in case a high magnitude earthquake take place. The results for an earthquake equal or near to the 2005 Kashmir earthquake may have even worst consequences as explained in Chapter 5.

9.2.2 North-East Zone

The second highest risk is in the North-East zone. Source for most of the earthquakes in this zone is the Hindu Kush and Pamir where continental earthquakes as deep as 250km take place. The latest of these earthquakes was the 2015 Mw 7.5 Hindu Kush earthquake with a death toll of 400 people and damage to about 12,000 houses in Afghanistan and Pakistan sides. Shallow earthquakes also take place in this zone and the latest of the later events was the 1998 twin earthquakes of Rustaq in Takhar with a death tool of 6,000 people and complete destruction of 7 and damage of as many as 35 villages. Landslides are usually associated with the earthquakes. The latest one was in May 2014 with the number killed or missing between few hundred and as many as 2,700. The Central Badakhshan fault system forms the local sources in the region. The Central Badakhshan fault and the Darvaz fault are the main faults with a slip rate in the order of 10mm/year. The density of past seismicity is the highest in this zone; however, the Hindu Kush seems to be the only source for release of earthquakes in this zone.

9.2.3 North Afghanistan Zone

In our analysis, we have put this zone at the third place where the risk is moderate. The latest instrumental earthquake in this zone was a series of the 2002 shallow event of Nahrin in Baghlan province with a death tool of about 1,200 deaths and destruction of the whole old city (Shahr Kona) of Nahrin. The earthquake was a shallow event and magnitude of Mw 5.9. Small magnitude earthquakes usually take place in this zone causing landslides. The zone is also affected from the Hindu Kush earthquakes taking place in North-East zone causing a lot of landslides. The zone doesn't have major faults in it; however, a shallow event of Mw 7.0 is reported in 819 with the specific characteristics unknown. Its reported that the earthquake destroyed a quarter of Balkh city, and ruined the masjid-i-jami. Sidreh desert (36.75N, 66.22E) was flooded by an excessive rise of the water table and turned the area into a fertile land. The earthquake also damaged many tens of kilometers to the west which is considered unlikely.

9.2.4 Southern-West Afghanistan Zone

This is the remaining Afghanistan bordering in the south with Pakistan and in the west with Iran. Although, earthquakes as high as Mw 7.0 take place in Iran and Pakistan near Afghanistan borders, however, the impact seems to be decreasing to negligible extent inside Afghanistan. Distribution of the earthquake is the least comparing to other risk zones. The sub-faults of the Hari-rud fault as well as the Chaman fault systems form the faults of this zone and are inactive both in instrumental as well as historic seismicity. Earthquakes as high as Mw<5.0 take place in this zone and have not had major impacts on life and properties.

9.3 Strong Motion Zoning

We estimated the strong motion for all Afghanistan using the Probabilistic Seismic Hazard Method (PSHA) in Chapter 4 of this thesis. We also estimated strong motion for Kabul City from a specific earthquake using deterministic approach. The strong motion for Kabul City can be as high as 1g (981 gals). The capitol of Badakhshan, Faizabad seems to be having the highest strong motion equal to about 2g. Baghlan follows with about 1.2g, then it is Jalalabad with about 0.9g, Kabul with 0.82g and Balkh with 0.47g. The ground motion for 10% and 2% probability of exceedance (PE) in 50 years resulted from the PSHA in Chapter 4 for the five big cities in the high seismicity zone is presented in Table 9.1. The ground motion in Kabul City from the hypothetical earthquake along Chaman fault segment is about 1g as discussed in Chapter 5.

Table 9.1 Probabilistic ground motion (%g) for 2% and 10% probability of exceedance in 50 years

Period (sec)	Baghlan	Balkh	Faizabad	Jalalabad	Kabul
2% Probability of Exceedance					
0.0	45	20	69	35	32
0.2	**121**	**47**	**204**	**91**	**82**
1.0	49	26	74	41	38
10% Probability of Exceedance					
0.0	26	11	42	19	19
0.2	**62**	**25**	**107**	**44**	**42**
1.0	25	13	39	19	19

As the historical earthquake catalogue of Afghanistan is very incomplete, one cannot ignore occurrence of earthquakes Mw≥7.0 in the nearby locations of the events documented by (Ambraseys & Bilham, 2003). We estimated the strong motion for a hypothetical earthquake near Kabul and found that the ground motions in few kilometers from the epicenter can be up to 1g. We

recommend this be considered in all the locations where earthquakes as high as Mw≥7.0 are reported. The results of PSHA in Chapter 4 and deterministic approach in Chapter 5 of this thesis for Kabul City region is that the ground motion can be up to 1g. We apply the results of the deterministic approach to all the historical earthquakes of Mw 7.0 reported in Bamiyan and in Faryab. In that case, the ground motion can be as high as 1g near the localities of those earthquakes as presented in Figure 9.2. The strong motion in NW and SW Afghanistan is very small and negligible.
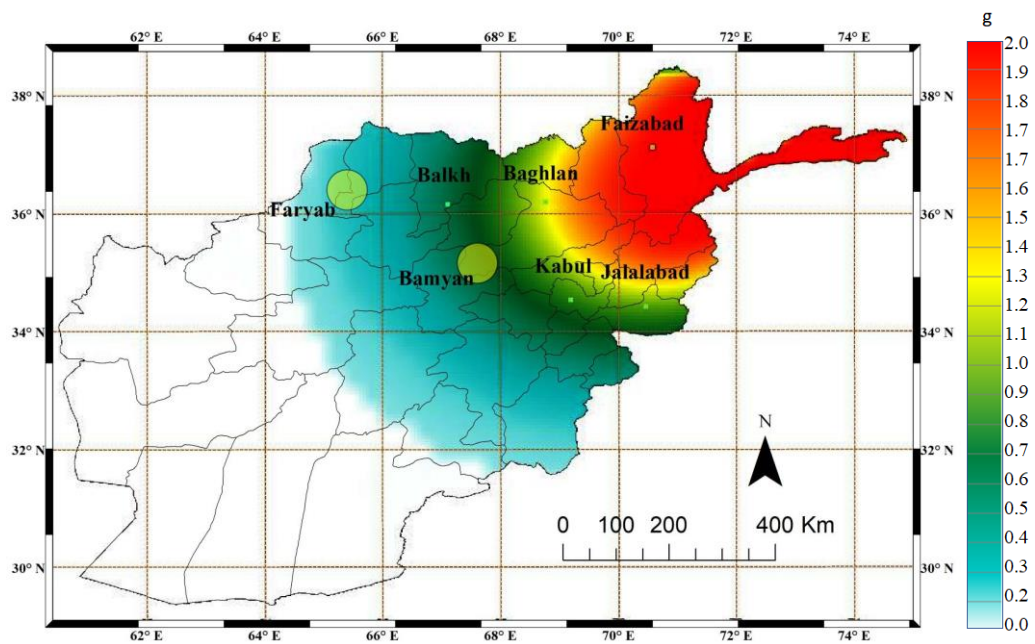
Figure 9.2 Strong motion contour map for Afghanistan, 0.2-second and 2%PE

9.4 Seismic Design Spectra

We calculated the seismic hazard response spectra for the five big cities in the high strong motion zones. Although the strong motion for Bamyan and Faryab provinces are small according to PSHA results in Chapter 4, historical events of Mw=7.0 are reported in the historical catalogue. As we calculated the strong motion for a hypothetical earthquake near Kabul with a result of about 1g strong motion, we apply this value to the localities of Bayman and Faryab where the events are reported, Figure 9.3. After three decades of civil war and violence, Afghanistan resumed to develop gradually about 15 years ago. There are almost no high-rise buildings in Afghanistan except very few 20 story buildings in Kabul City. Most of the structures built in the recent decades are 5-10 story therefore the spectral acceleration up to 1-sec time period is presented only. We also have presented the maximum considered earthquakes taking placing in different areas of Afghanistan in

Table 9.2. We recommend these values with the ground motions presented below be considered while designing buildings and other structures.
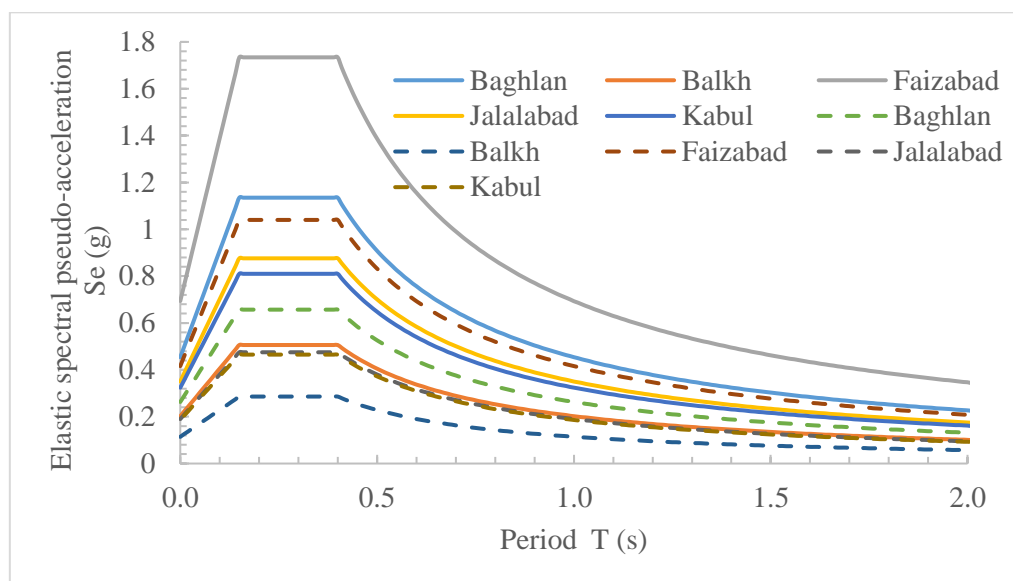
Figure 9.3 Earthquake Design response spectrum for 2% PE (solid lines) and 10% PE (broken lines) in 50 years.

Table 9.2 Maximum Considered Earthquakes for Afghanistan Provinces

Province	M_{wmax}	Province	M_{wmax}
Badakhshan	7.5	Kundoz	5.6
Badghis	4.4	Laghman	5.7
Baghlan	6.2	Logar	5.9
Balkh	7.0	Maidanwardag	4.9
Bamyan	7.2	Nangarhar	5.9
Farah	4.9	Nimroz	4.6
Faryab	7.3	Nuristan	7.2
Ghazni	6.2	Paktia	5.7
Ghor	4.9	Paktika	5.6
Helmand	6.1	Panjshir	7.0
Herat	5.8	Parwan	7.0
Jozjan	6.4	Samangan	7.0
Kabul	7.2	Sar-e-Pol	7.0
Kandahar	6.7	Takhar	5.5
Kapisa	5.4	Urozgan	NA
Khost	5.4	Zabul	5.7
Konar	7.4		

9.5 Retrofitting of Existing Structures

The death toll and damage to buildings in past earthquakes of Afghanistan region remakes the existing of some basic structural problems in the construction industry. There are several problems

contributing to this problem. Unavailability of experts, lower construction knowledge as well as the low level of experienced staff are few to name as example.

Most of the construction methods were copied from the neighboring countries and without modifying the methods and architectures, they were applied to structures in Afghanistan that has completely a different geography. In most parts of Afghanistan except the few very big cities, buildings seldom follow the normal flow of architecture, design, construction and maintenance; however, it is all done by one person/contractor who then builds the buildings. It is very seldom to see that either the builder is at least Architecture/Structural Engineer, or he employs such skilled people. An output of such a work is of course, deficient and unreliable. This is almost the case for all the owners of the buildings except those Afghans living in Europe and the US. Although those Afghans bring plans from those countries, they still face a lot of problems while implementing the construction as again the availability of skilled labor is a problem and in certain cases if it exists, it is difficult to afford their salary. Test of the construction material seldom take place as even the Afghan government does not have a complete engineering material laboratory. In such cases, the existing structures owe a lot of structural problems as well as unreliable earthquake safety precautions. The death toll and property loss from the past earthquakes, particularly those from 2005, M7.6 Kashmir earthquake is a very good evidence to prove the above statements. In Chapter 6 of this thesis, we have explained the issue in detail and will not repeat it here again. In the following section, I explain some of the retrofitting methods that fit the structures and environmental condition of the Afghanistan region.

9.5.1 Methods for Retrofitting of Existing Reinforced Concrete Buildings

Primary aim of strengthening a structure is to increase its ductility and load bearing capacity with respect to its previous condition. Only those aspects related to flexure are discussed here. Established techniques which have been in use successfully for several years are recognized as follows:

9.5.1.1 *Over Slabbing*

In this technique, a plain or reinforced concrete slab is overlaid on top of the existing slabs or beams to increase the section dimension in order to increase flexural strength. To ensure the composite action between the two, dowels or shear studs may be installed. This method may be advantageous when the member needing strengthening possesses reinforcement near or equal to balanced steel. However, as the flexural strength of a reinforced concrete member is usually limited by the capacity of the reinforcement rather than by the capacity of the concrete, over-slabbing may therefore, be of no significant value. Any strength increase may be offset by the increase in dead

load. It has been concluded that the chances of interface failure are increased when the existing beam is over-reinforced, and the depth of the overlay is too deep. This observation further limits the scope of its use. Apart from disruption to use of the structure, extensive surface preparation is required.

9.5.1.2 *Sprayed Concrete with Additional Reinforcement*

Sprayed concrete is a mixture of cement, aggregates and water which is projected into place at high velocity from nozzle. Many names have been associated with sprayed concrete including spray concrete, shotcrete and gunite. In the USA the "American Concrete Institute" described shotcrete as "mortar or concrete conveyed through a hose and pneumatically projected at high velocity onto a surface". In the UK Gunite is referred to "sprayed concrete where the aggregate size is less than 10mm, and where the size of aggregate exceeds 10mm, it is termed as shotcrete".

Strengthening of beams deficient in flexure is accompanied by addition of reinforcing steel in the tensile zone. The method is, therefore, sometimes referred to as tensile overlay. The method essentially requires removal of concrete cover, cutting recesses if necessary, to accommodate additional bars, either by providing enough anchorage length in the concrete, or by steel plates and bolts with anchoring yokes. Once the whole system is in place concrete is sprayed to the desired thickness. It is essential to have a satisfactory bond between existing and new concretes as the evaluation of new concrete section is based on the same principles as those of normal reinforced concrete. Apart from the capability of the joint to transfer shear stresses without relative movement, differences in creep and shrinkage properties of old and new concrete need careful evaluation. It is reported that most shotcrete durability failures do not involve failures of the material itself, but generally there is a peeling off sound shotcrete because of bond failure. The Department of Transport suggested the use of sprayed concrete where the reinforcement is not too congested. This method involves extensive surface preparation, and disruption to use of the structure is inevitable with this technique. Full advantage of the additional reinforcement can only be taken if the cross-section has enough capacity to incorporate additional reinforcement without becoming an over-reinforced section.

9.5.1.3 *Ferrocement*

Ferro cement is said to be the first form of reinforced concrete. Ferro cement is the type of reinforced concrete which uses wire mesh rather than heavy rods and bars as the primary part of its metal reinforcement and uses sand and cement mortar rather than a mixture of cement, sand and gravel as the primary part of its concrete mixture. Cement and sand mortar having a ratio of 1:2 is impregnated in the mesh reinforcement either by hand or by shotcrete to produce almost a fabric of steel packed and coated with mortar. Although there are many obstacles to the greater use of

ductility is attracting researchers to exploit its potential. Ferro cement have no apparent advantage over any other type of reinforced concrete either in direct tension or flexure, but it has a high level of control over cracking provided by the close spacing and specific surface area of the wire reinforcing mesh.

9.5.1.4 *Carbon Fiber Reinforced polymer (CFPR)*

Yuksel et al. (2010) reported a series of experimental studies focusing on the behavior of bare and carbon fiber reinforced polymer (CFPR)-retrofitted infilled RC frames with different bracing configurations. In their experiments, quasi-static experiments on 1/3-scaled infilled RC frames that were retrofitted using CFRP material in various schemes. The test results showed a significant increase in the yield and ultimate strength capacities of the frames with a decrease in relative story drifts, especially in the cross-braced and the cross diamond-braced type of retrofitting schemes. The energy dissipation capacities of the retrofitted frames turned out to be more than those of the bare infilled frame, thus reducing the seismic demand imposed on the frames. The cross diamond-braced type of retrofitting scheme, which was positioned on the infill wall and outside the beam–column connection regions of RC frame, showed the best behavior among the other schemes. This scheme not only prevented brittle shear failures of the infill wall, but also prevented the transfer of additional forces to the weak and brittle beam–column connections.

9.5.2 Recommendations of the Procedure for new Reinforced Concrete Buildings

The basic principle for Buildings should be such that they must be designed against ground shaking and they should show ductile behavior even under extreme dynamic loading conditions. In other words, the pan-cake mode of failure of RC buildings should not be allowed to occur. Most of casualties in many countries are due to weak floor (soft story) effect. The main cause is improper construction of beam-column connections and improper amount stir-ups and low workmanship. Furthermore, the infill walls are not integrated into the reinforced frame structures.

Karadogan et al (2009) performed a very interesting series of experiments a single frame under cyclic loading. Their test results are shown in Figure 9.4. They found that the integration of the infill wall into the frame increases the ductility and strength of the frame compared that of the bare reinforced concrete frame.

Figure 9.5 illustrates common practices in different parts of the world. The proposed T-Type procedure is illustrated in the figure. Number indicates the construction stages. The golden rule of the proposed T-Type procedure is to construct the frames as follow:

   1) First construct the wall

2) Next construct columns

3) Finally construct the floor slab.

However, it should be noted the resistance offered by the integrated walls must not be counted for.
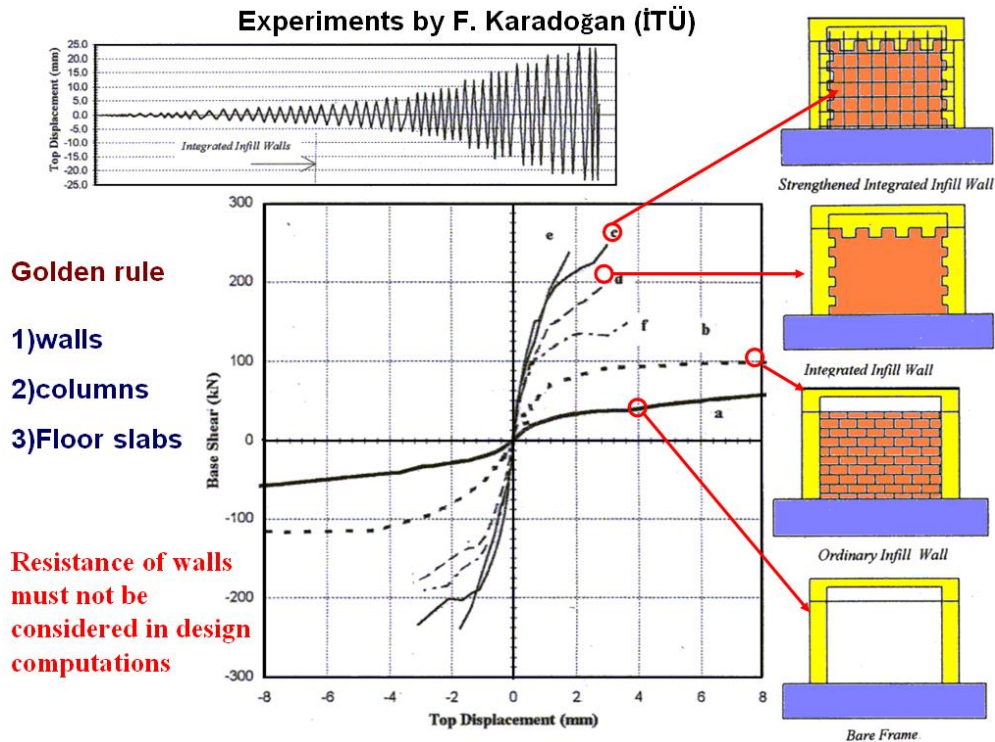
Figure 9.4 Experimental results on the effect of various construction procedures.

9.5.3 Masonry Structures

Masonry structures are quite common worldwide. The experiments and observations during earthquakes on masonry structures clearly showed that many such structures might collapse due to either inter-block sliding or toppling. The sliding failure purely depends upon the frictional properties of interfaces among the blocks.

- The toppling mode of failure, on the other hand, depends upon mainly the geometry of structures.
- For ordinary masonry structures, toppling or overturning failure would take place at lower intensity of shaking as compared with that related to sliding failure.
- The vertical walls are less resistant to shaking than that for inclined walls.

If masonry buildings are constructed using lime or cement mortar, they performed much better compared to those utilizing earthen mortar. Especially, the use of cement mortar together with well-spaced concrete lintels or slabs improved the integrity of the buildings. It is recommended to utilize

the lintels and reinforced concrete slabs at certain spacing such as 100 cm to increase the ductility and strength of the walls against sliding and out of plane failure (toppling failure) as illustrated in Figure 9.6.
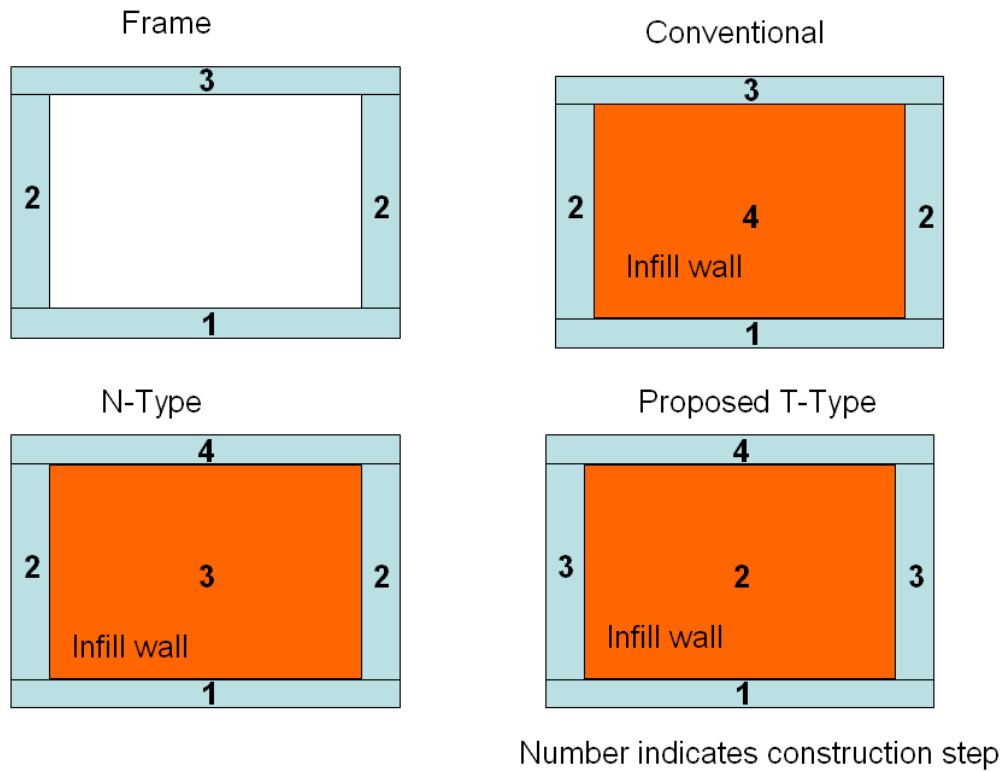
Figure 9.5 Illustration of various construction procedures and proposed procedure.
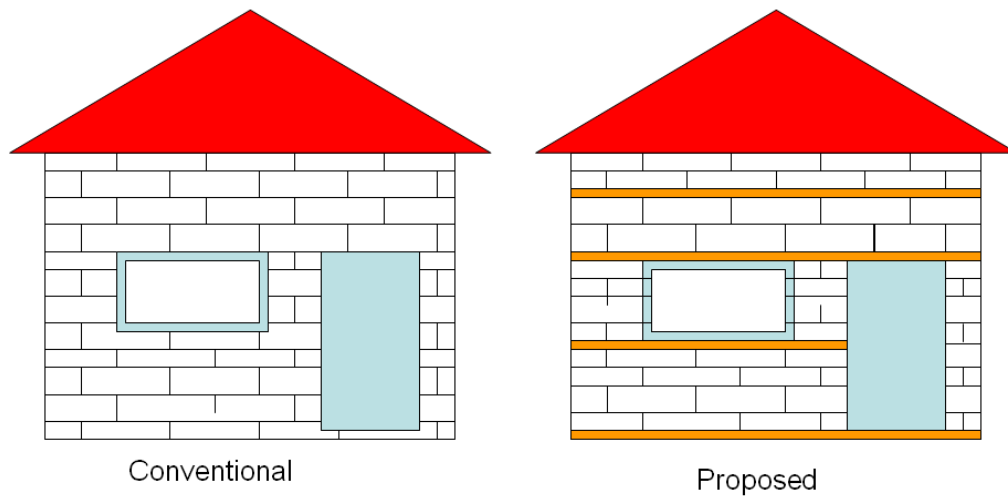
Figure 9.6 Illustrations of conventional and proposed masonry construction procedures.

CHAPTER 10 CONCLUSIONS

10.1 Summary

The findings of this study are summarized, and the results are presented in the following sections.

10.1.1 Overview

The primary goal of this thesis is to evaluate the earthquake hazard threatening the life and properties in Afghanistan. First and foremost, this requires a precise identification of the earthquake sources in the Afghanistan region. This study also aims evaluating the structural integrity of common type buildings, methods and material of construction.

The objectives of this research are primarily to develop seismic hazard maps and to evaluate the seismic collapse mechanisms of the common type buildings and to propose earthquake resistant model of common type buildings in Afghanistan. By assessing the tectonics and geologic activities in the region, earthquake catalogue is prepared for Afghanistan region as well as analyzed in order to develop earthquake risk and strong motion zoning. The crustal deformation, straining and stresses are analyzed, and stress state is discussed from the focal mechanism of past earthquakes. Numerous experiments and FEM simulations are conducted to identify appropriate construction methods for the common type buildings in order to increase life and property safety against future earthquake hazard. This work addresses many important issues involved in earthquake preparedness of Afghanistan some of which are summarized below.

- – Evaluation of the historical and instrumental regional seismicity and preparation of a homogenized earthquake catalogue.

- – Assessment of the tectonic settings and crustal deformation of the Afghanistan region.

- – Analysis of the seismic hazard using probabilistic approach, risk zonation of Afghanistan and strong motion estimation for Kabul city using deterministic seismic hazard analyze methods.

- – Analysis of the collapse mechanism of common type buildings in past earthquakes and evaluation of the characteristics of construction material and construction methods and proposal of modification in the construction methods.

– Photo-elasticity tests on fault models, masonry buildings, frames and frame structures, and evaluation of the stress distribution in these structures with different structural orientations. and

– Monitoring of the structural integrity of towers, frames, frame buildings, beams, RC buildings and bridges using the natural frequency and vibration frequency characteristics of common type structures.

The findings of every chapter are summarized in the following sections.

10.1.2 Tectonics and Seismicity

The seismicity in Afghanistan is fundamentally derived from the movement of Eurasia-India global fault in the East and South. Hindu Kush and Pamir is another major source of seismicity in the North-East Afghanistan from which Kabul is also affected. Afghanistan is divided into 9 seismotectonic domains, 8 of which induce shallow earthquakes and the 9th one is a deep earthquake zone. We retrieved instrumental earthquake data from two international agencies and the historical earthquakes from the earthquake catalogue of (Ambraseys & Bilham, 2003). We converted the different magnitude scales into moment magnitude and prepared a homogenized earthquake catalogue indicating the seismic distribution of the Afghanistan region. The faults in Afghanistan accommodate the movement of the Eurasia-India plate boundary. The focal mechanism of past earthquakes indicates that the faults in the Northern East Afghanistan are mainly thrust faults. The faults in the southern east have strike slip movement with some thrust fault components. The faults in the Northern West and Southern West are less active comparing to the Northern East Afghanistan and are mainly strike slip faults.

10.1.3 Crustal Deformation, Straining and Stresses

The crustal deformation and strain rates of the Afghanistan region is analyzed in Chapter 3. Although there is only one GPS station in Afghanistan, deformation rates from the GPS stations installed in the neighboring countries have been utilized. The strain rate is high in Northern East Afghanistan particularly in the Hindu Kush region. The strain rates are related with the seismicity and activity of the faults. It is noted that high seismicity is observed particularly in the regions undergoing high extension type straining rate.

10.1.4 Seismic Risk Analysis and Zonation

The completeness analysis of the earthquake catalogues discussed in Chapter 2 were evaluated. We found the seismic parameters and analyzed the seismicity using the probabilistic seismic hazard analysis approach. The attenuation relationship of the USA was used to predict the ground motion as these relations specific to Afghanistan are not developed yet. The ground motion is calculated for 0.0, 0.2 and 1.0 second time periods for 2% PE and 10% PE in 50 years, respectively. Results are presented in the form of contour maps. The hazard curves as well as the PE curves for 2% and 10% PE is also presented. Faizabad city in the NE has the highest strong motion followed by Baghlan, Nangarhar, Kabul and Balkh cities. Using these values and evaluating the regional geologic activities, Afghanistan is divided into 4 seismic risk zones.

10.1.5 Strong Motion Estimation for Kabul City

Three different deterministic seismic hazard analysis approaches are used to predict the effect of future earthquakes on Kabul city. Strong motions from Hindu Kush earthquakes in Kabul city seems to be very small. Although, the 2015 Hindu Kush earthquake created minor damages to some buildings, we believe that there might be some other construction factors also contributing to the damage in Kabul. This remarks the need of a thorough study of the seismic resistance of the current buildings in Kabul as well as the construction industries. There is high probability of a devastating earthquake along the Chaman fault near Kabul city. A hypothetical earthquake is simulated, and the effects show that the strong motion in Kabul city can be up to 1.0g and the PGV can be up to 100 kines. Considering the strong motion coverage in other countries like Japan, USA, Italy and Turkey, we recommend these values to be considered as the basis to build earthquake-resistant buildings in Kabul city.

10.1.6 Characteristics of Common Buildings and their Seismic Damage

Construction methods and material in Afghanistan are discussed. Type of common houses currently build are highlighted. The collapse mechanisms of adobe, masonry and frame buildings from the recent earthquakes in Afghanistan, Iran, India and Pakistan are evaluated. We notice from studies in other places that construction of a concrete beam on top of the windows/doors/openings add to the earthquake stability of masonry walls. For RCC buildings, the construction methods are changing but found in the experiments in Chapter 7 that construction of the partition walls before construction the columns and roof slab results in a more unit structure. In this case, partition walls work as load bearing walls and decreases the stress distribution in the frame elements. Although, this is deemed as a conventional construction method in Turkey, India and some other developing countries including Afghanistan, the findings of this study prefer this method over the construction

of frame and partition walls in separate steps. It is highly recommended that the partition wall strength shall not be included in the design strength; however, it results into more a unit resisting structure.

10.1.7 Photo-Elasticity Tests

Photo-elasticity tests are conducted on faults and numerous common type structures with different structural elements orientation in order to find appropriate earthquake resistant models. Furthermore, a series of FEM analyses were carried out on photo-elasticity models. The experimental and FEM results show that frame buildings with weak story are more vulnerable to earthquakes comparing to the frame buildings with infill wall and frame structures without infill wall. Stresses are less developed in the structural elements of frame buildings with infill wall all the way. In the case of weak floor (soft-story), stress concentration is observed at the beam-column joint of the soft story. Stress distribution is uniform in the frames without infill wall.

In the case of masonry structures, it is observed that construction of lintels below and on top of the opening, as well as along the height of the wall increased the ductility of the structure against lateral forces.

10.1.8 Evaluation of Natural Frequency of Structures

A series of tests are conducted to evaluate the structural integrity of common type structures using the natural frequency and vibration characteristics. Some model structures and actual structures in Afghanistan and elsewhere were investigated to obtain the vibration characteristics data. Three different methods are utilized, and it is noted that free vibration method is suitable for evaluating the structural integrity of structures and vibration characteristics. This method almost yields similar results to the forced vibration method and usage of micro-tremor device. This method is cheaper and is highly recommended to monitor slender structures, particularly in the countries like Afghanistan as research funds are seldom available. We also used the sandbag drop test and evaluated the integrity of some bridges in Afghanistan and some old and new buildings in Japan. It is noted that buildings are undergoing certain amount of degradation within time.

10.1.9 Proposals and Recommendations

Considering the overall results of this study, we made some proposal on risk zoning as well as strong motion zoning of Afghanistan. The shortcoming in earthquake resistance of existing buildings are discussed. Seismic design spectra are proposed for Afghanistan. Retrofitting methods

applicable to Afghanistan structures are recommended for the existing buildings. The main points are highlighted below.

– Several different earthquake hazard maps are used by Afghan government for as the reference for construction of earthquake resistance buildings. We recommend a unified, possible a latest version of the seismic hazard map is publicized for this purpose. The seismic hazard estimations in Chapter 4 and Chapter 5 of this study indicated that the strong ground motion and velocity in Kabul city can be up to 1.0 g and 100 kines: respectively. We recommend these be used as the basis for design of structures.

– For construction of earthquake resistant masonry buildings, usage of concrete lintels on top and bottom of the openings, windows and doors and at certain levels are recommended as they increase the ductility and strength of walls against collapse.

– Integration of the infill wall with the frame increases the base shear strength and decrease the lateral displacement. It is recommended that the infill walls shall be integrated with the frames so that they react as a unit system. It is recommended that strength of the infill wall should not be taken into account in the design strength of the structure.

– The free vibration method is a cheap and easy method to monitor the structural integrity of structures, particularly slender structures like towers, poles, long span bridges etc. It is no need to say that large and costly machines are needed to improve the construction industry in Afghanistan and similar countries as there are now adays small and cheap devices available to be used instead.

10.2 Limitations and Recommendations for Future Research

The limitations of this research and potential areas for future research include the following

10.2.1 Tectonics and Seismicity

– There is very little know about the activities of Afghanistan faults. There are a lot of faults believed to be active; however, the slip rate, actual measurements are not understood as there are no GPS devices installed in the region nor it is easy to conduct site visits due to security and financial limitations. We recommend a thorough faults study for the Afghanistan region.

– The historical earthquake catalogue of Afghanistan is almost nil. Although, there are few events reported, they are documented different by various author and the characteristics are still not well know. Further work to quantify these events are recommended.

– There are still a lot of earthquake events with unknow magnitude as well as unknown depth making it quite difficult to give a clear guide about future seismicity of the region.

10.2.2 Ground Motion and Risk Analysis

– There are still events reported in NW with unknow impacts on life and properties.

– We estimated ground motion for a hypothetical earthquake near Kabul City using earthquake parameters from other parts of the world. Necessary characteristics specific to Afghanistan geography are not developed or may not be available so for. In our calculations, we used attenuation relationships from the US. Future work is recommended on developing ground motion prediction equations specific to Afghanistan.

10.2.3 Construction Methods and Seismic Damage

– Effects of previous earthquakes on life and property is not documented. Although, there are some reports, but they are little and kind of a misleading information. Most of them are reports from journalists and other media sources and lack technical information.

– Record of damage to buildings in previous decades does not exist or they are probably not published or shared with people. The technical reports might not have been prepared or they are not published. Or the writers or compilers and even the government bodies believe either that they are confidential documents, or the compiler/writer assume it as his private piece of note. The publication of such documents that in fact increase the importance of the document by citations and reviews are still not understood as an important academic achievement causing the data remain unused in the cupboards. We recommend and propose it to the government to encourage and specify certain annual budget for publication and authorships until the importance of the issue is perceived.

10.2.4 Photo-Elasticity Tests

Results are quite useful. However, additional tests under forced conditions using shaking table are desirable. In such tests, some actual ground motions may also be imposed on models. Furthermore, some physical large-scale experiments using actual construction materials are desirable. Unfortunately, the research fund provided by JICE-JICA for studies leading to the PhD degrees is too small to carry out such experiments.

REFERENCES

Abdullah Sh. 1977, The Khula (North Afghanistan Earthquake of 19 March, 1976 (Abstract), International symposium on RCM, Stanford University, Palo Alto, California, USA

Abdullah, S. (1993). Seismic hazard assessment in the Islamic state of Afghanistan. The Practice of Earthquake Hazard Assessment, IDNDR Monograph. IASPEI/European Seismological Commission: Denver.

Aguilar-Meléndez A., Pujades L.G., Barbat A.H., Ordaz M.G., de la Puente J., Lantada N., and Rodríguez-Lozoya H.E. 2018. "A probabilistic approach for seismic risk assessment based on vulnerability functions. Application to Barcelona." Bulletin of Earthquake Engineering. In Press. DOI: 10.1007/s10518-018-0516-4.

Ahmad, N. 2015. A Note on The Strong Ground Motions and Behavior of Buildings During 26th Oct. 2015 Afghanistan–Pakistan Earthquake. UET Peshawar, 15p.: Earthquake Engineering Center, Department of Civil Engineering.

Ambraseys, N., & Bilham, R. 2003. "Earthquakes in Afghanistan." Seismological Research Letters, 74 (2) 107-123.

Atkinson, G.M., and D.M. Boore. 2003. "Empirical ground-motion relations for subduction zone earthquakes and their applications to Cascadia and other regions." Bulletin of the Seismological Society of America, v. 93 1703–1729.

Aydan, Ö. 2000. "A stress inference method based on GPS measurements for the directions and rate of stresses in the earth' crust and their variation with time." Yerbilimleri 22: 21-32.

Aydan, Ö. 2003a. "An experimental study on the dynamic responses of geomaterials during fracturing." Journal of School of Marine Science and Technology, Tokai University Vol.1 (No.2): 1-7.

Aydan, Ö. (2003b): The earthquake prediction and earthquake risk in Turkey and the applicability of Global Positioning System (GPS) for these purposes. Turkish Earthquake Foundation, TDV/KT 024-87, 1-73 (in Turkish).

Aydan, Ö. 2004. Implications of GPS-derived displacement, strain and stress rates on the 2003 Miyagi-Hokubu earthquakes, Yerbilimleri, No.30, 91-102.

Aydan, Ö. 2006. "The Possibility of Earthquake Prediction by Global Positioning System (GPS)." J. of School of Marine Science and Technology Vol. 4 (No.3): 77-89.

Aydan, Ö. 2008. "Some Thoughts on Seismic and Tsunami Hazard Potentials in Indonesia with a special emphasis on Sumatra Island." Journal of The School of Marine Science and Technology Vol.6 (No.3): 19-38.

References

Aydan, Ö. 2012. "Ground motions and deformations associated with earthquake faulting and their effects on the safety of engineering structures." Encyclopedia of Sustainability Science and Technology, Springer, R. Meyers (Ed.) 3233-3253.

Aydan, Ö. 2013. "The applicability of crustal deformation monitoring by global positioning system (GPS) to real-time earthquake prediction." Bulletin of Institute of Oceanic Research and Developments, Tokai University 34: 1-16.

Aydan, Ö. 2014. "Crustal stress changes and characteristics of damage to geo-engineering structures induced by the Great East Japan Earthquake of 2011." Bull Eng Geol Environ 74 (3): 1057-1070, DOI 10.1007/s10064-014-0668-7.

Aydan, Ö. 2020. "A revisiting of photo-elasticity techn:que and its renewed potential use in rock mechanics and rock engineering." Proc. the 47th Rock Mechanics Symposium, JSCE (in print).

Aydan, Ö., M. Hamada, J. Itoh, and K. 2009a Ohkubo. 2009a. "Damage to Civil Engineering Structures with an Emphasis on Rock Slope Failures and Tunnel Damage Induced by the 2008 Wenchuan Earthquake." Journal of Disaster Research, Vol.4, No.2 153-164.

Aydan, Ö., N. Tokashiki, N.Z. Nasiry, N. Iwata, and R. Kiyota. 2018. "Two-ways dynamic shear testing of rock discontinuities." The 3rd Int. Symp on Rock Dynamics, RocDyn3. Trondheim: Charlie C. Li, Xing Li, Zong-Xian Zhang. 89-95.

Aydan, Ö., N.Z. Nasiry, and Y., Ulusay, R. Ohta. 2018. "Effects of Earthquake Faulting on Civil Engineering Structures." Journal of Earthquake and Tsunami. Vol.12, No.4, 1841007.

Aydan, Ö., Ogura, Y., Daido, M., Tokashiki, N. (2003). A model study on the seismic response and stability of masonary structures through shaking table tests. Fifth National Conference on Earthquake Engineering, 26-30 May 2003, Istanbul, Turkey, Paper No: AE-123

Aydan, Ö., R. Ulusay, H. Kumsar, and E. Tuncay. 2000b. Site investigation and engineering evaluation of the Düzce-Bolu Earthquake of November 12,, 1999. Turkish Earthquake Foundation, TDV/DR 09-51, p.220.

Aydan, Ö., R. Ulusay, Z. Hasgür, and B. Taşkın. 2000a. A site investigation of Kocaeli Earthquake of August 17, 1999. Turkish Earthquake Foundation, TDV/DR 08-49, 180p. .

Aydan, Ö., Y. Ohta, M. Daido, H. Kumsar, M. Genis, N. Tokashiki, T. Ito, and M. Amini. 2011. "Chapter 15: Earthquakes as a rock dynamic problem and their effects on rock engineering structures. Advances in Rock Dynamics and Applications, Editors Y. Zhou and J. Zhao." CRC Press, Taylor and Francis Group, 341-422.

Aydan, Ö., Y. Ohta, M. Hamada, J. Ito, and 2009b K. Ohkubo. 2009b. "The response and damage of structures along the fault rupture traces of the 2008 Wenchuan Earthquake." Int. Conf. on Earthquake Engineering: the 1st Anniversary of Wenchuan Earthquake, Chengdu, pp 625-633.

Benz, H., Machette, M., Sipkin, S., & Wheeler, R. 2005. "Assessing the Seismic Hazards of Afghanistan." US Geological Survey Fact Sheet, 3038(3).

References

Bernard, M.,, B., Shen-Tu, W. E., Holt, and D. M. & Davis. 2000. "Kinematics of active deformation in the Sulaiman Lobe and Range, Pakistan." Journal of Geophysical Research: Solid Earth, 105(B6) 13253-13279.

Boore, D. M., and G. M. Atkinson. 2008. "Ground-motion prediction equations for the average horizontal component of PGA, PGV, and 5%-damped PSA at spectral periods between 0.01 s and 10.0 s." Earthquake Spectra, 24(1) 99-138.

Boore, M. D. 1983. "Stochastic simulation of high-frequency ground motions based on seismological models of the radiated spectra." Bulletin of the Seismological Society of America 73.6A 1865-1894.

Boyd, O. S., C. S. Mueller, and K. S. Rukstales. 2007. Preliminary Earthquake Hazard Map of Afghanistan. US Geological Survey Open-File Report, 2007, 1137.

Brewster, D. 1815. "Experiments on the depolarization of light as exhibited by various mineral, animal and vegetable bodies with a reference of the phenomena to the general principle of polarization." Phil. Tras 29–53.

Building Manual, Ministry of Rural Rehabilitation and Development of Afghanistan 2013

Eringen, A.C. 1980. Mechanics of Continua. Huntington, NY: Robert E. Krieger Publishing Co., 1980. 606 p .

Esri. n.d. National Geographic World Map. National Geographic, Esri, Garmin, HERE, UNEP-WCMC, USGS, NASA, ESA, METI, NRCAN, GEBCO, NOAA, increment P Corp.

Fowler, C.M.R. 1990. The solid earth – An introduction to Global Geophysics. Cambridge: Cambridge University Press.

Fresnel, A. 1820. "Resume d'une Memoire sur la reflexion da la lumiere." Annales de Chimie et de Physique Volume XV: 379-386.

Frocht, M.M. 1965. Photoelasticity. London: J. Wiley and Sons.

Gutenberg, B., and C. F. Richter. 1994. "Frequency of earthquakes in California." Bulletin of the Seismological society of America, 34(4) 185-188.

Hale, C., N. A. Abrahamson, and Y. Bozorgnia. 2018. "Probabilistic Seismic Hazard Analysis Code Verification." Pacific Earthquake Engineering Research Center. Berkeley, USA. PEER Report No. 2018/03 July 2018. Retrieved from https://peer.berkeley.edu/peer-reports.

Hanks, Thomas C., and Robin K. McGuire. 1981. "The character of high-frequency strong ground motion." Bulletin of the Seismological Society of America 71 (6): 2071–2095.

Harp, E. L.,, and A. J. Crone. 2006. Landslides triggered by the October 8, 2005, Pakistan earthquake and associated landslide-dammed reservoirs. No. 2006-1052.

Hayes, Gavin P., et al. 2017. Tectonic summaries of magnitude 7 and greater earthquakes from 2000 to 2015. No. 2016-1192. US Geological Survey.

Heuckroth, L. E., & Karim, R. A. (1970). Earthquake history, seismicity and tectonics of the regions of Afghanistan. Seismological Center, Kabul University.

References

ISC. 2016. "International Seismological Centre." On-line Bulletin, http://www.isc.ac.uk, Internatl. Seismol. Cent., Thatcham, United Kingdom, 2016 http://doi.org/10.31905/D808B830. Accessed December 2018

Ischuk, A., L. W. Bjerrum, M. Kamchybekov, K. Abdrakhmatov, and C Lindholm. 2018. "Probabilistic Seismic Hazard Assessment for the Area of Kyrgyzstan, Tajikistan, and Eastern Uzbekistan." Bulletin of the Seismological Society of America, 108(1) 130-144.

Kabul. 2017. Kabul-World Population Review. (http://worldpopulationreview.com/world-cities/kabul-population/). Accessed December 2018

Kafarsky, AKh, Chmyriov VM, Stazhilo-Alekseev KF, Abdullah Sh, Saikovsky VS. 1975. "Geological map of Afghanistan, scale 1:2, 500,000."

Karadogan F., S. Pala, A. Ilki, E. Yuksel, W. Mowrtage, P. Teymur, G. Erol, K. Taskin and R. Comlek. 2009. Improved infill walls and rehabilitation of existing low-rise buildings. In A. Ilki, F. Karadogan, S. Pala and E. Yuksel (eds) Seismic risk assessment and retrofitting with special emphasis on existing low rise structures, Springer

Lawrence, R. D., S. H. Khan, and T. Nakata. 1992. "Chaman Fault, Pakistan-Afghanistan." Ann. Tectonicae, 6 196-223.

M.A, Ordaz M. and Salgado-Gálvez. 2017. "R-CRISIS Validation and Verification Document. Technical Report."

Mahsuli, M., Rahimi, H., Bakhshi, A. 2019. "Probabilistic seismic hazard analysis of Iran using reliability methods." Bull. Earthq. Eng. 17, https://doi.org/10.1007/s10518-018-0498-2 (Bull. Earthq. Eng. 2019, 17) 1117–1143.

Manual of Construction Methods for Building in Afghanistan (USAID)

Mase, G. 1970. Theory and Problems of Continuum Mechanics. Schaum Outline Series.McGraw Hill Co., 230p. .

Masson, F., M. Anvari, Y. Djamour, A. Walpersdorf, F. Tavakoli, M. Daignieres, H. Nankali, and S. Van Gorp. 2007. "Large-scale velocity field and strain tensor in Iran inferred from GPS measurements: new insight for the present-day deformation pattern within NE Iran." Geophys. J. Int. (2007) 170: 436–440 .

Mohadjer, S., R. Bendick, A. Ischuk, S. Kuzikov, A. Kostuk, U. Saydullaev, S. Lodi, et al. 2010. "Partitioning of India-Eurasia convergence in the Pamir-Hindu Kush from GPS measurements." Geophysical Research Letters 37 (L04305): 6p.

MUDH, Guidelines for Earthquake Resistant Design, Construction and Retrofitting of Buildings in Afghanistan (2003)

Nasiry, N. Z., and Ö. Aydan. 2018. "Probabilistic Seismic Hazard Analysis of Southern-east Region of Afghanistan." 15th Japan Earthquake Engineering Symposium , 6-8 Dec. Sendai, Japan. 1310-1318.

References

Nasiry, N.Z., and Ö. Aydan. 2019. "Ground motion estimation at Kabul City for Mw 7.5 Hindu Kush earthquake." Proceedings of 2019 Rock Dynamics Summit in Okinawa, 7-11 May 2019. Okinawa, Japan, ISRM: Aydan, Ö., Ito, T., Seiki T., Kamemura, K., Iwata, N. 247-252.

NGDC/WDS. Significant Earthquake Database, National Geophysical Data Center / World Data Service. National Geophysical Data Center, NOAA. doi:10.7289/V5TD9V7K. Accessed July 2019.

Ordaz M., and Salgado-Gálvez M.A. 2017. "R-CRISIS Validation and Verification Document. Technical Report." Mexico City, Mexico.

Ordaz, M. 1991. Brief description of program CRISIS, Internal report. Norway,: Institute of Solid Earth Physics, University of Bergen, 16pp.

Ordaz, M. 1999. User's manual for program CRISIS1999. Technical report. Mexico City, Mexico. : Universidad Nacional Autónoma de México.

Pavlis, G. L., and S. Das. 2000. "The Pamir-Hindu Kush seismic zone as a strain marker for flow in the upper mantle." Tectonics, 19, (1) 103-115.

Prevot, R., Hatzfeld, D., Roecker, S. W., & Molnar, P. 1980. "Shallow earthquakes and active tectonics in eastern Afghanistan." Journal of Geophysical Research: Solid Earth, 85(B3) 1347-1357.

Rafi, Z., Lindholm, C., Bungum, H., Laghari, A., & Ahmed, N. 2012. "Probabilistic seismic hazard of Pakistan, Azad-Jammu and Kashmir." Natural hazards, 61(3) 1317-1354.

Ruleman, C. A.,, A. J., Crone, M. N., Machette, K. M., Haller, and K. S. Rukstales. 2007. Map and database of probable and possible Quaternary faults in Afghanistan (No. 2007-1103). Geological Survey (US).

Sadigh, K., Chang, C.-Y., Egan, J.A., Makdisi, F., and Youngs, R.R. 1997. "Attenuation relationships for shallow crustal earthquakes based on California strong motion data." Seismological Research Letters, v. 68, p 180–189.

Scordilis, E.M. 2006. "Empirical global relations converting Ms and mb to moment magnitude." J. Seismol. 10, 2 225-236, DOI: 10.1007/s10950-006-9012-4.

Shareq, A. (1981). Geological observations and geophysical investigations carried out in Afghanistan over the period of 1972–1979. Zagros Hindu Kush Himalaya Geodynamic Evolution, 75-86.

Stenz, E. (1945). Strong earthquakes in Afghanistan. Bulletin of the Polish Institute of Arts and Sciences in America, 398-411.

Sugito, M., Y. Furumoto, and T. and Sugiyama. 2000. "Strong Motion Prediction on Rock Surface by Superposed Evolutionary Spectra." 12th World Conference on Earthquake Engineering, CD-ROM, Aukland, New Zealand, January.

References

Tokashiki, N., Ö. Aydan, N. Z. Nasiry, T. Ito, and M. Geniş. 2018. "Dynamic response and stability of some historical masonry structures subjected to ground shaking." The 3rd Int. Symp on Rock Dynamics, RocDyn3. Trondheim : Charlie C. Li, Xing Li, Zong-Xian Zhang. 533-539.

Tromans, Iain J., et al. 2019. "Probabilistic seismic hazard assessment for a new-build nuclear power plant site in the UK." Bulletin of Earthquake Engineering 17.1 1-36.

UNISDR DRR sitrep (2015). 26 October 2015 Badakhshan Afghanistan and Pakistan Earthquake Disaster Risk Reduction Situation Report

USGS "United States Geological Survey." Earthquake Hazard Program. Accessed December 2018

Walpersdorf, A., I. Manighetti, Z. Mousavi, F. Tavakoli, M. Vergnolle, A. Jadidi, D. Hatzfeld, et al. 2014. "Present-day kinematics and fault slip rates in eastern Iran, derived from 11 years of GPS data." Journal of Geophysical Research: Solid Earth 1359-1383.

Waseem, M., Lateef, A., Ahmad, I., Khan, S., & Ahmed, W. 2019. "Seismic hazard assessment of Afghanistan." Journal of Seismology, 23(2) 217-242.

Wheeler, R. L., C. G. Bufe, M. L. Johnson, R. L. Dart, and G. A. Norton. 2005. Seismotectonic map of Afghanistan, with annotated bibliography. US Department of the Interior, US Geological Survey.

Youngs, R.R., Chiou, S.-J., Silva, W.J., and Humphrey, J.R. 1997. "Strong ground motion attenuation relationships for subduction zone earthquakes." Seismological Research Letters, v. 68 58–73.

Yuksel E., H. Ozkaynak, C. Buyukozturk, A. A. Yalcin, M. Dindar, D. Surmeli and B. Tastan. 2010. Performance of alternative CFRP retrofitting schemes used in infill RC frames. Construction and Building Materials 24(4): 596-609

Zare, M., Amini, H., Yazdi, P., Sesetyan, K., Demircioglu, M. B., Kalafat, D. & Tsereteli, N. 2014. "Recent developments of the Middle East catalog." Journal of Seismology, 18 (4) 749–772.

Zhang, J.,, D. R., Gurung, R., Liu, M. S. R., Murthy, and F. & Su. 2015. "Abe Barek landslide and landslide susceptibility assessment in Badakhshan Province, Afghanistan." Landslides 12 (3): 597-609.